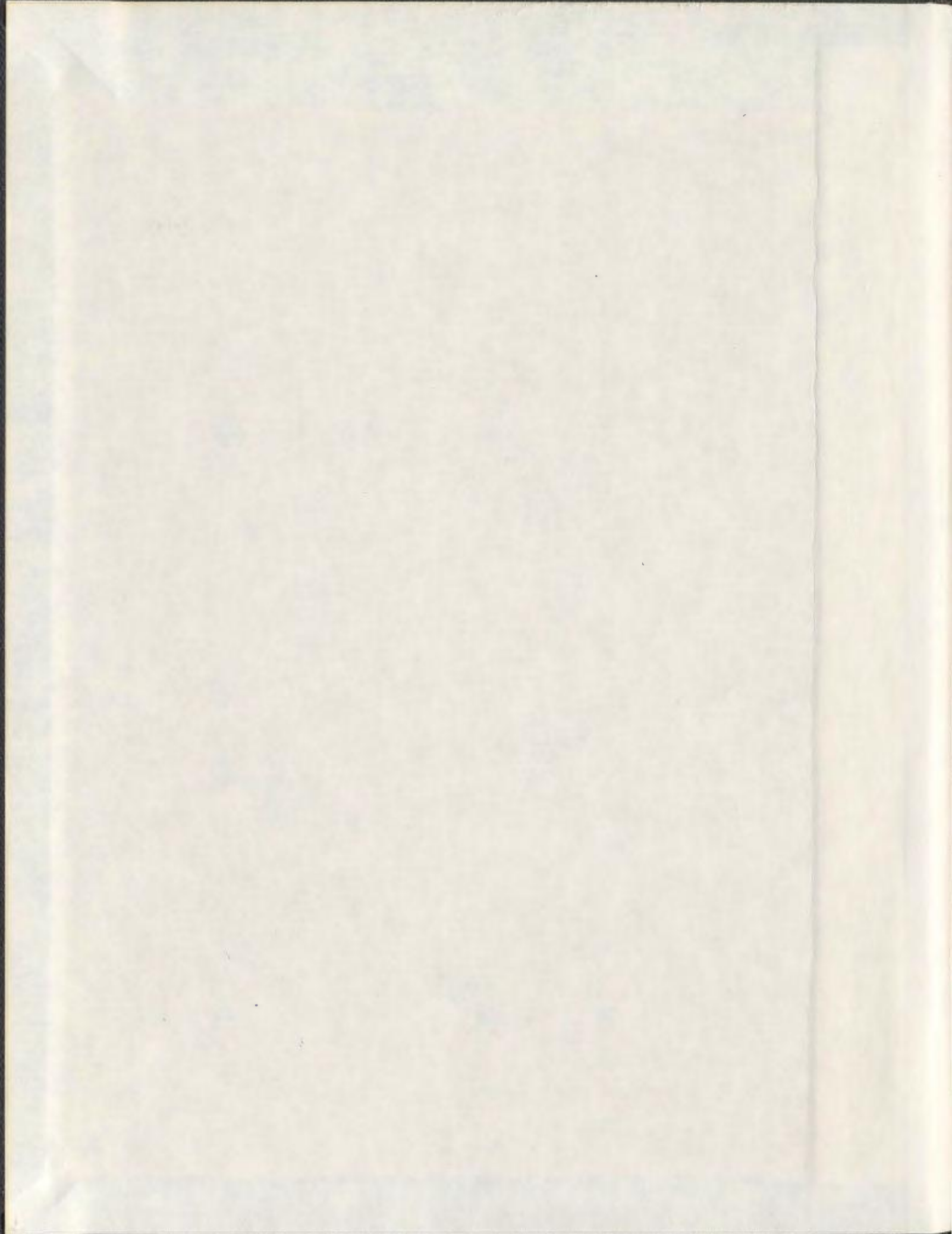


SYNTHESIS OF NEW MACROCYCLIC POLYAMIDES  
AND POLYSULFONAMIDES AND A STUDY OF THEIR  
COMPLEXATION BEHAVIOR USING  $^1\text{H}$ -NMR AND  
MASS SPECTROMETRY

HISHAM F. SLEEM



**Synthesis of New Macrocyclic Polyamides and Polysulfonamides and a Study  
of their Complexation Behavior using  $^1\text{H}$ -NMR and Mass Spectrometry**

By

© **Hisham F. Sleem**

A thesis submitted to the School of Graduate Studies  
in partial fulfillment of the requirements for the degree of  
Doctor of Philosophy

Department of Chemistry

Memorial University

2013

St. John's

Newfoundland and Labrador

## ***Dedication***

*To my family Enayat, Kareem and Fathy*

*To my Father, the memory of my Mother*

*And to all members of my family*

## Abstract

The reactions of isophthaloyl dichloride with “Jeffamine-176 and “Jeffamine-148” in the presence of triethylamine forms macrocyclic amide compounds. Also, the reaction of the chromotropic acid derivative with “Jeffamine-176” or with “Jeffamine-148” forms macrocyclic sulfonamides. The product ratios of these new macrocycles depend on the reaction conditions. The compounds have been found to be modest hosts for tetrabutylammonium and metal halides using  $^1\text{H}$  NMR titration experiments. These experiments are described in Chapters 2 and 3.

Their association constant ( $K_{\text{assoc}}$ ) values were determined using isothermal non-linear 1:1 binding curve fitting plots. Single-crystal X-ray structures for eight new compounds were obtained and confirmed the proposed structures. The photochemical behaviour of some of the chromotropic acid-based macrocyclic sulfonamides is also reported.

The titration properties of the tetrabutylammonium halides (TBAX, X = Cl, Br or I) alone with  $\text{CDCl}_3$  using  $^1\text{H}$  NMR chemical shift changes are described in Chapter 4. From the resulting titration curves a linear concentration-dependent relationship could be observed. A Single-crystal X-ray structure for  $\text{TBABr}:\text{CHCl}_3$  has been obtained.

## Acknowledgments

It's my great pleasure to thank the following people for their contributions to the work contained in this thesis. It is my privilege to acknowledge that without their efforts and assistance on my behalf, this work would never have been completed. To my supervisor Prof. Paris Georghiou go my profoundest thanks. Paris without your knowledge, desire, drive, encouragement and enthusiasm this degree would never have been completed. My thanks for the papers, discussions, ideas, and all the little things; things I could not have done without. To my supervisory committee members Dr. Christina Bottaro and Dr. Christopher Kozak, thank you for providing me with comments, suggestions during my doctoral program and for your critical evaluation of these documents. Thanks are also due to Prof. Graham Bodwell, Prof. Sunil Pansare, and Prof. Yuming Zhao for helpful discussions and encouragements.

I would like to thank my family, Dad, my brothers and sister, my aunts and my uncle, for support and encouragement. My wife Enayat, your love and support, belief, encouragement, and steadfast attitude stagger me beyond words and have kept me going, through the good and bad times, until the end.

My deep thanks to Dr. Louise Dawe for an X-ray crystal structure determination. Louise, your efforts are exemplary and much to be admired. Also, I would like to thank Ms. Linda Winsor, for training and support with mass spectroscopy and Ms. Julie Collins for training and support with NMR spectroscopy.

To the following people go my thanks for their support and help during my program. Ms. Ebony Penney, Ms. Mary Flinn, Ms. Roslaine Collins, Ms. Gina Jackson for the administrative support and Mr. Dave Murphy for his computer-related support throughout my program. I am thankful for the storeroom support provided by Mr. Steve Ballard, Ms. Bonita Smith, and Mr. John Power.

To the members of the Georghiou group, both past and present, it has been a great joy to me to work together over the past 4 years. The people I have worked with comprise the fondest memories of my studies, and have helped make the research and learning enjoyable.

And last, but not least, my appreciation is also extended to the Egyptian government for a scholarship and the Egyptian culture bureau staff in Montreal for their assistance, as well the NRC, Cairo, Egypt for their support.

## Table of Contents

	Page
Abstract.....	iii
Acknowledgments.....	iv
Table of Contents.....	vi
List of Tables.....	xi
List of Schemes.....	xii
List of Figures.....	xiii
List of Abbreviations.....	xvii
List of Appendices.....	xix

## CHAPTER 1

### Introduction

1.1 Supramolecular Chemistry.....	1
1.1.1 Non-covalent interactions.....	2
1.1.1.1 Hydrogen bonding.....	3
1.1.1.2 $\pi$ - $\pi$ -Stacking interactions.....	4
1.1.1.3 Electrostatic interactions.....	5
1.1.1.4 Van der Waals interactions.....	6
1.1.1.5 Hydrophobic effect.....	7
1.2 Macrocyclic amide receptors.....	7
1.3 Heteroditopic receptors.....	14
1.3.1 Heteroditopic receptors for separated ion pairs.....	15
1.3.2 Heteroditopic receptors for contact ion-pairs.....	18
1.4 Characterization of host-guest complexation.....	22
1.4.1 Mass spectrometry.....	23

1.4.2 Nuclear magnetic resonance (NMR) spectroscopy.....	23
1.4.3 UV-visible spectroscopy.....	26
1.4.4 Single-crystal X-ray diffraction.....	26
1.4.5 Determination of the association constant ( $K_{assoc}$ ).....	26
1.5 Objectives and results.....	28
1.6 References.....	30

## CHAPTER 2

### Synthesis and Complexation Properties of Amide-based Macrocyclic Receptors

2.1 Introduction.....	34
2.1.1 Anion receptors.....	34
2.1.2 Amide based receptors.....	35
2.1.3 Ditopic receptors.....	39
2.1.4 Diaryl ether coupling.....	42
2.2 Synthesis of the aryl diacid chloride-Jeffamines macrocyclic amides.....	43
2.2.1 Reaction of isophthaloyl dichloride ( <b>2c</b> ) with “Jeffamine <sup>®</sup> EDR-176” ( <b>19</b> ).....	43
2.2.2 Reaction of isophthaloyl dichloride ( <b>2c</b> ) with “Jeffamine <sup>®</sup> EDR-148” ( <b>15</b> ).....	44
2.2.3 Synthesis of macrocycles <b>36</b> and <b>37</b> .....	45
2.2.3.1 Synthesis of the starting material <b>32</b> .....	46
2.2.3.2 Reaction of diacyl chloride <b>35</b> with “Jeffamine <sup>®</sup> EDR-148” ( <b>15</b> ).....	48
2.3 X-Ray structures of <b>20</b> , <b>21</b> , <b>25</b> and <b>36</b> .....	48
2.4 Complexation studies.....	56
2.4.1 Complexation of macrocycles <b>20</b> and <b>21</b> with Group 1 and 2 metal chlorides .....	57
2.4.1.1 Complexation of macrocyclic amide <b>21</b> with anhydrous CaCl <sub>2</sub> .....	60
2.4.1.2 Complexation of macrocyclic amide <b>21</b> with anhydrous SrCl <sub>2</sub> .....	63
2.4.2 ESI-mass spectrometry of macrocyclic amide <b>21</b> with metal chlorides.....	65
2.4.3 Complexation of macrocycles <b>20</b> and <b>21</b> with tetrabutylammonium salts.....	66

2.4.3.1 Complexation of macrocyclic amide <b>21</b> with TBACl.....	68
2.4.3.2 Complexation of macrocyclic amide <b>21</b> with TBABr.....	70
2.4.3.4 Complexation of macrocyclic amide <b>21</b> with TBABF <sub>4</sub> .....	74
2.4.4 ESI-mass spectrometry data of macrocyclic amide <b>21</b> with TBAX.....	76
2.4.5 Complexation of macrocyclic amide <b>25</b> with tetrabutylammonium salts.....	77
2.4.5.1 Complexation of macrocyclic amide <b>25</b> with TBACl.....	77
2.4.5.2 Complexation of macrocyclic amide <b>25</b> with TBABr.....	79
2.4.5.3 Complexation of macrocyclic amide <b>25</b> with TBAI.....	81
2.4.6 Comparison between the $K_{assoc}$ values of macrocycles <b>21</b> and <b>25</b> .....	83
2.5 Uranium complex.....	85
2.6 Conclusions.....	87
2.7 Experimental section.....	89
2.7.1 Experimental.....	89
2.8 References.....	95

### CHAPTER 3

#### Synthesis and Structures of New Macrocyclic Chromotropic Acid-based Sulfonamides; Their Complexation Properties and an Unexpected Photochemical Reaction

3.1 Introduction.....	100
3.1.1 Chromotropic acid.....	100
3.1.2 Sulfonamides as drugs.....	102
3.1.3 Macrocyclic sulfonamides.....	103
3.2 Synthesis of the CTA-Jeffamines macrocyclic sulfonamides.....	107
3.2.1 Synthesis of the starting material.....	107

3.2.2 Synthesis of the CTA-Jeffamines macrocycles.....	107
3.2.2.1 Synthesis of macrocycles <b>21</b> and <b>22</b> .....	107
3.2.2.2 Synthesis of macrocycles <b>24</b> and <b>25</b> .....	108
3.3 X-Ray structure of macrocycle <b>24</b> .....	109
3.4 Complexation studies.....	111
3.4.1 Complexation studies with Group 1 and 2 metal chlorides.....	112
3.4.2 Complexation studies with tetrabutylammonium salts.....	113
3.4.2.1 Complexation of macrocyclic sulfonamide <b>22</b> with TBAX.....	113
3.4.2.1.1 Complexation of macrocyclic sulfonamide <b>22</b> with TBACl.....	114
3.4.2.1.2 Complexation of macrocyclic sulfonamide <b>22</b> with TBABr.....	116
3.4.2.1.3 Complexation of macrocyclic sulfonamide <b>22</b> with TBAI.....	118
3.4.2.2 ESI-mass spectral data of macrocyclic sulfonamide <b>22</b> with TBAX.....	120
3.4.2.3 Complexation of macrocyclic sulfonamide <b>25</b> with TBAX.....	121
3.4.2.3.1 Complexation of macrocyclic sulfonamide <b>25</b> with TBACl.....	121
3.4.2.3.2 Complexation of macrocyclic sulfonamide <b>25</b> with TBABr.....	123
3.4.2.3.3 Complexation of macrocyclic sulfonamide <b>25</b> with TBAI.....	125
3.4.2.4 Comparison between the $K_{assoc}$ values of macrocycles <b>22</b> and <b>25</b> with TBAX...	127
3.4.2.5 ESI-mass spectral data of <b>25</b> with TBAX.....	128
3.5 Photochemistry of sulfonamides.....	129
3.5.1 Photochemical reaction of macrocyclic sulfonamide <b>25</b> .....	130
3.5.2 Photochemical reaction of macrocyclic sulfonamide <b>22</b> .....	133
3.6 Conclusions.....	136
3.7 Experimental section.....	137
3.7.1 Experimental.....	137
3.8 References.....	141

## Chapter 4

### <sup>1</sup>H-NMR Spectroscopic Studies of Tetrabutylammonium Halides

4.1 Introduction.....	144
4.1.1 NMR studies of the complexation of TBAX.....	144
4.2 Complexation studies of different TBAX halides in CDCl <sub>3</sub> .....	147
4.2.1 Titration of TBACl with CDCl <sub>3</sub> .....	148
4.2.2 Titration of TBABr with CDCl <sub>3</sub> .....	150
4.2.3 Titration of TBAI with CDCl <sub>3</sub> .....	151
4.2.4 Titration of TBABF <sub>4</sub> with CDCl <sub>3</sub> .....	152
4.2.5 Comparison between the slopes observed with the TBAX salts in CDCl <sub>3</sub> .....	154
4.3 X-Ray structure of TBABr with CDCl <sub>3</sub> .....	155
4.4 Conclusion.....	158
4.5 References.....	159

## List of Tables

	Page
Table 2.1. Hydrogen-bond geometry (Å).....	51
Table 2.2. Hydrogen-bond geometry (Å).....	53
Table 2.3. Hydrogen-bond geometry (Å).....	55
Table 2.4. <sup>1</sup> H NMR titration chemical shift data of <b>21</b> with anhydrous CaCl <sub>2</sub> .....	61
Table 2.5. <sup>1</sup> H NMR titration chemical shift data of <b>21</b> with anhydrous SrCl <sub>2</sub> .....	64
Table 2.6. <sup>1</sup> H NMR titration chemical shift data of <b>21</b> with TBACl.....	69
Table 2.7. <sup>1</sup> H NMR titration chemical shift data of <b>21</b> with TBABr.....	71
Table 2.8. <sup>1</sup> H NMR titration chemical shift data of <b>21</b> with TBAI.....	73
Table 2.9. <sup>1</sup> H NMR titration chemical shift data of <b>21</b> with TBABF <sub>4</sub> .....	75
Table 2.10. <sup>1</sup> H NMR titration chemical shift data of <b>25</b> with TBACl.....	78
Table 2.11. <sup>1</sup> H NMR titration chemical shift data of <b>25</b> with TBABr.....	81
Table 2.12. <sup>1</sup> H NMR titration chemical shift data of <b>25</b> with TBAI.....	83
Table 2.13. <i>K<sub>assoc</sub></i> values of macrocycles <b>21</b> and <b>25</b> with TBAX.....	84
Table 3.1. <sup>1</sup> H NMR titration chemical shift data of <b>22</b> with TBACl.....	115
Table 3.2. <sup>1</sup> H NMR titration chemical shift data of <b>22</b> with TBABr.....	117
Table 3.3. <sup>1</sup> H NMR titration data of <b>22</b> with TBAI.....	119
Table 3.4. <sup>1</sup> H NMR titration data of <b>25</b> with TBACl.....	122
Table 3.5. <sup>1</sup> H NMR titration data of <b>25</b> with TBABr.....	124
Table 3.6. <sup>1</sup> H NMR titration data of with TBAI.....	126
Table 3.7. <i>K<sub>assoc</sub></i> values of macrocycles <b>22</b> and <b>25</b> with TBAX.....	127
Table 4.1. Comparison between <sup>1</sup> H NMR CIS changes of trihalomethane.....	145
Table 4.2. <sup>1</sup> H NMR titration data from Figure 4.2.....	149
Table 4.3. <sup>1</sup> H NMR titration data from Figure 4.4.....	150
Table 4.4. <sup>1</sup> H NMR expanded titration data from Figure 4.6.....	152
Table 4.5. <sup>1</sup> H NMR titration data from Figure 4.10.....	153
Table 4.6. Slope values of CDCl <sub>3</sub> with TBAX (X= Cl <sup>-</sup> , Br <sup>-</sup> , I <sup>-</sup> and BF <sub>4</sub> <sup>-</sup> ) salts.....	155
Table 4.7. Bromide anion and chloroform hydrogen atoms distances.....	156

## List of Schemes

	Page
Scheme 1.1. Synthesis of macrocyclic amide <b>13</b> .....	10
Scheme 1.2. Synthesis of macrocyclic tetramides <b>16-19</b> .....	11
Scheme 1.3. Synthesis of macrocyclic tetramides <b>22-24</b> .....	12
Scheme 1.4. Synthesis of receptor <b>43</b> as described by Beer and co-workers.....	20
Scheme 2.1. Synthesis of diamide homo-15-crown-5-calix[4]arene.....	36
Scheme 2.2. Synthesis of tetra-, hexa- and octamide macrocycles.....	38
Scheme 2.3. Synthesis of macrocycle <b>13</b> .....	42
Scheme 2.4. General scheme for diaryl ether formation.....	43
Scheme 2.5. General mechanism for copper acetate-mediated coupling.....	43
Scheme 2.6. Reaction conditions of isophthaloyl dichloride and compound <b>19</b> .....	44
Scheme 2.7. Reaction conditions of isophthaloyl dichloride and compound <b>15</b> .....	45
Scheme 2.8. Preparation of arylboronic acid <b>32</b> .....	46
Scheme 2.9. Preparation of diacid chloride <b>35</b> .....	47
Scheme 2.10. Reaction of diacid chloride <b>35</b> and <b>15</b> .....	48
Scheme 3.1. Deuterium exchange of the CTA protons.....	101
Scheme 3.2. Poh's synthesis of cyclotetrachromotropyrene.....	102
Scheme 3.3. Metabolic conversion of pro-drug Prontosil ( <b>5</b> ) to sulfonamide <b>6</b> .....	103
Scheme 3.4. Synthesis of macrocyclic tetrasulfonamides <b>11</b> .....	104
Scheme 3.5. Synthesis of macrocyclic bis-sulfonamides <b>17</b> .....	106
Scheme 3.6. Synthesis of 4,5-ditosyloxynaphthalene-2,7-disulfonyl chloride.....	107
Scheme 3.7. Synthesis of macrocyclic sulfonamides <b>21</b> and <b>22</b> .....	108
Scheme 3.8. Synthesis of macrocyclic sulfonamides <b>24</b> and <b>25</b> .....	109
Scheme 3.9. Gomberg's free radical reaction.....	129
Scheme 3.10. Lancaster and Smith sulfonamide photochemical reaction.....	130
Scheme 3.11. Synthesis and equilibrium process between the bis- and tetra-imines.....	130

## List of Figures

Chapter 1	Page
Figure 1.1. Categories of supramolecular chemistry.....	2
Figure 1.2. Types of different hydrogen bonding geometries.....	3
Figure 1.3. Multiple hydrogen bonding systems and hydrogen bonds in the DNA.....	4
Figure 1.4. Different types of $\pi$ - $\pi$ stacking.....	5
Figure 1.5. Types of electrostatic interactions.....	6
Figure 1.6. Hydrophobic effect in host-guest chemistry.....	7
Figure 1.7. The acyclic amide receptors <b>1-4</b> .....	8
Figure 1.8. Macrocyclic tetramide <b>5</b> .....	9
Figure 1.9. Bowman-James macrocyclic tetraamide.....	9
Figure 1.10. Chiral calix[4]arenes <b>8</b> and <b>9</b> .....	10
Figure 1.11. X-ray structure of <b>17</b> .....	11
Figure 1.12. Structures of different macrocyclic bisamide compounds <b>25-29</b> .....	13
Figure 1.13. Calcium complex of macrocycle <b>25</b> .....	13
Figure 1.14. The structure of tricyclic amide receptor <b>30</b> .....	14
Figure 1.15. Common designs of ditopic receptors.....	15
Figure 1.16. Solubilization of sodium chloride ion-pairs in the calix[4]arene.....	15
Figure 1.17. Receptor <b>32</b> for CsF ion-pairs.....	16
Figure 1.18. Anti-cooperative binding in the presence of two equivalents of sodium.....	17
Figure 1.19. (a) Macrocycle <b>34</b> (b) X-ray structure of complex <b>34</b> :LiCl·H <sub>2</sub> O and (c) X-ray structure of complex <b>34</b> :LiBr·H <sub>2</sub> O.....	17
Figure 1.20. Ferrocene receptor <b>35</b> binds NaBr.....	18
Figure 1.21. Uranyl salophen receptor <b>36</b> binds CsCl.....	19
Figure 1.22. Chemical structure of receptor <b>37</b> .....	19
Figure 1.23. Optimised CAChe model of <b>43</b> :KCl complex.....	21

Figure 1.24. Chemical structures of resorcin[4]arene-based receptors <b>44a-e</b> .....	21
Figure 1.25. Two different views of the X-ray structure of <b>44a</b> :TMACl.....	22
Figure 1.26. The <sup>1</sup> H NMR spectra of cyclohexane-d11 as a function of temperature.....	25

## Chapter 2

Figure 2.1. Isophthaloyldiamides <b>2a-b</b> and isophthaloyl dichloride ( <b>2c</b> ).....	37
Figure 2.2. The trisbiphenyl macrocyclic amides <b>3a-b</b> and <b>4</b> .....	37
Figure 2.3. Limiting ion-pair interactions relevant to receptor-mediated ion-pair.....	39
Figure 2.4. (a) Macrocycle <b>12</b> (b) X-ray structure of complex <b>12</b> :KCl and (c) X-ray structure of complex <b>12</b> :NaCl.....	40
Figure 2.5. First supramolecular ion triplet complex of macrocyclic <b>13</b> :CaCl <sub>2</sub> .....	41
Figure 2.6. X-ray structure of <b>20</b> .....	49
Figure 2.7. X-ray structure of <b>21</b> .....	50
Figure 2.8. Asymmetric unit for macrocycle <b>24</b> .....	51
Figure 2.9. Hydrogen bonding (dashed lines) for macrocycle <b>24</b> .....	52
Figure 2.10. Asymmetric unit for macrocycle <b>25</b> .....	53
Figure 2.11. Hydrogen bonding for macrocycle <b>25</b> .....	54
Figure 2.12. The $\pi$ - $\pi$ stacking for macrocycle <b>25</b> .....	54
Figure 2.13. Asymmetric unit for macrocycle <b>36</b> .....	55
Figure 2.14. Hydrogen bonding (dashed lines) for macrocycle <b>36</b> .....	56
Figure 2.15. Downfield NH protons chemical shift changes for solutions of <b>13</b> and <b>21</b> ..	58
Figure 2.16. <sup>1</sup> H NMR titration spectra of macrocyclic <b>20</b> with CaCl <sub>2</sub> .....	59
Figure 2.17. <sup>1</sup> H NMR titration spectra of macrocyclic <b>21</b> with CaCl <sub>2</sub> .....	61
Figure 2.18. <sup>1</sup> H NMR titration curves of <b>21</b> with CaCl <sub>2</sub> .....	62
Figure 2.19. <sup>1</sup> H NMR titration spectra of macrocyclic <b>21</b> with SrCl <sub>2</sub> .....	63
Figure 2.20. <sup>1</sup> H NMR titration curves of <b>21</b> with SrCl <sub>2</sub> .....	64
Figure 2.21. <sup>1</sup> H NMR chemical shift changes of <b>21</b> with TBAX.....	66
Figure 2.22. <sup>1</sup> H NMR titration spectra of macrocyclic <b>20</b> with TBACl.....	67

Figure 2.23. <sup>1</sup> H NMR titration spectra of macrocyclic <b>21</b> with TBACl.....	68
Figure 2.24. <sup>1</sup> H NMR titration curves of <b>21</b> with TBACl.....	70
Figure 2.25. <sup>1</sup> H NMR titration spectra of macrocyclic <b>21</b> with TBABr.....	70
Figure 2.26. <sup>1</sup> H NMR titration curves of <b>21</b> with TBABr.....	72
Figure 2.27. <sup>1</sup> H NMR titration spectra of macrocyclic amide <b>21</b> with TBAI.....	72
Figure 2.28. <sup>1</sup> H NMR titration curves of <b>21</b> with TBAI.....	74
Figure 2.29. <sup>1</sup> H NMR titration spectra of <b>21</b> with TBABF <sub>4</sub> .....	74
Figure 2.30. <sup>1</sup> H NMR titration curve of <b>21</b> with TBABF <sub>4</sub> .....	76
Figure 2.31. <sup>1</sup> H NMR titration spectra of macrocyclic amide <b>25</b> with TBACl.....	77
Figure 2.32. <sup>1</sup> H NMR titration curves of <b>25</b> with TBACl.....	79
Figure 2.33. <sup>1</sup> H NMR titration spectra of macrocyclic amide <b>25</b> with TBABr.....	80
Figure 2.34. <sup>1</sup> H NMR titration curves of <b>25</b> with TBABr.....	81
Figure 2.35. <sup>1</sup> H NMR titration spectra of macrocyclic amide <b>25</b> with TBAI.....	82
Figure 2.36. <sup>1</sup> H NMR titration curves of <b>25</b> with TBAI.....	83
Figure 2.37. Uranium complex <b>38</b> .....	86

### Chapter 3

Figure 3.1. Biernat and co-workers' macrocyclic sulfonamide compounds.....	105
Figure 3.2. Macrocyclic bis-sulfonamides synthesized by Eshghi.....	106
Figure 3.3. Asymmetric unit for <b>24</b> .....	109
Figure 3.4. Hydrogen bonding (dashed lines) for <b>24</b> .....	110
Figure 3.5. $\pi$ - $\pi$ stacking between naphthalene ring.....	111
Figure 3.6 <sup>1</sup> H NMR titration spectra of macrocyclic <b>22</b> with TBACl.....	114
Figure 3.7. <sup>1</sup> H NMR titration curves of <b>22</b> with TBACl.....	115
Figure 3.8. <sup>1</sup> H NMR titration spectra of macrocyclic <b>22</b> with TBABr.....	116
Figure 3.9. <sup>1</sup> H NMR titration curves of <b>22</b> with TBABr.....	117
Figure 3.10. <sup>1</sup> H NMR titration spectra of macrocyclic <b>22</b> with TBAI.....	118
Figure 3.11. <sup>1</sup> H NMR titration curves of <b>22</b> with TBAI.....	119

Figure 3.12. $^1\text{H}$ NMR titration spectra of macrocyclic <b>25</b> with TBACl.....	121
Figure 3.13. $^1\text{H}$ NMR titration curves of <b>25</b> with TBACl.....	123
Figure 3.14. $^1\text{H}$ NMR titration spectra of <b>25</b> with TBABr.....	123
Figure 3.15. $^1\text{H}$ NMR titration curves of <b>25</b> with TBABr.....	124
Figure 3.16. $^1\text{H}$ NMR titration spectra of macrocyclic <b>25</b> with TBAI.....	125
Figure 3.17. $^1\text{H}$ NMR titration curves of <b>25</b> with TBAI.....	126
Figure 3.18. $^1\text{H}$ NMR step-wise photochemical reaction spectra of <b>25</b> .....	132
Figure 3.19. Expanded sections of $^1\text{H}$ NMR photochemical reaction spectra of <b>25</b> .....	133
Figure 3.20. $^1\text{H}$ NMR stepwise photochemical reaction spectra of <b>22</b> .....	134
Figure 3.21. Expanded sections of $^1\text{H}$ NMR photochemical reaction spectra of <b>22</b> .....	135

## Chapter 4

Figure 4.1. Proton shielding of 0.1 M $\text{CHCl}_3$ in $\text{CH}_3\text{CN}$ as a function of TBABr.....	146
Figure 4.2. $^1\text{H}$ NMR expanded titration spectra for $\text{CDCl}_3$ with TBACl.....	148
Figure 4.3. Least-squares linear regression plot for the $\text{CDCl}_3$ : TBACl.....	149
Figure 4.4. $^1\text{H}$ NMR expanded titration spectra of the $\text{CDCl}_3$ with TBABr.....	150
Figure 4.5. Least-squares linear regression plot for $\text{CDCl}_3$ : TBABr.....	151
Figure 4.6. $^1\text{H}$ NMR expanded titration spectra for $\text{CDCl}_3$ with TBAI.....	151
Figure 4.7. Least-squares linear regression plot for $\text{CDCl}_3$ : TBABr.....	152
Figure 4.8. $^1\text{H}$ NMR titration spectra of the $\text{CDCl}_3$ with $\text{TBABF}_4$ .....	153
Figure 4.9. Least-squares linear regression plot for the $\text{CDCl}_3$ : TBABr.....	154
Figure 4.10. Asymmetric unit of $\text{TBABr}:\text{CHCl}_3$ .....	155
Figure 4.11. SpartanPro'10 molecular modeling of $(\text{TBABr})_2(\text{CHCl}_3)_6$ complex.....	156
Figure 4.12. $^1\text{H}$ NMR titration curve of <b>1</b> :TBACl in $\text{CDCl}_3$ .....	157
Figure 4.13. X-ray crystal structure of <b>1</b> :TBACl.....	158

## List of Abbreviations

Å	angstrom (s)
aq	aqueous
APCI-MS	atmospheric pressure chemical ionization mass spectrometry
ESI-MS	electron spray ionization mass spectrometry
Bn	benzyl
bs	broad singlet (in NMR)
bd	broad doublet (in NMR)
δ	chemical shift in ppm downfield from tetramethylsilane
DMF	<i>N,N</i> -dimethylformamide
DMSO	dimethyl sulfoxide
Et	ethyl
h	hour (s)
Hz	Hertz
<i>J</i>	coupling constant (Hz)
m	multiplet (in NMR)
M <sup>+</sup>	molecular ion
Me	methyl
mol equiv	molar equivalent (s)
mp	melting point
MS	mass spectrometry
DCM	dichloromethane
CTA	chromotropic acid

NMR	nuclear magnetic resonance
<i>p</i>	<i>para</i>
Ph	phenyl
PLC	preparative layer chromatography
ppm	parts per million
q	quartet (in NMR)
rt	room temperature
s	singlet (in NMR)
t	triplet (in NMR)
<i>tert</i>	tertiary
THF	tetrahydrofuran
TLC	thin-layer chromatography
TMS	tetramethylsilane (in NMR)
$K_{assoc}$	association or binding constant
H	host
G	guest
DNA	deoxyribonucleic acid
TBA	tetra- <i>n</i> -butylammonium
TBACl	tetra- <i>n</i> -butylammonium chloride
TBABr	tetra- <i>n</i> -butylammonium bromide
TBAI	tetra- <i>n</i> -butylammonium iodide
TBABF <sub>4</sub>	tetra- <i>n</i> -butylammonium tetrafluoroborate
CIS	chemically induced shift (in NMR)

## List of Appendices

- Appendix A.  $^1\text{H}$ ,  $^{13}\text{C}$  NMR and ESI-mass spectra for compounds described in Chapter 2...160
- Appendix B.  $^1\text{H}$ ,  $^{13}\text{C}$  NMR and ESI-mass spectra for compounds described in Chapter 3...202
- Appendix C. X-ray data reports for compounds in the order presented in Chapters 2-4.....223

# **Chapter 1**

## **Introduction**

# Chapter 1

## Introduction

### 1.1 Supramolecular Chemistry

Supramolecular chemistry is one of the most important and active areas of science, since it has many applications in biology, new materials, chemical technologies and medicine. In 1987, a definition of supramolecular chemistry was introduced for the first time by Jean-Marie Lehn as “the chemistry of molecular assemblies and of the intermolecular bond” or “the chemistry of noncovalent bonds”.<sup>1</sup>

Supramolecular chemistry is concerned with the assembly of two or more molecules via intermolecular interactions rather than covalent bonding, as a result of molecular recognition processes. These processes can be defined as specific interactions between two or more molecules, which are complementary in their geometric and electronic features through non-covalent interactions.<sup>2</sup> In biological systems there are different types of molecular recognition processes (e.g. DNA-protein, sugar-lectin, RNA-ribosome, etc.). Supramolecular chemistry can be divided into two main categories:

- (a) *Host-guest chemistry*, which describes complexes formed in solution, in the solid state, or in clathrates between two or more molecules or ions that are held together by non-covalent interactions (Figure 1a-b).
- (b) *Self-assembly*, defined as a process by which molecules can arrange themselves spontaneously only by intermolecular non-covalent interactions, leading to aggregations as shown in Figure 1c.

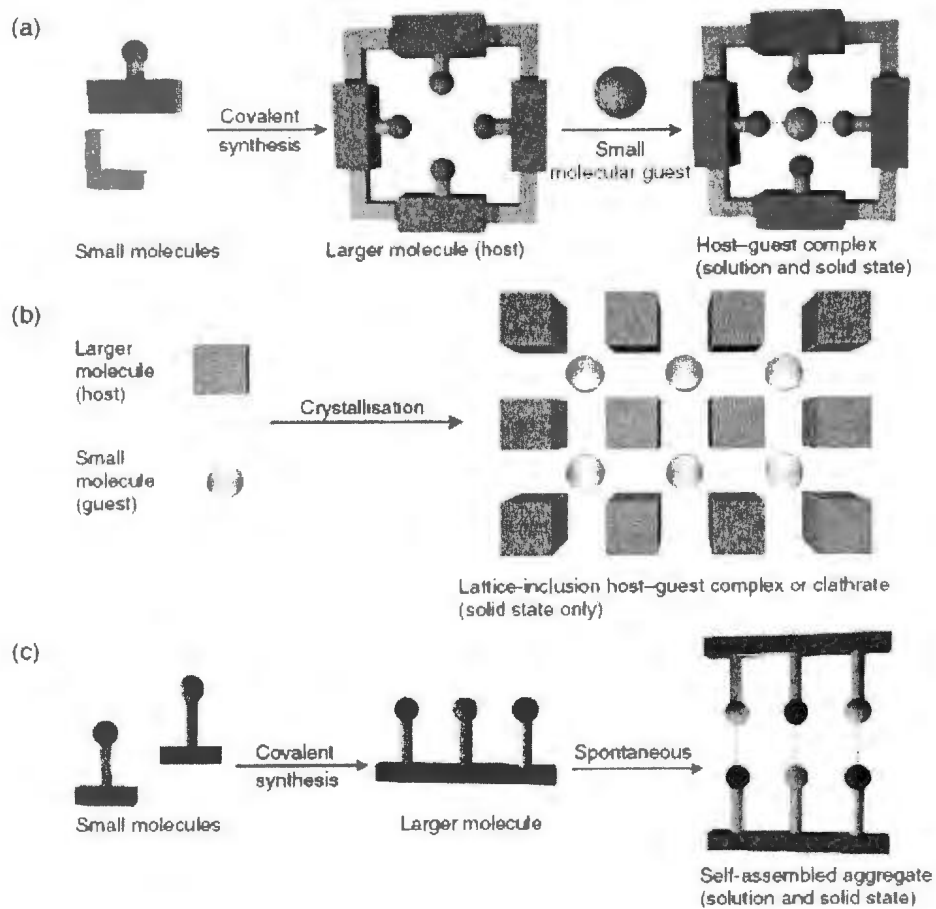


**Figure 1.1.** Categories of supramolecular chemistry: (a) host-guest complexation; (b) lattice inclusion; (c) self-assembly.<sup>1</sup>

### 1.1.1 Non-covalent interactions

Non-covalent interactions which are weaker than covalent bonds play an important role in holding supramolecular systems together.<sup>3</sup> There are different types of non-covalent interactions, such as hydrogen bonding,  $\pi$ - $\pi$  stacking, electrostatic interactions, Van der Waals interactions and the hydrophobic effect. Each type will be described briefly below.

### 1.1.1.1 Hydrogen bonding

Hydrogen bonding can be defined as “a special type of intermolecular attraction between the hydrogen atom in a polar bond (particularly H—F, H—O and H—N) and a non-bonding electron pair on a nearby small electronegative ion or atom usually F, O, or N (in another molecule)”<sup>4</sup> as illustrated in Figure 1.2a.

Figure 1.2b shows the different types of hydrogen bonding geometries: Type (1) shows a nearly linear geometry with a favoured hydrogen bond angle close to 180°. Type (2) shows the “accepting bifurcated” arrangement. Types (3) and (4) are called “donating bifurcated” and “three centers bifurcated” respectively.<sup>5</sup>

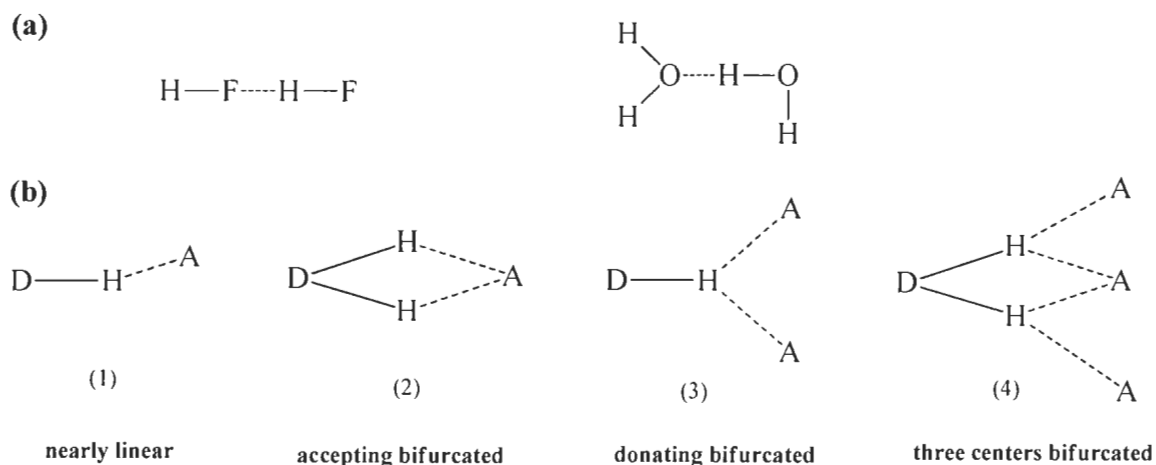


**Figure 1.2.** Types of different hydrogen bonding geometries, where (D) is a proton donor group; and (A) is a proton acceptor group.

Some molecular assemblies can contain different numbers of donor or acceptor sites, and the components are held together by arrays of double or triple hydrogen bonds which lead to an increase in the stability of the resulting structure (Figure 1.3). Jorgenson and

co-workers<sup>6</sup> showed that the stability of the assembly depends not only on the number of hydrogen bonds, but also on the arrangement of the donor and acceptor sites.

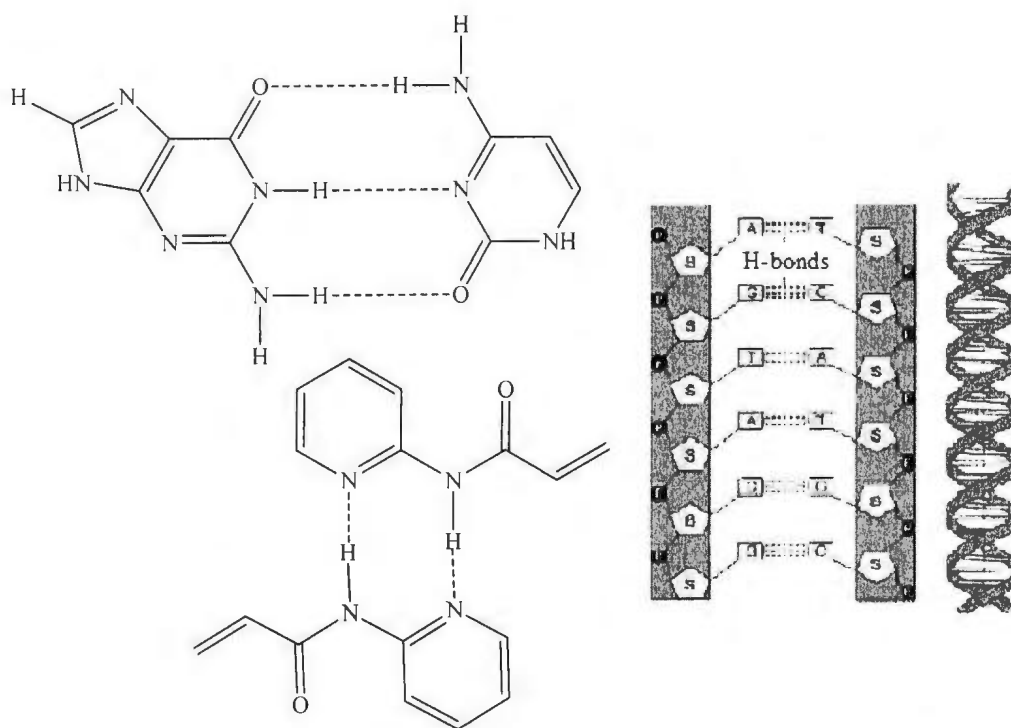


**Figure 1.3.** Multiple hydrogen bonding systems and hydrogen bonds in the DNA structure. [Adapted from <http://cnx.org/content/m12382/latest/dna.gif>]

### 1.1.1.2 $\pi$ - $\pi$ - interactions

These interactions can be considered to be a mixture of both electrostatic and dispersion interactions and generally involve aromatic rings which contain delocalized  $\pi$  electrons. The outer edge of the aromatic ring tends to be slightly electropositive due to the polarized C-H bond, and the  $\pi$  molecular orbitals tend to be slightly electronegative.<sup>7,8</sup>

There are three different types of  $\pi$ - $\pi$  stacking:

- a) *Offset face-to-face interactions*, in which the aromatic rings are parallel to each other and at the same time are offset from each other (Figure 1.4a).

- b) *Edge-to-face interactions or (T-stacking)*, in which the slightly positively-charged hydrogen atoms in one aromatic ring are attracted to the slightly negatively-charged  $\pi$  electrons of another ring. The two rings are perpendicular to each other (Figure 1.4b).
- c) *Face-to-face interactions*, in which the two aromatic rings planes are parallel but not offset from each other (Figure 1.4c).

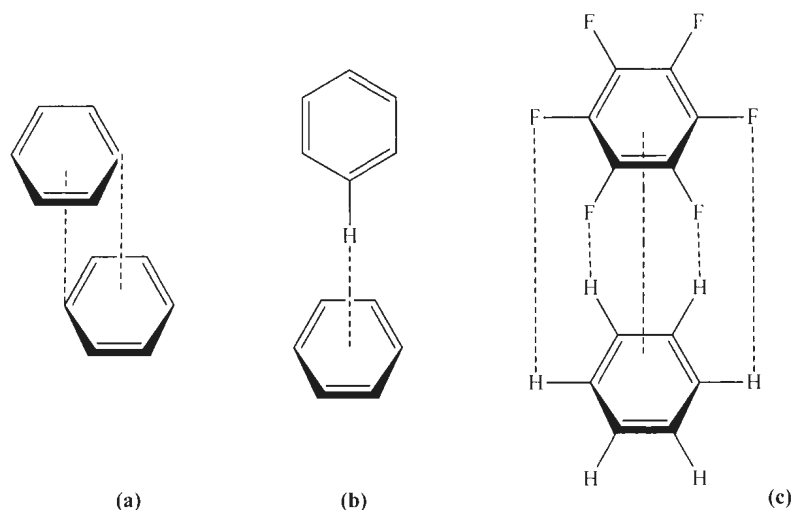


**Figure 1.4.** Different types of  $\pi$ - $\pi$  stacking. a) Offset, b) Edge-to-face, c) Face-to-face.

### 1.1.1.3 Electrostatic interactions

The interactions between two oppositely-charged molecules such as ion-ion, ion-dipole and dipole-dipole interactions are called *electrostatic interactions*. In contrast with ion-ion interactions, ion-dipole interactions should be arranged in a particular direction, where the partially-positive end of the dipole should be facing a negative ion and vice versa. Figure 1.5 shows different types of electrostatic interactions.<sup>9</sup>

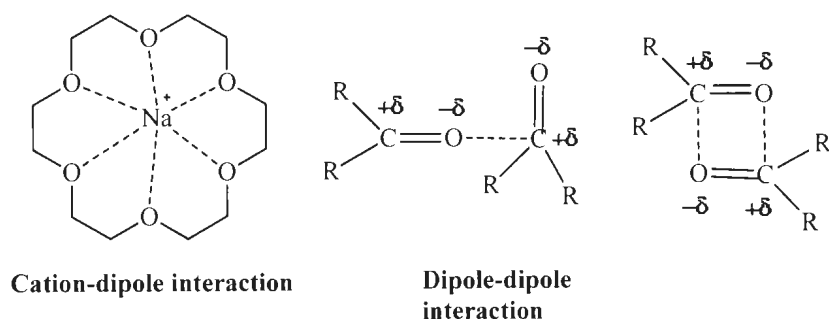


**Figure 1.5.** Types of electrostatic interactions.

#### 1.1.1.4 Van der Waals interactions

In 1873, it was discovered that gases show less pressure than would be normally expected. Upon investigation it was found that there are interactions between molecules that have induced dipole and instantaneous dipoles, which became known as Van der Waals forces.<sup>10</sup> Van der Waals forces have bond energies around 8 kJ/mol. These forces depend on the distances between the atoms or molecules. The forces could be increased in the case of an assembly of large numbers of molecules. These interactions arise not only from permanent charges but also from the polarization of the electron cloud of the molecules which are involved.<sup>11</sup> Van der Waals forces can be classified into different types:

- a) *Induced dipole interactions*, are weak forces in which ion or a dipole induces a dipole in an atom or a molecule with no dipole.
- b) *Instantaneous dipole-induced dipole interactions*, sometimes called London forces or dispersion forces, in which the electron density of the molecule is not symmetric at a given instant of time, so this makes the molecule partially polarized.

- c) *Permanent dipole-induced dipole interactions*, in which the electrons are situated closer to one side of the molecule more than another at any particular moment of time.

### 1.1.1.5 Hydrophobic effect

The hydrophobic effect can be defined as an aggregation of non-polar substances in aqueous solution to exclude water molecules (Figure 1.6). It can be considered as a driving force for different phenomena, such as protein folding and the poor solubility of non-polar solutes in aqueous solution.

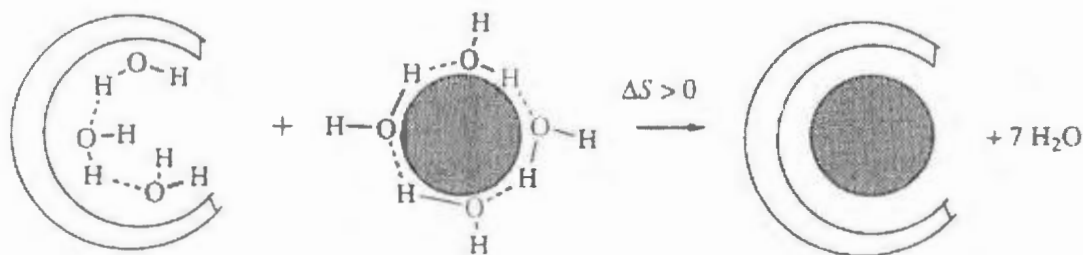


**Figure 1.6.** Hydrophobic effect in host-guest chemistry. [Adapted from <http://online-media.uni-marburg.de/chemie/bioorganic/vorlesung1/grafik/k1e008.jpg>]

The Frank-Evans hypothesis concerns the reduction in the number of water molecules needed to solvate the solute by reducing the surface area of the non-polar solute, sometimes called the “iceberg” model. On the other hand, the hydrophobic effect is very important in host-guest complexation phenomena in which cyclophane and cyclodextrin hosts bind guests.<sup>12</sup>

## 1.2 Macrocyclic amide receptors

The design of effective anion receptors has been of interest to many scientists in the field of supramolecular chemistry, since anions play an important role not only in

industry but also in health and the environment. Anion receptors have medical applications since they can be used for transferring chloride anions through cell membranes.<sup>13</sup>

Pascal *et al.*<sup>14</sup> reported the synthesis of the first anion receptors containing secondary amide groups. Subsequently, Sessler and co-workers<sup>15</sup> synthesized the new acyclic amide-containing anion receptors, **1-4** (Figure 1.7).

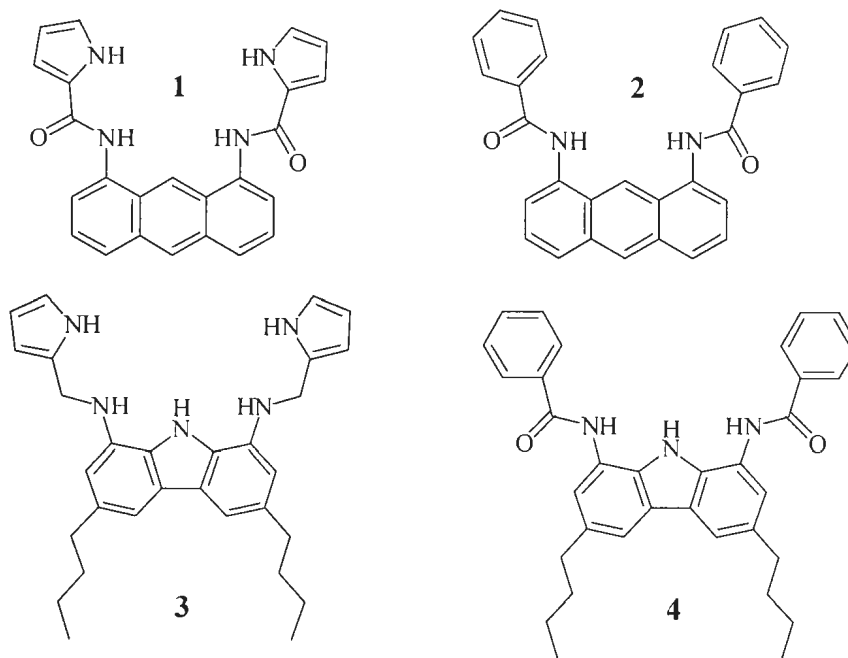


**Figure 1.7.** The acyclic amide receptors **1-4**.

Szumna and Jurczak<sup>16</sup> reported the synthesis of macrocyclic tetraamide **5** and the open-chain analogue **6** (Figure 1.8). The <sup>1</sup>H-NMR complexation study showed that macrocycle tetraamide **5** had high binding affinity with acetate and fluoride anions *via* hydrogen bonding in a 1:1 host-guest ratio.

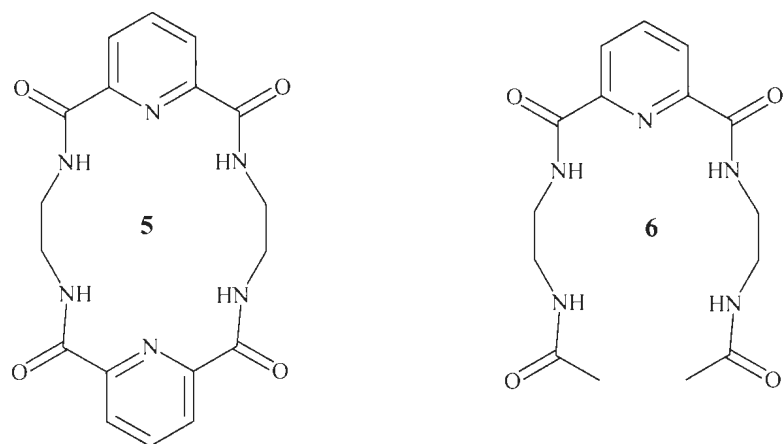


**Figure 1.8.** Macrocyclic tetramide **5** (left) and its open-chain analogue **6** (right).

Bowman-James and co-workers<sup>17</sup> described a rigid macrocyclic tetraamide **7** which contains two tertiary amine groups (Figure 1.9). This compound showed a 1:1 binding ratio with both  $\text{HSO}_4^-$  and  $\text{H}_2\text{PO}_4^-$  anions.

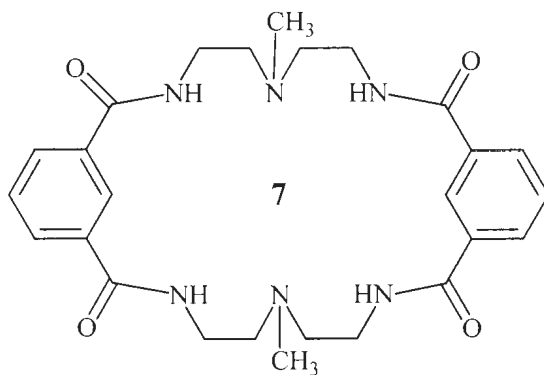


**Figure 1.9.** Bowman-James macrocyclic tetraamide, **7**.

Macrocyclic calix[4]arene-based tetraamides **8** and **9** (Figure 1.10) have also been synthesized by Ungaro and co-workers,<sup>18</sup> and showed high selectivity to bind with benzoate anion *via*  $\pi$ - $\pi$  stacking and H-bonding. Beer *et al.*<sup>19</sup> developed the bis-calix[4]arene macrocyclic diamide **10** (Figure 1.10), which binds  $\text{F}^-$  anion with a binding constant of  $1330 \text{ M}^{-1}$ .

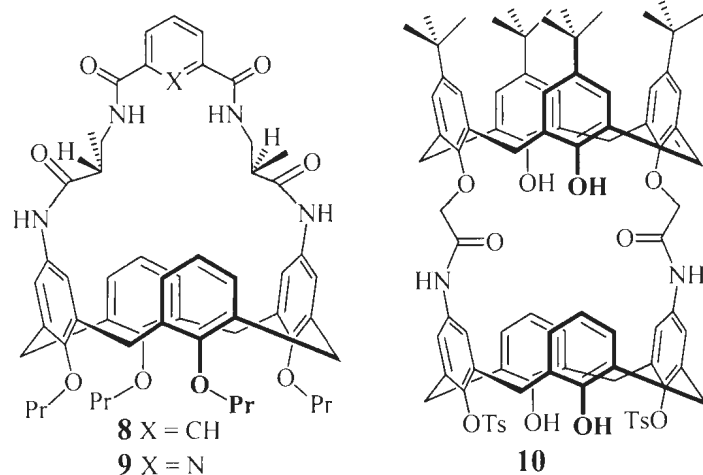
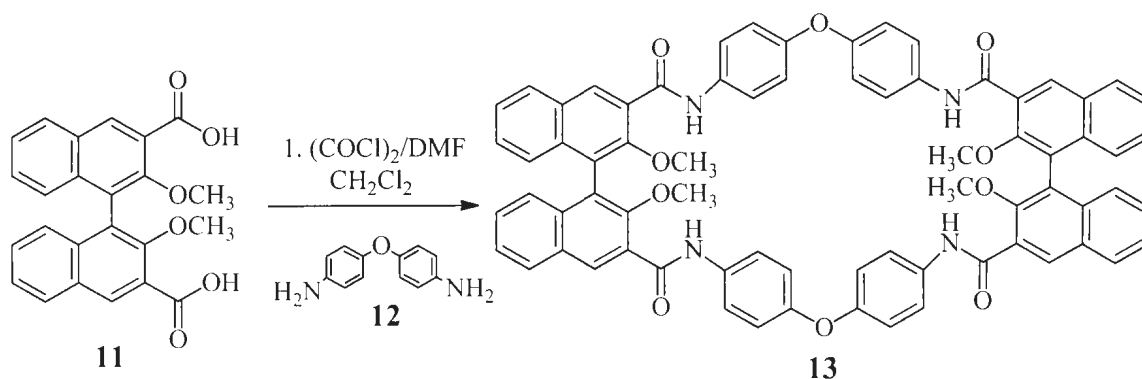


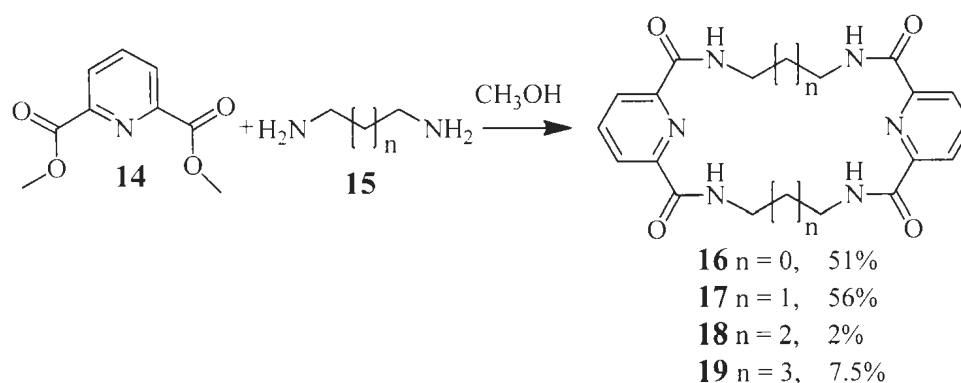
**Figure 1.10.** Chiral calix[4]arenes **8** and **9** (left) and a biscalix[4]arene **10** (right).

In 2012, Pasini and co-workers<sup>20</sup> reported the synthesis of the binaphthyl-based macrocyclic amide **13** by reacting **11** with oxalyl chloride followed by condensation with diamine **12** in the presence of triethylamine and  $\text{CH}_2\text{Cl}_2$  under high dilution conditions, as shown in Scheme 1.1. A  $^1\text{H-NMR}$  titration study of macrocycle **13** conducted with tetrabutylammonium halide salts, showed a downfield chemical shift of the amide proton signal, indicating that the binding with the halides occur *via* H-bonding.



**Scheme 1.1.** Synthesis of macrocyclic amide **13**.

Jurczak and co-workers<sup>21</sup> reported the synthesis and complexation properties of other macrocyclic tetraamides, **16-19** (Scheme 1.2), by condensation between diester **14** with diamines **15** ( $n = 0-3$ ) using methanol as a solvent. Their complexation study showed that the 20-membered macrocycle **17** has a higher affinity for complexing anions, as compared with the other macrocycles. An X-ray structure of the **17**:( $n$ -Pr)<sub>4</sub>NCl complex was also obtained showing the chloride ion complexed *via* H-bonding (Figure 1.11).



**Scheme 1.2.** Synthesis of macrocyclic tetraamides **16-19**.

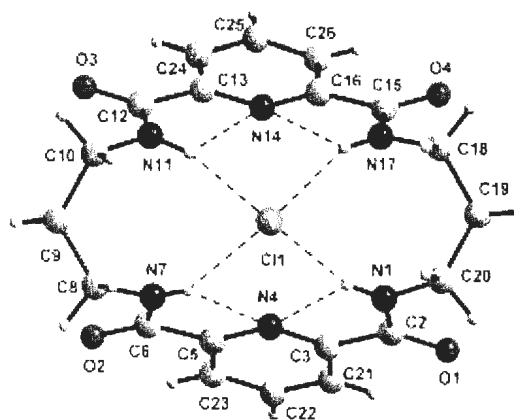
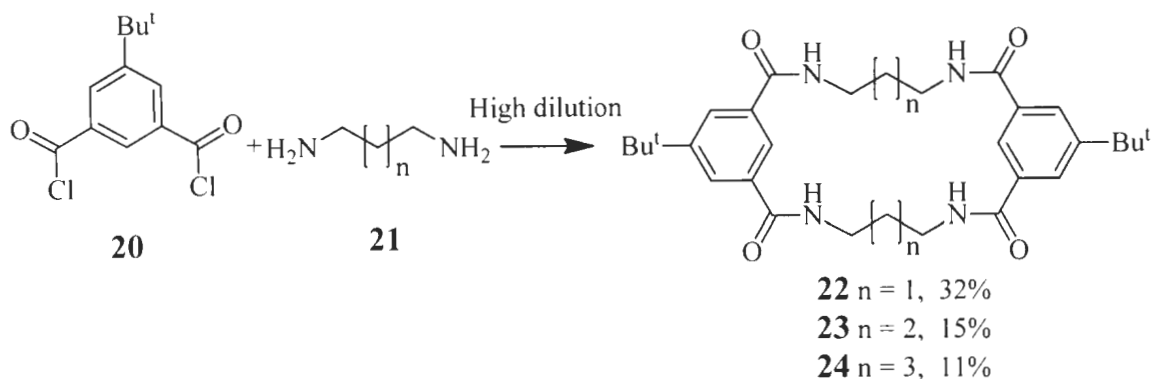


**Figure 1.11.** X-ray structure of **17** showing the encapsulated chloride anion. [Adapted with permission from reference 21]

The same authors also synthesized macrocyclic tetraamides **22-24**, by reacting 5-*tert*-butyl-isophthaloyl chloride **20** with the diamines **21** at high dilution conditions, as shown in Scheme 1.3.



**Scheme 1.3.** Synthesis of macrocyclic tetraamides **22-24**.

Consistent with the previous study, the complexation study on macrocyclic amides **22-24** also showed the higher affinity of the 20-membered macrocycle **23** to complex with anions in preference to the other macrocycles.

Jurczak and co-workers<sup>22</sup> also described complexation studies with  $\text{Ca}^{2+}$  ions in  $\text{CD}_3\text{CN}$  of macrocyclic diamide compounds **25-29**, (Figure 1.12). The stoichiometry of these complexes were found to have a 2:1 host:guest stoichiometry, except for macrocycle **25** which complexed with 1:1 stoichiometry.

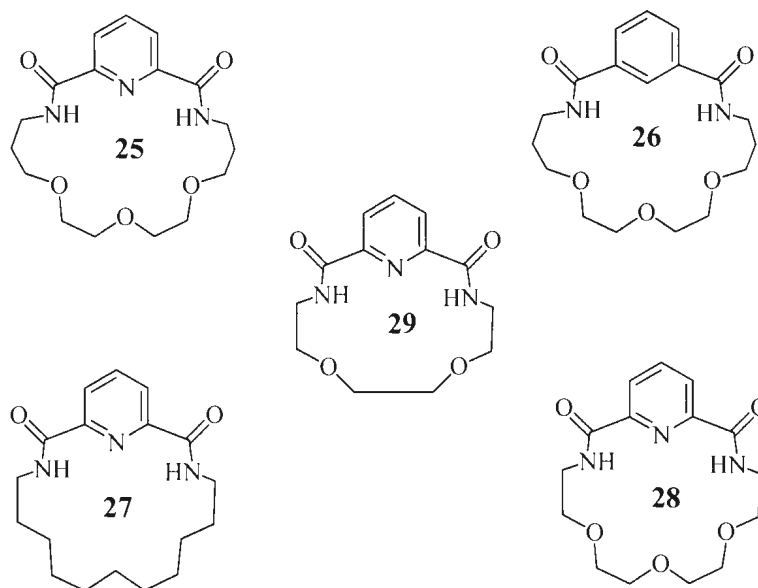


**Figure 1.12.** Structures of different macrocyclic bisamide compounds **25-29**.

An X-ray structure reported by these authors shows that the **25**:Ca<sup>2+</sup> complex crystallized in two different conformations, as illustrated in Figure 1.13.

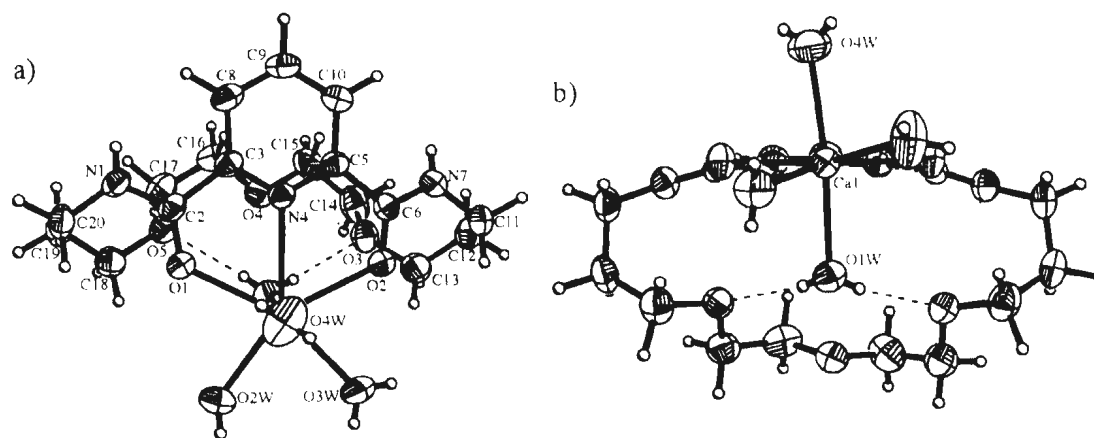


**Figure 1.13.** Calcium complex of macrocycle **25**. A view (a) perpendicular and (b) parallel to the mean plane passing through the pyridine ring. [Adapted with permission from reference 22]

Bowman-James and co-workers<sup>23</sup> synthesized the tricyclic amide **30**, (Figure 1.14), by using selective protection and deprotection techniques. The <sup>1</sup>H NMR titration studies

of **30** with various tetrabutylammonium halide salts in DMSO- $d_6$  revealed that **30** forms stable complexes with hydrogen bifluoride ( $\text{FHF}^-$ ) and azide ( $\text{N}_3^-$ ) linear anions selectively over the spherical  $\text{Cl}^-$ ,  $\text{Br}^-$  or  $\text{I}^-$  anions.

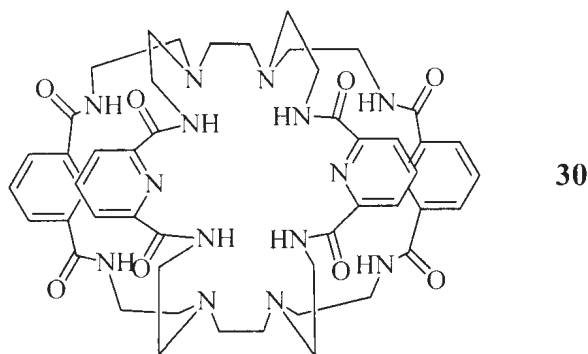


**Figure 1.14.** The structure of tricyclic amide receptor **30**.

### 1.3 Heteroditopic receptors

Ion-pair recognition is considered to be a very important area in supramolecular chemistry, where there are many potential applications, including sensors, membrane transport and salt solubilization agents. Ditopic receptors include two binding sites in the same molecular receptor for both cation and anion. Ion-pair receptors can have three different design forms:<sup>24</sup>

- a) A *cascade complex*, in which the anionic guest bridges two encapsulated cations (Figure 1.15a).
- b) A *heteroditopic receptor*, in which the anion and cation are bound as separated ions (Figure 1.15b).
- c) A *contact ion-pair*, in which both cation and anion are bound in close proximity to each other (Figure 1.15c).

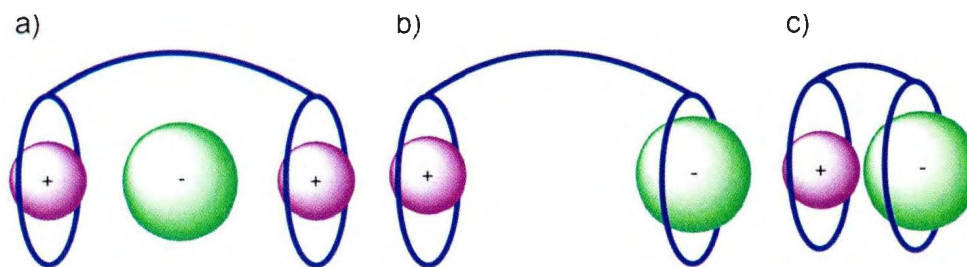


**Figure 1.15.** Common designs of ditopic receptors: a) Cascade complex; b) Heteroditopic receptor; c) Contact ion pairs. [Adapted with permission from reference 24]

### 1.3.1 Heteroditopic receptors for separated ion pairs

Some of the ion-pair receptors are designed to bind ions as separated ion-pairs due to both solvent and conformation effects, where the cation and anion binding sites are relatively distant from one another. Scheerder *et al.*<sup>25</sup> showed the calix[4]arene-based receptor (Figure 1.16) has ability to solubilize sodium chloride in  $\text{CDCl}_3$  through cation-dipole interactions between the  $\text{Na}^+$  ions and the oxygen atoms of the side-chain ester groups, and through hydrogen bonding between the  $\text{Cl}^-$  anions and the hydrogen atoms of the side-chain urea groups, as shown in Figure 1.16.

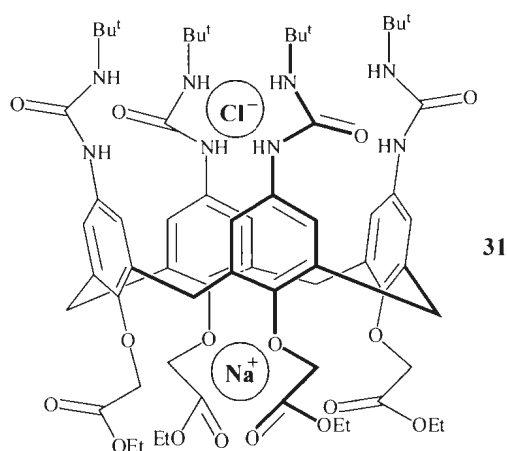


**Figure 1.16.** Solubilization of sodium chloride ion-pairs in the calix[4]arene-based receptor **31**.

In contrast, cesium salts did not bind to the calix[4]arene-based receptor **31** since the cesium atom is too large to fit in the cavity. Cesium however could bind with other receptors which have larger cavities, as shown by Sessler *et al.*<sup>26</sup>

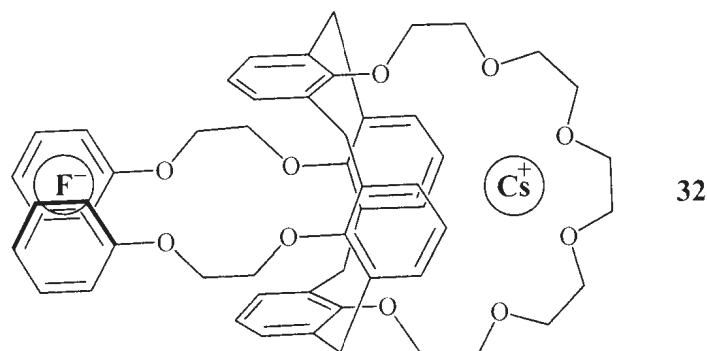


**Figure 1.17.** Receptor **32** for CsF ion-pairs as reported by Sessler *et al.*

Calix[4]arene **32** (Figure 1.17) can bind CsF, where the Cs<sup>+</sup> cation fits within the crown ether cavity while the F<sup>-</sup> anion fits between the two aromatic rings, as shown in Figure 1.17. Evans and Beer<sup>27</sup> reported anti-cooperative binding between the calix[4]arene-based receptor **33** (Figure 1.18) and two equivalents of NaCl, where the two Na<sup>+</sup> ions fit within the crown ether cavities, and the Cl<sup>-</sup> ions are not complexed to the amide protons. The electrostatic repulsion forces between the two complexed sodium cations prevent the conformational changes needed for anion binding (Figure 1.18).

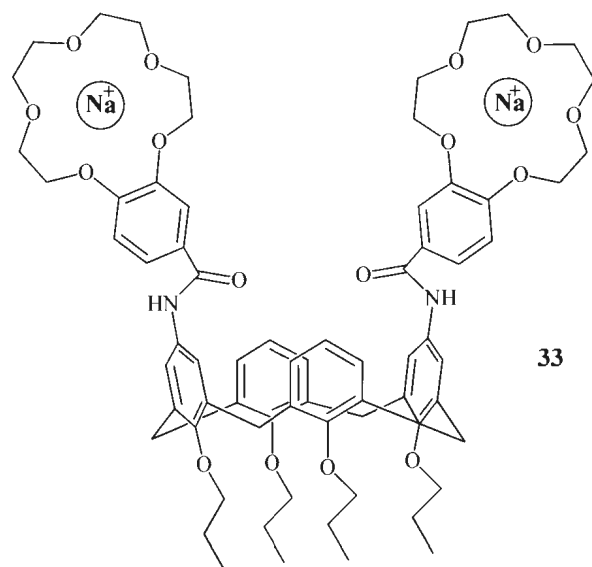


**Figure 1.18.** Anti-cooperative binding in the presence of two equivalents of sodium.

Furthermore, Smith and co-workers<sup>28</sup> described the synthesis of macrocycle **34** and they have shown that it can extract LiCl and LiBr from the solid state as water-separated ion-pairs, where the Li<sup>+</sup> binds within the crown ether cavity and the anions (Cl<sup>-</sup> and Br<sup>-</sup>) bind *via* hydrogen bonding with the amide NH protons as shown in Figure 1.19. X-ray structures of these complexes were also obtained.

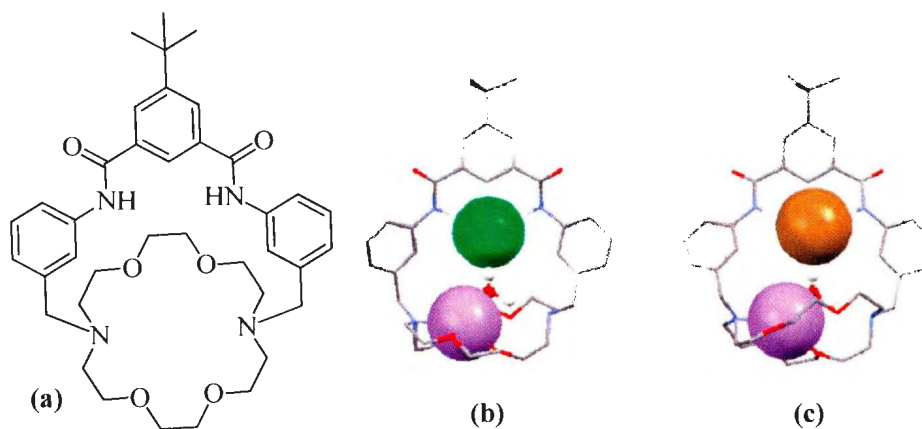


**Figure 1.19.** (a) Macrocycle **34** (b) X-ray structure of complex **34**:LiCl·H<sub>2</sub>O and (c) X-ray structure of complex **34**:LiBr·H<sub>2</sub>O. [X-ray structures adapted with permission from reference 28]

### 1.3.2 Heteroditopic receptors for contact ion-pairs

Binding of a guest as a contact ion-pair to a receptor is energetically favored, since it can overcome the energy required to break the Coulombic forces between the two ions. Suksai *et al.*<sup>29</sup> reported the synthesis and complexation behavior of the ferrocene receptor **35**, which binds NaBr more strongly than other sodium and potassium halides as contact ion-pairs in CD<sub>3</sub>CN/CDCl<sub>3</sub> 95:5 (Figure 1.20).

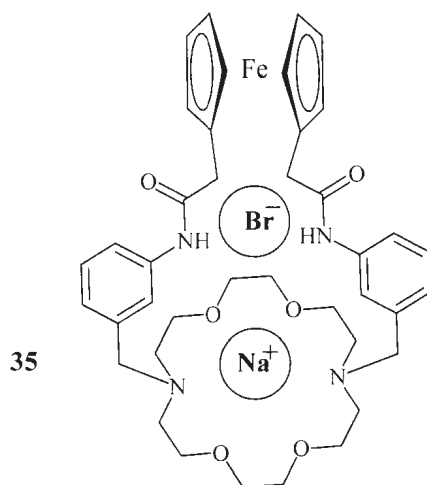


**Figure 1.20.** Ferrocene receptor **35** binds NaBr as reported by Suksai *et al.*

An interesting example of a contact ion-pair is that shown in compound **36**. The uranyl salophen:CsCl complex has a Cl<sup>-</sup> bound to the positively-charged uranyl center, and the Cs<sup>+</sup> binds *via* electrostatic interaction with the Cl<sup>-</sup> as well as by cation- $\pi$  interactions with the aromatic rings, as illustrated in Figure 1.21.<sup>30</sup>

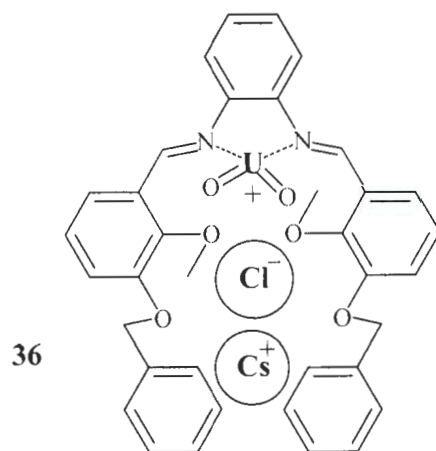


**Figure 1.21.** Uranyl salophen receptor **36** binds CsCl as a contact ion-pair.

Gale and co-workers<sup>31</sup> prepared the macrobicyclic receptor **37** which contains a bridging 2,5-diamidopyrrole group; also they reported the complexation of receptor **37** with NaCl as shown in the X-ray structure (Figure 1.22), where the Cl<sup>-</sup> binds *via* hydrogen bonding with both amide protons and the pyrrole NH proton as shown in Figure 1.22.

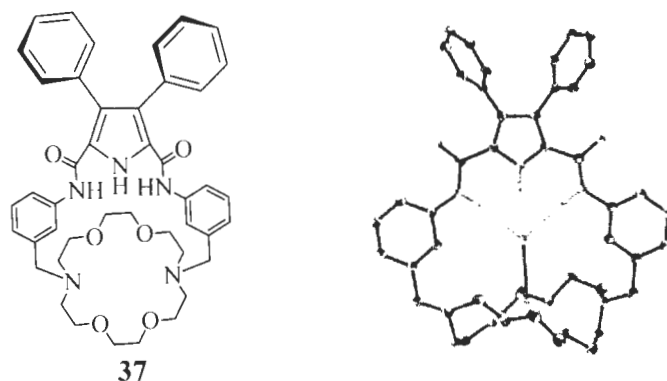


**Figure 1.22.** Chemical structure of receptor **37** and X-ray structure of (**37**:NaCl). [X-ray structure adapted with permission from reference 31]

Beer and co-workers<sup>32</sup> synthesized the calix[4]diquinone receptor **43** through the synthetic procedure shown in Scheme 1.4.



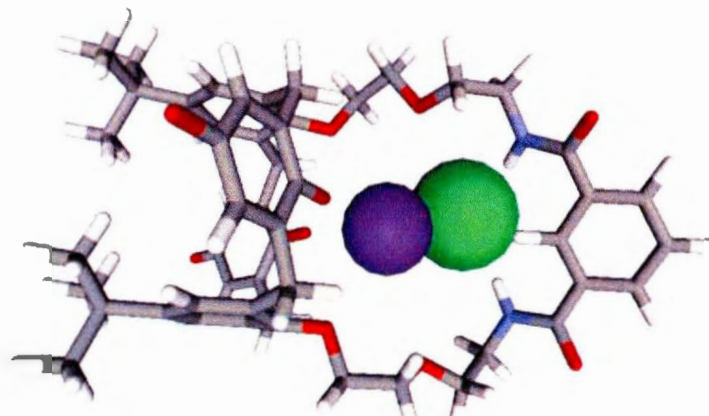


**Figure 1.23.** Optimised CAChe model of **43**:KCl complex; K = purple and Cl = green.  
[Adapted with permission from reference 32]

In 2002, Atwood *et al.*<sup>33,34</sup> reported different types of resorcin[4]arene based-receptors **44a-e** (Figure 1.24) which have both hydrophobic cavities and four amide groups on the upper rim capable of forming H-bonding.

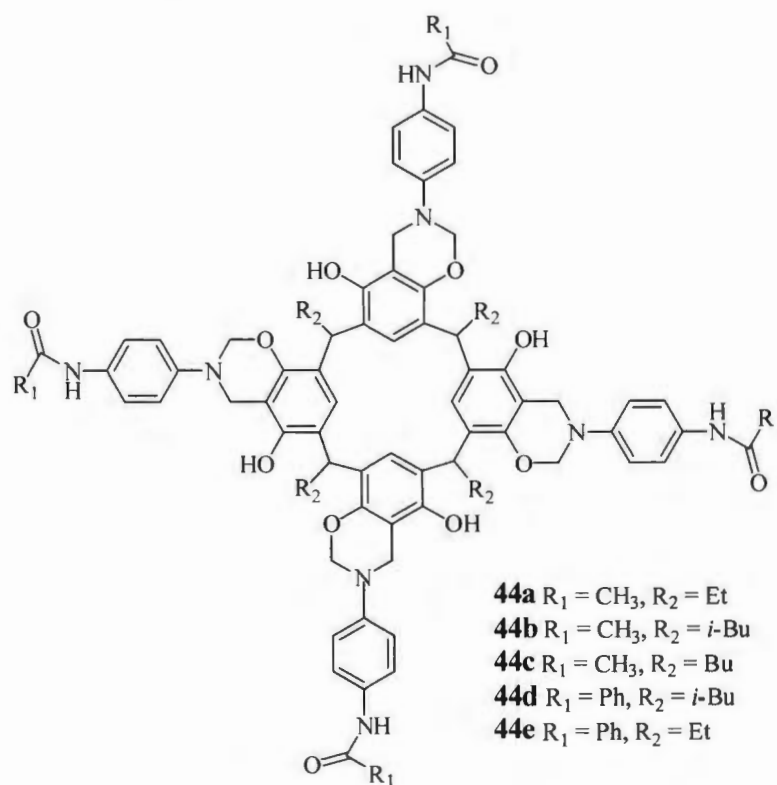


**Figure 1.24.** Chemical structures of resorcin[4]arene-based receptors **44a-e**.

Complexation studies for receptors **44a-e** have been conducted with excess amounts of TMACl (tetramethylammonium chloride) using  $^1\text{H}$  NMR spectroscopy in  $\text{CDCl}_3$ , resulting in the conclusion that the chloride anion is hydrogen bonded to the amide NH protons in agreement with the findings of others, while the  $\text{TMA}^+$  cation is encapsulated in the cavity. Figure 1.25 shows the X-ray structure of complex **44a**:TMACl, where the receptor forms a simultaneous complex with both the anion and cation as a contact ion-pair.

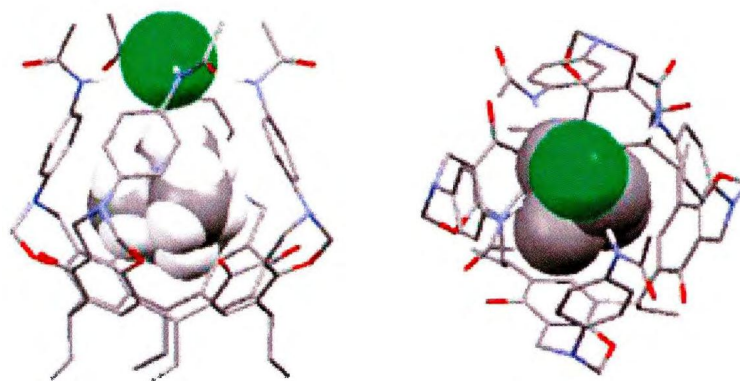


**Figure 1.25.** Two different views of the X-ray structure of **44a**:TMACl. [Adapted with permission from reference 34]

#### 1.4 Characterization of host-guest complexation

There are different analytical techniques that can be used to determine host-guest complexation, such as mass spectrometry (MS), nuclear magnetic resonance (NMR) spectroscopy, fluorescence spectroscopy, UV-visible spectroscopy (UV-vis) and single-crystal X-ray diffraction. The most used techniques are NMR and UV-vis spectroscopies because they have the advantage of being able to characterize the complexation by detecting the spectroscopic feature changes of either the guest and/or the host. As well, these techniques can provide information about the binding constant, the stoichiometry of the host-guest complexation and the host-guest binding location.

#### 1.4.1 Mass spectrometry

Mass spectrometry can be used as a quantitative technique to provide information about the mass of a host-guest complex, whose components are held together by weak intermolecular forces. Soft ionization methods are needed in these cases and the methods used include electrospray ionization (ESI) and matrix-assisted laser desorption ionization (MALDI).<sup>35</sup>

#### 1.4.2 Nuclear magnetic resonance (NMR) spectroscopy

NMR spectroscopy is one of the most useful and applicable techniques which can be used for detecting and measuring the extent of host-guest complexation. It is used to detect chemical shift changes ( $\Delta\delta$  ppm) which arise due to the changes of the environments of the respective protons which either shield or deshield the host and/or guest.<sup>36</sup> Thus, useful information about the location of the interaction between the host and guest, as well the values of the observed chemical shift changes ( $\delta$  ppm) can be used to determine the binding constants between host and guest. The variation of the chemical shift changes of the host and guest protons depend on how fast the exchange occurs between the host and guest with respect to the NMR time-scale ( $\delta\nu$ ), which is defined as the difference in frequency (Hz) between the exchanging sites. The NMR time-scale depends on the spectrometer frequency and the nucleus considered ( $^1\text{H}$ ,  $^{13}\text{C}$ , etc.). There are two different cases for system exchange.<sup>37</sup>

- a) *Slow exchange system*, in which the nucleus' exchange rate between the two states (guest/host-guest) is slower than the NMR time-scale.

- b) *Fast exchange system*, where the nucleus' exchange rate between the two states is faster than the NMR time-scale.

If a guest proton shows fast exchange behavior, both free and bound proton resonances appear as one signal, which represents the average of the free and bound proton resonances. If, on the other hand, the host-guest exchange takes place on the same time-scale of the NMR, the signals that representing the free and bound nuclei will be broad.<sup>38</sup>

A good example of this process is the  $^1\text{H}$  NMR study of cyclohexane- $d_{11}$  at different temperatures. Cyclohexane- $d_{11}$  contains a single proton which can exist in a distinct axial and equatorial position. At room temperature only one sharp signal is observed. This is because the proton has the same chemical shift average since the molecule is in rapid equilibrium between its two chair conformers (Figure 1.26). Since the rate of this process is greater than the chemical shift difference between the position for the axial and equatorial proton, the  $^1\text{H}$  NMR cannot distinguish these and only one signal is observed (this is an example of fast exchange) as shown in Figure 1.26. At lower temperatures however, the rate of the process can be reduced and can become smaller than the chemical shift difference between the two conformers. In this case,  $^1\text{H}$  NMR can distinguish the two conformers' protons and two signals are observed (this is an example of a slow exchange) as illustrated in Figure 1.26.<sup>39,40</sup>

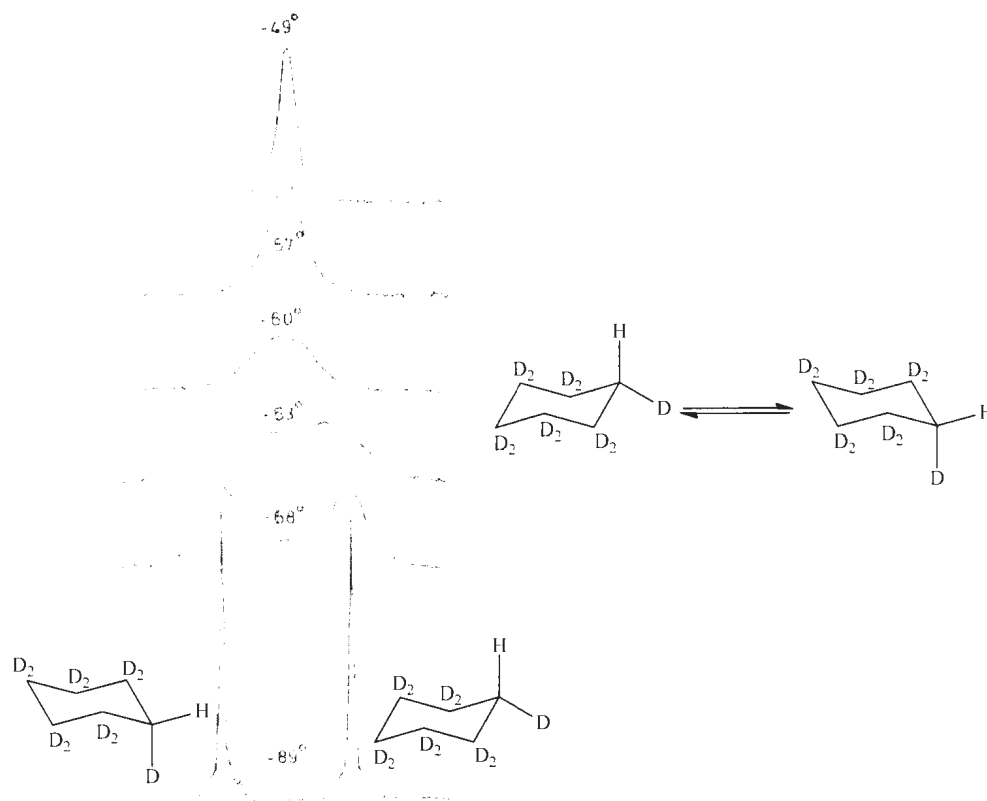


**Figure 1.26.** The  $^1\text{H}$  NMR spectra of cyclohexane- $d_{11}$  as a function of temperature. [This figure has been adapted with permission from reference 40]

Figure 1.26 shows that by gradually decreasing the temperature from  $-49\text{ }^\circ\text{C}$  to  $-60\text{ }^\circ\text{C}$  the conversion rate of the process decreases and consequently the  $^1\text{H}$  NMR spectra can distinguish the two different protons. The signal gradually becomes broadened until, at  $-63\text{ }^\circ\text{C}$  it starts to split into two different signals, until it finally splits completely into two sharp signals at  $-89\text{ }^\circ\text{C}$ .

$^1\text{H}$  NMR when compared with  $^{13}\text{C}$  and  $^{31}\text{P}$  NMR is the more useful technique for studying host-guest complexation since protons are closer to the exterior of the molecule and consequently are more exposed to the other guest molecules or ionic species. Also,  $^{13}\text{C}$  NMR chemical shifts are less responsive to intermolecular interactions and longer

acquisition times are needed because the sensitivity of the  $^{13}\text{C}$  nucleus is relatively poor (natural abundance only 1.1%).<sup>41</sup>

### 1.4.3 UV-visible spectroscopy

The sensitivity of UV-vis spectroscopy is greater than that of NMR for the detection of host-guest complexation, since small concentrations of the host ( $10^{-4}$  to  $10^{-5}$  M) can be used. Even though UV-vis can be used for determining the binding constants, the method has the disadvantage in that it does not provide information about the binding location as relatively unambiguously as does NMR spectroscopy.<sup>36</sup>

### 1.4.4 Single-crystal X-ray diffraction

Single-crystal X-ray diffraction can be used for determining the solid-state structure of host-guest complexes, provided suitable crystals are obtained. In addition, X-ray crystallography can provide valuable information about how molecules are positioned with respect to one another; as well it can give information about individual bond angles and bond lengths within the complex in the solid state.<sup>36</sup>

### 1.4.5 Determination of the association constant ( $K_{assoc}$ )

The most common methods used for quantitative measurements of the relative strengths of complexation in host-guest solution chemistry are spectrophotometry, potentiometry and NMR spectroscopy. Generally, the stronger the host-guest interactions in solution, the larger the association (or binding or stability constants)<sup>42</sup> which are given as  $K_{assoc}$  values. In 1928, Job<sup>43</sup> reported a method for determining the stoichiometry of host-guest binding. In this method, the mole fraction of the guest can be plotted against the observed UV-vis absorbance changes at a specific wavelength, or using the NMR

observed chemical shift changes of the guest or host protons ( $\Delta\delta$ ). The stoichiometry of binding can be determined from the shape of the resulting titration curves.

To calculate the  $K_{assoc}$  the concentrations of the free host, free guest and host-guest complex should be taken into account. In case of 1:1 binding the equilibrium can be represented as follows:



Where, H and G are the free host and guest respectively, and H•G is the host-guest complex. The  $K_{assoc}$  of this system can be calculated by the following equation:

$$K_{assoc} = [H \cdot G] / ([H] \cdot [G])$$

Where, [H] and [G] are the concentration of the host and guest respectively, and [H•G] is the concentration of the host-guest complex at equilibrium. If one more host is able to bind to the guest, in this case the equilibrium can be represented as follow:



And the  $K_{assoc}$  of this system can be calculated using this equation:

$$K_{assoc} = [H_2 \cdot G] / ([H] [H \cdot G])$$

Using  $^1\text{H-NMR}$  titration the association constant can be calculated by plotting the concentration of the guest ([G]) or host ([H]) against the changes in the chemical shifts ( $\Delta\delta$  Hz) and using a non-linear curve 1:1 binding constant isotherm according to Connors.<sup>42</sup> In the Benesi-Hildebrand treatment ( $1 / [G]$ ) or ( $1 / [H]$ ) is plotted vs ( $1 / \Delta\delta$ )

which should give a straight line. The  $K_{assoc}$  of this system can be calculated by the following equation.<sup>44</sup>

$$K_{assoc} = \text{Slope} / \text{intercept}$$

## 1.5 Objectives and results

The research that was pursued in this thesis and will be described in the following Chapters, involved a number of parallel studies. These were focused on the synthesis of macrocyclic amides and sulfonamides compounds and studying their complexation behavior using different types of guest species. The families of guests which were studied in this work included Group 1 and 2 metal salts, and tetra-*n*-butylammonium (“tetrabutylammonium” or “TBA”) halides.

Chapter 1 describes the background and principles of supramolecular chemistry and as it pertains to the host-guest chemistry which formed the basis of the research conducted by the author and more fully described in this Thesis.

In Chapter 2, the syntheses of new macrocyclic amides derived from different diacyl dichlorides with both 1,8-diamino-3,6-dioxaoctane or with 1,10-diamino-4,7-dioxadecane<sup>45</sup> at low temperatures under high dilution conditions are described. The structures of these macrocycles were determined by <sup>1</sup>H NMR, <sup>13</sup>C NMR, mass spectrometry and single-crystal X-ray analysis. Also described in this Chapter is a complexation study of these macrocyclic amides with selected Group 1 and 2 metal salts and tetrabutylammonium halides (TBAX, X=Cl, Br or I) using <sup>1</sup>H NMR chemical shift changes. The binding or association constants ( $K_{assoc}$ ) were calculated using isothermal non-linear 1:1 binding curve fitting plots according to Connors using the ORIGINPro 7.5 program from OriginLab Corporation.<sup>46</sup>

In Chapter 3, the synthesis of bis- and the tetrakis-macrocyclic sulfonamides derived from chromotropic acid (CTA) with both “Jeffamine<sup>®</sup> EDR-148” (1,8-diamino-3,6-dioxaoctane) and “Jeffamine<sup>®</sup> EDR-176” (1,10-diamino-4,7-dioxadecane) at low temperatures and under high dilution conditions is described. The structures of these macrocycles were also determined by <sup>1</sup>H NMR, <sup>13</sup>C NMR, mass spectrometry and single-crystal X-ray analysis. A complexation study of these new macrocyclic sulfonamides with selected Group 1 and 2 metal salts and tetrabutylammonium halides (TBAX, X = Cl, Br or I) using <sup>1</sup>H NMR chemical shift changes. The resulting binding or association constants ( $K_{assoc}$ ) were calculated as described in Chapter 2, using similar isothermal non-linear 1:1 binding curve fitting plots and using the ORIGINPro 7.5 program from OriginLab Corporation.

In Chapter 4, the titration properties of the tetrabutylammonium halides (TBAX, X = Cl, Br or I) themselves with CDCl<sub>3</sub> using <sup>1</sup>H NMR chemical shift changes are described. From the resulting titration curves a linear concentration-dependent relationship could be observed.

## 1.6 References

1. (a) Lehn, J. *Supramolecular Chemistry*, Wiley VCH: Weinheim, Germany, 1995.
2. Atwood, J. L.; Davies, J. E. D.; MacNicol, D. D.; Vögtle, F.; Lehn, J.-M.  
*Comprehensive Supramolecular Chemistry*, Oxford, U. K., 1996.
3. Beer, P.; Gale, P.; Smith, D. *Supramolecular Chemistry*, Oxford University Press:  
Oxford, 2003.
4. Brown, T. L.; LeMary, H. E.; Brusten, B. E.; Murphy, C. J.; Woodward, P. M.  
*Chemistry The Central Science*, 12<sup>th</sup> Ed. Glenview, IL: Pearson Prentice Hall.
5. Steed, J. W.; Atwood, J. L. *Supramolecular Chemistry*, Wiley-VCH: Weinheim,  
Germany, 2009.
6. (a) Pranata, J.; Wierschke, S. G.; Jorgenson, W. L. *J. Am. Chem. Soc.* **1991**, *113*, 2810-  
2819. (b) Jorgenson, W. L.; Pranata, J. *J. Am. Chem. Soc.* **1990**, *112*, 2008-2010.
7. Dance, I.  $\pi$ - $\pi$  Interactions: Theory and Scope, In *Encyclopedia of Supramolecular  
Chemistry*, Atwood and Steed (eds.), Marcel Dekker, Inc.: New York, 2004.
8. Hunter, C. A. *Chem. Soc. Rev.* **1994**, *23*, 101-109.
9. Steed, J. W.; Turner, D. R.; Wallace, K. J. *Core Concepts in Supramolecular  
Chemistry*, John Wiley & Sons, Ltd.: Chichester, 2007.
10. Schneider, H. J. *Van der Waals Forces*, In *Encyclopedia of Supramolecular  
Chemistry*, Marcel Dekker, Inc.: New York, 2004.
11. Parsegian, V. A. *Van der Waals Forces: A Handbook for Biologists, Chemists,  
Engineers, and Physicists*, Cambridge University Press, 2006.
12. Southall, N. T.; Dill, K. A.; Haymet, A. D. J. *J. Phys. Chem.* **2002**, *106*, 521-533.
13. Gale, P. A. *Acc. Chem. Res.* **2011**, *44*, 216-226.

14. Pascal, R. A.; Spergel, J.; van Engen, D. *Tetrahedron Lett.* **1986**, *27*, 4099-4108.
15. Gross, D. E.; Mikkilineni, A. V.; Lynch, V. M.; Sessler, J. L. *Supramol. Chem.* **2010**, *22*, 135-141.
16. Szumna, A.; Jurczak, J. *Eur. J. Org. Chem.* **2001**, 4031-4039.
17. Hossain, M. A.; Llinares, J. M.; Powell, A. D.; Bowman-James, K. *Inorg. Chem.* **2001**, *40*, 2936-2937.
18. Sansone, F.; Baldini, L.; Casnati, A.; Lazzarotto, M.; Ugozzoli, F.; Ungaro, R. *Proc. Natl. Acad. Sci.* **2002**, *99*, 4842-4847.
19. Beer, P. D.; Gale, P. A.; Heseck, M. D. *Tetrahedron Lett.* **1995**, *36*, 767-770.
20. Caricato, M.; Leza, N.; Gargiulli, C.; Gattuso, G.; Dondi, D.; Pasini, D. *Beilstein J. Org. Chem.* **2012**, *8*, 967-976.
21. Chmielewski, M.; Zieliński, T.; Jurczak, J. *Pure Appl. Chem.* **2007**, *79*, 1087-1096.
22. Szumna, A.; Gryko, D.; Jurczak, J. *J. Chem. Soc., Perkin Trans.* **2000**, *2*, 1553-1558.
23. Kang, S. O.; Powell, D.; Day, V. W.; Bowman-James, K. *Angew. Chem. Int. Ed.* **2006**, *45*, 1921-1925.
24. McConnell, A.; Beer, P. *Angew. Chem. Int. Ed.* **2012**, *51*, 5052-5061.
25. Scheerder, J.; van Duynhoven, J.; Engbersen, J.; Reinhoudt, D. *Angew. Chem.* **1996**, *108*, 1172-1175.
26. Sessler, J. L.; Kim, S. K.; Gross, D. E.; Lee, C. H.; Kim, J. S.; Lynch, V. M. *J. Am. Chem. Soc.* **2008**, *130*, 13162-13166.
27. Evans, A. J.; Beer, P. D. *Dalton Trans.* **2003**, *23*, 4451-4456.

28. Mahoney, J. M.; Beatty, A. M.; Smith, B. D. *Inorg. Chem.* **2004**, *43*, 7617–7621.
29. Suksai, C.; Leeladee, P.; Jainuknan, D.; Tuntulani, T.; Muangsin, N.; Chailapakul, O.; Kongsaree, P.; Pakavatchai, C. *Tetrahedron Lett.* **2005**, *46*, 2765–2769.
30. Cametti, M.; Nissinen, M.; Dalla Cort, A.; Mandolini, L.; Rissanen, K. *J. Am. Chem. Soc.* **2005**, *127*, 3831–3837.
31. Mahoney, J. M.; Marshall, R. A.; Beatty, A. M.; Smith, B. D.; Camiolo, S.; Gale, P.A. *J. Supramol. Chem.* **2001**, *1*, 289–292.
32. Lankshear, M.; Cowley, A.; Beer, P. *Chem. Commun.* **2006**, *6*, 612–614.
33. Atwood, J. L.; Szumna, A. *J. Am. Chem. Soc.* **2002**, *124*, 10646–10647.
34. Atwood, J. L.; Szumna, A. *Chem. Commun.* **2003**, *12*, 940–941.
35. Schalley, C. A. *Mass Spectrom. Rev.* **2001**, *20*, 253–309.
36. Schneider, H. J.; Yatsimirsky, A. K. *Principles and Methods in Supramolecular Chemistry*, John Wiley & Sons Ltd.: Chichester, 2000.
37. Sanders, J. K. M.; Hunter, B. K. *Modern NMR Spectroscopy. A Guide for Chemists*, Oxford University Press: Oxford, 1988.
38. Hirose, K. *J. Incl. Phenom. Macrocycl. Chem.* **2001**, *39*, 193–209.
39. Lambert, J. P.; Mazzola, E. P. *Nuclear Magnetic Resonance Spectroscopy, An Introduction to Principles, Applications and Experimental Methods*, Pearson Ed. Inc., 2004.
40. Bovey, F. A.; Hood, F. P.; Anderson, E. W.; Kornegay, R. L. *J. Chem. Phys.* **1964**, *41*, 2042–2044.
41. Moser, A.; Detellier, C. *Nuclear Magnetic Resonance Spectroscopy*, In *Encyclopedia of Supramolecular Chemistry*, Marcel Dekker Inc.: New York, 2004.

42. Connors, K. A. *Binding Constants*, Wiley: New York, 1987.
43. Job, P. *Ann. Chim.* **1928**, 9, 113-203.
44. Fielding, L. *Tetrahedron* **2000**, 56, 6151-6170.
45. Jeffamines are the trade names for these amines supplied by Huntsman International.
46. Association constants were calculated using a non-linear curve fitting using the program ORIGINPro 7.5 from OriginLab Corporation.

## Chapter 2

### Synthesis and Complexation Properties of Amide-based Macrocyclic Receptors

Part of this work described in this chapter has been published in

*New J. Chem.* **2012**, *36*, 2451–2455.

&

*Acta Cryst.* **2011**, *E67*, 1880–1881.

## Chapter 2

### Synthesis and Complexation Properties of Amide-based Macrocyclic Receptors

#### 2.1 Introduction

The synthesis of new macrocyclic amides derived from different diacyl dichlorides with both “Jeffamine<sup>®</sup> EDR-148” and “Jeffamine<sup>®</sup> EDR-176”<sup>1</sup> at low temperatures under high dilution conditions are described in this Chapter. Also described is a complexation study of these new macrocyclic amides with selected Group 1 and 2 metal halides and tetrabutylammonium salts (TBAX) using 300 and 500 MHz <sup>1</sup>H NMR chemical shift changes. From the resulting titration curves, the association constants ( $K_{assoc}$ ) were calculated using isothermal non-linear 1:1 binding curve fitting plots according to Connors<sup>2</sup> using the ORIGINPro 7.5 program from OriginLab Corporation. Part of this chapter has been published in *New J. Chem.* **2012**, *36*, 2451–2455 and *Acta Cryst.* **2011**, *E67*, 1880–1881.

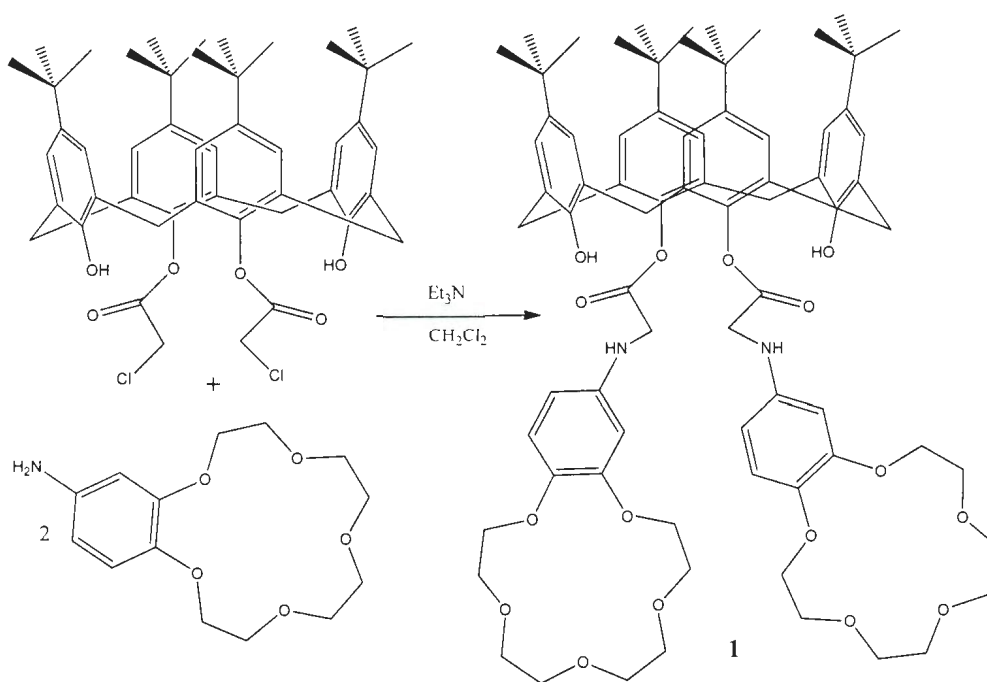
##### 2.1.1 Anion receptors

Shriver and Biallas<sup>3</sup> reported the first anion receptor in the late 1960s. Since anions play an important role not only in industry but also in health and the environment, researchers have for many years focused on studying anion receptors.<sup>4,5</sup> Designing anion receptors is much more complex than designing cation receptors since there are many factors which have to be considered *e.g.* size, geometry and the pH of the medium. The

cavity size of the anion receptors in many cases should be large enough to accommodate the desired anion. Anions also have different types of geometries: they can be spherical (e.g.  $F^-$ ,  $Cl^-$ ,  $Br^-$  and  $I^-$ ); linear (e.g.  $CN^-$ ,  $SCN^-$  and  $N_3^-$ ); tetrahedral (e.g.  $SO_4^{2-}$ ,  $PO_4^{2-}$  and  $ClO_4^-$ ) and octahedral (e.g.  $[Fe(CN)_6]^{4-}$ ). Anion receptors have many applications where they can be used in chemical reactions as catalysts and as bases; as well, they could be used for the selective separation of anions.<sup>6</sup> They also have medical applications since they can be used for transferring chloride anions through cell membranes.<sup>7</sup>

### 2.1.2 Amide based receptors

The development of novel macrocyclic ionic receptors, in particular organic-soluble heteroditopic macrocycles capable of binding to both cations and anions, either as contact ion-pairs or as separated ions is actively being pursued by many research groups. Beer *et al.*<sup>8</sup> reported the synthesis of an early example of such an organic solvent-soluble receptor **1** (Scheme 2.1). This calixarene-based diamido-benzo-15-crown-5-calix[4]arene could bind ion-pair salts as separated ions.<sup>9</sup> Beer *et al.* showed that this receptor could bind a cation in the crown ether residues, and the anionic counter-ion at the amide NH residues.



**Scheme 2.1.** Synthesis of diamido-benzo-15-crown-5-calix[4]arene **1**.

In 1997, Crabtree<sup>10</sup> reported that diamido compounds **2a-b** (Figure 2.1), which are derived from isophthaloyl dichloride (**2c**), had the ability to bind halide anions in  $\text{CD}_2\text{Cl}_2$  solutions. Using  $^1\text{H}$  NMR titration studies in  $\text{CD}_2\text{Cl}_2$  they showed that **2a-b** formed 1:1 complexes with relatively high affinities and selectivity for chloride and bromide ions over iodide ions. Since then, the isophthaloyl or isophthalamide motif has become a popular choice for designing new macrocyclic ion-pair receptors.<sup>11,12,13</sup> Beer's group also reported a calix[4]diquinone-isophthalamide host, which could bind alkali metal and ammonium chlorides as contact ion-pairs, since both cation and anion binding were found to be co-operatively enhanced in the presence of an appropriate co-bound counterion.<sup>14,15</sup>

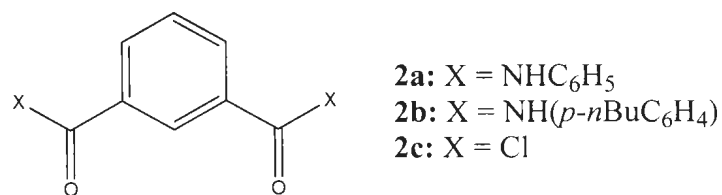


**Figure 2.1.** Isophthaloyldiamides **2a-b** and isophthaloyl dichloride (**2c**).

Hamilton and Choi<sup>16</sup> synthesized the tris(biphenyl) macrocyclic amides **3a-b** and **4**, (Figure 2.2). These compounds were synthesized using a stepwise protocol *via* Suzuki coupling.

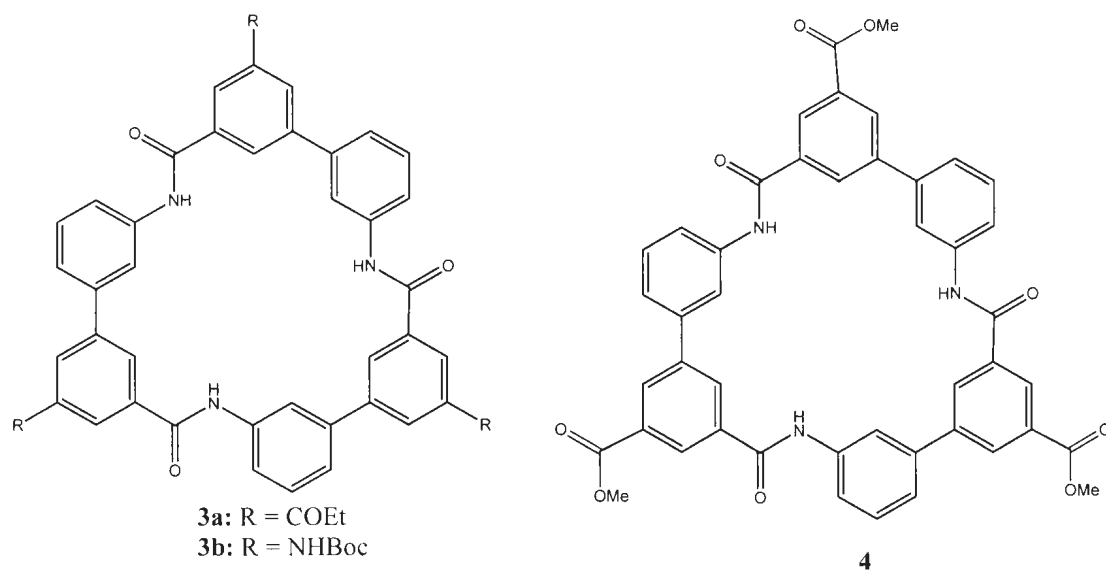
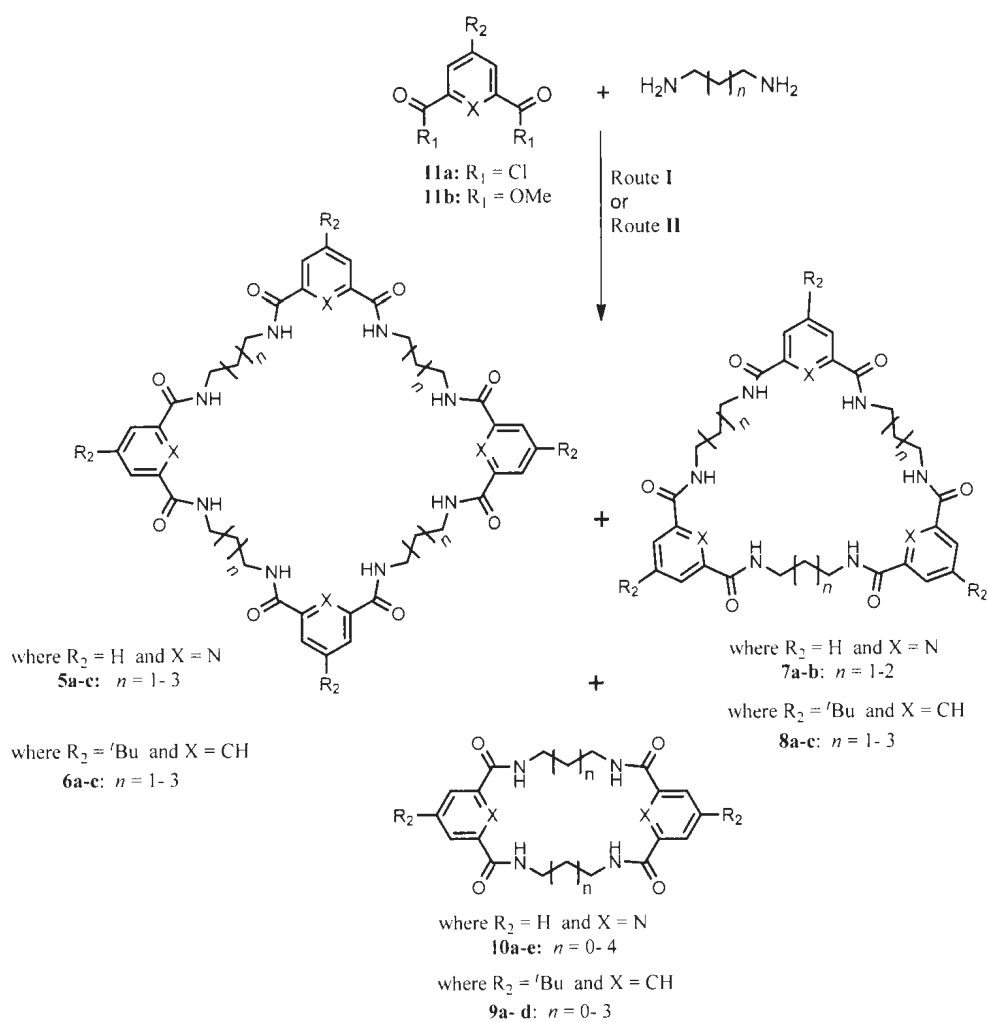


**Figure 2.2.** The tris(biphenyl) macrocyclic amides **3a-b** and **4**.

Jurczak and co-workers<sup>17,18</sup> reported the synthesis of different macrocyclic octa- (**5a-c** and **6a-c**), hexa- (**7a-b** and **8a-c**), and tetraamides (**9a-d** and **10a-e**), by two different synthetic routes.



**Scheme 2.2.** Synthesis of tetra-, hexa- and octaamide macrocycles using Route I (**11a**,  $\text{Et}_3\text{N}$ , DCM) or Route II (**11b**,  $\text{CH}_3\text{OH}$ ).

The first route (Route I, Scheme 2.2) involved the condensation of 5-*tert*-butylisophthalic acid dichloride (**11a**) with the appropriate diamine(s) under high dilution conditions in the presence of triethylamine in dichloromethane at room temperature. The second route, (Route II, Scheme 2.2) involved the condensation of dimethyl 2,6-pyridinedicarboxylate (**11b**) using different diamines, in methanol, at room temperature.

Jurczak and co-workers<sup>17</sup> also showed that the increase of the macrocycle ring sizes from an 18-membered ring (**10a**) to a 20-membered ring (**10b**) resulted in a 30-fold increase in the binding constant of the anions. However, any further increases of the macrocycle receptors size (**10c-e**) reduced the binding constant toward the tested anions.

### 2.1.3 Ditopic receptors

Receptors with two distinct binding sites are called ditopic receptors and they can be classified according to their binding mode to both cations and anions into three different types: (a) *contact ion pair* receptors, in which the anion and the cation are in a direct contact (Figure 2.3a); (b) *solvent-bridged ion pair* receptors, in which one or more solvent molecules bridges the gap between the anion and cation (Figure 2.3b); and (c) *host-separated ion pair* receptors, in which the anion is bound far from the cation (Figure 2.3c).<sup>19</sup>

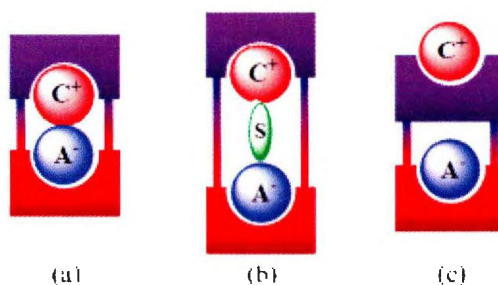


**Figure 2.3.** Limiting ion-pair interactions relevant to receptor-mediated ion-pair recognition: (a) contact, (b) solvent-bridged, and (c) host-separated. In this schematic, the anion is shown as “A<sup>-</sup>”, the cation as “C<sup>+</sup>”, and the solvent is represented as “S”. [Adapted with permission from reference 19]

Smith and co-workers<sup>20</sup> reported that alkali metal salts can bind with different receptors depending on the receptor cavity. In 2001, Smith and co-workers<sup>21</sup> also described the synthesis and complexation properties of a ditopic salt receptor **12** (Figure 2.4a).

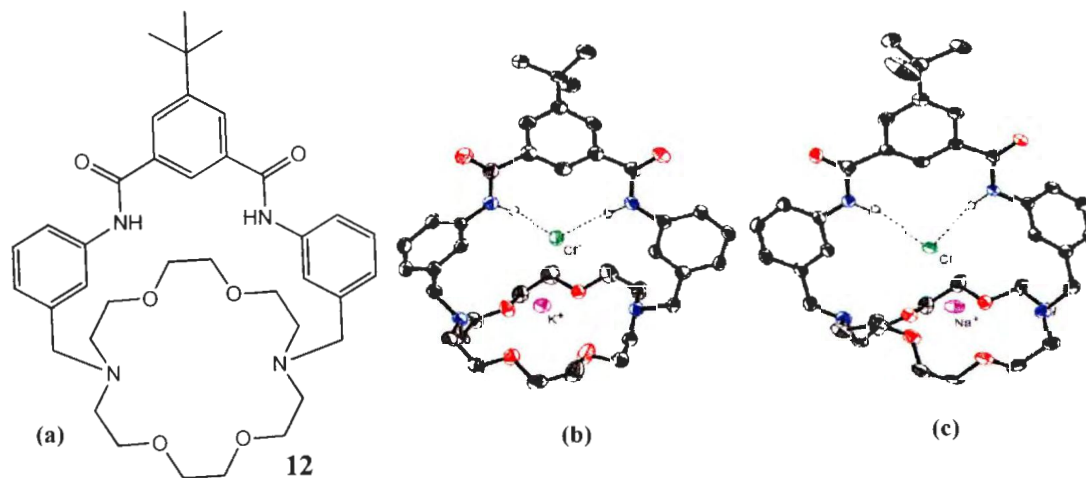


**Figure 2.4.** (a) Macrocycle **12** (b) X-ray structure of complex **12**:KCl and (c) X-ray structure of complex **12**:NaCl. [X-ray structures are adapted with permission from reference 21]

A quantitative evaluation of the binding constants of receptor **12** with KCl and with NaCl was obtained using <sup>1</sup>H NMR titration experiments in DMSO-*d*<sub>6</sub>. Also, single crystals of both **12**:KCl and **12**:NaCl complexes were obtained by slow evaporation of ethyl acetate solutions of receptor **12** saturated with KCl and NaCl, respectively, and their X-ray structures are shown in Figure 2.4 b-c.

A recent paper by Lüning and co-workers<sup>22</sup> reported the “first supramolecular ion triplet complex” of macrocyclic tetramide **13** with CaCl<sub>2</sub> (Figure 2.5).

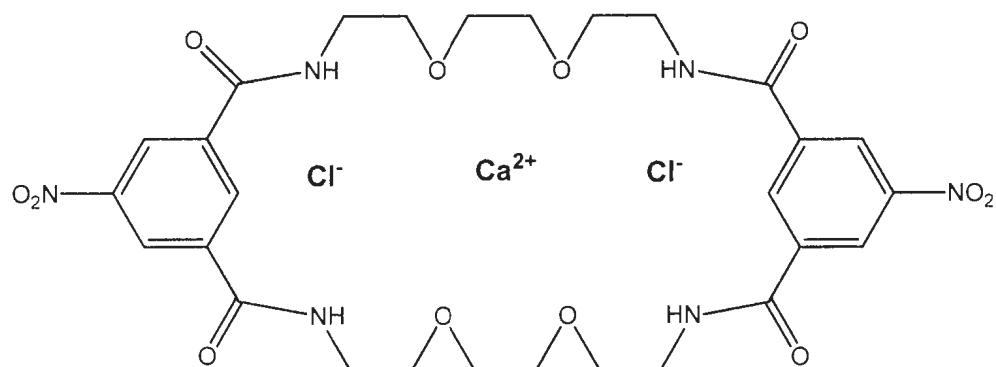
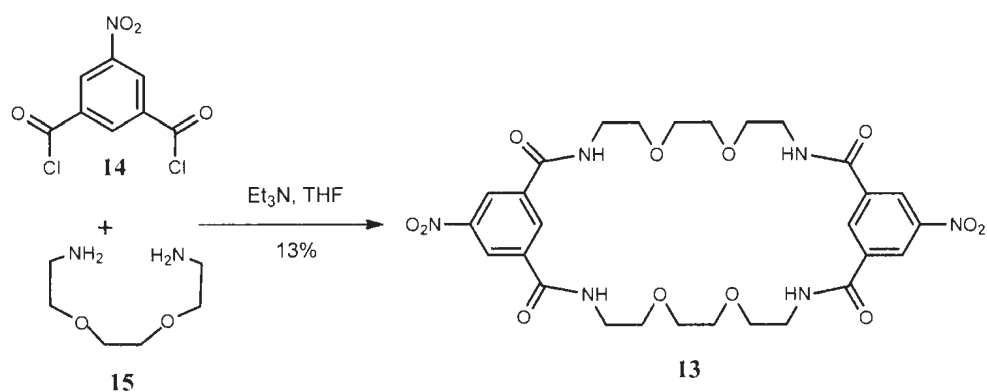


**Figure 2.5.** First supramolecular ion triplet complex of macrocyclic **13**:CaCl<sub>2</sub>.

The synthesis of macrocyclic **13** was obtained by reacting 5-nitroisophthaloyl dichloride (**14**) with 1,8-diamino-3,6-dioxaoctane (**15**) in the presence of triethylamine in anhydrous THF, as shown in Scheme 2.3. This compound contains three binding sites, which can bind anions via hydrogen bonding, and cations via the ether oxygen atoms. In addition, they studied the complexation properties of this macrocycle **13** with saturated solutions of metal halides in a solvent mixture of CDCl<sub>3</sub>:DMSO-*d*<sub>6</sub> 95:5, using <sup>1</sup>H NMR spectroscopy. The resulting spectra were analyzed, based on the differences in chemical shift changes. The study showed that the macrocycle **13** selectively binds lithium chloride and calcium chloride in preference to other metal chlorides examined. Furthermore, the results were supported by using electrospray ionization mass spectroscopy (ESI-MS) suggesting that macrocycle **13** formed a “ternary” complex with CaCl<sub>2</sub>.



**Scheme 2.3.** Synthesis of macrocycle **13**.

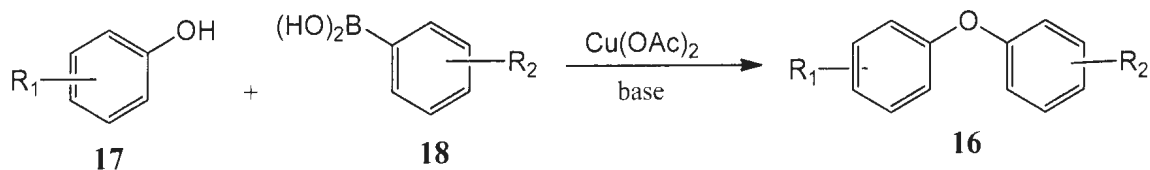
As Lüning has pointed out, despite the fact that many ditopic receptors for contact ion-pairs have been synthesized and characterized in recent years, tritopic molecular hosts for complexing alkaline earth metal salts and hence rendering them organic solvent-soluble are less well-known. Considering these facts, reported in this Chapter are the syntheses and binding properties of a new isophthalamide tetraamido macrocyclic receptor, which supports Lüning's contentions. The complexation properties of this new receptor with some tetrabutylammonium salts are also reported.

The synthesis and properties of a new diaryl ether-based macrocyclic amide which has not yet been published are also described in this Chapter. A general review of the diaryl ether coupling methodology employed for this latter macrocycle is presented in the following section.

#### 2.1.4 Diaryl ether coupling

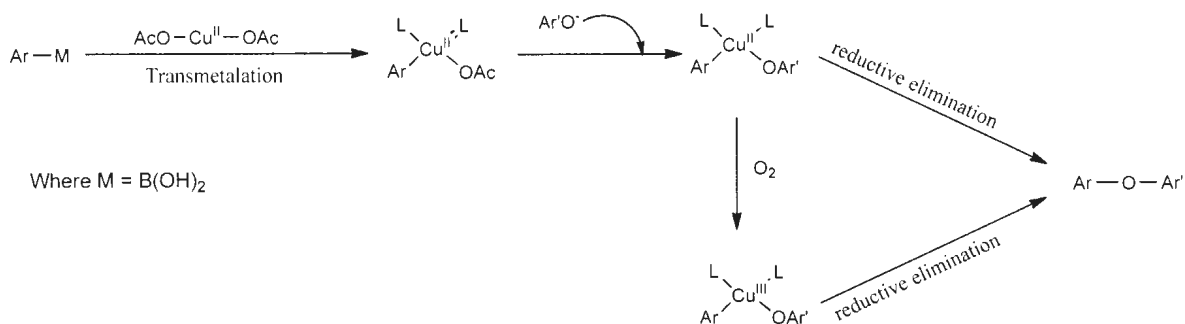
Diaryl ethers such as **16** can be synthesized as described by Evans *et al.*<sup>23</sup> using the copper-promoted arylation of phenols **17** with arylboronic acids **18** to produce the

corresponding diaryl ethers in high yields at room temperature (Scheme 2.4). Evans described the use of various substrates and in most cases yields were generally good, especially in case of the electron-rich phenols arylation was affected more efficiently.



**Scheme 2.4.** Scheme for diaryl ether formation using copper acetate mediated coupling.

It has been found that the product yields can be increased by the addition of powdered 4 Å molecular sieves, which prevents the formation of phenol and diphenyl ether side-products which were generated, even under anhydrous conditions. The general mechanism for the  $\text{Cu(OAc)}_2$ -mediated coupling is shown in Scheme 2.5.



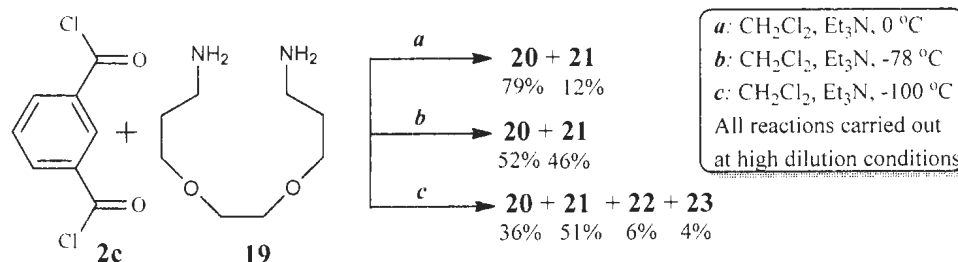
**Scheme 2.5.** General mechanism for copper acetate-mediated coupling.

## 2.2 Synthesis of the aryl diacid chloride-Jeffamines macrocyclic amides

Two different diacid chlorides were used for the macrocyclic amides reported in this study: isophthaloyl dichloride (**2c**) and diaryl ether diacyl chloride **35**.

### 2.2.1 Reaction of isophthaloyl dichloride (**2c**) with “Jeffamine<sup>®</sup> EDR-176” (**19**)

The synthesis of macrocycles **20-23** (see page 87 for the structures), which are the “[1+1]”-, “[2+2]”-, “[3+3]”- and “[4+4]”- macrocyclic amide compounds respectively, derived from the reaction of **2c** with 1,10-diamino-4,7-dioxadecane (“Jeffamine<sup>®</sup> EDR-176”, **19**) in dry DCM are summarized in Scheme 2.6. Of several reaction conditions which were investigated, using conditions “a” (Scheme 2.6) the [2+2]-macrocyclic amide **21** was produced in 12% yield, in addition to [1+1]-macrocyclic amide **20** in 79% yield. Using conditions “b” (Scheme 2.6) however, along with **21** (46% yield), the [1+1] product, **20**, could be isolated in 52% yield.

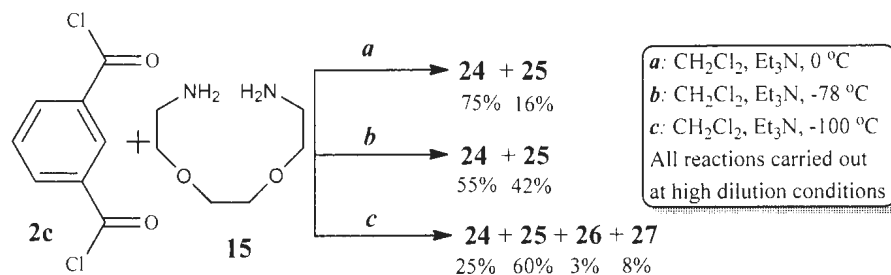


**Scheme 2.6.** Reaction conditions used with isophthaloyl dichloride (**2c**) and 1,10-diamino-4,7-dioxadecane (**19**).

The [2+2]-macrocyclic amide **21** was optimally produced in 51% yields (conditions “c”, Scheme 2.6), compared with the 8% yield of **13** reported by Lünig and co-workers for their synthesis of **13** from the reaction of 3-nitroisophthaloyl dichloride with 1,8-diamino-3,6-dioxaoctane (**15**) in THF. Under the initial lower temperature conditions (conditions “c”, Scheme 2.6), it was also possible to isolate small amounts of the [3+3]-macrocyclic amide **22** (6% yield) and the [4+4]-macrocyclic amide **23** (4% yield).

## 2.2.2 Reaction of isophthaloyl dichloride (**2c**) with “Jeffamine<sup>®</sup> EDR-148” (**15**)

The synthesis of macrocyclic amides **24-27** (see page 89 for the structures), derived from the reaction of **2c** with 1,8-diamino-3,6-dioxaoctane (**15**) in dry DCM are summarized in Scheme 2.7. Using conditions “a” (Scheme 2.7) produced the [2+2]-macrocyclic amide **25** in 16% yield, in addition to the [1+1]-macrocyclic amide **24** which was formed in 75% yield. Conditions “b” (Scheme 2.7) afforded a mixture of macrocyclic amides **24** and **25** in 55% and 42% yields respectively. The [2+2]-macrocyclic amide **25** was optimally produced in 60% yields using conditions “c”, (Scheme 2.7), compared with the 8% yield of **13** reported by Lünig and co-workers.



**Scheme 2.7.** Reaction conditions used with isophthaloyl dichloride (**2c**) and 1,8-diamino-3,6-dioxaoctane (**15**).

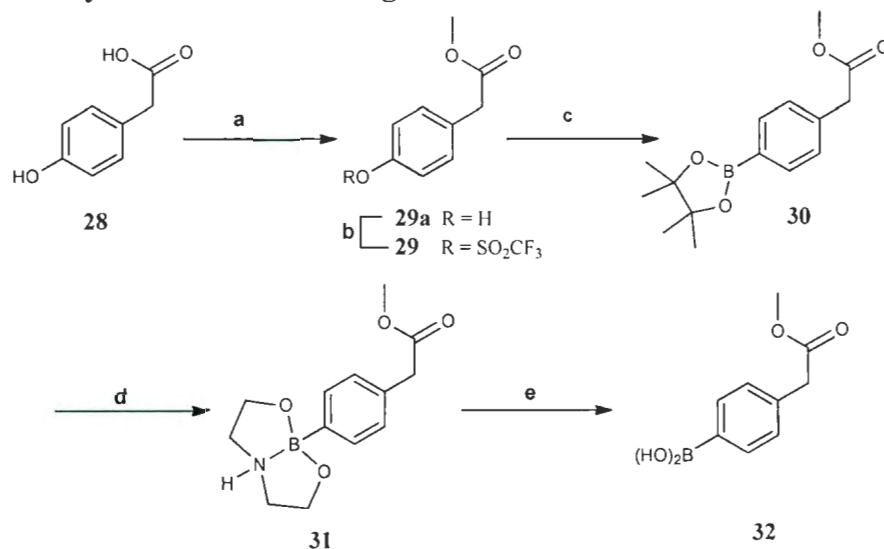
Further decreasing of the temperature, conditions “c” (Scheme 2.7), it was also possible to isolate small amounts of the [3+3]-macrocyclic amide **26** (3% yield) and the [4+4]-macrocyclic amide **27** (8% yield).

## 2.2.3 Synthesis of macrocycles **36** and **37**

The syntheses of macrocycles **36** and **37** were conducted in co-operation with Dr. Ahmed Zein, of the Chemistry Department, Memorial University. The precursor

compounds were derived from compound **32** which Zein had used during his Ph.D studies toward the synthesis of some selected bisbenzyltetrahydroisoquinolines.

### 2.2.3.1 Synthesis of the starting material **32**<sup>24</sup>



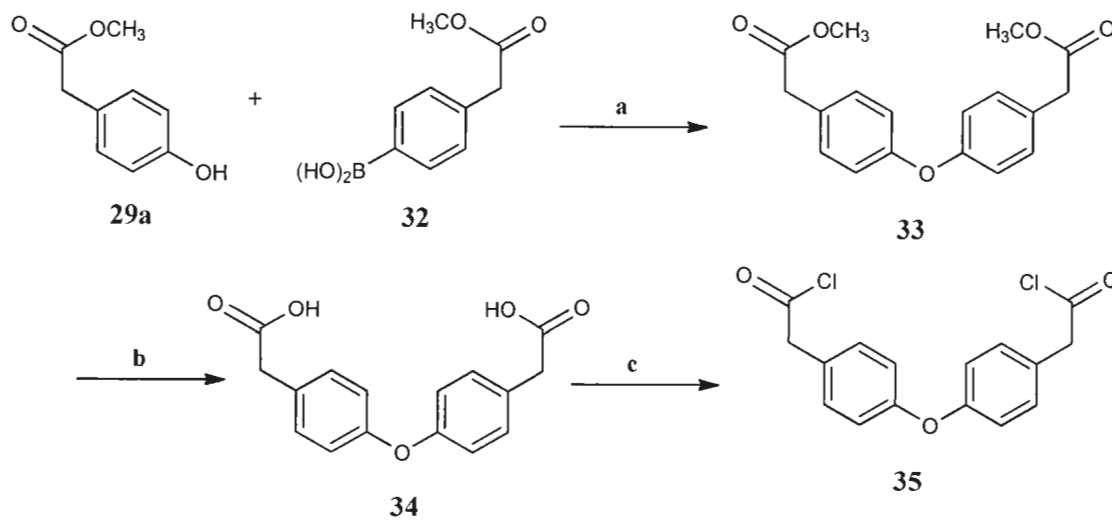
**a:** SOCl<sub>2</sub>, MeOH, reflux, 95%; **29a**; **b:** Tf<sub>2</sub>O, pyridine, 0 °C, 98%; **29**; **c:** 4,4,5,5-tetramethyl-1,3,2-dioxaborolane, PdCl<sub>2</sub>(dppf), Et<sub>3</sub>N, dioxane, 100 °C, 90%; **d:** diethanolamine, 2-propanol, 77%; **e:** aq 1 M HCl, THF, 85%.

### Scheme 2.8. Preparation of arylboronic acid **32**

The arylboronic acid **32** was synthesized from the commercially-available 4-hydroxyphenylacetic acid (**28**). Esterification of the carboxylic acid using thionyl chloride in methanol gave the methyl 4-hydroxyphenylacetate (**29a**) in 95% yield, followed by activation of the phenolic group as the triflate **29** using triflic anhydride in pyridine. This activation is necessary for the palladium-catalyzed borylation step.<sup>25</sup> PdCl<sub>2</sub>(dppf)-catalyzed coupling of triflate **29** with tetramethyl dioxaborolane afforded the intermediate arylboronate **30** in 90% yield. Without any purification, this aryl boronate **30** was converted into the corresponding cyclic aminoboronate intermediate **31** with

diethanolamine using a procedure similar to that described by Jung and Lazarova.<sup>26</sup> The cyclic aminoboronate intermediate **31** could be more easily hydrolyzed than **30**, to **32** under acidic conditions (Scheme 2.8).

After stirring **29a** and **32** with  $\text{Cu}(\text{OAc})_2$ , pyridine, and 4 Å molecular sieves in DCM for 48 h at room temperature, diaryl ether **33** was formed in reasonably good yield (72%). Further reaction of **33** with LiOH in water afforded diacid **34** in 68% yield. Reaction of **34** with oxalyl chloride in DMF and benzene afforded the target diacyl chloride **35** in 73% yield (Scheme 2.9).

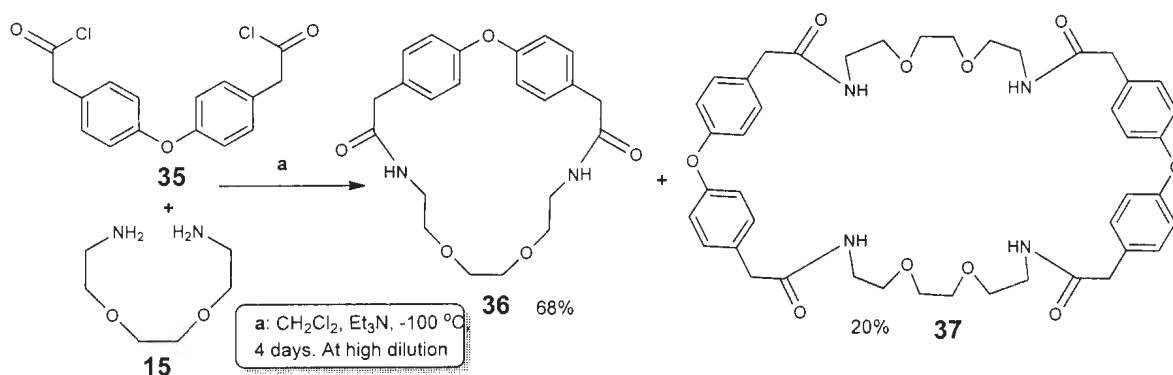


**a:**  $\text{Cu}(\text{OAc})_2$ , pyridine, 4 Å molecular sieves,  $\text{CH}_2\text{Cl}_2$ , rt, 48 h, 72%;  
**b:** LiOH, THF,  $\text{H}_2\text{O}$ , 68%; **c:**  $(\text{COCl})_2$ , DMF, benzene, 73%.

**Scheme 2.9.** Preparation of diacyl chloride **35**.

### 2.2.3.2 Reaction of diacyl chloride **35** with “Jeffamine<sup>®</sup> EDR-148” (**15**)

The diacyl chloride **35** was reacted with “Jeffamine<sup>®</sup> EDR-148” (**15**) under low temperature and high dilution conditions in dry DCM and Et<sub>3</sub>N, to afford a mixture of the [1+1]-macrocyclic amide **36** and the corresponding [2+2]-macrocyclic amide **37** (Scheme 2.10).



**Scheme 2.10.** Reaction of diacyl chloride **35** and 1,8-diamino-3,6-dioxaoctane (**15**).

### 2.3 X-Ray structures of **20**, **21**, **25** and **36**

Crystals of **20** were obtained by the slow evaporation at room temperature of the aqueous methanol/ethyl acetate solvent mixture used to dissolve the macrocycle to give colorless crystals which were suitable for X-ray diffraction analysis and its structure is shown in Figure 2.6.

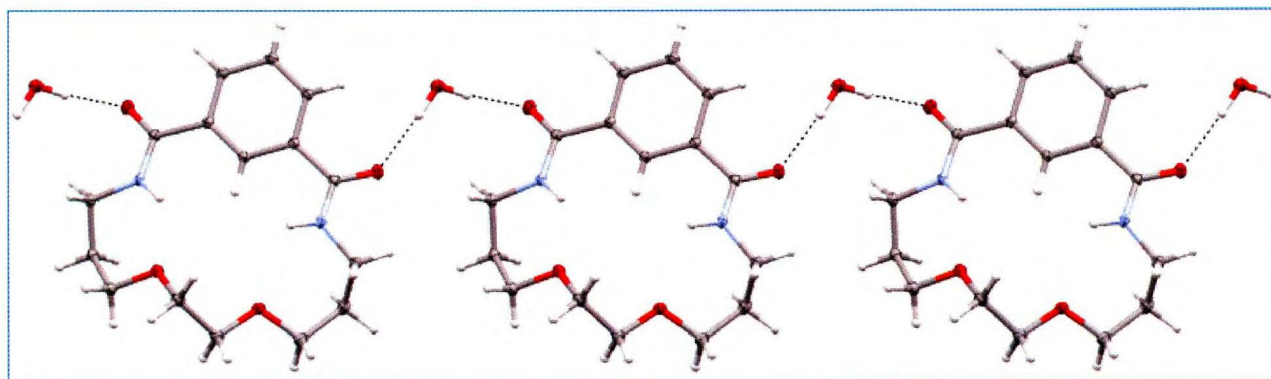


**Figure 2.6.** X-ray structure of **20**, with 30% displacement ellipsoids, looking along an *a*-axis, showing the water molecule hydrogen-bonded to adjacent molecules of **20**.

The X-ray structure of **20** (Figure 2.6)<sup>27</sup> reveals it to be a channel-type clathrate<sup>28</sup> with water molecules which are hydrogen-bond ( $\text{O}\cdots\text{H}$  1.99 Å) between pairs of molecules in the unit cell and their counterparts in neighbouring unit cells. The hydrogen-bonding chain motif can be described using graph set theory as  $\text{C}_2^2(10)$ .<sup>29</sup>

Crystals of **21** were obtained by the slow evaporation at room temperature of the aqueous methanol solution used to dissolve the macrocycle. The colorless crystals obtained were suitable for X-ray diffraction analysis and its structure is shown in Figure 2.7.

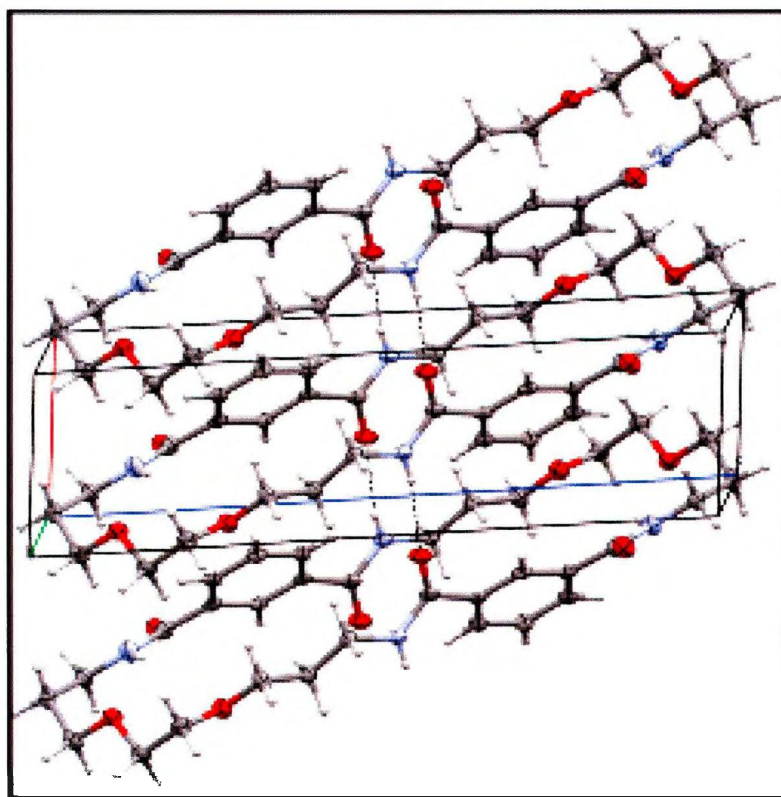


**Figure 2.7.** X-ray structure of **21**, with 30% displacement ellipsoids, showing the unit cell and the intermolecular short contacts.

The single-crystal X-ray structure of **21** (Figure 2.7) shows that there are no solvent molecules included in this crystal. The structure shows intermolecular (O $\cdots$ H 2.10 Å) H-bonding interactions, leading to formation of H-bonded chains that run parallel to the crystallographic a-axis.<sup>30</sup>

Crystals of **24** were also obtained from a chloroform solution maintained at 0 °C. The colorless crystals obtained were suitable for single-crystal X-ray diffraction analysis and the structure of **24** is shown in Figure 2.8 and Figure 2.9. Macrocyclic **24** co-

crystallized with a lattice solvent chloroform molecule in the non-centrosymmetric monoclinic space group  $P2_1$ .<sup>31</sup>

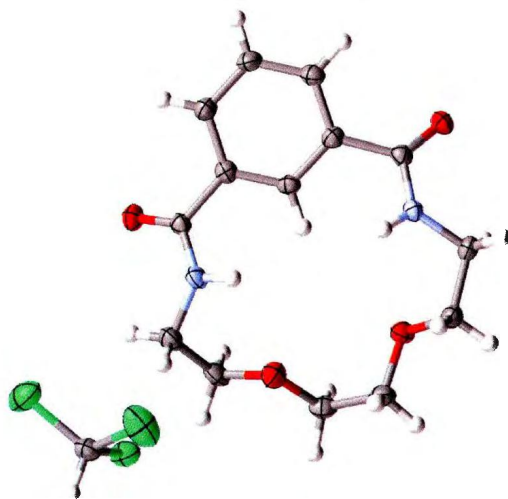


**Figure 2.8.** Asymmetric unit for macrocycle **24** with 50 % probability ellipsoids. grey = carbon, light grey = hydrogen, green = chlorine, red = oxygen, blue = nitrogen.

The intermolecular hydrogen bonding in this structure results in an infinite one-dimensional chain with base vector  $[0\ 1\ 0]$  (i.e. parallel to the  $b$ -axis), that is coincident with a two-fold screw axis (Figure 2.9 and Table 2.1).

**Table 2.1.** Hydrogen-bond geometry (Å), symmetry operations used to generate equivalent atoms: (i)  $1-x, y-1/2, 1-z$ .

$D-H\cdots A$	$D-H$	$H\cdots A$	$D\cdots A$	$D-H\cdots A$
$N2-H2N\cdots O1^i$	0.86 (3)	2.12 (3)	2.973 (3)	175 (3)

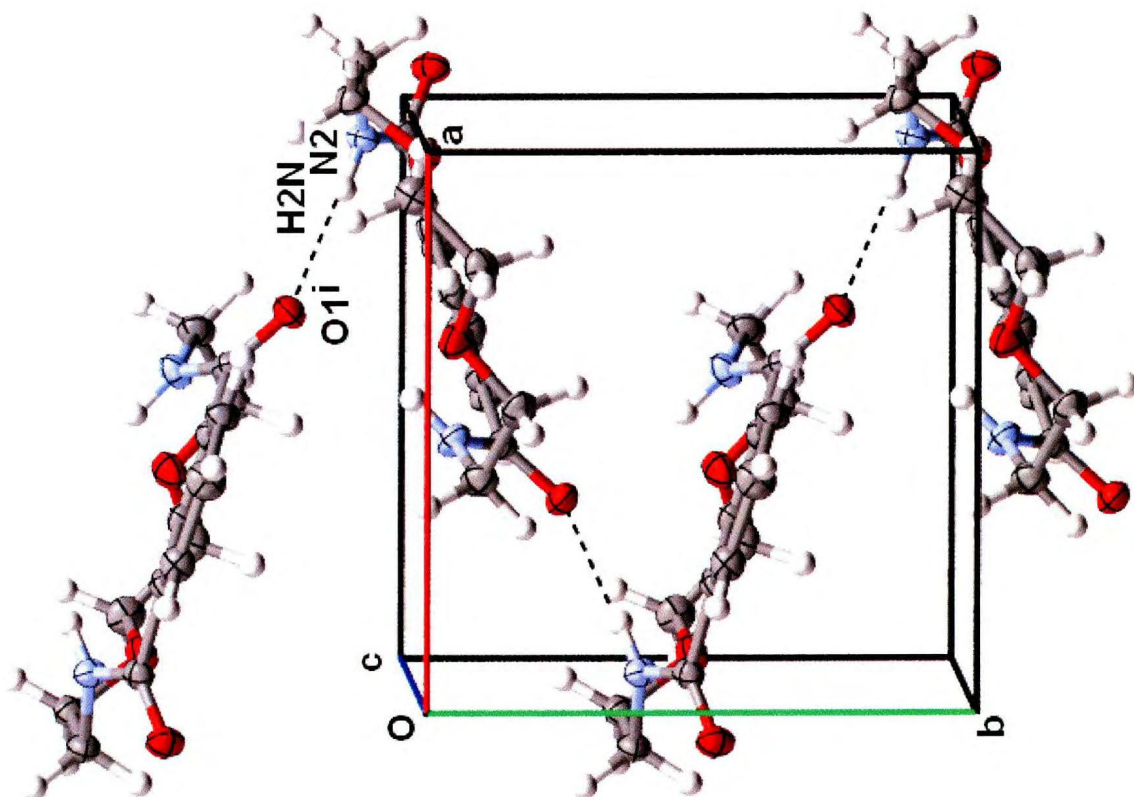


**Figure 2.9.** Hydrogen bonding (dashed lines) for macrocycle **24** leading to an infinite one-dimensional chain parallel to the *b*-axis. Lattice solvent molecules ( $\text{CHCl}_3$ ) omitted for clarity. Symmetry operations used to generate equivalent atoms: (i)  $1-x, y-1/2, 1-z$ .

Crystals of **25** were obtained by the slow evaporation at room temperature of the aqueous methanol/DMSO solution of the macrocycle. The colorless crystals obtained were suitable for X-ray diffraction analysis, and the structure of **25** is shown in Figure 2.10.

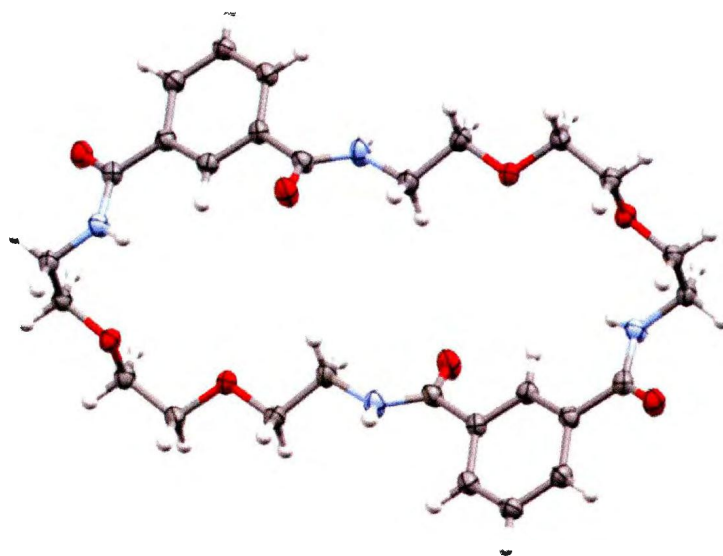


**Figure 2.10.** Asymmetric unit for macrocycle **25** with 50% probability ellipsoids. grey = carbon, light grey = hydrogen, red = oxygen, blue = nitrogen.

The macrocycle crystallized in the centrosymmetric triclinic space group  $P\bar{1}$  with half the molecule contained in the asymmetric unit.<sup>32</sup> Extensive intermolecular hydrogen bonding leading to the formation of a two dimensional infinite polymer in the  $ac$ -plane was also present (see Figure 2.11 and Table 2.2).

**Table 2.2.** Hydrogen-bond geometry (Å). Symmetry operations used to generate equivalent atoms: (ii)  $x+1, y, z$ ; (iii)  $-x, -y, -z$ .

$D-H\cdots A$	$D-H$	$H\cdots A$	$D\cdots A$	$D-H\cdots A$
N1—H1N $\cdots$ O4 <sup>ii</sup>	0.91 (3)	2.00 (3)	2.883 (3)	163 (3)
N2—H2N $\cdots$ O3 <sup>iii</sup>	0.93 (3)	2.08 (3)	2.973 (3)	162 (3)

Finally, the intermolecular interactions in the form of  $\pi$ - $\pi$  stacking present in the crystal structure can also be seen in Figure 2.12.

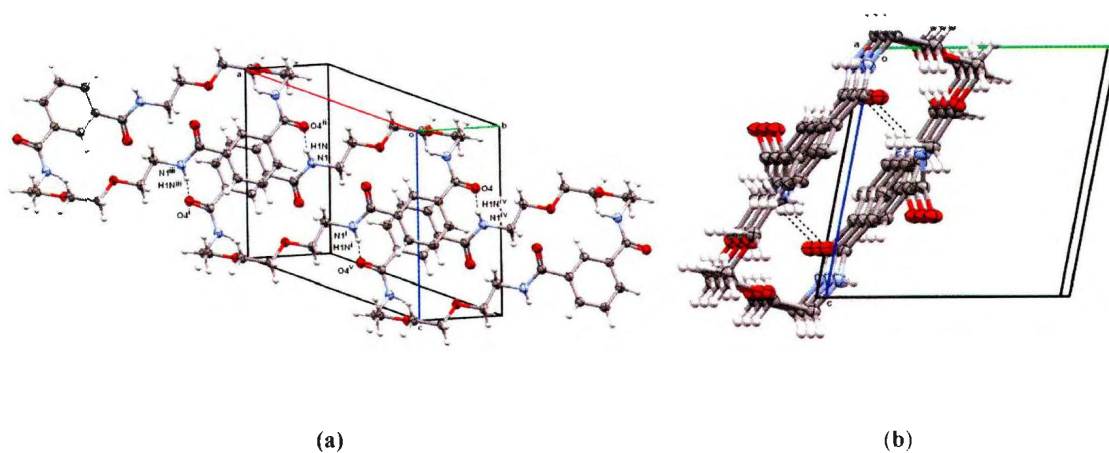


**Figure 2.11.** (a) Hydrogen bonding (dashed lines) leading to an infinite 2D polymer in the (0 1 0) plane for macrocycle **25**. (b) Viewed down the *a*-axis. Symmetry operations used to generate equivalent atoms: (i) =  $1-x, -y, 1-z$ ; (ii) =  $x+1, y, z$ ; (iii) =  $2-x, -y, 1-z$ , (iv) =  $x-1, y, z$ , (v) =  $-x, -y, z-1$ .

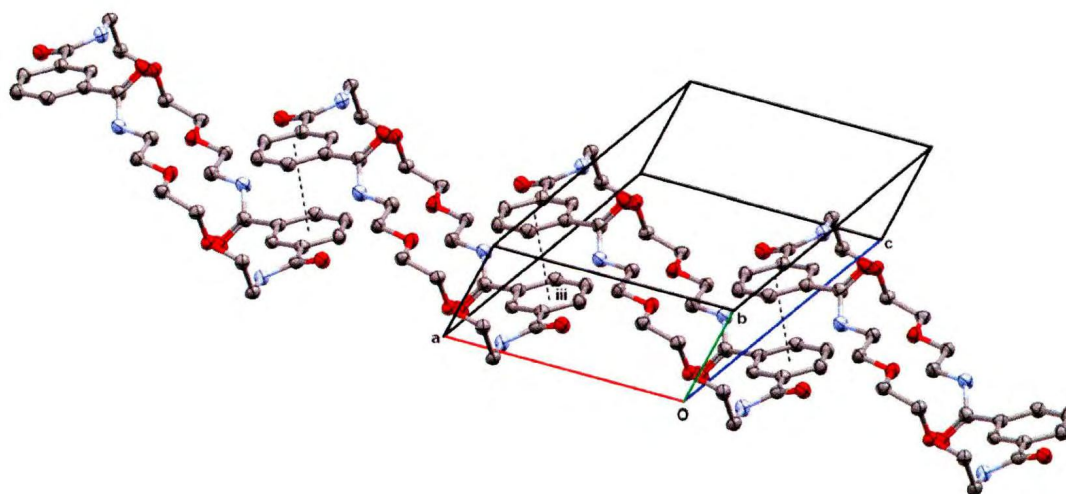


**Figure 2.12.** The  $\pi$ - $\pi$  stacking between the [C1 – C6; Plane 1] ring and its symmetry generated equivalent (Plane 2; symmetry operator =  $2 - x, - y, 1 - z$ ) can be seen for macrocycle **25**. Plane 1 to Plane 2 angle:  $0.0(3)^\circ$ ; Plane 1 centroid to Plane 2 centroid distance:  $3.626(2)$  Å; Plane 1 to Plane 2 centroid distance:  $3.501(3)$  Å; Plane 1 to Plane 2 shift:  $0.947(5)$  Å.

Colorless crystals of **36** suitable for X-ray diffraction analysis were obtained after allowing a methanol solution to stand at 0 °C for several weeks. The structure of **36** is shown in Figure 2.13. The macrocycle **36** crystallized in the monoclinic space group  $C^2/c$ .<sup>33</sup> The asymmetric unit contains one half of the molecule, with the other half generated by a two-fold proper rotation (Figure 2.13).

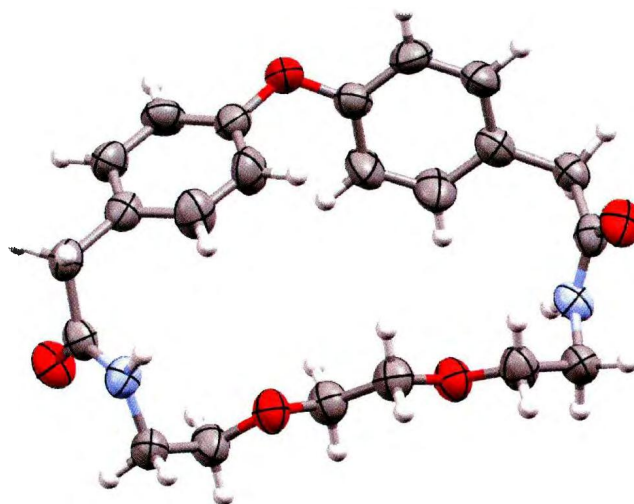


**Figure 2.13.** Asymmetric unit for macrocycle **36** with 50 % probability ellipsoids. grey = carbon, light grey = hydrogen, red = oxygen, blue = nitrogen.

The aromatic plane-plane angle is 72.08°. Intermolecular hydrogen bonding results in two (symmetry generated) interactions between each pair of macrocycles and leads to an infinite one-dimensional chain with base vector [1 0 0] (i.e. parallel to the *a*-axis; Figure 2.14 and Table 2.3).

**Table 2.3.** Hydrogen-bond geometry (Å), Symmetry operations used to generate equivalent atoms: (i)  $x-1, y, z$ .

$D-H\cdots A$	$D-H$	$H\cdots A$	$D\cdots A$	$D-H\cdots A$
N1—H1 <sup>i</sup> ⋯O2 <sup>i</sup>	0.98 (5)	1.96 (5)	2.904 (5)	162 (3)

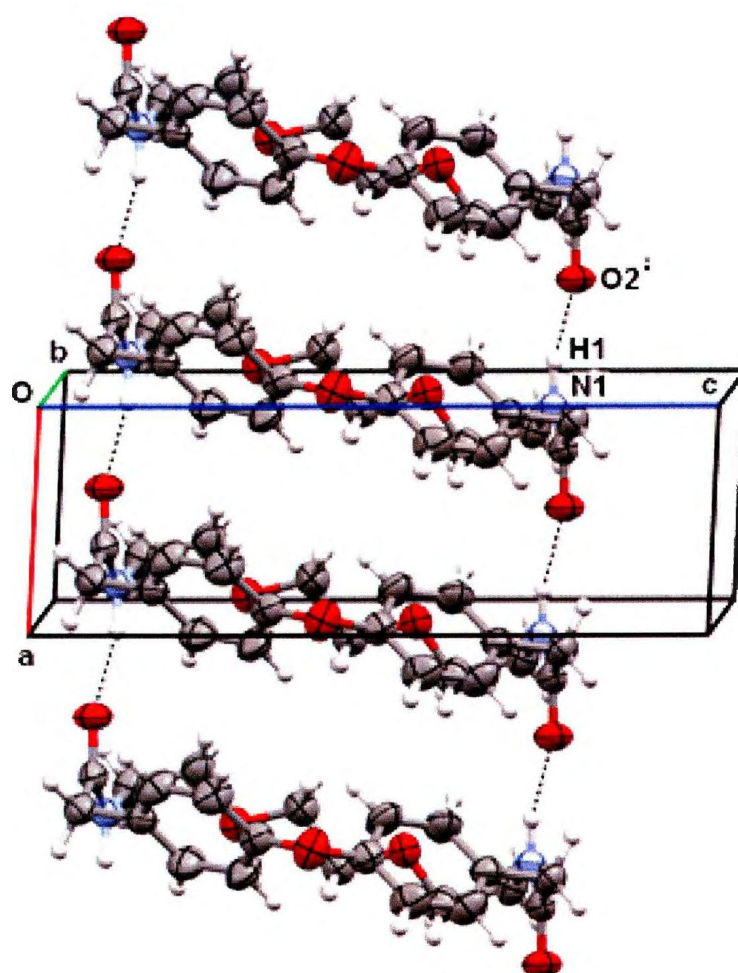


**Figure 2.14.** Hydrogen bonding (dashed lines) for macrocycle **36** leading to an infinite chain parallel to the *a*-axis. Symmetry operations used to generate equivalent atoms: (i)  $x-1, y, z$ .

## 2.4 Complexation studies

Stock solutions of macrocyclic amides ( $\sim 1.00 \times 10^{-3}$  M) were prepared in a 9:1  $\text{CDCl}_3$ : $\text{DMSO-}d_6$  solvent mixture or, in the case of the titration studies with TBA salts, in  $\text{CDCl}_3$ . After maximum chemical shift changes using saturated solutions of the guests

were determined in preliminary studies, solid aliquots of the guests to be studied were weighed (+/- 0.01 mg) into separate sample vials using a Sartorius microbalance. To these samples, 1.00 mL amounts of the stock solution were added and the resulting solutions were sonicated at room temperature for 5 min and then allowed to stand for 24 h before measuring their  $^1\text{H}$  NMR spectra and calculating binding constants from the observed chemical shift changes using a non-linear curve fitting according to Connors<sup>2</sup> using the ORIGINPro 7.5 program from OriginLab Corporation.

#### **2.4.1 Complexation of macrocycles **20** and **21** with Group 1 and 2 metal chlorides**

Complexation studies with Group 1 and 2 metal chlorides were conducted to test whether macrocyclic amides **20** and **21** behaved in a manner similar to that of Lünig's compound **13**. A similar experiment was conducted in which solutions of **20** and **21** were saturated with respect to the metal salts. The mixtures were sonicated and thereafter allowed to stand at room temperature for 24 h before their  $^1\text{H}$  NMR spectra were measured. Figure 2.15 summarizes the changes in the NH chemical shifts observed and are compared with Lünig's macrocycle **13**. It should be noted that Lünig used a 95:5  $\text{CDCl}_3$ : $\text{DMSO}-d_6$  solvent mixture, but due to solubility differences between **13** and **21**, a 9:1  $\text{CDCl}_3$ : $\text{DMSO}-d_6$  solvent mixture instead was employed in our determinations. The largest chemical shift changes (1.15 and 0.54 ppm downfield shifts, respectively) were observed with  $\text{CaCl}_2$  and **21** for the amide protons, which appear as a triplet, and the intra-annular aromatic singlet.

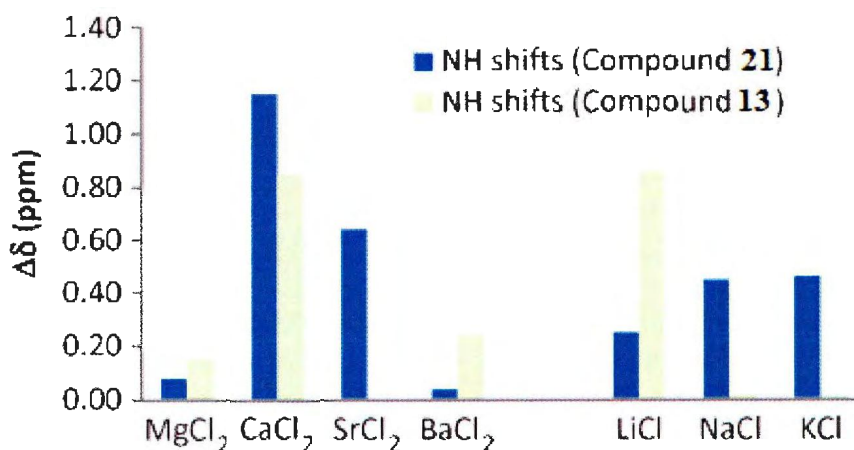


**Figure 2.15.** Downfield NH protons chemical shift changes for solutions of **13** and **21** which were saturated with the Group 1 and 2 metal halides shown in 9:1 CDCl<sub>3</sub>:DMSO-*d*<sub>6</sub>. Data for **13** are taken from Lüning and co-workers.<sup>22</sup>

These results are basically similar to Lüning's observations. Where our data differs is in the case of LiCl where for this particular ion pair, no selectivity over NaCl or KCl, or any comparable downfield chemical shift changes were observed: 0.25 ppm for LiCl with **21** compared with 0.88 ppm for LiCl with Lüning's compound **13**. Possible reasons for this difference could be at least threefold: (i) compound **13** has a strongly electron-withdrawing nitro substituent in the *para* positions of the aromatic rings; (ii) the solvent used with **21** had a larger relative percentage of DMSO and was therefore more polar thus making a solvophobic effect more difficult to overcome by the host molecules; and (iii) macrocycle **21** is larger, and hence a larger entropic effect could be needed to be overcome in order to accommodate a LiCl ion-pair. On the other hand, a downfield chemical shift change of 0.70 ppm for the NH proton of **21** with SrCl<sub>2</sub> was observed.

Lüning did not report any study with  $\text{SrCl}_2$  but did report a downfield shift of 0.24 ppm with  $\text{BaCl}_2$  which in our case, revealed a downfield shift of only 0.05 ppm.

In all cases there was no evidence to support any 2:1 binding as determined by subjecting the complexation data to the corresponding 2:1 binding isotherm analyses.<sup>2</sup>

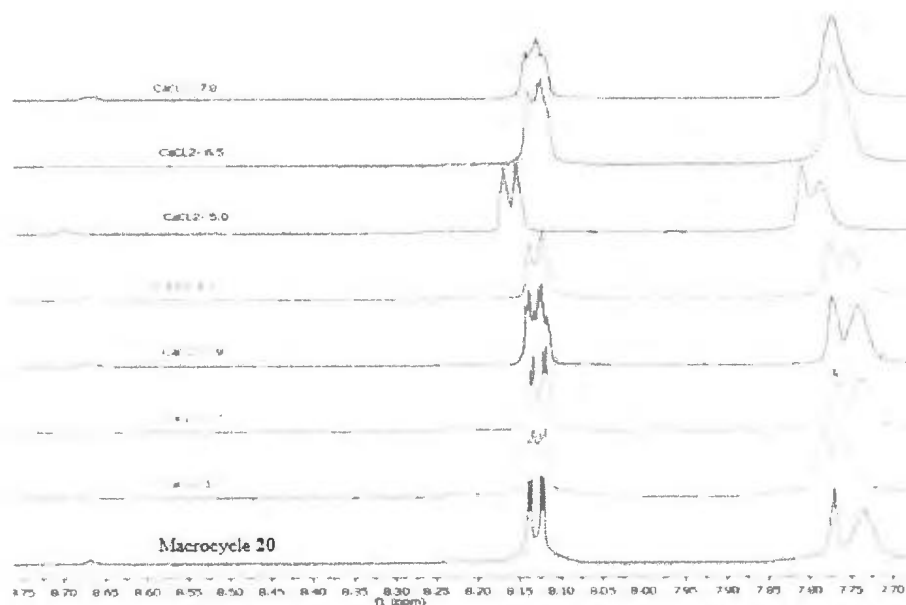


**Figure 2.16.** Expanded <sup>1</sup>H NMR (300 MHz) titration spectra of macrocyclic amide **20** with anhydrous  $\text{CaCl}_2$ .

In contrast with the [2+2] macrocycle **21**, the [1+1] macrocycle **20** showed negligibly small chemical shift changes in the titration with anhydrous  $\text{CaCl}_2$  under similar conditions (Figure 2.16).

#### 2.4.1.1 Complexation of macrocyclic amide **21** with anhydrous CaCl<sub>2</sub>

To determine a binding constant for the complexation of **21** with CaCl<sub>2</sub> we initially sought to use deuterated methanol as a solvent since the solubility of our host compound in this solvent is greater. However, as was noted by Smith and co-workers,<sup>20</sup> methanol and water bind strongly to the amido protons and in the cavity, and as a result, it was not possible to follow the shift changes for those protons' signal(s) since exchange with the solvent results in considerable broadening. Instead, using the same 9:1 CDCl<sub>3</sub>:DMSO-*d*<sub>6</sub> solvent ratio used for the saturation study above, it was possible to titrate the addition of solid anhydrous CaCl<sub>2</sub> to a solution of **21** and measure the NH and intra-annular aromatic proton chemical shift changes.

Figure 2.17 shows the titration spectra of **21** with anhydrous CaCl<sub>2</sub>. It can be seen that by increasing the added amounts of CaCl<sub>2</sub> to the solution of **21**, a downfield change in chemical shift occurs for both the triplet signals due to the NH protons and also the aromatic intra-annular proton singlet signals. The NH signals shifted downfield from 7.67 ppm to 8.49 ppm, whereas the singlet also shifted downfield from 8.21 ppm to 8.59 ppm (Table 2.4), indicating that complexation occurred between macrocycle **21** and CaCl<sub>2</sub>.

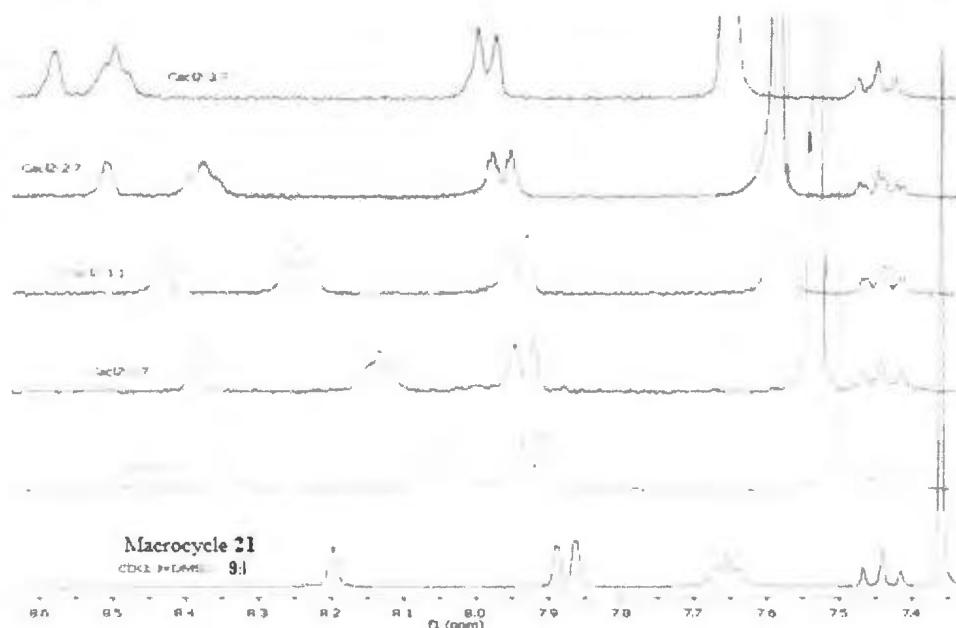


**Figure 2.17.** Expanded  $^1\text{H}$  NMR (300 MHz) titration spectra of macrocyclic amide **21** with anhydrous  $\text{CaCl}_2$ .

The extent of this complexation was determined by measuring the binding, or association constant ( $K_{\text{assoc}}$ ), using the non-linear 1:1 binding isotherm for both the NH and aromatic intra-annular proton singlet chemical shift changes (Table 2.4).

**Table 2.4.**  $^1\text{H}$  NMR (300 MHz) titration chemical shift data for both singlet and NH signals of **21** ( $9.12 \times 10^{-7}$  M) with anhydrous  $\text{CaCl}_2$ .

Sample	Guest (g)	[Guest] (M)	[G]/[H]	Singlet $\delta$	$\Delta\delta$ Hz	NH $\delta$	$\Delta\delta$ Hz
Free host				8.210		7.670	
1	4.00E-04	3.60E-03	4	8.339	38.7	8.042	111.6
2	7.00E-04	6.31E-03	7	8.386	52.8	8.134	139.2
3	1.10E-03	9.91E-03	11	8.435	67.5	8.245	172.5
4	2.70E-03	2.43E-02	27	8.51	90.0	8.378	212.4
5	3.90E-03	3.51E-02	39	8.585	112.5	8.497	248.1

Using the Origin program the concentration of the guest ( $[Guest]$ ) was plotted against the observed chemical shift changes ( $\Delta\delta$ ) in Hz. The association constants values were determined to be  $133 \pm 6$  and  $207 \pm 15 \text{ M}^{-1}$  respectively, based on the singlet and NH proton chemical shift changes (Figure 2.18).

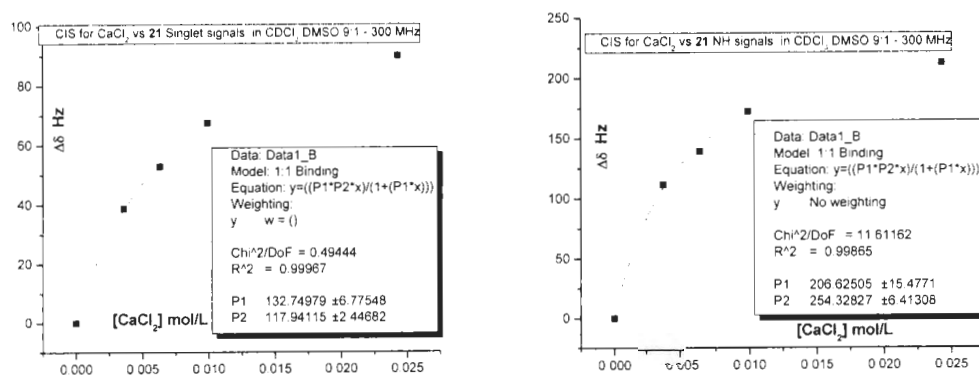


**Figure 2.18.**  $^1\text{H}$  NMR (300 MHz) titration curves for both singlet and NH signals of **21** ( $9.12 \times 10^{-7}$ ) with anhydrous  $\text{CaCl}_2$ .

Lüning quoted binding constants for his host with  $\text{CaCl}_2$  “in the range of  $10^3$  to  $10^4$  in  $\text{CHCl}_3/\text{DMSO}$ ” but used a  $\text{Ca}(\text{ClO}_4)_2/n\text{Bu}_4\text{NCl}$  mixture for his determinations and cautioned that the ionic strength changes in the resulting solutions need to be taken into account. When  $\text{Ca}(\text{ClO}_4)_2$  alone was used with **21** however, no chemical shift changes could be discerned.

### 2.4.1.2 Complexation of macrocyclic amide **21** with anhydrous SrCl<sub>2</sub>

Since SrCl<sub>2</sub> showed significant chemical shift changes in the saturated solution study, a similar binding constant determination was also conducted using a 9:1 CDCl<sub>3</sub>:DMSO-*d*<sub>6</sub> solvent mixture. Figure 2.19 shows the titration spectra for **21** with strontium chloride (SrCl<sub>2</sub>). It can be seen that by increasing the added amounts of SrCl<sub>2</sub> to the solution of **21** a downfield chemical shift change occurs for both the triplet signals due to the NH protons and also the aromatic intra-annular proton singlet signals. The NH signals shifted downfield from 7.67 ppm to 8.43 ppm, whereas the singlet also shifted downfield from 8.21 ppm to 8.50 ppm (Table 2.5), indicating that complexation occurred between macrocycle **21** and SrCl<sub>2</sub>.

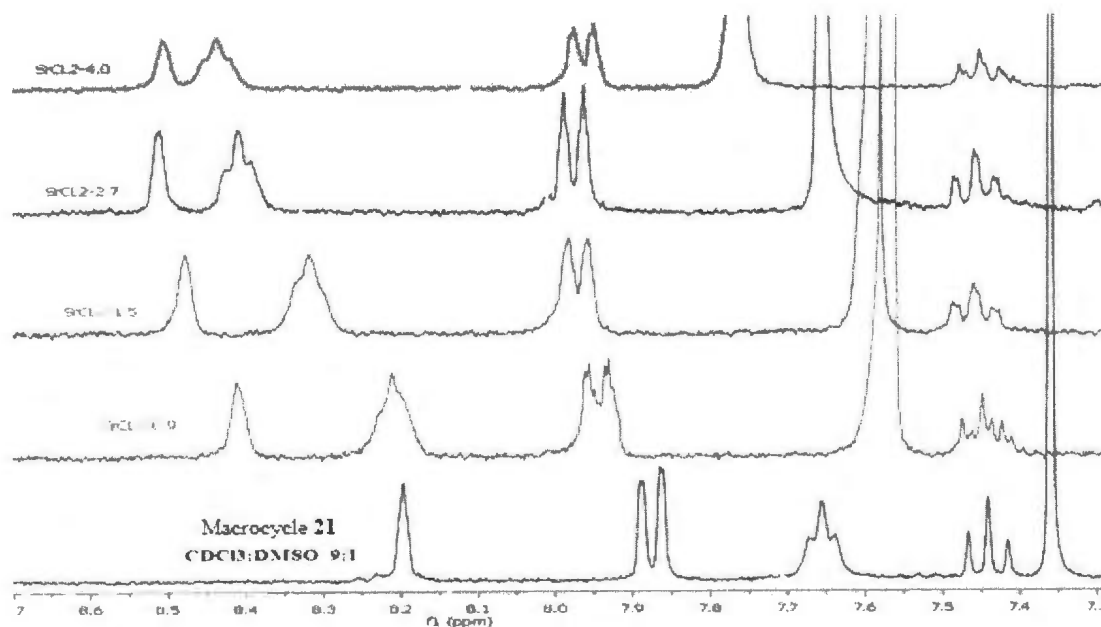


**Figure 2.19.** Expanded <sup>1</sup>H NMR (300 MHz) titration spectra of macrocyclic amide **21** with anhydrous SrCl<sub>2</sub>.

The extent of this complexation was determined as before, by measuring the  $K_{assoc}$  values, using the non-linear 1:1 binding isotherm for both the NH and aromatic intramolecular proton singlet chemical shift changes (Table 2.5). Using the Origin program the concentration of the guest ( $[Guest]$ ) was plotted against the observed chemical shift change ( $\Delta\delta$ ) in Hz. The  $K_{assoc}$  values were determined to be  $268 \pm 17$  and  $286 \pm 7 \text{ M}^{-1}$  respectively, based on the singlet and NH proton chemical shift changes (Figure 2.20).

**Table 2.5.**  $^1\text{H}$  NMR (300 MHz) titration chemical shift data for both singlet and NH signals of **21** ( $1.06 \times 10^{-6} \text{ M}$ ) with anhydrous  $\text{SrCl}_2$ .

Sample	Guest (g)	[Guest] (M)	[G]/[H]	Singlet $\delta$	$\Delta\delta$ Hz	NH $\delta$	$\Delta\delta$ Hz
Free host				8.210		7.670	
1	9.00E-04	5.68E-03	5	8.412	60.6	8.211	162.3
2	1.50E-03	9.46E-03	9	8.479	80.7	8.318	194.4
3	2.70E-03	1.70E-02	16	8.513	90.9	8.408	221.4
4	4.00E-03	2.52E-02	24	8.506	88.8	8.437	230.1

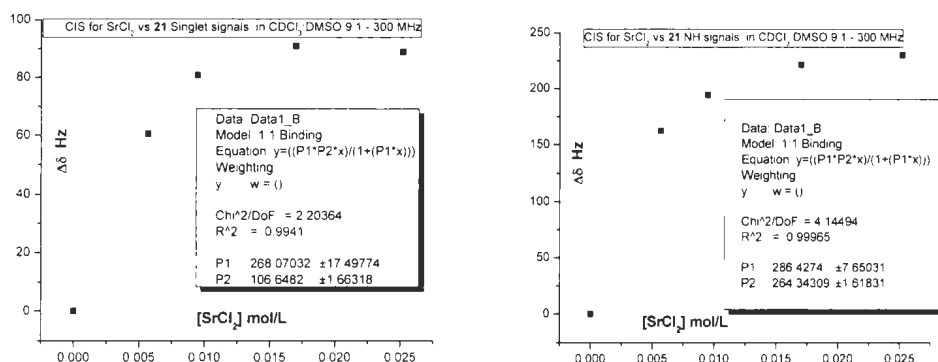


**Figure 2.20.**  $^1\text{H}$  NMR (300 MHz) titration curves for both singlet and NH signals of **21** ( $1.06 \times 10^{-6} \text{ M}$ ) with anhydrous  $\text{SrCl}_2$ .

#### 2.4.2 ESI-mass spectrometry of macrocyclic amide **21** with metal chlorides

A study of the complexation of macrocycle **21** with  $\text{CaCl}_2$  and  $\text{SrCl}_2$  was determined qualitatively using ESI-mass spectrometry in both positive and negative modes. These were conducted using an Agilent 1100 series SL LC/MSD (Trap) in the ESI mode with the following method parameters: nebulizer pressure (50 psi), drying gas flow (11 L/min), dry temperature (350 °C), for compound stability (50%), trap drive level (100%) and chloroform as a solvent.

The ESI-mass spectrometry data in the negative-ion mode of the solution of **21** with  $\text{CaCl}_2$ , which was diluted with chloroform for the MS analysis, shows mass signals at  $m/z$  647.6 corresponding to the charged host-guest complex  $[\mathbf{21}+\text{Cl}]^-$ . In positive-ion mode, signals including  $m/z$  744.8 and 799.2 corresponding to  $[\mathbf{21}+\text{CaCl}_2+\text{Na}]^+$  and  $[\mathbf{21}+\text{CaCl}_2+\text{Na}+3(\text{H}_2\text{O})]^+$  are present. The MS-MS of the  $m/z$  744.8 signal gave ions at  $m/z$  723.5  $[\mathbf{21}+\text{CaCl}_2+\text{H}]^+$  and  $m/z$  665.3  $[\mathbf{21}+3(\text{H}_2\text{O})+\text{H}]^+$  and also  $m/z$  613.3  $[\mathbf{21}+\text{H}]^+$ . The NMR and ESI-MS data, therefore, also support the contention that the  $\text{CaCl}_2$  is being complexed by **21** as an ion-triplet.

The ESI-MS of the solutions of **21** with  $\text{SrCl}_2$  also revealed analogous mass signals. In the negative-ion mode a mass signal at  $m/z$  647.6 again corresponding to the molecular ion of  $[\mathbf{21}+\text{Cl}]^-$  and in the positive-ion mode, the most prominent mass signal at  $m/z$  893.0 corresponds to  $[\mathbf{21}+\text{SrCl}_2+5(\text{H}_2\text{O})+\text{CH}_3\text{OH}+\text{H}]^+$  indicating that  $\text{SrCl}_2$  is also associated as an ion triplet with macrocycle **21**. The MS-MS of the  $m/z$  893.0 peak includes ions centred around those at  $m/z$  806.6, 769.8 and 711.7 corresponding to

$[\mathbf{21}+\text{SrCl}_2+2(\text{H}_2\text{O})+\text{H}]^+$ ,  $[\mathbf{21}+\text{SrCl}_2+\text{H}]^+$  and  $[\mathbf{21}+2(\text{H}_2\text{O})+2(\text{CH}_3\text{OH})+\text{H}]^+$  respectively, confirming this. It is presumed that the methanol originated from the eluent solvent used to purify **21**.

The positive-mode ESI-MS of the Group 1 metal salts with **21**, were not unequivocal with the limitations of the instrument to be factored in: with LiCl and NaCl, signals corresponding to  $[\mathbf{21}+\text{Li}]^+$  and  $[\mathbf{21}+\text{Na}]^+$  at  $m/z$  619.4 and 635.4, respectively, were present, but signals corresponding to the ditopic species were not obvious. With all three metals, however, masses corresponding to **21** plus  $\text{Cl}^-$  in the ESI-MS negative-ion mode were present as the major signals.

#### 2.4.3 Complexation of macrocycles **20** and **21** with tetrabutylammonium salts

A study of the complexation of **21** with several tetrabutylammonium salts (TBAX; X = halide;  $\text{BF}_4^-$  or  $\text{PF}_6^-$ ) was also undertaken to evaluate the effect of the different anions.

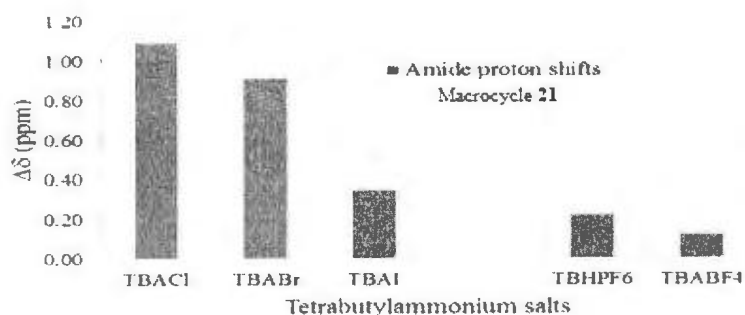


**Figure 2.21.** Downfield NH  $^1\text{H}$  NMR (500 MHz) chemical shift changes for saturated solutions of **21** in 9:1  $\text{CDCl}_3$ : $\text{DMSO}-d_6$  saturated with TBA salts.

Figure 2.21 shows the relative changes for each of the TBAX salts tested as saturated solutions, using the 9:1 CDCl<sub>3</sub>:DMSO-*d*<sub>6</sub> solvent mixture, by analogy with the approach used for the metal halides whose data is shown in Figure 2.21.

Again, the chloride salt showed the largest relative chemical shift changes for the NH protons. Since these TBA salts and also **21** were soluble in CDCl<sub>3</sub>, binding studies were conducted in this solvent. The chemical shift changes for the NH signals of **21** with CaCl<sub>2</sub> and TBACl (saturated solutions) were similar, suggesting a similar mode of binding of the chloride anion as an associated cation-anion complex with the macrocycle. In all cases there was no evidence to support any 2:1 binding as determined by subjecting the complexation data to the corresponding 2:1 binding isotherm analyses.<sup>2</sup>

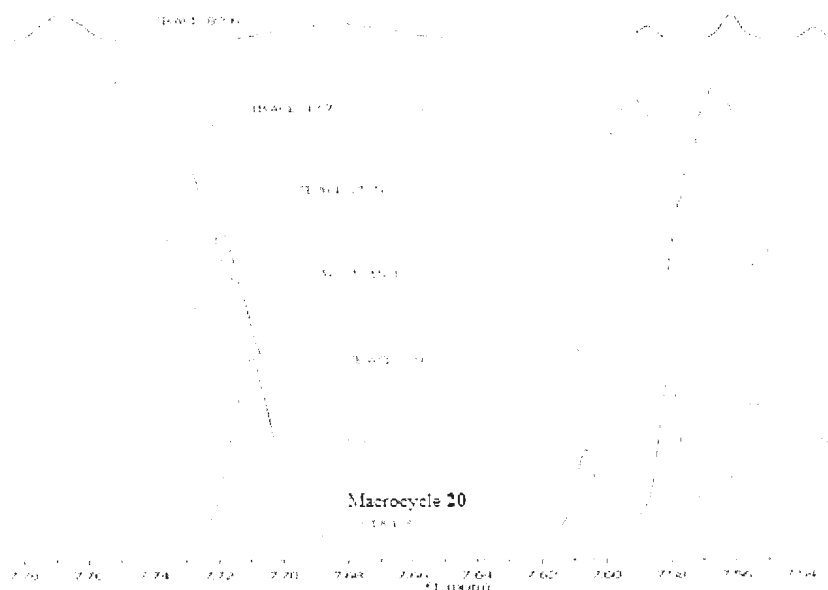


**Figure 2.22.** Expanded <sup>1</sup>H NMR (300 MHz) titration spectra of macrocyclic amide **20** with TBACl.

In contrast with the [2+2] macrocycle **21**, the [1+1] macrocycle **20** showed negligible chemical shift changes with TBACl under similar conditions (Figure 2.22).

#### 2.4.3.1 Complexation of macrocyclic amide **21** with tetrabutylammonium chloride

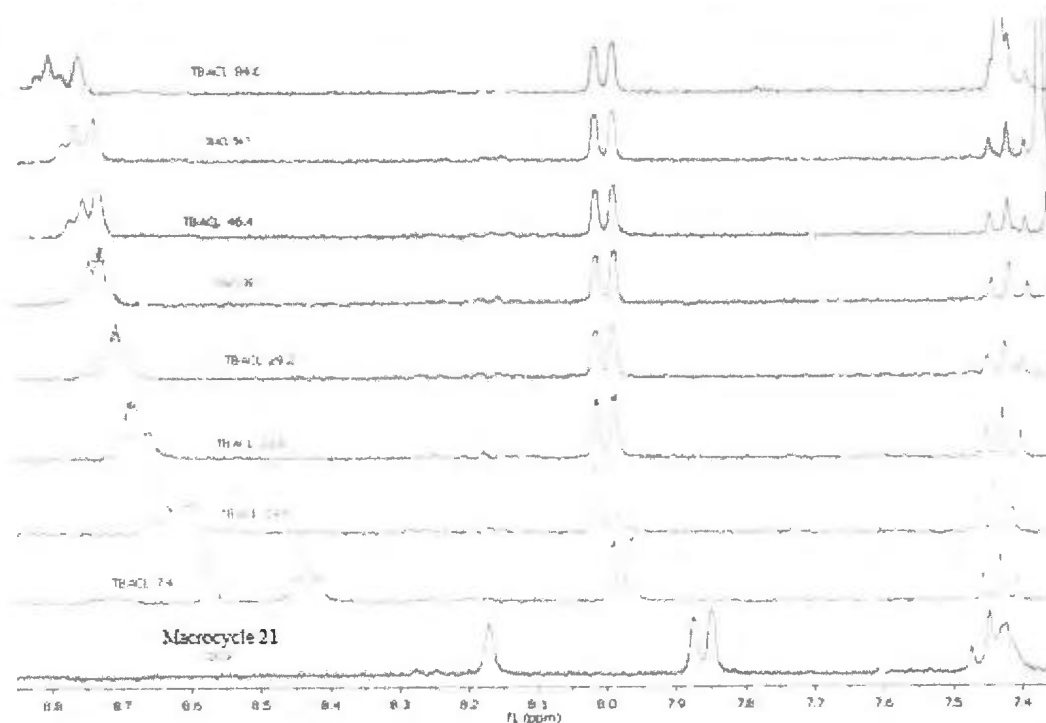


**Figure 2.23.** Expanded  $^1\text{H}$  NMR (300 MHz) titration spectra of macrocyclic amide **21** with TBACl.

Figure 2.23 shows the titration spectra for **21** with tetrabutylammonium chloride (TBACl) in  $\text{CDCl}_3$ . Increasing the added amounts of TBACl to the solution of **21** results in a downfield chemical shift change occurs for both the triplet signals due to the NH protons and also the aromatic intra-annular proton singlet signals. The NH signals shifted downfield from 7.72 ppm to 8.81 ppm, whereas the singlet also shifted downfield from 8.19 ppm, to 8.77 ppm (Table 2.6), indicating that complexation occurred between

macrocycle **21** and TBACl.

The extent of this complexation was determined as before, by measuring the  $K_{assoc}$  values using the non-linear 1:1 binding isotherm for both the NH and aromatic intramolecular proton singlet chemical shift changes in **21** (Table 2.6). The resulting  $K_{assoc}$  values were  $65 \pm 2$  and  $95 \pm 2 \text{ M}^{-1}$  respectively, based on the singlet and NH proton chemical shift changes (Figure 2.24).

**Table 2.6.** Expanded  $^1\text{H}$  NMR (300 MHz) titration chemical shift data of **21** ( $1.70 \times 10^{-6}$  M) with TBACl.

Sample	Guest (g)	[Guest] M	[G]/[H]	Singlet $\delta$	$\Delta\delta$ Hz	NH $\delta$	$\Delta\delta$ Hz
<b>Free host</b>				<b>8.19</b>	<b>0</b>	<b>7.42</b>	<b>0</b>
1	7.40E-03	2.66E-02	16	8.57	114	8.44	306
2	1.46E-02	5.25E-02	31	8.66	141	8.62	360
3	2.26E-02	8.13E-02	48	8.69	150	8.68	378
4	2.92E-02	1.05E-01	62	8.7	153	8.71	387
5	3.93E-02	1.41E-01	83	8.73	162	8.75	399
6	4.64E-02	1.67E-01	98	8.74	165	8.76	402
7	5.47E-02	1.97E-01	116	8.74	165	8.77	405
8	8.46E-02	3.04E-01	179	8.77	174	8.81	417

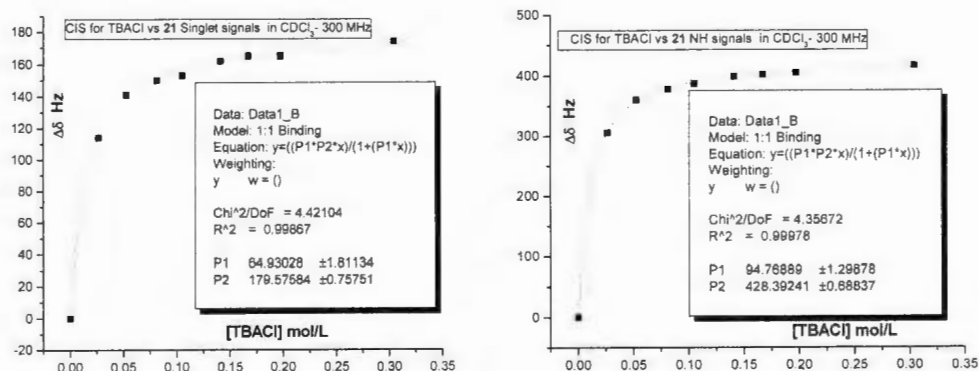


**Figure 2.24.** <sup>1</sup>H NMR (300 MHz) titration curves for both singlet and NH signals of **21** ( $1.70 \times 10^{-6}$  M) with TBACl.

#### 2.4.3.2 Complexation of macrocyclic amide **21** with tetrabutylammonium bromide

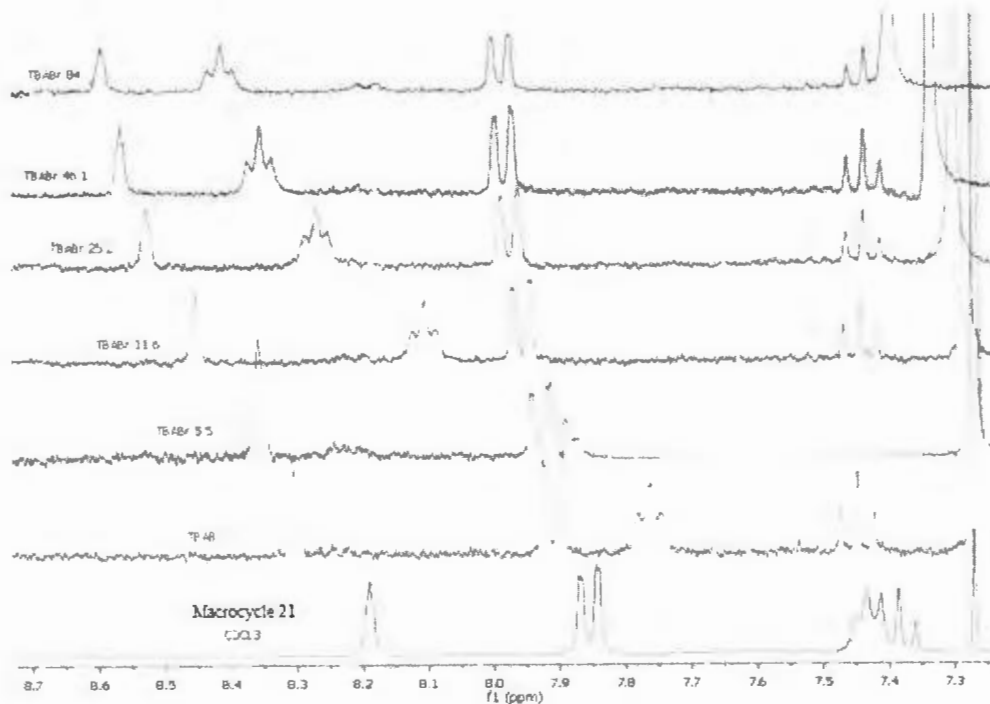


**Figure 2.25.** Expanded <sup>1</sup>H NMR (300 MHz) titration spectra of macrocyclic amide **21** with TBABr.

The titration spectra of macrocyclic **21** with tetrabutylammonium bromide (TBABr) are shown in Figure 2.25. Increasing the added amounts of TBABr to the solution of **21** results in downfield chemical shift changes for both the triplet NH and aromatic intra-annular proton singlet signals. The NH signal shifted from 7.42 ppm to 8.42 ppm, whereas the singlet signal shifted from 8.19 ppm to 8.60 ppm (Table 2.7) indicating the complexation between **21** and TBABr.

The  $K_{assoc}$  values using the non-linear 1:1 binding isotherm for both the NH and aromatic intra-annular proton singlet chemical shift changes (Table 2.7), were determined to be  $36 \pm 1$  and  $46 \pm 0.5 \text{ M}^{-1}$  respectively (Figure 2.26).

**Table 2.7.**  $^1\text{H}$  NMR (300 MHz) titration chemical shift data for both singlet and NH signals of **21** ( $9.35 \times 10^{-7} \text{ M}$ ) with TBABr.

Sample	Guest (g)	[Guest] M	[G]/[H]	Singlet $\delta$	$\Delta\delta$ Hz	NH $\delta$	$\Delta\delta$ Hz
Free host				8.19	0	7.42	0
1	3.30E-03	1.02E-02	11	8.31	36	7.76	102
2	5.50E-03	1.71E-02	18	8.36	51	7.89	141
3	1.16E-02	3.60E-02	38	8.45	78	8.11	207
4	2.52E-02	7.82E-02	84	8.53	102	8.27	255
5	4.61E-02	1.43E-01	153	8.57	114	8.36	282
6	8.40E-02	2.61E-01	279	8.60	123	8.42	300

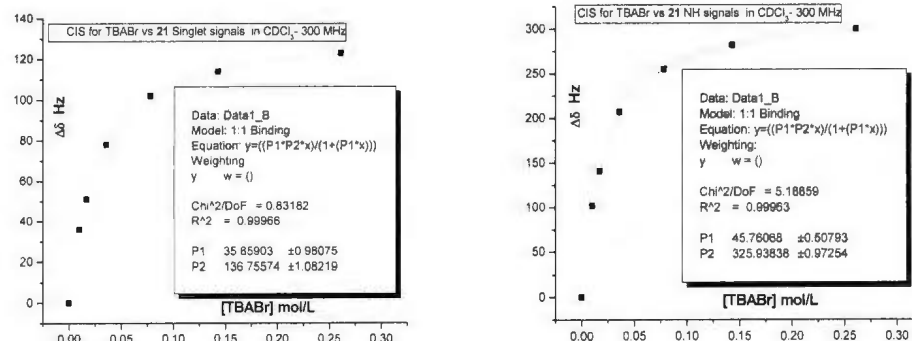


**Figure 2.26.** <sup>1</sup>H NMR (300 MHz) titration curves for both singlet and NH signals of **21** ( $9.35 \times 10^{-7}$  M) with TBABr.

#### 2.4.3.3 Complexation of macrocyclic sulfonamide **21** with TBAI

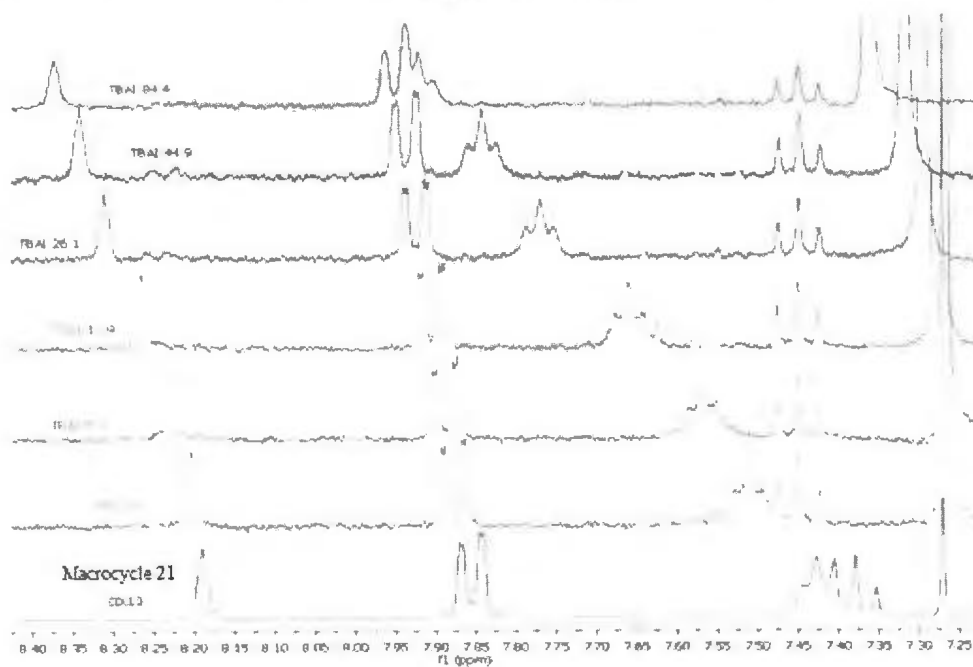


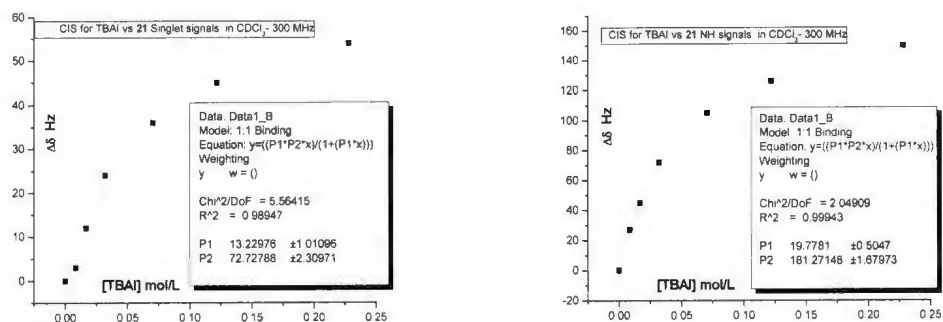
**Figure 2.27.** Expanded <sup>1</sup>H NMR (300 MHz) titration spectra of macrocyclic amide **21** with TBAI.

The titration spectra of macrocyclic **21** with tetrabutylammonium iodide (TBAI) are shown in Figure 2.27. Increasing the added amount of TBAI to a solution of macrocycle **21** results in downfield chemical shift changes for both the triplet (NH) and aromatic intra-annular proton singlet signals. The NH signals shifted from 7.42 ppm to 7.92 ppm, whereas the singlet shifted from 8.19 ppm to 8.37 ppm (Table 2.8) indicating complexation between **21** and TBAI.

The extent of this complexation was determined as before, and were determined to be  $13 \pm 1$  and  $20 \pm 0.5 \text{ M}^{-1}$  respectively, based on the singlet and NH proton chemical shift changes (see Figure 2.28 and Table 2.8).

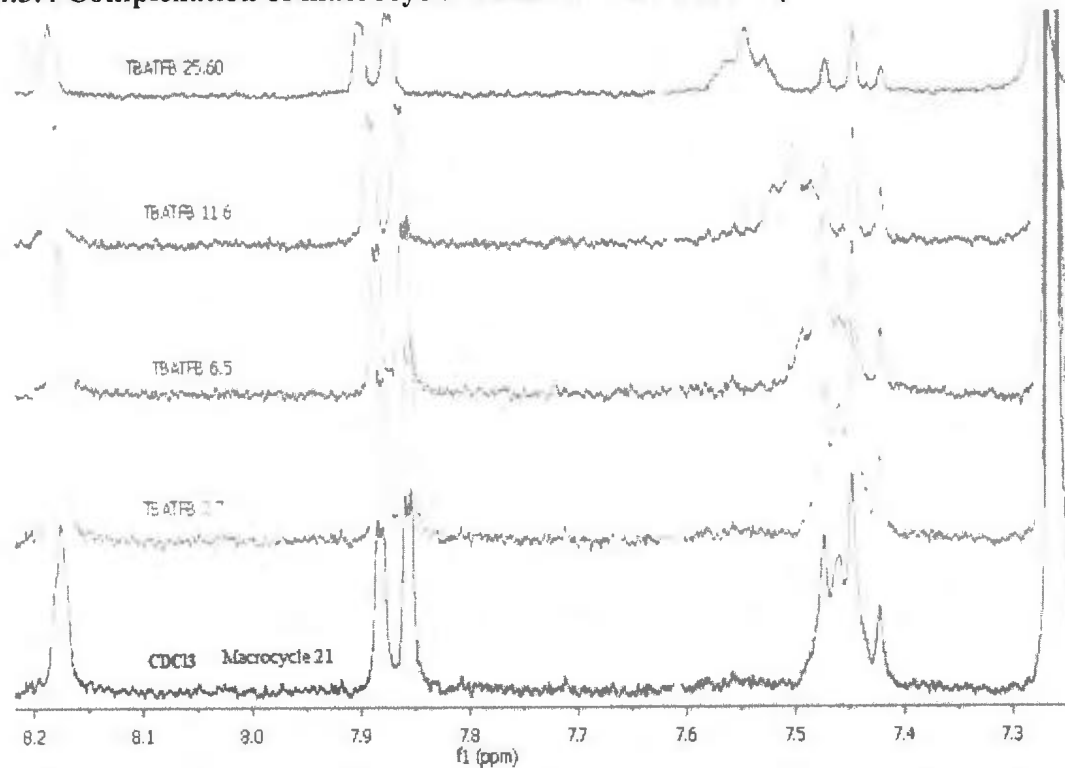
**Table 2.8.**  $^1\text{H}$  NMR (300 MHz) titration chemical shift data for both singlet and NH signals of **21** ( $9.35 \times 10^{-7} \text{ M}$ ) with TBAI.

Sample	Guest (g)	[Guest] M	[G]/[H]	Singlet $\delta$	$\Delta\delta$ Hz	NH $\delta$	$\Delta\delta$ Hz
Free host				8.19	0	7.42	0
1	3.20E-03	8.66E-03	9	8.2	3	7.51	27
2	6.20E-03	1.68E-02	18	8.23	12	7.57	45
3	1.19E-02	3.22E-02	34	8.27	24	7.66	72
4	2.61E-02	7.07E-02	76	8.31	36	7.77	105
5	4.49E-02	1.22E-01	130	8.34	45	7.84	126
6	8.44E-02	2.28E-01	244	8.37	54	7.92	150



**Figure 2.28.** <sup>1</sup>H NMR (300 MHz) titration curves for both singlet and NH signals of **21** (9.35 x 10<sup>-7</sup> M) with TBAI.

#### 2.4.3.4 Complexation of macrocyclic amide **21** with TBABF<sub>4</sub>



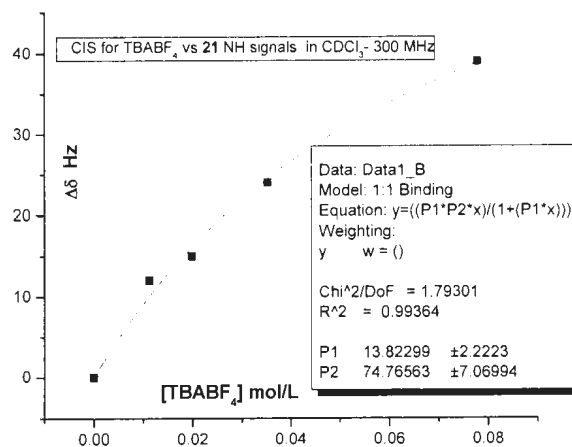
**Figure 2.29.** Expanded <sup>1</sup>H NMR (300 MHz) titration spectra of macrocyclic amide **21** with TBABF<sub>4</sub>.

Figure 2.29 shows the titration spectra for **21** with tetrabutylammonium tetrafluoroborate (TBABF<sub>4</sub>) in CDCl<sub>3</sub>. Increasing the added amounts of TBABF<sub>4</sub> to the solution of **21** causes the NH signals to be shifted downfield from 7.42 ppm to 7.60 ppm, whereas the singlet did not show any change (Table 2.9).

The extent of this complexation was determined as before, by measuring the  $K_{assoc}$  values, using the non-linear 1:1 binding isotherm for the NH chemical shift changes (Table 2.9). Using the Origin program the concentration of the guest ([Guest]) was plotted against the chemical shift changes ( $\Delta\delta$ ) in Hz. The  $K_{assoc}$  value was determined to be  $13 \pm 2 \text{ M}^{-1}$  based on the NH proton chemical shift changes (Figure 2.30).

**Table 2.9.** <sup>1</sup>H NMR (300 MHz) titration chemical shift data for both singlet and NH signals of **21** ( $9.35 \times 10^{-7} \text{ M}$ ) with TBABF<sub>4</sub>.

Sample	Guest (g)	[Guest] M	[G]/[H]	NH $\delta$	$\Delta\delta$ Hz
<b>Free host</b>				<b>7.42</b>	<b>0</b>
1	3.70E-03	1.12E-02	12	7.46	12
2	6.50E-03	1.98E-02	21	7.47	15
3	1.16E-02	3.53E-02	38	7.5	24
4	2.56E-02	7.78E-02	83	7.55	39



**Figure 2.30.**  $^1\text{H}$  NMR (300 MHz) titration curve for NH signal of **21** ( $9.35 \times 10^{-7}$  M) with TBABF<sub>4</sub>.

#### 2.4.4 ESI-mass spectrometry data of macrocyclic amide **21** with TBAX

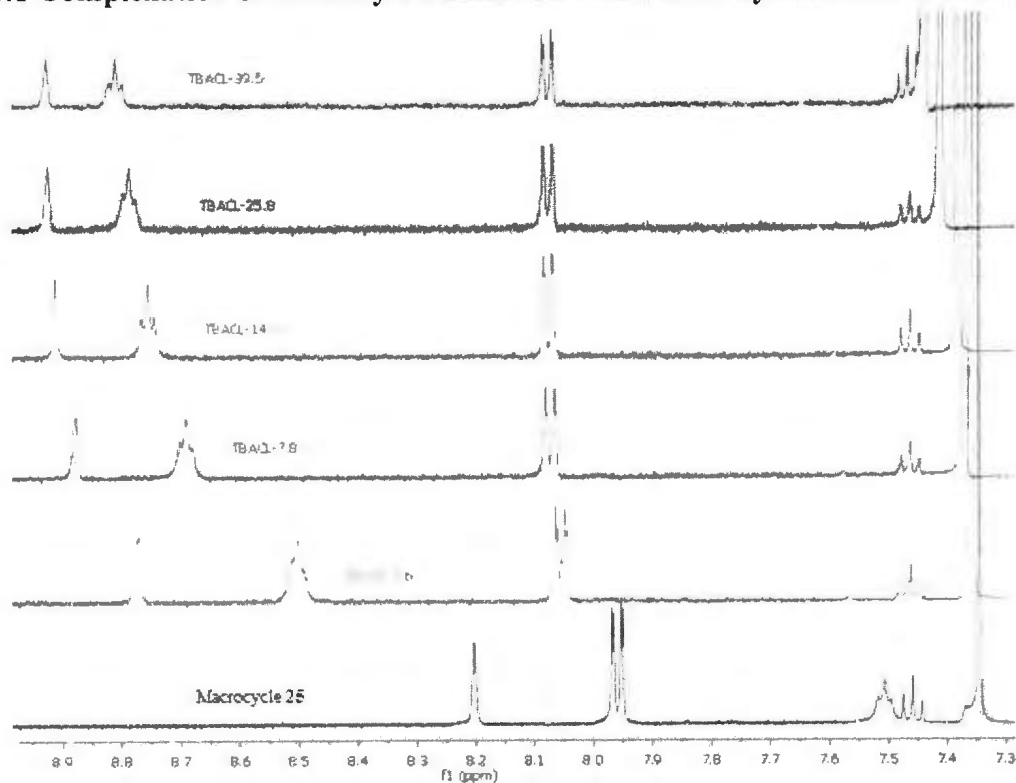
Studies of the complexation of macrocycle **21** with tetrabutylammonium salts were determined qualitatively using ESI-mass spectra in both positive and negative mode, which were conducted using an Agilent 1100 series SL LC/MSD (Trap) in the ESI mode with the following method parameters: Nebulizer (50 psi), dry gas (11 L/min), dry temperature (350 °C), for compound stability (50%), trap drive level (100%) and chloroform as a solvent. Unexpectedly, however, the ESI-MS spectra in the positive-ion mode did not reveal any mass signals corresponding to a TBACl:**21** complex, but only a mass corresponding to  $[\text{TBA}+\mathbf{21}]^+$  at  $m/z$  855.1. In the negative-ion mode a signal could be seen at  $m/z$  647.6 corresponding to  $[\mathbf{21}+\text{Cl}]^-$ . With the exception of the TBAPF<sub>6</sub>, the ESI-MS of the other TBA salts showed the presence of signals corresponding to the masses of the host plus the associated ion-pairs: e.g.  $m/z$  932.9 for  $[\mathbf{21}+\text{TBABr}+\text{H}]^+$ ;  $m/z$

1126.8 for  $[\mathbf{21} + \text{TBAI}_2 + \text{H}_2\text{O} + \text{H}]^+$  and 1131 for  $[\text{TBAI}_2 + \text{Na}]^+$  and  $m/z$  959.0 for  $[\mathbf{21} + \text{TBABF}_4 + \text{H}]^+$  in the positive-ion mode. In the negative ion mode the masses corresponding to  $[\mathbf{21} + \text{X}]^-$  are observed for the respective cases where  $\text{X} = \text{Br}^-$ ,  $\text{I}^-$  or  $\text{BF}_4^-$ .

#### 2.4.5 Complexation of macrocyclic amide **25** with tetrabutylammonium salts

For the [1+1] macrocyclic compound **24**, no changes were observed with TBAX salts or with the metal halides. Subsequent complexation studies were therefore conducted only with the [2+2] compound, **25**.

##### 2.4.5.1 Complexation of macrocyclic amide **25** with tetrabutylammonium chloride



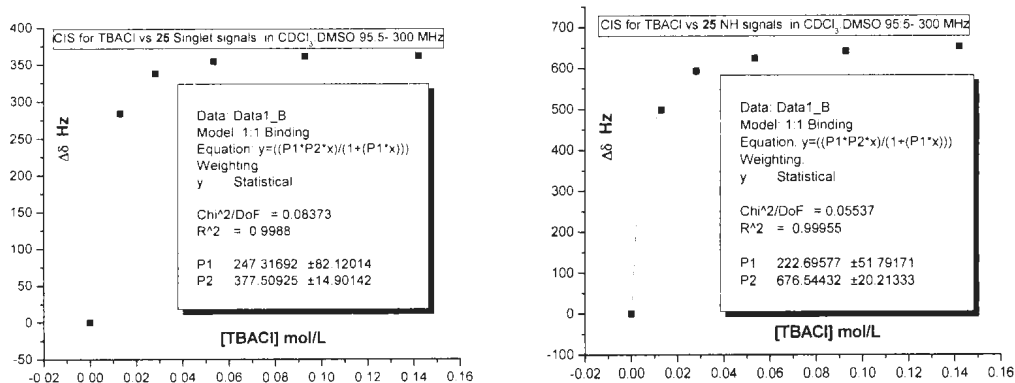
**Figure 2.31.** Expanded  $^1\text{H}$  NMR (500 MHz) titration spectra of macrocyclic amide **25** with TBACl.

Figure 2.31 shows the titration spectra for **25** with tetrabutylammonium chloride (TBACl) using 95:5 CDCl<sub>3</sub>:DMSO-*d*<sub>6</sub> solvent mixture. It can be seen that by increasing the added amounts of TBACl to the solution of **25** a downfield chemical shift change occurs for both the triplet signals due to the NH protons and also the aromatic intra-annular proton singlet signals. The NH signals shifted downfield from 7.51 ppm to 8.81 ppm, whereas the singlet also shifted downfield from 8.20 ppm, to 8.93 ppm (Table 2.10), indicating that complexation occurred between macrocycle **25** and TBACl.

The association constants ( $K_{assoc}$ ), were determined using the non-linear 1:1 binding isotherms for both the NH and aromatic intra-annular proton singlet chemical shift changes (Table 2.10). Using the Origin program the molar concentrations of the guest ([Guest]) were plotted against the observed chemical shift changes ( $\Delta\delta$ ) in Hz. The resulting  $K_{assoc}$  values were determined to be  $247 \pm 82$  and  $223 \pm 51 \text{ M}^{-1}$  respectively, based on the singlet and NH proton chemical shift changes (Figure 2.32).

**Table 2.10.** <sup>1</sup>H NMR (500 MHz) titration chemical shift data for both singlet and NH signals of **25** ( $1.39 \times 10^{-6} \text{ M}$ ) with TBACl.

Sample	Guest (g)	[Guest] M	[G]/[H]	Singlet $\delta$	$\Delta\delta$ Hz	NH $\delta$	$\Delta\delta$ Hz
Free host				8.204		7.505	
1	3.60E-03	1.30E-02	9	8.772	284	8.502	498.5
2	7.80E-03	2.81E-02	20	8.879	337.5	8.691	593
3	1.48E-02	5.33E-02	38	8.912	354	8.754	624.5
4	2.58E-02	9.28E-02	67	8.926	361	8.789	642
5	3.95E-02	1.42E-01	102	8.927	361.5	8.812	653.5



**Figure 2.32.** <sup>1</sup>H NMR (500 MHz) titration curves for both singlet and NH signals of **25** ( $1.39 \times 10^{-6}$  M) with TBACl.

#### 2.4.5.2 Complexation of macrocyclic amide **25** with tetrabutylammonium bromide

The titration spectra of macrocycle **25** with tetrabutylammonium bromide (TBABr) are shown in Figure 2.33. Increasing the added amounts of TBABr to the solution of **25** in a 95:5 CDCl<sub>3</sub>:DMSO-*d*<sub>6</sub> solvent mixture, results in downfield chemical shift changes for both the triplet NH and aromatic intra-annular proton singlet signals. The NH signal shifted from 7.51 ppm to 8.32 ppm, whereas the singlet signal shifted from 8.20 ppm to 8.67 ppm (Table 2.11) indicating the complexation between **25** and TBABr.

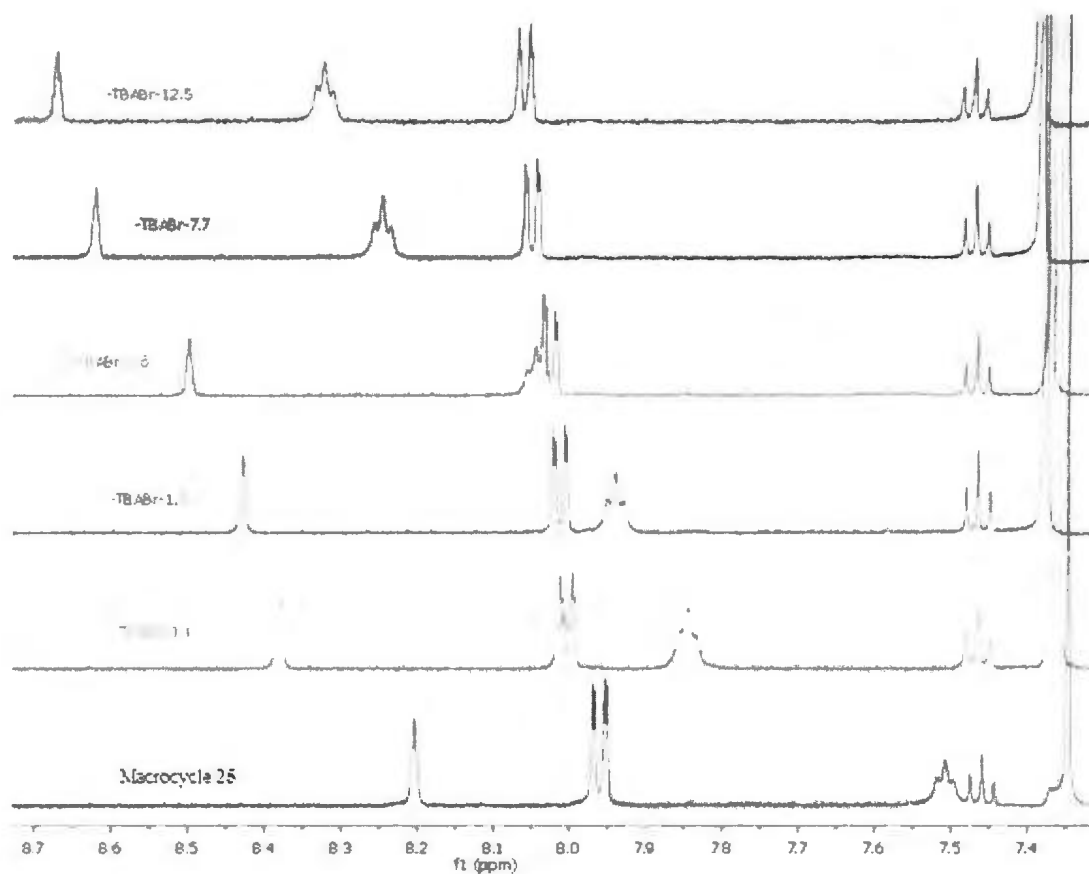


**Figure 2.33.** Expanded  $^1\text{H}$  NMR (500 MHz) titration spectra of macrocyclic amide **25** with TBABr.

The association constants, as in all cases previously described, were determined using the non-linear 1:1 binding isotherm for both the NH and aromatic intra-annular proton singlet chemical shift changes (Table 2.11). Using the Origin program, the concentrations of the guest ( $[\text{Guest}]$ ) were plotted against the observed chemical shift changes ( $\Delta\delta$ ) in Hz. The  $K_{\text{assoc}}$  values were determined to be  $174 \pm 39$  and  $215 \pm 38 \text{ M}^{-1}$  respectively, based on the singlet and NH proton chemical shift changes (Figure 2.34).

**Table 2.11.** Expanded  $^1\text{H}$  NMR (300 MHz) titration chemical shift data of **25** ( $1.39 \times 10^{-6}$  M) with TBABr.

Sample	Guest (g)	[Guest]	[G]/[H]	Singlet $\delta$	$\Delta\delta$ Hz	NH $\delta$	$\Delta\delta$ Hz
Free host				<b>8.204</b>		<b>7.505</b>	
1	1.30E-03	4.03E-03	3	8.429	112.5	7.941	218
2	2.60E-03	8.07E-03	6	8.499	147.5	8.045	270
3	7.70E-03	2.39E-02	17	8.621	208.5	8.247	371
4	1.25E-02	3.88E-02	28	8.671	233.5	8.324	409.5

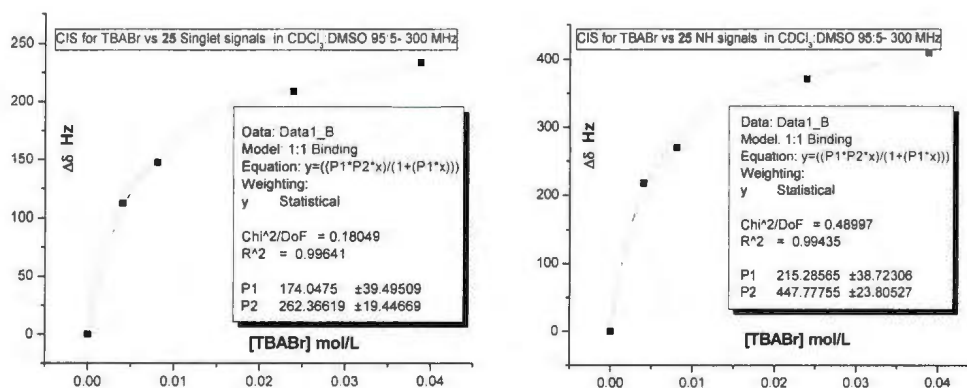


**Figure 2.34.**  $^1\text{H}$  NMR (300 MHz) titration curves for both singlet and NH signals of **25** ( $1.39 \times 10^{-6}$  M) with TBABr.

#### 2.4.5.3 Complexation of macrocyclic amide **25** with tetrabutylammonium iodide

The titration spectra of macrocyclic **25** with tetrabutylammonium iodide (TBAI) are shown in Figure 2.35. Increasing the added amounts of TBAI to the solution of **25** in the 95:5 CDCl<sub>3</sub>:DMSO-*d*<sub>6</sub> solvent mixture, results in downfield chemical shift changes for both the triplet NH and aromatic intra-annular proton singlet signals. The NH signal

shifted from 7.51 ppm to 7.85 ppm, whereas the singlet signal shifted from 8.20 ppm to 8.41 ppm (Table 2.12).

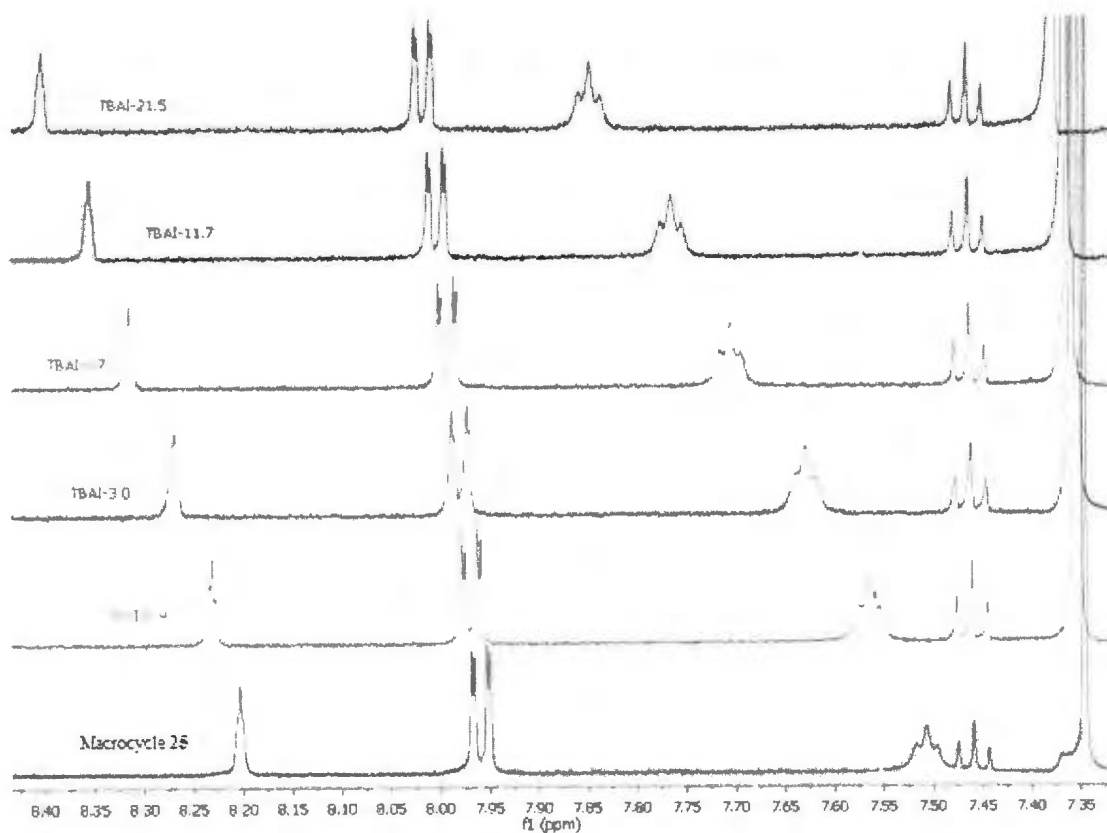
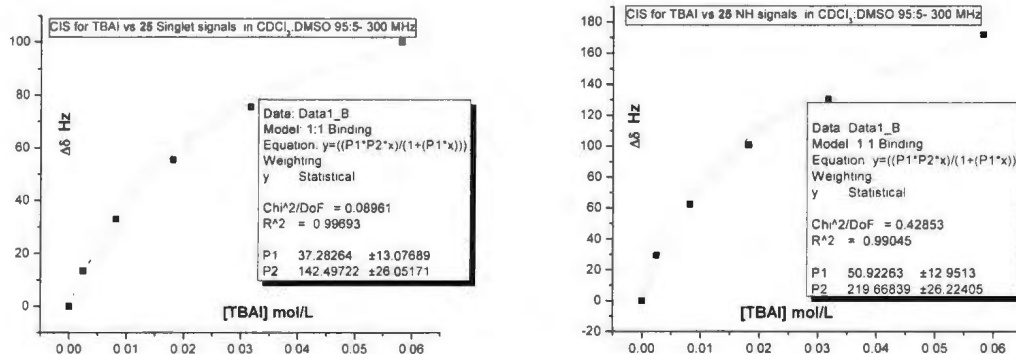


**Figure 2.35.** Expanded  $^1\text{H}$  NMR (500 MHz) titration spectra of macrocyclic amide **25** with TBAI.

The association constants, as before, were determined using the non-linear 1:1 binding isotherm for both the NH and aromatic intra-annular proton singlet chemical shift changes (Table 2.12). Using the Origin program the concentrations of the guest ( $[\text{Guest}]$ ) were plotted against the observed chemical shift changes ( $\Delta\delta$ ) in Hz. The  $K_{\text{assoc}}$  values were determined to be  $37 \pm 13$  and  $51 \pm 13 \text{ M}^{-1}$  respectively, based on the singlet and NH proton chemical shift changes (Figure 2.36).

**Table 2.12.**  $^1\text{H}$  NMR (500 MHz) titration chemical shift data for both singlet and NH signals of **25** ( $1.39 \times 10^{-6}$  M) with TBAI.

Sample	Guest (g)	[Guest] M	[G]/[H]	Singlet $\delta$	$\Delta\delta$ Hz	NH $\delta$	$\Delta\delta$ Hz
Free host				<b>8.204</b>		<b>7.505</b>	
1	9.00E-04	2.44E-03	2	8.231	13.5	7.564	29.5
2	3.00E-03	8.12E-03	6	8.27	33	7.63	62.5
3	6.70E-03	1.81E-02	13	8.315	55.5	7.707	101
4	1.17E-02	3.17E-02	23	8.355	75.5	7.766	130.5
5	2.15E-02	5.82E-02	42	8.404	100	7.849	172

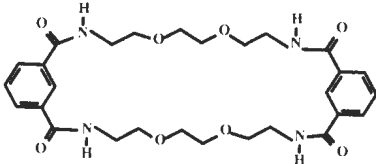
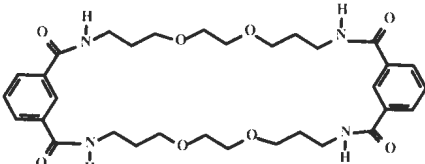


**Figure 2.36.**  $^1\text{H}$  NMR (500 MHz) titration curves for both singlet and NH signals of **25** ( $1.39 \times 10^{-6}$  M) with TBAI.

#### 2.4.6 Comparison between the $K_{assoc}$ values of macrocycles **21** and **25** with TBAX salts

A comparison between the association constant values measured for the complexation of macrocycles **21** and **25** with TBAX salts is summarized in Table 2.13. The  $K_{assoc}$  values for **25** compared with those of macrocycle **21** are nearly 3-, 5- and 2.5-fold higher for the  $\text{Cl}^-$ ,  $\text{Br}^-$  and  $\text{I}^-$  salts respectively.

**Table 2.13.**  $K_{assoc}$  values of macrocycles **21** and **25** with TBAX (X= halide) salts.

TBAX	$K_{assoc}$ ( $M^{-1}$ )	Macrocycle <b>25</b> 	Macrocycle <b>21</b> 
TBACl		235	80
TBABr		195	41
TBAI		44	17

There are several possible factors which could account for these differences between **25** and **21**. Firstly, it should be recalled (*see* Figure 2.4) that the mode of complexation of the halide ion is presumed to be *via* hydrogen-bonding between the halide ions and the protons of the NH groups and as found by others in similar studies, the trend is:  $Cl^- > Br^- > I^-$ . The tetrabutylammonium ion is non-coordinating so it is presumed that the ether oxygen atoms are not significant in the cases of the TBAX salts as compared with the metal halides. Since presumably the distances between the NH groups in the two macrocycles are not different, a factor that could be more significant is the difference in the ring sizes leading to more conformational possibilities and a larger entropic effect therefore which needs to be overcome in the case of **21**.

## 2.5 Uranium complex

In connection with these studies on the metal-binding properties of the macrocyclic polyamide compounds reported in this Chapter, we were particularly interested in determining whether our polyamides, by analogy with salen-*N,N'*-ethylenebis(salicylimine) compounds,<sup>34,35</sup> could form stable complexes with the uranyl ion. While studying the complexation behavior of the [2+2] macrocyclic tetraamide **21** with  $\text{UO}_2(\text{AcO})_2$  (uranyl acetate), it was noticed that light yellow crystals formed which initially were thought to be the complex of **21** with uranyl acetate. Unexpectedly, however, a new uranyl acetate complex **38** (Figure 2.37) was formed. When the same experiment was repeated but without using macrocyclic **21**, the same complex was obtained. The X-ray structure was solved by Dr. Louise Dawe of this Department and was published in *Acta Cryst.* **2011**, *E67*, 1880–1881 and her report is summarized below:

The complex was found to be a centrosymmetric tetramer,  $[\text{U}_4(\text{C}_2\text{H}_3\text{O}_2)_4\text{O}_{10}(\text{H}_2\text{O})_4] \cdot 2\text{CH}_4\text{O}$ , which has a near planar core [maximum deviation from the least squares plane of 0.294 (6) Å]. It consisted of two hexagonal-bipyramidally coordinated  $\text{U}^{\text{VI}}$  atoms connected *via*  $\mu_2$ -O (acetate) and  $\mu_3$ -O (oxide) bridges in the equatorial plane to two pentagonal bipyramidally-coordinated  $\text{U}^{\text{VI}}$  atoms. The equatorial plane of each  $\text{U}^{\text{VI}}$  atom is completed by a bound water molecule, while the axial positions are occupied by uranyl ( $\text{UO}_2$ )<sup>2+</sup> O atoms. Multiple O-H $\cdots$ O hydrogen bonds are present, including a lattice methanol molecule bound to one of the pentagonal bipyramidal uranyl O atoms, as well as two different  $C^1_1(6)$  chains originating from a donor water molecule,

via a uranyl oxygen acceptor and an acetate acceptor on different, adjacent tetramers. Finally, the unit cell contains four  $U^{VI}$  tetramers, all connected by hydrogen bonding, forming a supramolecular  $R^4_4(24)$  ring.

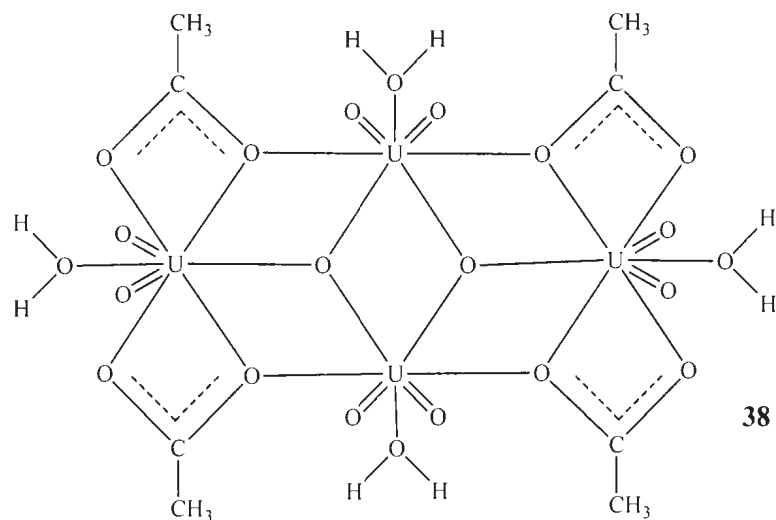


**Figure 2.37.** Tetra- $\mu_2$ -acetato-tetraaqua-di- $\mu_3$ -oxido-octa-oxido-tetrauranium (VI) methanol disolvate tetrahydrate **38**.

## 2.6 Conclusions

Several new macrocyclic amides **20-23** and **24-27** were synthesized by reacting isophthaloyldichloride (**2c**) with 1,10-diamino-4,7-dioxadecane (or “Jeffamine<sup>®</sup> EDR-176”, **19**) and 1,8-diamino-3,6-dioxaoctane (or “Jeffamine<sup>®</sup> EDR-148”, **15**) respectively. Also macrocyclic amides **36** and **37** were synthesized in a similar manner by reacting the diaryldiacyl chloride **35** with **15**, and their structures were characterized. Suitable crystals of five new macrocyclic amides **20**, **21**, **24**, **25** and **36** were obtained for single-crystal X-ray crystallography and their structures were determined. Complexation studies of tetramide macrocycles **21** and **25** with both alkali metal halides and tetrabutylammonium salts were conducted and were characterized using both <sup>1</sup>H NMR and ESI mass spectra. The association constants ( $K_{assoc}$ ) were calculated using an isothermal 1:1 binding formula according to Connors<sup>2</sup> and a using non-linear curve fitting program using the ORIGINPro 7.5 program from OriginLab Corporation.

In addition, the new isophthaloyl tetraamido macrocycle **21** complements the earlier observation by Lüning and co-workers since it is also capable of binding with CaCl<sub>2</sub> as an “ion-triplet” or tritopic receptor, and is also capable of binding with the larger SrCl<sub>2</sub> as well. No complexation was observed between uranyl acetate with the macrocyclic amide **21** reported in this chapter. A new uranyl acetate complex, **38**, however was unexpectedly formed and its X-ray structure determined. Finally, two new macrocyclic amides **36** and **37** have been synthesized by reacting diaryldiacyl chloride **35** with **15**, but their complexation properties have yet to be investigated in detail.

## Experimental

### General

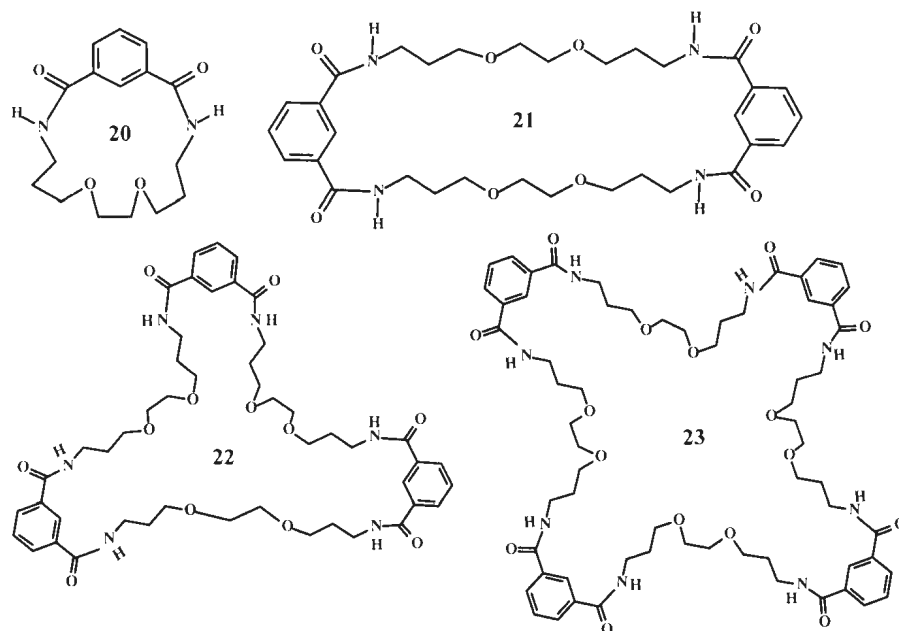
All reactions requiring anhydrous conditions were performed under a positive pressure of nitrogen using oven-dried glassware (120 °C) that was cooled under nitrogen. <sup>1</sup>H and <sup>13</sup>C NMR spectra were recorded on a Bruker AVANCE 500 MHz or 300 MHz NMR spectrometer and were referenced to the solvent (CDCl<sub>3</sub>) and TMS unless otherwise specified. Overlap may have prevented the reporting of all resonances. LC-MS and ESI-MS were conducted using a GCT Premier Micromass spectrometer, while HRMS was conducted using a MALDI-TOF spectrometer. X-ray structures were measured with a Rigaku Saturn CCD area detector equipped with a SHINE optic using Mo K $\alpha$  radiation. Silicycle Ultrapure silica gel (0-20  $\mu$ m) G and F-254 was used for the preparative-layer TLC, and Silicycle Silia-P Ultrapure Flash silica gel (40-63  $\mu$ m) was used for flash column chromatography. TLC was conducted on Polygram SIL G/UV254 precoated plastic sheets. All solvents and reagents used were either of the highest commercial grades available or were distilled. In all of the spectra which were recorded and reported in this thesis, tetramethylsilane (TMS) was used as an internal standard and CIS were referenced to TMS at  $\delta = 0.00$  ppm.

## 2.7 Experimental section

General methods, materials, and instrumentation used were identical to those described previously. The Huntsman Petrochemical Corporation is gratefully acknowledged for the generous gift of 1,8-diamino-3,6-dioxaoctane (“Jeffamine<sup>®</sup> EDR-148”) and 1,10-diamino-4,7-dioxadecane (“Jeffamine<sup>®</sup> EDR-148”).

### 2.7.1 Experimental

#### General conditions for the synthesis of macrocyclic amides 20-23

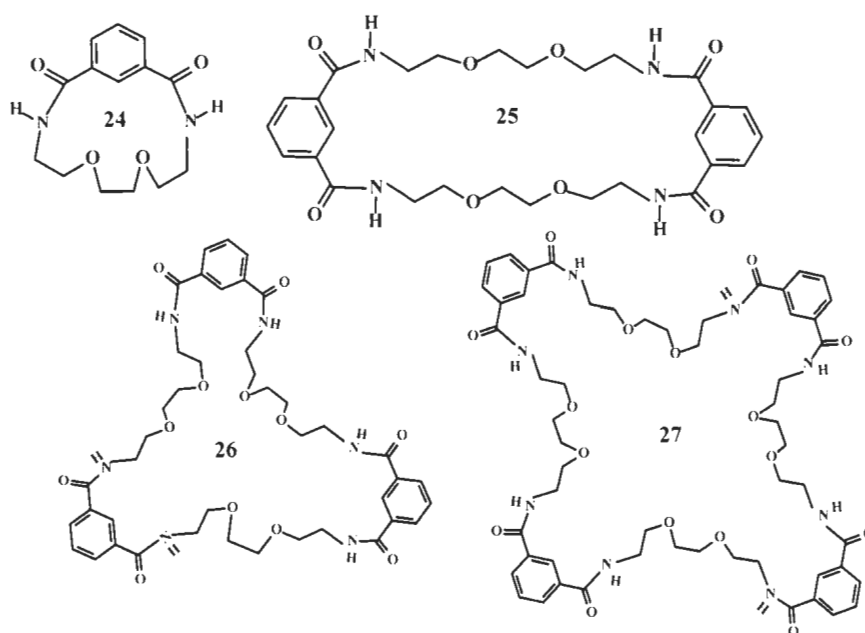


A solution of isophthaloyl dichloride (**2c**, 2.00 g, 9.85 mmol) in dry DCM (700 mL) was added dropwise over 2 h to a stirred solution of 1,10-diamino-4,7-dioxadecane (**19**), (1.76 mL, 10.0 mmol) and triethylamine (2.80 mL, 27.7 mmol) in dry DCM (2 mL) at -78 °C (Conditions “b”, Scheme 2.6) or at -100 °C (Conditions “c”, Scheme 2.6). In

each case, the reaction solutions were maintained at the respective temperatures for 2 h and then allowed to warm to room temperature, with stirring over a period of 48 h. The reaction solutions were filtered and washed with brine (3 x 100 mL) and then with water (2 x 100 mL). The extracts were dried with anhydrous MgSO<sub>4</sub> and evaporated under reduced pressure to yield yellow solids, which were purified by SiO<sub>2</sub> flash column chromatography using ethyl acetate/methanol (80:20) as eluent. Conditions “a” afforded **20** (1.03 g; 79%) as a colorless solid: mp 151-152 °C (from methanol); <sup>1</sup>H NMR (CDCl<sub>3</sub>, 300 MHz): δ 1.92-1.99 (m, 4H), 3.63-3.68 (m, 4H), 3.70 (s, 4H), 3.79 (t, *J* = 5.0 Hz, 4H); 7.58 (overlap) (t, *J* = 7.6 Hz, 3H), 7.72 (t, *J* = 2.8 Hz, 1H), 8.21 (dd, *J* = 7.6, 2.8 Hz, 2H); <sup>13</sup>C NMR (CDCl<sub>3</sub>, 75 MHz): δ 28.2, 40.6, 71.6, 73.9, 121.4, 129.6, 131.7, 134.2, 165.5; (+)-APCI-MS (*m/z*): 307.4 (M+1, 100); **21** (157 mg, 12%) as a colorless solid: mp 187-188 °C (from methanol); <sup>1</sup>H NMR (CDCl<sub>3</sub>, 300 MHz): δ 1.69-1.77 (m, 8H), 3.31-3.37 (m, 8H), 3.58 (t, *J* = 9.4 Hz, 8H), 3.62 (s, 8H), 7.43 (t, *J* = 7.6 Hz, 2H), 7.49 (t, *J* = 9.2 Hz, 4H), 7.85 (dd, *J* = 7.6 and 2.8 Hz, 4H), 8.17 (t, *J* = 2.8 Hz, 2H); <sup>13</sup>C NMR (CDCl<sub>3</sub>, 75 MHz): δ 28.7, 38.8, 70.3, 70.5, 125.5, 128.6, 129.9, 135.4, 167.1; (+)-APCI-MS (*m/z*): 613.3 (M+1, 100). Conditions “b” afforded **20** (680 mg; 52%) and **21** (602 mg; 46%) whose spectral data were identical to those obtained above. Conditions “c” afforded **20** (470 mg; 36%) ; **21** (670 mg; 51%) and **22** (80 mg, 6%) as a colorless solid: mp 223-224 °C; <sup>1</sup>H NMR (CDCl<sub>3</sub>, 500 MHz): δ 1.66-1.71 (m, 12H), 3.30-3.35 (m, 12H), 3.52 (t, *J* = 5.7 Hz, 12H), 3.60 (s, 12H), 7.44 (t, *J* = 7.5 Hz, 3H), 7.60 (t, *J* = 2.5 Hz, 6H), 7.88 (dd, *J* = 7.5, 1.4 Hz, 6H), 8.18 (t, *J* = 1.4 Hz, 3H); <sup>13</sup>C NMR (CDCl<sub>3</sub>, 75 MHz): δ 28.5,

38.7, 70.2, 70.4, 128.6, 130.0, 135.6, 167.1, 167.2; ; (+)-APCI-MS ( $m/z$ ): 920.1 (M+1, 100); and **23** (50 mg, 4%) as a colorless solid: mp 246-247°C;  $^1\text{H}$  NMR ( $\text{CD}_3\text{OD}$ , 300 MHz):  $\delta$  1.76-1.84 (m, 16H), 3.30-3.45 (m, 16H), 3.57 (t,  $J = 6.0$  Hz, 16H), 3.61 (s, 16H), 7.50 (t,  $J = 7.8$  Hz, 4H), 7.89 (dd,  $J = 7.8$  and 1.7 Hz, 8H), 8.20 (t,  $J = 1.7$  Hz, 4H);  $^{13}\text{C}$  NMR ( $\text{DMSO}-d_6$ , 75 MHz):  $\delta$  29.4, 36.8, 68.3, 69.7, 126.1, 128.4, 129.7, 134.9, 165.9; ; (+)-APCI-MS ( $m/z$ ): 1225.8 (M+1, 100).

### General conditions for the synthesis of macrocyclic amides **24-27**

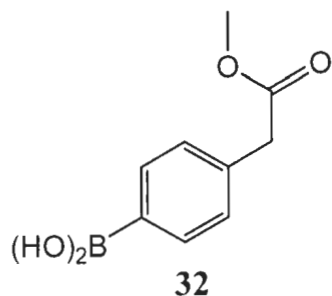


A solution of isophthaloyl dichloride (**2c**, 601 mg, 2.95 mmol) in dry DCM (500 mL) was added dropwise over 1 h to a stirred solution of 1,8-diamino-3,6-dioxadecane (**15**), (0.45 mL, 2.97 mmol) and triethylamine (0.6 mL, 60 mmol) in dry DCM (2 mL) at -78 °C (Conditions “b”, Scheme 2.7) or at -100 °C (Conditions “c”, Scheme 2.7). In each

case, the reaction solutions were maintained at the respective temperatures for 2 h and then allowed to warm to room temperature, with stirring over a period of 48 h. The reaction solutions were filtered and washed with brine (3 x 100 mL) and then with water (2 x 100 mL). The extracts were dried with anhydrous MgSO<sub>4</sub> and evaporated under reduced pressure to yield yellow solids, which were purified by SiO<sub>2</sub> flash column chromatography using ethyl acetate/methanol (85:15) as eluent. Conditions "a" afforded **24** (370 mg; 75%) as a colorless solid: mp 198-199 °C (from methanol); <sup>1</sup>H NMR (CD<sub>2</sub>Cl<sub>2</sub>, 300 MHz): δ 3.67 (t, 8H, ), 3.79 (s, 4H); 6.85 (t, *J* = 7.5 Hz, 2H), 7.61 (t, *J* = 7.5 Hz, 1H), 7.95 (d, *J* = 4.5 Hz, 2H), 8.10 (t, *J* = 4.5 Hz, 1H); <sup>13</sup>C NMR (CD<sub>2</sub>Cl<sub>2</sub>, 75 MHz): δ 39.8, 69.7, 71.4, 127.3, 130.1, 130.2, 136.9, 167.8; (+)-APCI-MS (*m/z*): 279.4 (M+1, 100); **25** (81 mg, 16%) as a colorless solid: mp 219-220 °C; <sup>1</sup>H NMR (CD<sub>3</sub>OD, 300 MHz): δ 3.52-3.56 (m, 8H), 3.66-3.70 (m, 16H), 7.41 (t, *J* = 7.8 Hz, 2H), 7.87 (dd, *J* = 7.8 and 3.0 Hz, 4H), 8.21 (t, *J* = 3.0 Hz, 2H); <sup>13</sup>C NMR (DMSO-*d*<sub>6</sub>, 75 MHz): δ 68.5, 68.7, 69.3, 125.7, 128.2, 129.6, 134.2, 165.6; (+)-APCI-MS (*m/z*): 557.3 (M+1, 100). Conditions "b" (Scheme 2.7) afforded **24** (270 mg; 55%) and **25** (210 mg; 42%) whose spectral data were identical to those obtained above. Conditions "c" (Scheme 2.7) afforded **24** (120 mg; 25%) ; **25** (300 mg; 60%) and **26** (10 mg, 3%) as a colorless solid: mp 213.5-214 °C; <sup>1</sup>H NMR (CD<sub>3</sub>OD, 300 MHz): δ 3.59-3.62 (m, 12H), 3.62-3.72 (m, 24H), 7.53 (t, *J* = 7.8 Hz, 3H), 7.97 (d, *J* = 7.8 Hz, 6H), 8.31 (t, 3H); <sup>13</sup>C NMR (CD<sub>3</sub>OD, 75 MHz): δ 42.1, 71.6, 72.4, 128.6, 131.4, 132.7, 137.4, 170.8; (+)-APCI-MS (*m/z*): 835.3 (M+1, 100); and **27** (40 mg, 8%) as a colourless solid: mp 208-209 °C; <sup>1</sup>H NMR

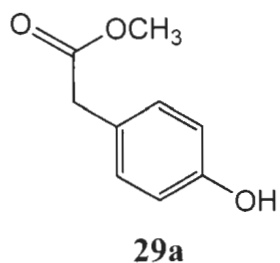
(CD<sub>3</sub>OD, 300 MHz):  $\delta$  3.50-3.53 (m, 16H), 3.63-3.66 (m, 32H), 7.44 (t,  $J = 7.8$  Hz, 4H), 7.88 (d,  $J = 7.8$  Hz, 8H), 8.22 (t, 4H); <sup>13</sup>C NMR (CD<sub>3</sub>OD, 75 MHz):  $\delta$  39.3, 68.7, 69.6, 125.6, 128.1, 129.6, 134.3, 167.5; (+)-APCI-MS ( $m/z$ ): 1113.4 (M+1, 100).

#### General conditions for the synthesis of arylboronic acid **32**



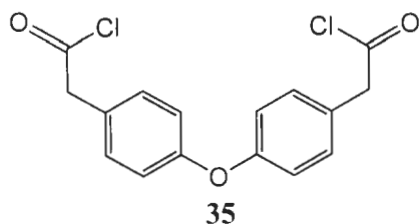
Arylboronic acid **32** was prepared as described by Zein, A.<sup>24</sup>

#### General conditions for the synthesis of methyl (4-hydroxyphenyl) acetate (**29a**)



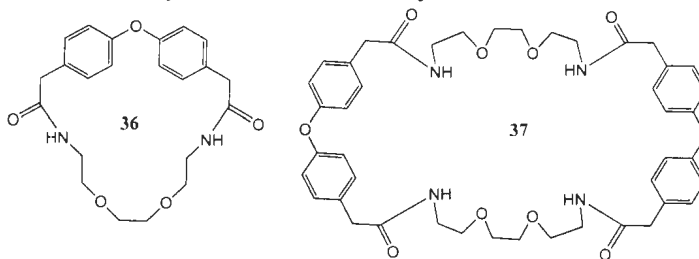
Methyl (4-hydroxyphenyl) acetate (**29a**) was prepared as described by Zein, A.<sup>24</sup>

#### General conditions for the synthesis of diacyl dichloride **35**



Diacyl dichloride **35** was prepared as described by Zein, A.<sup>24</sup>

### General conditions for the synthesis of macrocyclic amides **36** and **37**



A solution of diacyl dichloride **35** (240 mg, 0.75 mmol) in dry DCM (200 mL) was added dropwise over 1 h to a stirred solution of 1,8-diamino-3,6-dioxadecane (**15**), (0.12 mL, 0.81 mmol) and triethylamine (0.28 mL, 2.77 mmol) in dry DCM (2 mL) at -100 °C (Conditions “a”, Scheme 2.10), the reaction solution was maintained at the respective temperatures for 2 h and then allowed to warm to room temperature, with stirring over a period of 4 d. The reaction solutions were filtered and washed with brine (3 x 100 mL) and then with water (2 x 100 mL). The extracts were dried with anhydrous Na<sub>2</sub>SO<sub>4</sub> and evaporated under reduced pressure to yield yellow solids, which were purified by SiO<sub>2</sub> flash column chromatography using chloroform/methanol (95:5) as eluent. Conditions “a” afforded **36** (102 mg; 68%) as a colorless solid: mp 218-219 °C; <sup>1</sup>H NMR (CDCl<sub>3</sub>, 300 MHz): 3.33 (s, 4H), 3.37-3.42 (m, 8H), 3.59 (s, 4H); 5.71 (t, 2H), 6.99 (d, *J* = 8.7 Hz, 4H), 7.22 (d, *J* = 8.7 Hz, 4H); <sup>13</sup>C NMR (CD<sub>3</sub>OD, 75 MHz): δ 40.4, 43.4, 64.0, 70.3, 120.4, 131.1, 132.1, 158.6, 174.1; (+)-APCI-MS (*m/z*): 399.0 (M+1, 100); **37** (30 mg, 20%) as a colourless solid: mp 206-206 °C; <sup>1</sup>H NMR (CD<sub>3</sub>OD, 300 MHz): δ 3.32-3.38 (m, 16H), 3.47 (s, 8H), 3.59 (s, 8H), 6.87 (d, *J* = 8.7 Hz, 8H), 7.30 (d, *J* = 8.7 Hz, 8H); <sup>13</sup>C NMR (CD<sub>3</sub>OD, 75 MHz): δ 35.3, 38.2, 58.9, 65.1, 115.2, 126.1, 126.8, 153.4, 169.1; (+)-APCI-MS (*m/z*): 797.3 (M+1, 100).

## 2.8 References

1. Jeffamines are the trade names for these amines supplied by Huntsman International.
2. (a) Connors, K. A. *Binding Constants*, Wiley, New York, 1987. (b) Association constants were calculated using a non-linear curve fitting using the program ORIGINPro 7.5 from OriginLab Corporation.
3. Shriver, D.; Biallas, M. *J. Am. Chem. Soc.* **1967**, *89*, 1078-1081.
4. (a) Steed, J. W.; Atwood, J. L. *Supramolecular Chemistry*, Wiley VCH: Weinheim, Germany, 2009. (b) Beer, P. D.; Gale, P. A.; Smith, D. K. *Supramolecular Chemistry*, Oxford University Press, Oxford, UK, 1999.
5. (a) Dietrich, B. *Pure Appl. Chem.* **1993**, *65*, 1457-1464. (b) Bowman-James, K. *Acc Chem. Res.* **2005**, *38*, 671-678.
6. (a) Gale, P. A. *Chem. Soc. Rev.* **2010**, *39*, 3746-3758. (b) Wenzel, M.; Hiscock, J. R.; Gale, P. A. *Chem. Soc. Rev.* **2012**, *41*, 480-520.
7. Gale, P. A. *Acc. Chem. Res.* **2011**, *44*, 216-226.
8. (a) McConnell, A.; Beer, P. *Angew. Chem. Int. Ed.* **2012**, *51*, 5052-5061; (b) Kim, M.; Sessler, J. *Chem. Soc. Rev.* **2010**, *39*, 3784-3809; (c) Smith, B. *Ion-pair Recognition by Ditopic Receptors in Macrocyclic Chemistry: Current Trends and Future*. Gloe, K. and Antonioli, B. Eds. Kluwer, London, 2005.
9. Beer, P. D.; Chen, Z. E.; Gale, P. A.; Heath, J. A.; Knubley, R. J.; Ogden, M. I. *J. Incl. Phenom.* **1994**, *19*, 343-359.

10. Kavallieratos, K.; de Gala, S. R.; Austin, D. J.; Crabtree, H. R. *J. Am. Chem. Soc.* **1997**, *119*, 2325-2326.
11. (a) Mahoney, J. M.; Beatty, A. M.; Smith B. D. *J. Am. Chem. Soc.* **2001**, *123*, 5847-5848. (b) Mahoney, J. M.; Beatty, A. M.; Smith B. D. *Inorg. Chem.* **2004**, *43*, 7617-7621, and references cited therein.
12. Gale, P. A. *Acc. Chem. Res.* **2006**, *39*, 465-475.
13. Wisner, J. A.; Beer, P. D.; Berry, N. G.; Tomapatanaget, B. *Proc. Natl. Acad. Sci. USA* **2002**, *99*, 4983-4986.
14. Lankshear, M. D.; Cowley, A. R.; Beer, P. D. *Chem. Commun.* **2006**, 612-614.
15. Lankshear, M. D.; Dudley, I. M.; Can, K.-M.; Beer, P. D. *New J. Chem.* **2007**, *31*, 684-690.
16. Choi, K.; Hamilton, A. D. *J. Am. Chem. Soc.* **2001**, *123*, 2456-2457.
17. (a) Chmielewski, M. J.; Zieliński, T.; Jurczak, J. *Pure Appl. Chem.* **2007**, *79*, 1087-1096. (b) Chmielewski, M. J.; Jurczak, J. *Chem. Eur. J.* **2006**, *12*, 7605-7605. (c) Chmielewski, M. J.; Jurczak, J. *Chem. Eur. J.* **2005**, *11*, 6080-6094. (d) Chmielewski, M.; Szumna, A.; Jurczak, J. *Tetrahedron Lett.* **2004**, *45*, 8699-8703. (e) Szumna, A.; Jurczak, J. *Eur. J. Org. Chem.* **2001**, 4031-4039.
18. (a) Chmielewski, M.; Jurczak, J. *Tetrahedron Lett.* **2004**, *45*, 6007-6010. (b) Chmielewski, M. J.; Jurczak, J. *Tetrahedron Lett.* **2005**, *46*, 3085-3088.
19. Kim, S.; Sessler, J. *Chem. Soc. Rev.* **2010**, *39*, 3784-3809.
20. Shukla, R.; Kida, D.; Smith, B. D. *Org. Lett.* **2000**, *2*, 3099-3102.

21. Mahoney, J. M.; Beatty, A. M.; Smith, B. D. *J. Am. Chem. Soc.* **2001**, *123*, 5847-5848.
22. Eckelmann, J. M. Saggiomo, V. A.; Sönnichsen, F. D.; Lüning, U. B.; *New J. Chem.* **2010**, *34*, 1247-1250.
23. Evans, D. A.; Katz, J. L.; West, T. R. *Tetrahedron Lett.* **1998**, *39*, 2937-2940.
24. Zein, A. Ph.D. Dissertation, Memorial University, 2011.
25. Murata, M.; Oyama, T.; Watanabe, S.; Masuda, Y. *J. Org. Chem.* **2000**, *65*, 164-168.
26. Jung, M. E.; Lazarova, T. I. *J. Org. Chem.* **1999**, *64*, 2976-2977.
27. Crystal data for **20**: C<sub>16</sub>H<sub>22</sub>N<sub>2</sub>O<sub>4</sub>•H<sub>2</sub>O, *M* = 324.38, monoclinic, *a* = 11.336(3) Å, *b* = 10.813(3) Å, *c* = 16.926(5) Å,  $\alpha = 90.00^\circ$ ,  $\beta = 129.643(6)^\circ$ ,  $\gamma = 90.00^\circ$ , *V* = 1597.6(8) Å<sup>3</sup>, *T* = 153(2) K, space group *P*2<sub>1</sub>/*c*, *Z* = 4,  $\mu(\text{MoK}\alpha) = 0.100 \text{ mm}^{-1}$ , 21578 reflections measured, 3649 independent ( $R_{\text{int}} = 0.0230$ ). *R*1 = 0.0389 (*I* > 2 $\sigma$ (*I*)),  $wR(F^2) = 0.0992$  (all data),  $\text{GOF}(F^2) = 1.064$ .
28. (a) *Topics in Current Chemistry: Molecular Inclusion and Molecular Recognition. Clathrates I*, 140; Weber, E., Ed.; Springer-Verlag: New York, 1987.
- (b) *Supramolecular Chemistry*, Steed, J. W.; Atwood, J. L. John Wiley and Sons, Ltd., 2<sup>nd</sup> Edition, 2009.
29. Etter, M. C.; MacDonald, J. C.; Bernstein, J. B. *Acta Cryst. B.* **1990**, *46*, 256-262.
30. Crystal data for **21**: C<sub>32</sub>H<sub>44</sub>N<sub>4</sub>O<sub>8</sub>, *M* = 612.72, triclinic, *a* = 5.0083(18) Å, *b* = 9.048(3) Å, *c* = 17.725(6) Å,  $\alpha = 85.179(8)^\circ$ ,  $\beta = 82.023(9)^\circ$ ,  $\gamma = 75.645(9)^\circ$ , *V* = 769.6(5) Å<sup>3</sup>, *T* = 163(2) K, space group *P* $\bar{1}$ , *Z* = 1,  $\mu(\text{MoK}\alpha) = 0.095 \text{ mm}^{-1}$ , 8677

reflections measured, 2656 independent ( $R_{int} = 0.1457$ ).  $R_1 = 0.1365$  ( $I > 2\sigma(I)$ ),  $wR(F^2) = 0.3084$  (all data),  $GOF(F^2) = 1.107$ . Note: multiple attempts were made to grow suitable X-ray diffraction single crystals, however, the only successful collection, reported here, was performed on a very tiny needle that diffracted poorly. The high data statistics are the result of this weak data-set.

31. Crystal data for macrocycle **24**:  $C_{14}H_{18}N_2O_4 \cdot CHCl_3$ ,  $M = 397.69$ , monoclinic,  $a = 8.662(7)$  Å,  $b = 8.329(7)$  Å,  $c = 12.672(10)$  Å,  $\alpha = 90.00^\circ$ ,  $\beta = 99.006(11)^\circ$ ,  $\gamma = 90.00^\circ$ ,  $V = 903.0(13)$  Å<sup>3</sup>,  $T = 123(2)$  K, space group  $P2_1$ ,  $Z = 2$ ,  $\mu(MoK\alpha) = 0.529$  mm<sup>-1</sup>, 8478 reflections measured, 3076 independent reflections ( $R_{int} = 0.0357$ ).  $R_1 = 0.0368$  ( $I > 2\sigma(I)$ ),  $wR(F^2) = 0.0953$  (all data). The goodness of fit on  $F^2$  was 1.062. Flack parameter = 0.07(7).
32. Crystal data for macrocycle **25**:  $C_{28}H_{36}N_4O_8$ ,  $M = 556.61$ , triclinic,  $a = 9.293(10)$  Å,  $b = 9.4262(10)$  Å,  $c = 9.600(9)$  Å,  $\alpha = 91.525(8)^\circ$ ,  $\beta = 110.407(3)^\circ$ ,  $\gamma = 115.256(16)^\circ$ ,  $V = 697.4(10)$  Å<sup>3</sup>,  $T = 123(2)$  K, space group  $P\bar{1}$ ,  $Z = 1$ ,  $\mu(MoK\alpha) = 0.098$  mm<sup>-1</sup>, 7058 reflections measured, 3149 independent reflections ( $R_{int} = 0.0485$ ).  $R_1 = 0.0711$  ( $I > 2\sigma(I)$ ),  $wR(F^2) = 0.2045$  (all data). The goodness of fit on  $F^2$  was 1.088.
33. Crystal data for macrocycle **36**:  $C_{22}H_{26}N_2O_5$ ,  $M = 398.46$ , monoclinic,  $a = 4.7848(10)$  Å,  $b = 18.335(4)$  Å,  $c = 23.767(6)$  Å,  $\alpha = 90.00^\circ$ ,  $\beta = 93.032(7)^\circ$ ,  $\gamma = 90.00^\circ$ ,  $V = 2082.1(8)$  Å<sup>3</sup>,  $T = 163(2)$  K, space group  $C2/c$ ,  $Z = 4$ ,  $\mu(MoK\alpha) = 0.090$  mm<sup>-1</sup>, 8693 reflections measured, 1752 independent reflections ( $R_{int} = 0.1174$ ).  $R_1 = 0.0907$  ( $I > 2\sigma(I)$ ),  $wR(F^2) = 0.2483$  (all data). The goodness of fit on  $F^2$  was 1.049.

34. Cametti, M.; Nissinen, M.; Cort, A. D.; Mandolini, L.; Rissanen, K. *Chem. Commun.* **2003**, *19*, 2420–2421.
35. Rudkevich, D. M.; Scheerder, J.; Reinhoudt, D. N. *Molecular Design and Bioorganic Catalysis*, Kluwer publishes, Netherlands, 1996.

## **Chapter 3**

### **Synthesis and Structures of New Macrocyclic Chromotropic Acid-based Sulfonamides; Their Complexation Properties and an Unexpected Photochemical Reaction.**

Part of this work described in this chapter has been published

*Tetrahedron Lett.* **2013**, *54*, 3444–3448.

## Chapter 3

### Synthesis and Structures of New Macrocyclic Chromotropic Acid-based Sulfonamides; Their Complexation Properties and an Unexpected Photochemical Reaction.

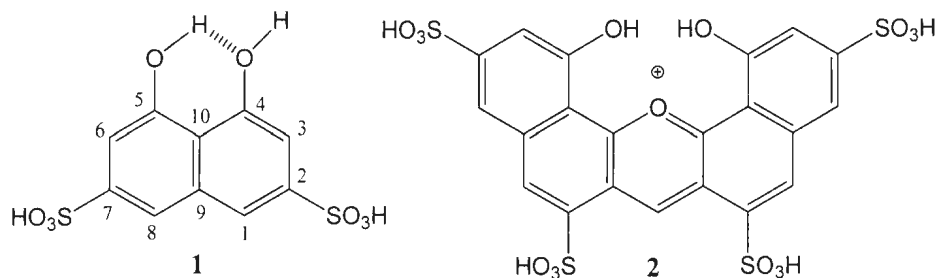
#### 3.1 Introduction

This chapter describes the synthesis of new macrocyclic sulfonamides derived from chromotropic acid (CTA) **1** with both “Jeffamine<sup>®</sup> EDR-148” (1,8-diamino-3,6-dioxaoctane) and “Jeffamine<sup>®</sup> EDR-176” (1,10-diamino-4,7-dioxadecane) at low temperatures and under high dilution conditions. Also described is a complexation study of these new macrocyclic sulfonamides with selected Group 1 and 2 metal halides and tetrabutylammonium salts (TBAX) using 300 MHz <sup>1</sup>H NMR chemical shift changes. From the resulting titration curves the association constants ( $K_{assoc}$ ) were calculated using isothermal non-linear 1:1 binding curve fitting plots according to Connors.<sup>1</sup> Part of this chapter has been published in *Tetrahedron Lett.* **2013**, *54*, 3444-3448.

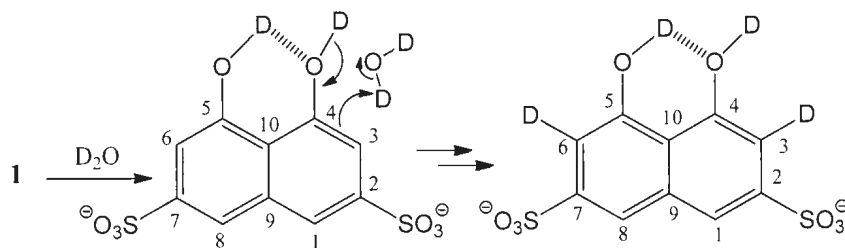
##### 3.1.1 Chromotropic acid

Chromotropic acid (CTA) **1** (4,5-dihydroxy-2,7-naphthalenedisulfonic acid) is a reactive and highly water-soluble reagent which has been used in many diverse applications. Among these applications, CTA is used as a highly-selective formaldehyde analytical reagent, Eegriwe<sup>2</sup> being the first to describe its use in 1937 as a formaldehyde-specific reagent. More recently, the mechanism of the reaction of this reagent in the

formaldehyde reaction has been studied.<sup>3</sup> CTA is also used as a key intermediate in the syntheses of various azo derivatives, which can be used not only in the dye industry, but also in a variety of analytical chemistry applications.<sup>4</sup>

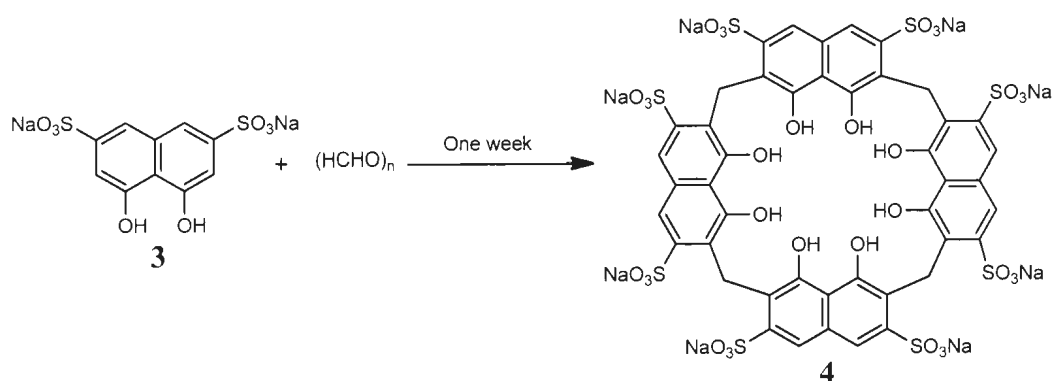


In the analysis of aqueous formaldehyde solutions using method P&CAM 125, as recommended by the National Institute for Occupational Safety and Health (NIOSH), Ho and Georghiou<sup>3</sup> showed that in the presence of concentrated sulfuric acid CTA forms the oxanthilium-type chromogen **2**, which is directly related to the amount of formaldehyde present in the solution.<sup>5</sup> Another study conducted by Georghiou *et al.*<sup>6</sup> using <sup>1</sup>H NMR spectroscopy in D<sub>2</sub>O showed that rapid deuterium exchange of the CTA protons *ortho* to the hydroxyl groups at C-3 and C-6 occurred, in addition to those of both hydroxyl groups as shown in Scheme 3.1.



**Scheme 3.1.** Deuterium exchange of the CTA protons.

In contrast to the work of Ho and Georghiou, Poh *et al.*<sup>7</sup> showed that the aqueous reaction of the disodium salt of CTA with formaldehyde in the absence of concentrated sulfuric acid produced a water-soluble cyclic tetramer which he called “cyclotetrachromotropylenene” (**4**) as a calixarene<sup>8</sup> analogue (Scheme 3.2). This compound could not be crystallized and was mainly characterized by its mass spectrum.

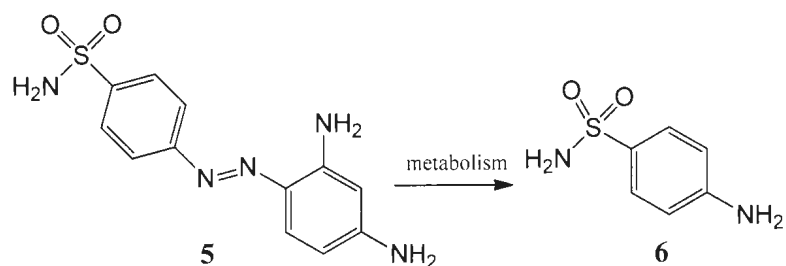


**Scheme 3.2.** Poh's synthesis of cyclotetrachromotropylenene.

### 3.1.2 Sulfonamides as drugs

The chemotherapeutic activities of sulfonamides have been studied for many years.<sup>9</sup> The first sulfonamide-based medicine, the antibiotic Prontosil (**5**), was discovered in 1932. It is a pro-drug which is converted to the active form, the *p*-aminosulfonamide **6**, during metabolism (Scheme 3.3).<sup>10,11</sup>

Since then, sulfonamides have been shown to possess a wide range of medicinal applications in which they can be used as *e.g.* antimicrobial agents, competitive inhibitors of dihydropteroate synthetase (DHPS), anti-impotence and also as loop diuretic drugs.<sup>12</sup>



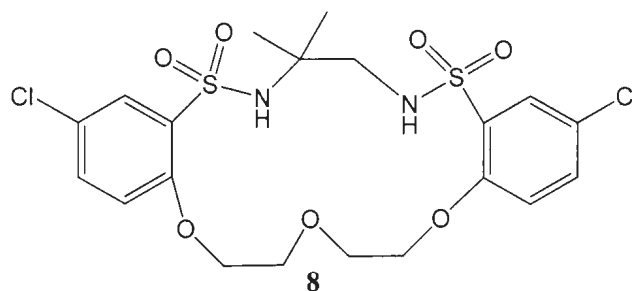
**Scheme 3.3.** Metabolic conversion of pro-drug Prontosil (**5**) to sulfonamide **6**.

### 3.1.3 Macrocyclic sulfonamides

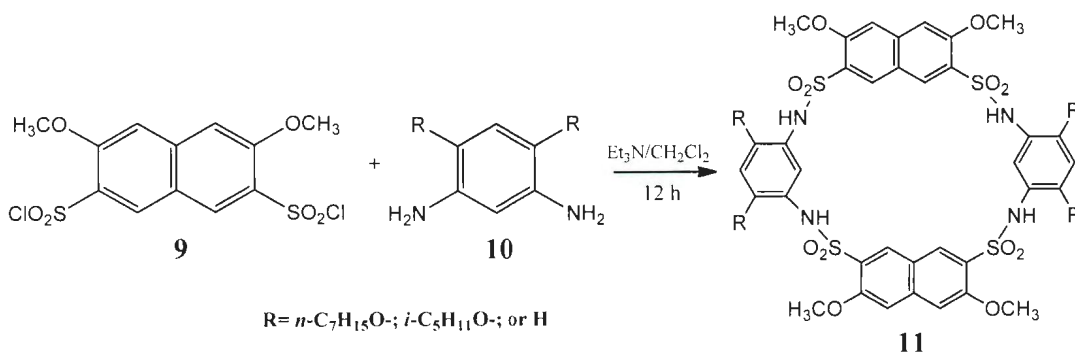
Host-guest chemistry<sup>13</sup> is an important branch of chemistry which has expanded in the last 20 years and has widespread applications. An important class of host molecules includes macrocyclic sulfonamides, which play a significant role in both organic chemistry and drug discovery. Most notable are the “*sulfa*” antibiotics, which were discovered in the 1930s for treating bacterial infections and more recently, for HIV treatment.<sup>14, 15</sup>

In 1993, Reinhoudt and co-workers<sup>16</sup> reported the synthesis of a series of trissulfonamides **7**, to test their binding properties as receptors with different anion species. These receptors showed selective binding to the phosphate anion in acetonitrile solution.

On the other hand, a series of bis-sulfonamide crown compounds was reported by Bradshaw *et al.* as very good alkali metal carriers in biological membranes.<sup>17</sup> In 2011, Kihanyan and co-workers<sup>18</sup> reported the synthesis of the macrocyclic bis-sulfonamide **8** which has high antibacterial activity and is a good biosensor for some microorganisms.



Gong and co-workers<sup>19</sup> reported the synthesis of several cyclic aromatic tetrasulfonamides and studied their conformations using 2D NMR (NOESY). They found that these compounds could be used as good hosts for small solvent molecules such as *N,N*-dimethylformamide (DMF). In 2006, Gong reported the reaction of disulfonyl chloride **9** with diamine **10** in the presence of triethylamine afforded the naphthalene-ring macrocyclic tetrasulfonamides **11** (Scheme 3.4). These new compounds were reported to be good hosts for pyridine, and tetrahydrofuran (THF).<sup>20</sup>



**Scheme 3.4.** Synthesis of macrocyclic tetrasulfonamides **11**.

Biernat and co-workers<sup>21</sup> reported the synthesis of several new macrocyclic sulfonamide compounds (Figure 3.1) which can be used as ion-selective ionophores for  $K^+$ ,  $Rb^+$  and  $Cs^+$  cations.

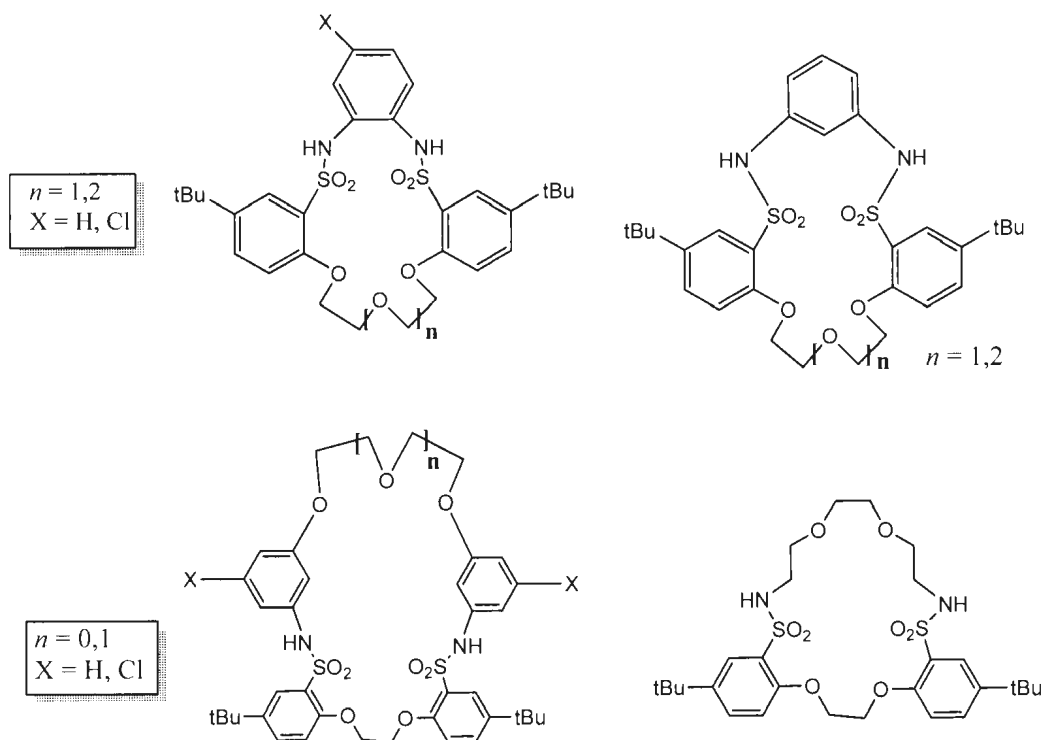


**Figure 3.1.** Biernat and co-workers' macrocyclic sulfonamide compounds.

In 2008, Eshghi<sup>22</sup> reported the synthesis of the macrocyclic bis-sulfonamides (shown in Figure 3.2), by reacting bis-sulfonyl chlorides (**15a,b**) with diamines **16** using a fast-addition method (Scheme 3.5).

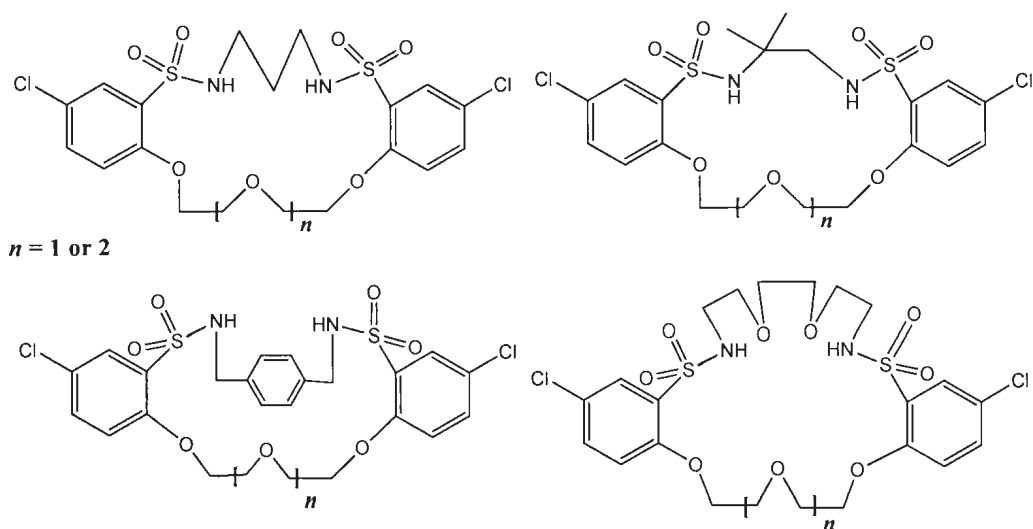
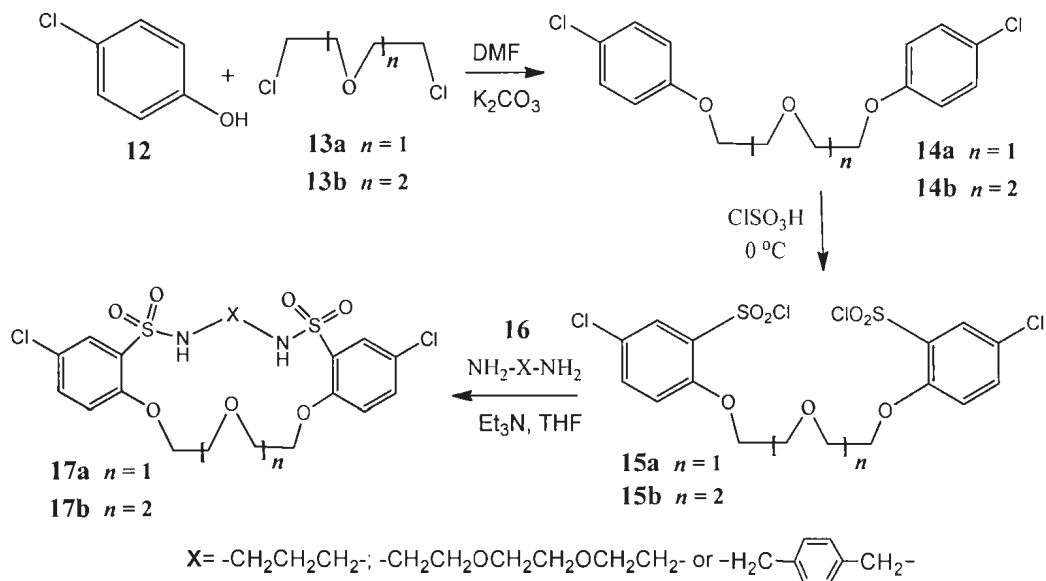


**Figure 3.2.** Macrocyclic bis-sulfonamides synthesized by Eshghi.



**Scheme 3.5.** Synthesis of macrocyclic bis-sulfonamides **17**.

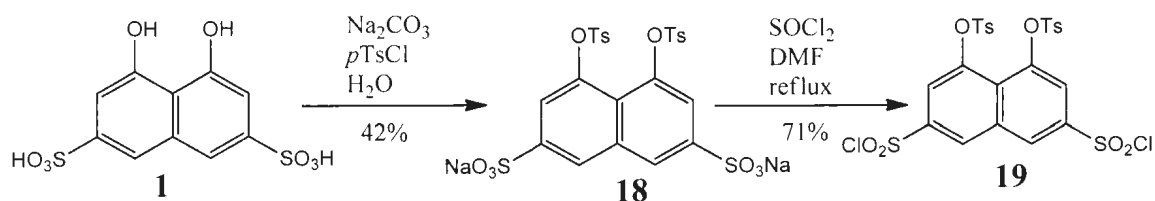
*p*-Chlorophenol (**12**) was reacted with dichlorides **13a** or **13b** in DMF in the presence of potassium carbonate to yield podands **14a** or **14b** in 76% and 64% yields,

respectively. Further chlorosulfonation of these podands afforded bis-sulfonyl chlorides **15a** or **15b** in 86% and 73% yields, respectively. Cyclization using vigorous stirring and fast addition of a mixture of triethylamine and diamine **16** in THF, into the suspension of the bis-sulfonyl chlorides **15a** or **15b** kept at 25 °C afforded bis-sulfonamides **17a** or **17b** as shown in Scheme 3.5.

### 3.2 Syntheses of the CTA-Jeffamines macrocyclic sulfonamides

#### 3.2.1 Syntheses of the starting material<sup>23</sup>

4,5-Ditosyloxynaphthalene-2,7-disulfonyl chloride (**19**) can be prepared by converting CTA (**1**) to its ditosylate disodium salt **18** and then reacting it with thionyl chloride under reflux for 3 h to yield the CTA-disulfonyl chloride **19** in 71% yield, as shown in Scheme 3.6.



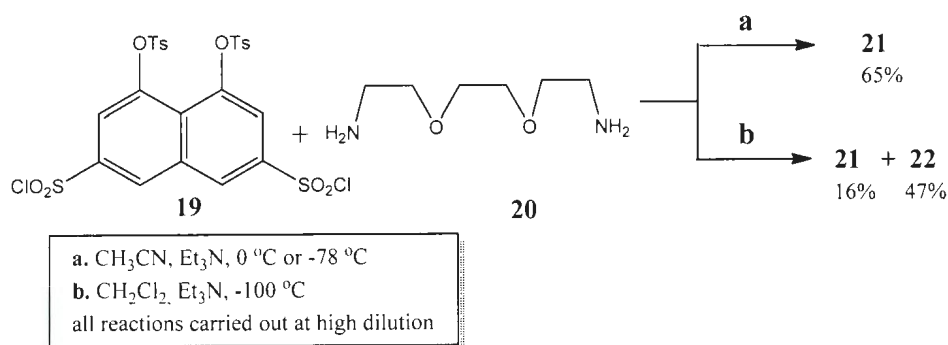
**Scheme 3.6.** Synthesis of 4,5-ditosyloxynaphthalene-2,7-disulfonyl chloride (**19**).

#### 3.2.2 Synthesis of the CTA-Jeffamines macrocycles

##### 3.2.2.1 Synthesis of macrocycles **21** and **22**

The syntheses of **21** and **22** (see page 138 for the structures), which are the “[1+1]” and “[2+2]” macrocyclic sulfonamide compounds respectively, derived from the reaction

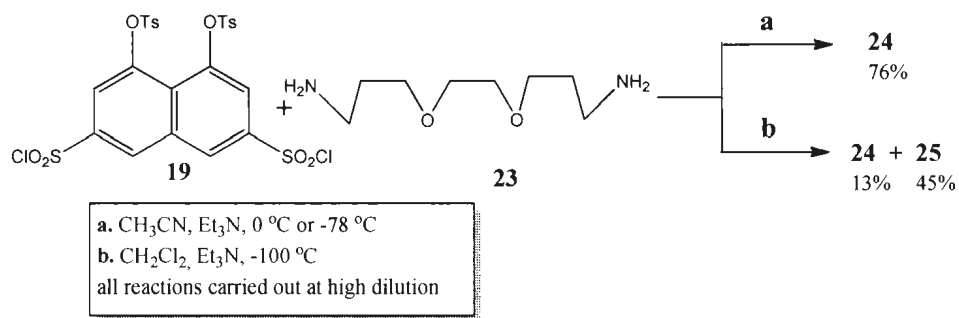
of disulfonyl dichloride **19** with 1,8-diamino-3,6-dioxaoctane (**20**) or “Jeffamine<sup>®</sup> EDR-148”<sup>24</sup> are summarized in Scheme 3.7. Of the different reaction conditions which were investigated, the [1+1] product, **21**, was isolated in 65% yield under initial lower temperature and high dilution conditions (Conditions “a”, Scheme 3.7). The [2+2]-macrocylic sulfonamide **22** was optimally produced in 47% yield in addition to the [1+1] product **21** which was formed in 16% yield (Conditions “b”, Scheme 3.7).



**Scheme 3.7.** Synthesis of macrocyclic sulfonamides **21** and **22**.

### 3.2.2.2 Synthesis of macrocycles **24** and **25**

The synthesis of **24** and **25** (see page 139 for the structures), the “[1+1]” and “[2+2]” macrocyclic sulfonamide compounds respectively, were also derived from the reaction of compound **19** with 1,10-diamino-4,7-dioxadecane (**23**) or “Jeffamine<sup>®</sup> EDR-176”, are summarized in Scheme 3.8. The [1+1] product **24** was isolated in 76% yield under the initial lower temperature and high dilution conditions used (Conditions “a”, Scheme 3.8). The [2+2]-macrocylic sulfonamide **25** however, was optimally produced in 45% yield, in addition to the [1+1] product **24** which was also formed, in 13% yield (Conditions “b”, Scheme 3.8).



**Scheme 3.8.** Synthesis of macrocyclic sulfonamides **24** and **25**.

### 3.3 X-Ray structure of macrocycle **24**

Crystals of **24** were obtained by the slow evaporation of the aqueous methanol/ethyl acetate solvent mixture used to dissolve the macrocycle. Slow evaporation of the solvent at room temperature gave colorless crystals which were suitable for X-ray diffraction analysis. Its structure is shown in Figure 3.3.

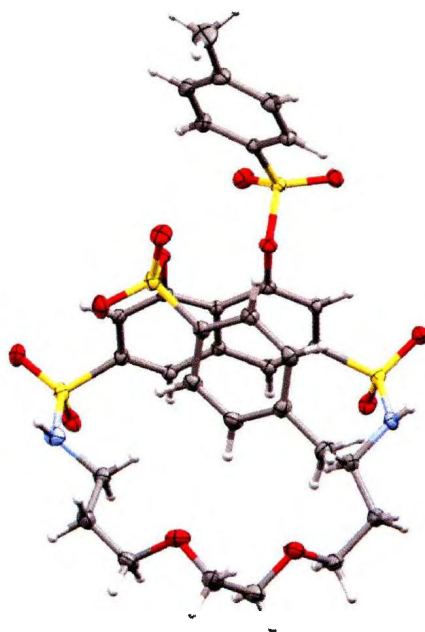


**Figure 3.3.** Asymmetric unit for **24** with 50% probability ellipsoids. Grey = carbon, light grey = hydrogen, yellow = sulfur, red = oxygen, blue = nitrogen.

The X-ray analysis of **24** was conducted by Dr. Louise Dawe of the Chemistry Department, Memorial University and the following images and text are taken directly from her analysis:

Macrocycle **24** (Figure 3.3) crystallized in the non-centrosymmetric orthorhombic space group  $P2_12_12_1$ . Extensive intermolecular hydrogen bonding, leading to the formation of a two dimensional infinite polymer in the  $ab$ -plane, was present (Figure 3.4). Further, intermolecular interactions, in the form of  $\pi$ - $\pi$  stacking between naphthalene rings were observed (Figure 3.5).

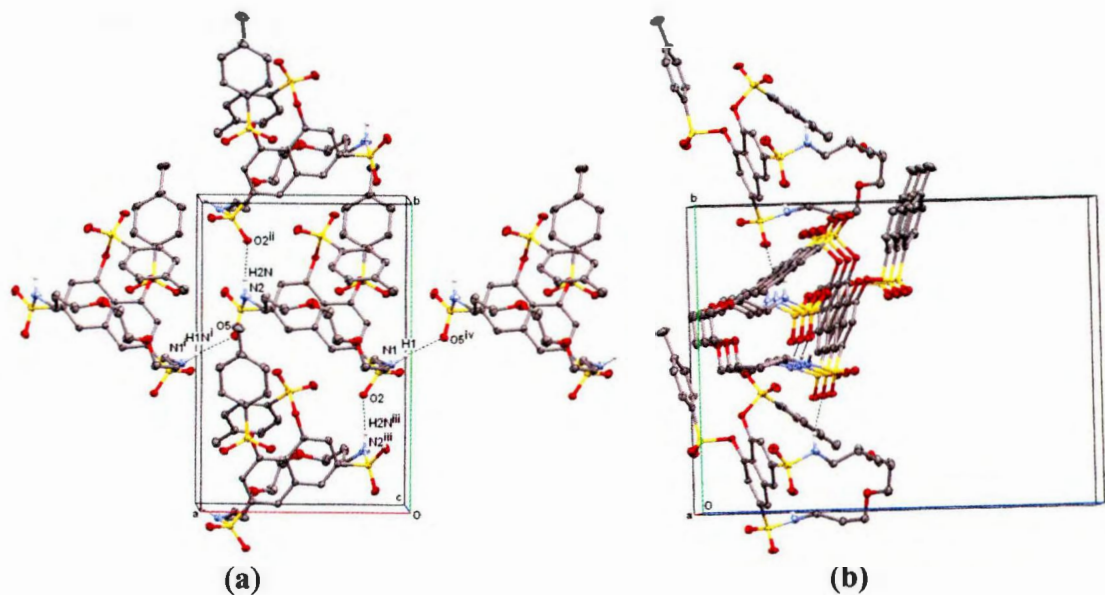


**Figure 3.4.** (a) Hydrogen bonding (dashed lines) leading to an infinite 2D polymer in the  $(0\ 0\ 1)$  plane for **24**. (b) View in (a) rotated by  $90^\circ$ . Hydrogen atoms omitted for clarity. Symmetry operations: (i) =  $1+x, y, z$ ; (ii) =  $1-x, \frac{1}{2}+y, \frac{1}{2}-z$ ; (iii) =  $1-x, y-\frac{1}{2}, \frac{1}{2}-z$ , (iv) =  $x-1, y, z$ .

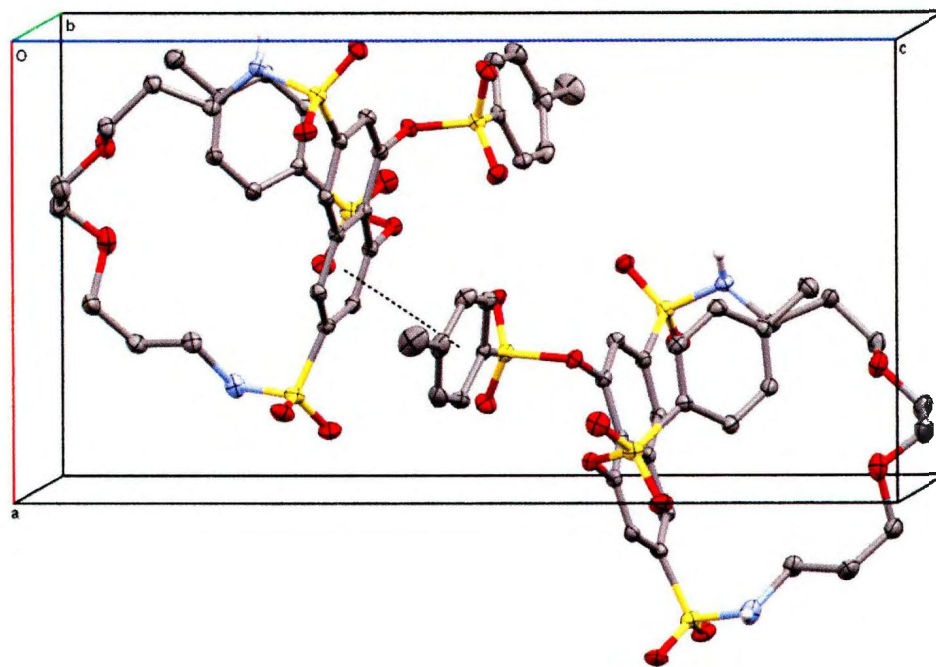


**Figure 3.5.**  $\pi$ - $\pi$  stacking between naphthalene ring [C3 C4 C5 C6 C7 C8; Plane 1] and the ring formed by [C29 C30 C31 C32 C33 C34; Plane 2; symmetry operator =  $\frac{1}{2} + x$ ,  $\frac{3}{2} - y$ ,  $1 - z$ ] for HS-24b. Plane 1 to Plane 2 angle:  $1.23(6)^\circ$ ; Plane 1 centroid to Plane 2 centroid distance:  $3.6801(10)$  Å; Plane 1 to Plane 2 centroid distance:  $3.5418(13)$  Å; Plane 1 to Plane 2 shift:  $1.000(2)$  Å.

### 3.4 Complexation studies

$^1\text{H}$  NMR spectroscopy was chosen as the most convenient technique for studying the binding or association constants ( $K_{\text{assoc}}$ ) in different solvents and avoids the potential problems encountered using absorption spectroscopy.<sup>25,26</sup>

Stock solutions of the macrocyclic CTA-Jeffamine sulfonamides ( $\sim 1.00 \times 10^{-3}$  M) were prepared in a 9:1  $\text{CDCl}_3$ : $\text{DMSO-}d_6$  solvent mixture or, in the case of the tetrabutylammonium salts (TBAX), in  $\text{CDCl}_3$  alone. After maximum chemical shift changes using saturated solutions of the guests were determined in preliminary studies, solid aliquot amounts of the guests to be studied were weighed ( $\pm 0.01$  mg) into separate sample vials using a Sartorius microbalance. To these samples, 1.00 mL

amounts of the stock solution were added and the resulting solutions were sonicated at room temperature for 5 min and then allowed to stand for 24 h before measuring their  $^1\text{H}$  NMR spectra. Binding constants were calculated from the observed chemical shift changes using a non-linear curve fitting formula according to Connors<sup>1</sup> using the ORIGINPro 7.5 program from OriginLab Corporation.

### 3.4.1 Complexation studies with Group 1 and 2 metal chlorides

Complexation studies of the macrocyclic CTA-sulfonamides were conducted with Group 1 and 2 metal chlorides to test whether these new macrocyclic sulfonamides behaved in a similar manner to those of the isophthaloyl macrocyclic amides<sup>27</sup> which had previously been synthesized and were described in Chapter 2. A similar experiment was therefore conducted in which the metal salts were added to solutions in a 9:1  $\text{CDCl}_3$ : $\text{DMSO}-d_6$  solvent mixture of each of the macrocycles **21**, **22**, **24** and **25** such that the solutions were saturated with respect to the salts. The samples were sonicated and allowed to stand for 24 h before their  $^1\text{H}$  NMR spectra were determined. Surprisingly, no changes were seen in the  $^1\text{H}$  NMR spectra for either the [1+1] and [2+2] macrocyclic sulfonamide compounds, suggesting that there was no apparent complexation. A molecular mechanics modeling study using the Spartan'10 program<sup>28</sup> showed that in case of the [1+1] macrocycles **21** or **24**, the cavities might not be large enough to host the metal cations as was also seen in the case of the isophthaloyl [1+1] macrocyclic amides. On the other hand, with the [2+2] macrocycles **22** and **25**, the cavities could be too large for the cations to be complexed easily and overcome entropic or solvation effects. Chmielewski and co-workers<sup>29</sup> have shown in their studies with TBAX ( $X = \text{Cl}, \text{Br}$  or  $\text{I}$ )

that an increase of the macrocycle ring size from an 18-membered ring to a 20-membered ring resulted in a 30-fold increase in the binding constant of the anions. On the other hand, increasing the macrocycle receptor's size beyond a 20-membered ring reduced the binding constant toward the anions tested.

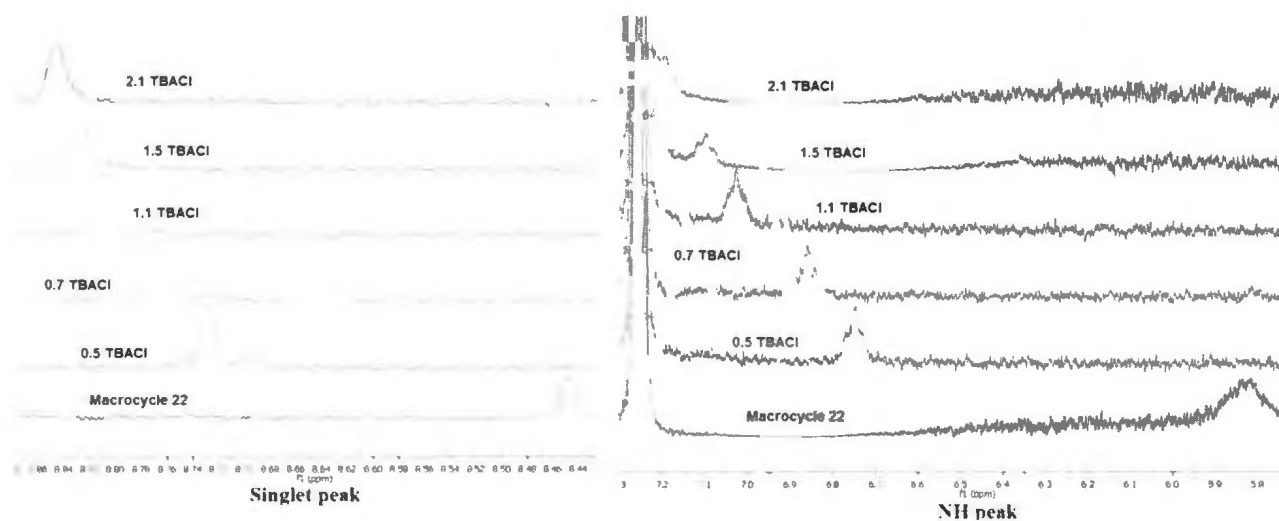
### **3.4.2 Complexation studies with tetrabutylammonium salts**

For the [1+1] macrocyclic compounds **21** and **24**, no changes were observed with TBAX salts or with the metal halides. Subsequent complexation studies were therefore conducted only with the [2+2] compounds, **22** and **25**.

#### **3.4.2.1 Complexation of macrocyclic sulfonamide **22** with tetrabutylammonium salts**

A study of the complexation of macrocyclic sulfonamide **22** with the tetrabutylammonium halides (TBAX; where X = Cl, Br and I) was undertaken to evaluate the potential effect of the different halide anions. Average  $K_{assoc}$  values of  $808 \pm 18$ ;  $229 \pm 16$  and  $222 \pm 21 \text{ M}^{-1}$  respectively for the chloride, bromide and iodo salts could be determined using the non-linear 1:1 binding isotherm for the NH and aromatic intramolecular proton singlet chemical shift changes. These results confirmed the stronger relative affinity for the chloride anion seen previously also with the isophthaloyl amide.<sup>27</sup> The other “non-complexing” anions tested, namely the tetrafluoroborate and phosphorus hexafluoride showed negligible chemical shift changes for which association constants could not be determined.

### 3.4.2.1.1 Complexation of macrocyclic sulfonamide **22** with tetrabutylammonium chloride



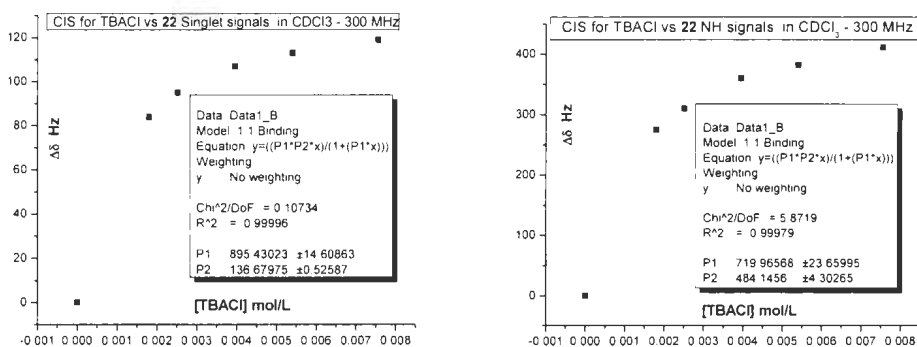
**Figure 3.6.**  $^1\text{H}$  NMR (300 MHz) titration spectra for both singlet and NH signals of macrocyclic sulfonamide **22** with TBACl.

Figure 3.6 shows the titration spectra for **22** with tetrabutylammonium chloride (TBACl). It can be seen that by increasing the added amounts of TBACl to the solution of **22** a downfield chemical shift change occurs for both the triplet signals due to the NH protons and also the aromatic intra-annular proton singlet signals. The NH signals shifted downfield from 5.83 ppm to 7.20 ppm, whereas the singlet also shifted downfield from 8.45 ppm, to 8.85 ppm (Table 3.1), indicating that complexation occurred between macrocycle **22** and TBACl. The association constants ( $K_{assoc}$ ), were determined using the non-linear 1:1 binding isotherms for both the NH and aromatic intra-annular proton singlet chemical shift changes (Table 3.1). Using the Origin program the molar concentrations of the guest ( $[\text{Guest}]$ ) were plotted against the observed chemical shift changes ( $\Delta\delta$ ) in Hz. The resultant association constants ( $K_{assoc}$ ) were  $895 \pm 14$  and  $720 \pm$

23 M<sup>-1</sup>, respectively, based on the singlet and NH proton chemical shift changes (Figure 3.7).

**Table 3.1.** <sup>1</sup>H NMR (300 MHz) titration chemical shift data for both singlet and NH signals of **22** (6.19 x 10<sup>-4</sup> M) with TBACl.

Sample	Guest (g)	[Guest]	[G]/[H]	NH δ	Δδ Hz	Singlet δ	Δδ Hz
Free host				5.830	0	8.450	0
1	5.00E-04	1.80E-03	3	6.747	275	8.729	84
2	7.00E-04	2.52E-03	4	6.863	310	8.765	95
3	1.10E-03	3.96E-03	6	7.029	360	8.808	107
4	1.50E-03	5.40E-03	9	7.103	382	8.827	113
5	2.10E-03	7.56E-03	12	7.199	411	8.846	119



**Figure 3.7.** <sup>1</sup>H NMR (300 MHz) titration curves for both singlet and NH signals of **22** (6.19 x 10<sup>-4</sup> M) with TBACl.

### 3.4.2.1.2 Complexation of macrocyclic sulfonamide **22** with tetrabutylammonium bromide

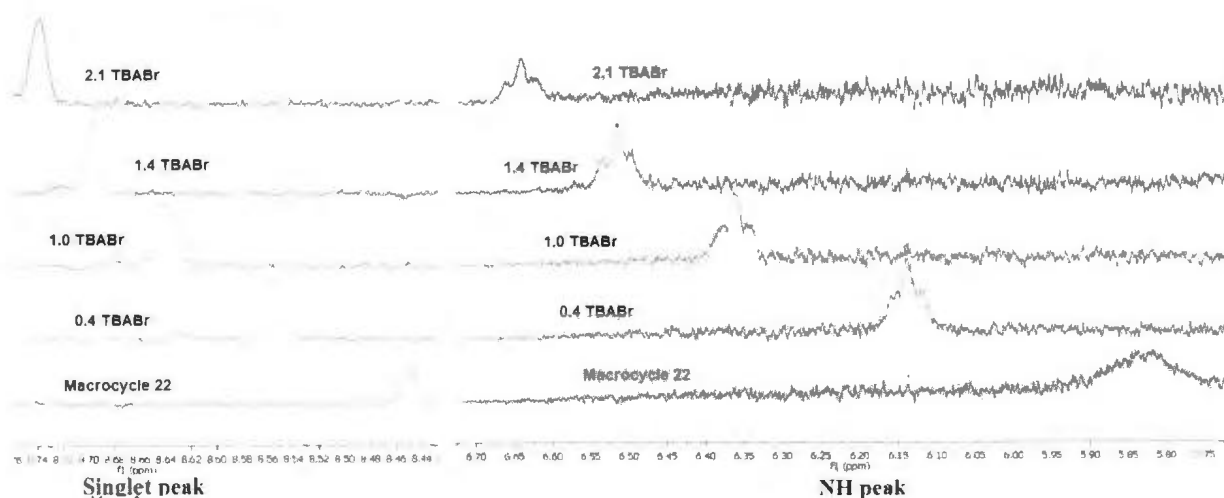


**Figure 3.8.** Expanded  $^1\text{H}$  NMR (300 MHz) titration spectra of macrocyclic sulfonamide **22** ( $6.19 \times 10^{-4}$  M) with TBABr.

The titration spectra of macrocyclic **22** with tetrabutylammonium bromide (TBABr) are shown in Figure 3.8, where it can be seen that by increasing the added amounts of TBABr to the solution of **22** there are downfield chemical shift changes for both the triplet NH and aromatic intra-annular proton singlet signals. The NH signal shifted from 5.83 ppm to 6.64 ppm, whereas the singlet signal shifted from 8.45 ppm to 8.74 ppm (Table 3.2) indicating the complexation between **22** and TBABr.

The association constants ( $K_{assoc}$ ), as in all cases, were determined using the non-linear 1:1 binding isotherm for both the NH and aromatic intra-annular proton singlet chemical shift changes (Table 3.2).

**Table 3.2.**  $^1\text{H}$  NMR (300 MHz) titration chemical shift data for both singlet and NH signals of **22** ( $6.19 \times 10^{-4}$  M) with TBABr.

Sample	Guest (g)	[Guest]	[G]/[H]	NH $\delta$	$\Delta\delta$ Hz	Singlet $\delta$	$\Delta\delta$ Hz
Free host				5.830	0	8.450	0
1	4.00E-04	1.24E-03	2	6.141	93	8.555	32
2	1.00E-03	3.10E-03	5	6.362	160	8.640	57
3	1.40E-03	4.34E-03	7	6.515	206	8.697	74
4	2.10E-03	6.51E-03	11	6.643	244	8.739	87

Using the Origin program the concentration of the guest ([Guest]) were plotted against the observed chemical shift changes ( $\Delta\delta$ ) in Hz, the association constants ( $K_{\text{assoc}}$ ) were  $245 \pm 76$  and  $212 \pm 16 \text{ M}^{-1}$  respectively based on the singlet and NH proton chemical shift changes (Figure 3.9).

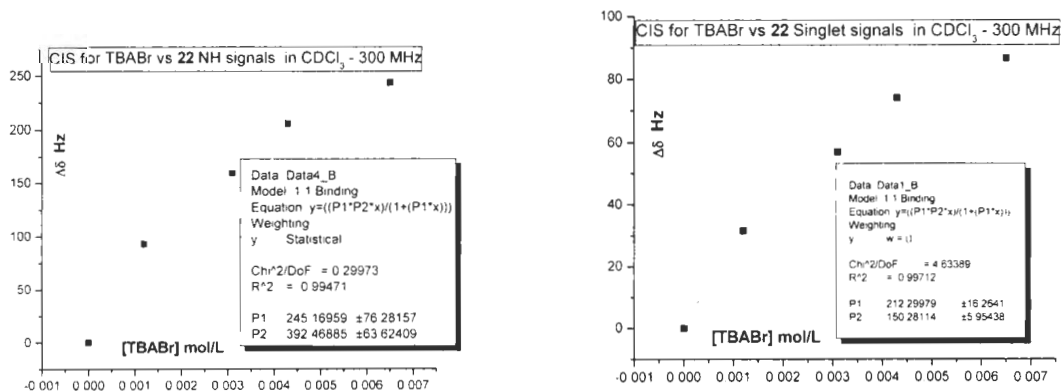


**Figure 3.9.**  $^1\text{H}$  NMR (300 MHz) titration curves for both singlet and NH signals of **22** ( $6.19 \times 10^{-4}$  M) with TBABr.

### 3.4.2.1.3 Complexation of macrocyclic sulfonamide **22** with tetrabutylammonium iodide

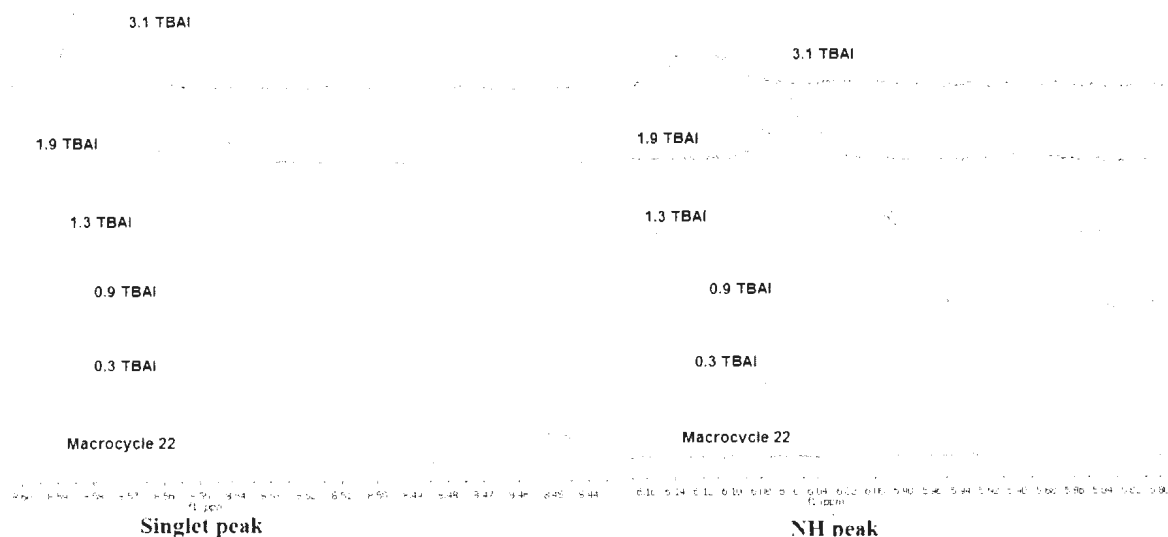


**Figure 3.10.** Expanded  $^1\text{H}$  NMR (300 MHz) titration spectra of macrocyclic sulfonamide **22** with TBAI.

The titration spectra of macrocyclic **22** with tetrabutylammonium iodide (TBAI) are shown in Figure 3.10. Increasing the added amount of TBAI to a solution of macrocyclic **22** results in downfield chemical shift changes for both the triplet (NH) and aromatic intra-annular proton singlet signals. The NH signals shifted from 5.83 ppm to 6.12 ppm, whereas the singlet shifted from 8.45 ppm to 8.58 ppm (Table 3.3) indicating complexation between **22** and TBAI.

The association constants ( $K_{assoc}$ ) were calculated using the non-linear 1:1 binding isotherm for both the NH and aromatic intra-annular proton singlet chemical shift changes shown in Table 3.3.

**Table 3.3.**  $^1\text{H}$  NMR (300 MHz) titration data for both singlet and NH signals of **22** ( $7.84 \times 10^{-4}$  M) with TBAI.

Sample	[Guest]	[G]/[H]	NH $\delta$	$\Delta\delta$ Hz	Singlet $\delta$	$\Delta\delta$ Hz
Free host			5.830	0	8.450	0
1	8.12E-04	1	5.910	24	8.480	9
2	2.44 E-03	3	5.990	48	8.520	21
3	3.52 E-03	4	6.020	57	8.530	24
4	5.14 E-03	7	6.060	69	8.550	30
5	8.39 E-03	11	6.120	87	8.580	39

Using the Origin program the concentrations of the guest ([Guest]) were plotted against the chemical shift changes ( $\Delta\delta$ ) in Hz, the association constants ( $K_{assoc}$ ) were  $195 \pm 28$  and  $248 \pm 15 \text{ M}^{-1}$  respectively based on the singlet and NH proton chemical shift changes (Figure 3.11).

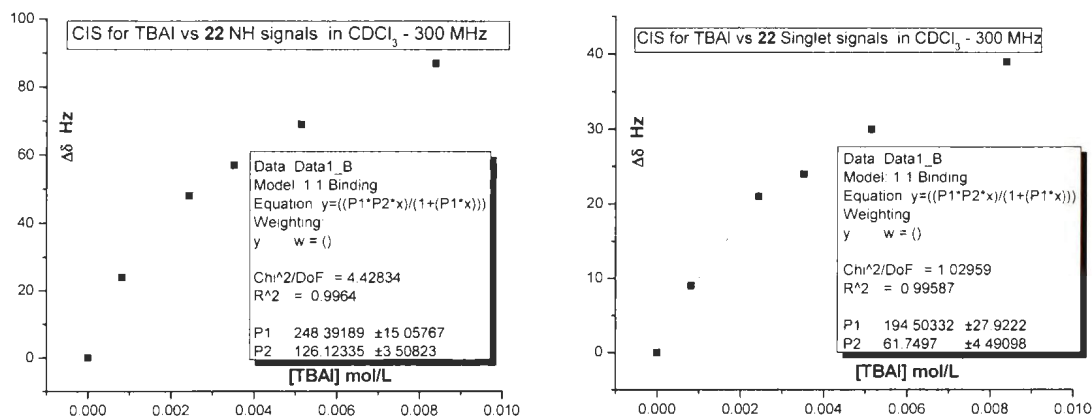


**Figure 3.11.**  $^1\text{H}$  NMR (300 MHz) titration curves for both singlet and NH signals of **22** ( $7.84 \times 10^{-4}$  M) with TBAI.

### 3.4.2.2 ESI-mass spectral data of macrocyclic sulfonamide **22** with TBAX salts

A study of the complexation of macrocycle **22** with the tetrabutylammonium salts (TBAX) with the different counteranions was also determined qualitatively using ESI-mass spectra in both positive and negative modes, using an Agilent 1100 series SL LC/MSD (Trap) in the ESI mode with the following method parameters: Nebulizer (50 psi), dry gas (11 L/min), dry temperature (350 °C), for compound stability (50%), trap drive level (100%) and chloroform as a solvent.

The ESI-MS in the negative-ion mode, for the **22**:TBACl solution in chloroform, showed a mass signal at  $m/z$  1515.8 corresponding to [**22** + Cl<sup>-</sup>], and in the positive-ion mode mass signals at  $m/z$  1722 and 1781 corresponding to [**22** + TBA<sup>+</sup>] and [**22** + TBACl + Na<sup>+</sup>], respectively. The ESI-MS spectra for TBABr in the negative-ion mode showed a mass signal at  $m/z$  1561.8 corresponding to [**22** + Br<sup>-</sup>], and in the positive-ion mode mass signals at  $m/z$  1722 and 1803 corresponding to [**22** + TBA<sup>+</sup>] and [**22** + TBABr + H<sup>+</sup>], respectively.

Using the same conditions and parameters for the ESI-MS spectra used in the previous cases for TBAI did not show signals in the positive-ion mode indicating any complexation. However, when the solvent was changed from chloroform to methanol, and decreasing the dry temperature on the instrument to 200 °C, the ESI-MS spectra in the negative-ion mode showed a mass signal at  $m/z$  1607.9 corresponding to [**22** + I<sup>-</sup>], and in the positive-ion mode, mass signals at  $m/z$  1799 and 1849 corresponding to [**22** + TBA + 3H<sub>2</sub>O + Na<sup>+</sup>] and [**22** + TBAI + H<sup>+</sup>], respectively.

### 3.4.2.3 Complexation of macrocyclic sulfonamide **25** with TBAX salts

A study of the complexation of macrocyclic sulfonamide **25** with the tetrabutylammonium salts (TBAX, X= Cl, Br and I) was undertaken using the same methodologies that were conducted with macrocyclic sulfonamide **22**. Average  $K_{assoc}$  values of  $252 \pm 8$ ;  $87 \pm 6$  and  $52 \pm 5 \text{ M}^{-1}$  respectively for the TBA-chloride, bromide and iodo salts could be determined using the non-linear 1:1 binding isotherm for the NH and aromatic intra-annular proton singlet chemical shift changes, as before. These results confirmed the stronger relative affinity for the chloride anion seen previously also with the isophthaloyl amides.<sup>27</sup> The other “non-complexing” anions tested, namely the tetrafluoroborate and phosphorus hexafluoride again, as with **22** showed negligible changes for which association constants could not be determined.

#### 3.4.2.3.1 Complexation of macrocyclic sulfonamide **25** with tetrabutylammonium chloride

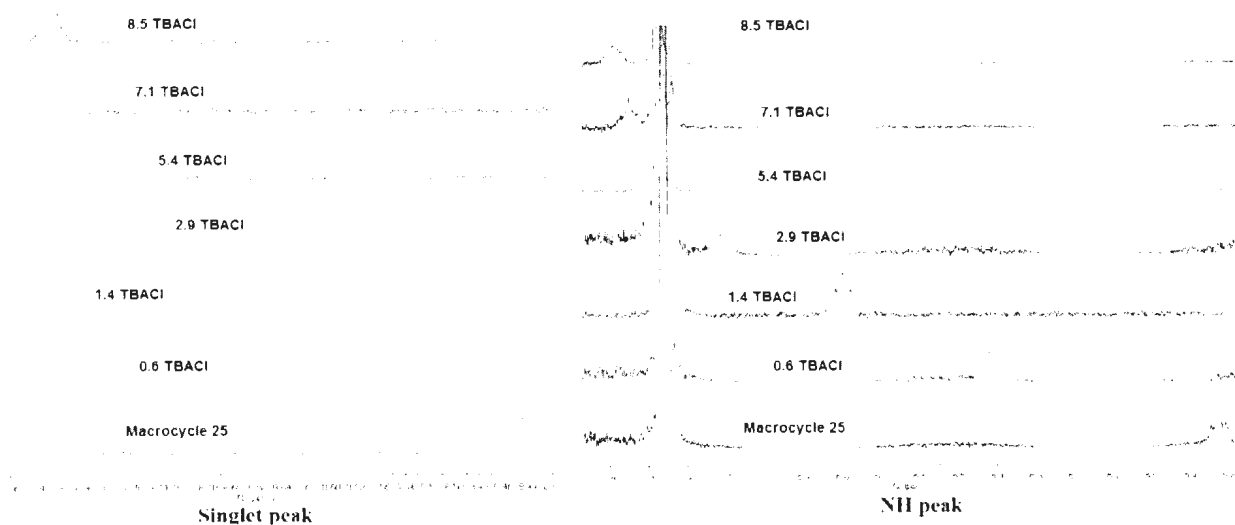


**Figure 3.12.** Expanded <sup>1</sup>H NMR (300 MHz) titration spectra of macrocyclic sulfonamide **25** with TBACl.

Figure 3.12 shows the titration spectra for **25** with TBACl. Increasing the added amounts of TBACl to the solution of **25** results in downfield chemical shift changes for both the triplet signals due to the NH protons and also the aromatic intra-annular proton singlet signals. The NH signals shifted downfield from 5.83 ppm to 7.39 ppm, whereas the singlet also shifted downfield from 8.44 ppm to 8.83 ppm (Table 3.4), indicating that complexation occurred between macrocycle **25** and TBACl. The association constants ( $K_{\text{assoc}}$ ) were determined using the non-linear 1:1 binding isotherm for both the NH and aromatic intra-annular proton singlet chemical shift changes (Table 3.4).  $K_{\text{assoc}}$  values were  $267 \pm 11$  and  $238 \pm 5 \text{ M}^{-1}$  respectively, based on the singlet and NH proton chemical shift changes (Figure 3.13).

**Table 3.4.**  $^1\text{H}$  NMR (300 MHz) titration data for both singlet and NH signals of **25** ( $4.38 \times 10^{-4} \text{ M}$ ) with TBACl.

Sample	[Guest]	[G]/[H]	Singlet $\delta$	$\Delta\delta$ Hz	NH $\delta$	$\Delta\delta$ Hz
Free host			8.442	0	5.829	0
1	2.16E-03	5	8.596	46	6.422	178
2	5.04E-03	12	8.695	76	6.796	290
3	1.04E-02	24	8.769	98	7.102	382
4	1.94E-02	44	8.810	110	7.273	433
5	2.55E-02	58	8.820	113	7.346	455
6	3.06E-02	70	8.828	116	7.389	468

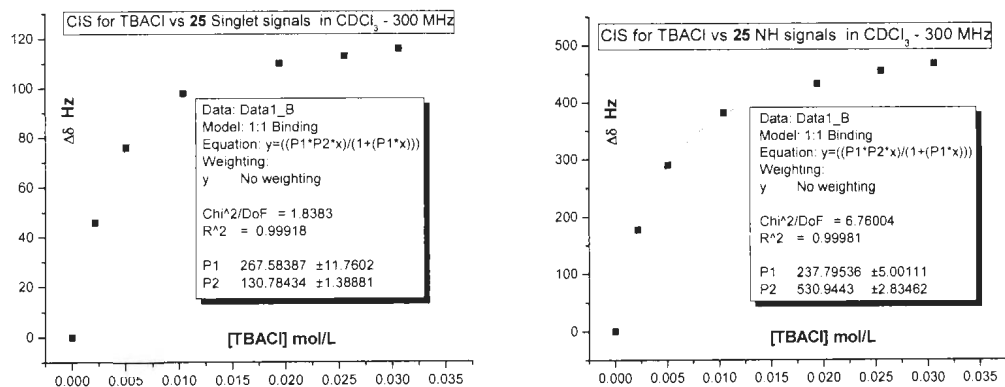


**Figure 3.13.** <sup>1</sup>H NMR (300 MHz) titration curves for both singlet and NH signals of **25** ( $4.38 \times 10^{-4}$  M) with TBACl.

#### 3.4.2.3.2 Complexation of macrocyclic sulfonamide **25** with tetrabutylammonium bromide

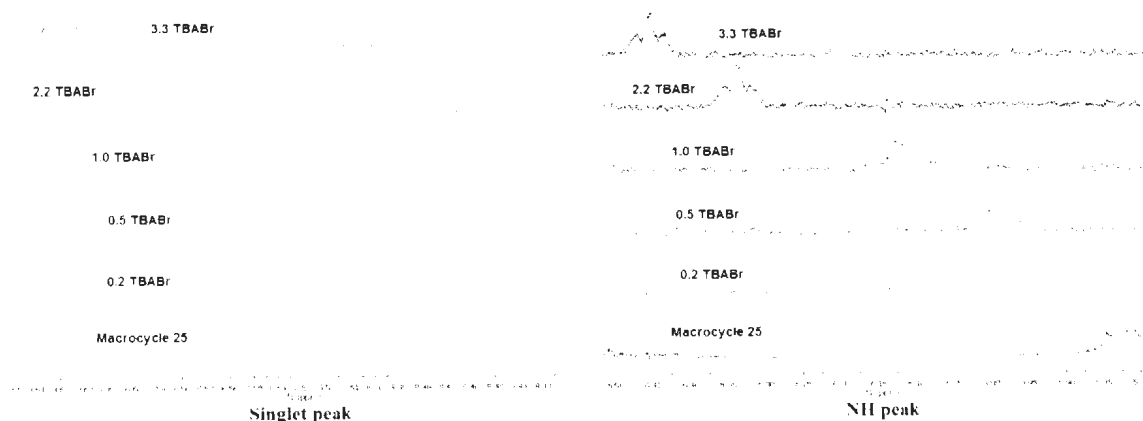


**Figure 3.14.** Expanded <sup>1</sup>H NMR (300 MHz) titration spectra of **25** with TBABr.

Titration spectra of macrocycle **25** with TBABr (Figure 3.14) show that as the amounts of TBABr are added to the solution of **25**, downfield chemical shift changes for both the triplet NH and aromatic intra-annular proton singlet signals result. The NH

signal shifted from 5.83 ppm to 6.45 ppm, and the singlet peak shifted from 8.44 ppm to 8.63 ppm (Table 3.5) indicating the complexation between **25** and TBABr.

**Table 3.5.**  $^1\text{H}$  NMR (300 MHz) titration data for both singlet and NH signals of **25** ( $4.38 \times 10^{-4}$  M) with TBABr.

Sample	[Guest]	[G]/[H]	Singlet $\delta$	$\Delta\delta$ Hz	NH $\delta$	$\Delta\delta$ Hz
Free host			8.442	0	5.829	0
1	6.20 E-04	1	8.463	6	5.916	26
2	1.55 E-03	4	8.487	14	5.992	49
3	3.10 E-03	7	8.524	25	6.106	83
5	6.82 E-03	16	8.593	45	6.339	153
6	1.02 E-02	23	8.631	57	6.452	187

$K_{\text{assoc}}$  values using the non-linear 1:1 binding isotherm were  $79 \pm 1.5$  and  $94 \pm 11 \text{ M}^{-1}$  respectively, based on the singlet and NH proton chemical shift changes (Figure 3.15).

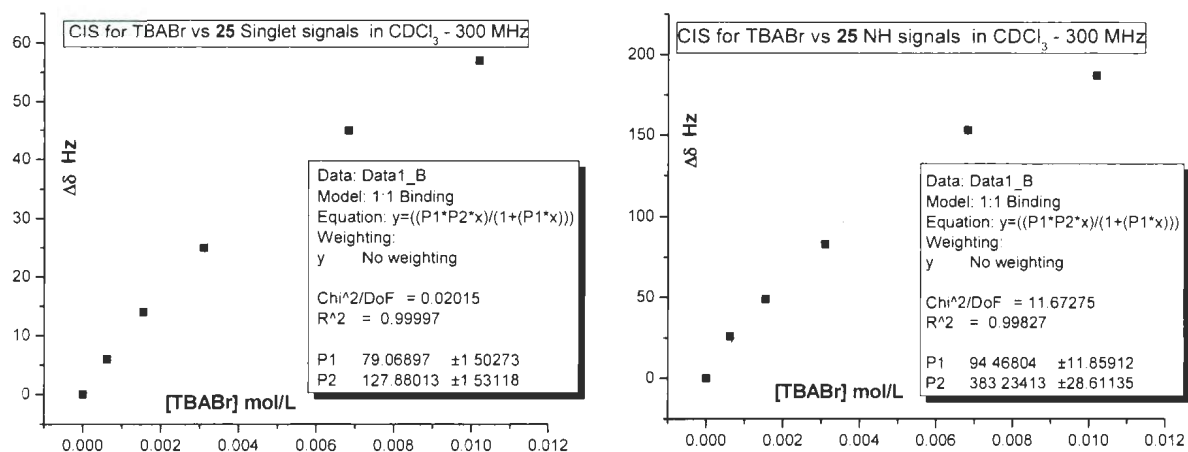


**Figure 3.15.**  $^1\text{H}$  NMR (300 MHz) titration curves for both singlet and NH signals of **25** ( $4.38 \times 10^{-4}$  M) with TBABr.

### 3.4.2.3.3 Complexation of macrocyclic sulfonamide **25** with tetrabutylammonium iodide

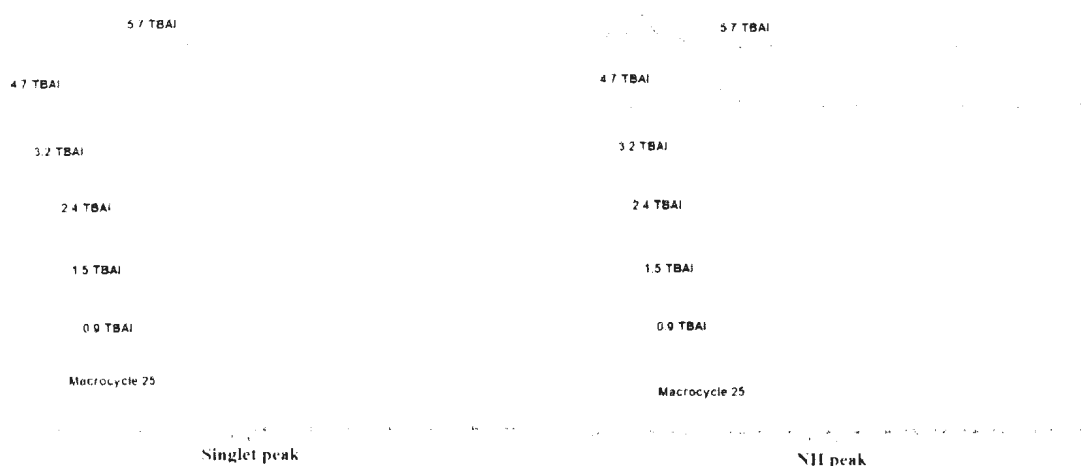


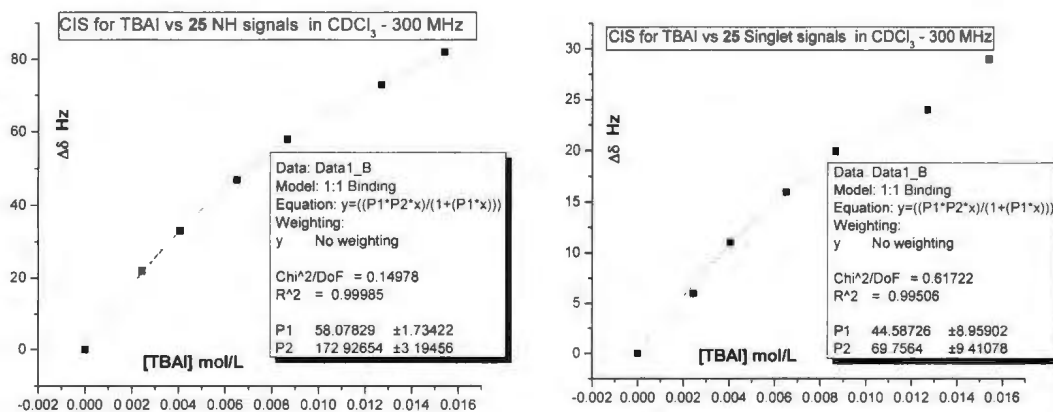
**Figure 3.16.** Expanded  $^1\text{H}$  NMR (300 MHz) titration spectra of macrocyclic sulfonamide **25** with TBAI.

The titration spectra of **25** with TBAI (Figure 3.16) show that, as the amounts of TBAI are added to the solution of **25** there are downfield chemical shift changes for both triplet (NH) and aromatic intra-annular proton singlet signals, the NH signal shifted from 5.83 ppm to 6.10 ppm, and the singlet signal shifted from 8.44 ppm to 8.54 ppm indicating complexation between compound **25** and TBAI. (Table 3.6).

Using the Origin program the concentration of the guest ([Guest]) was plotted against the difference in the chemical shift changes ( $\Delta\delta$ ) in Hz and the  $K_{assoc}$  values were  $45 \pm 9$  and  $58 \pm 2 \text{ M}^{-1}$ , respectively based on the singlet and NH proton chemical shift changes (Figure 3.17).

**Table 3.6.**  $^1\text{H}$  NMR (300 MHz) titration data for both singlet and NH signals of **25** ( $4.38 \times 10^{-4}$  M) with TBAI.

Sample	[Guest]	[G]/[H]	Singlet $\delta$	$\Delta\delta$ Hz	NH $\delta$	$\Delta\delta$ Hz
Free host			<b>8.442</b>	<b>0</b>	<b>5.829</b>	<b>0</b>
1	2.44 E-03	6	8.463	6	5.902	22
2	4.06 E-03	9	8.479	11	5.940	33
3	6.50 E-03	15	8.494	16	5.986	47
4	8.66 E-03	20	8.508	20	6.021	58
5	1.27 E-02	29	8.523	24	6.071	73
6	1.54 E-02	35	8.538	29	6.103	82

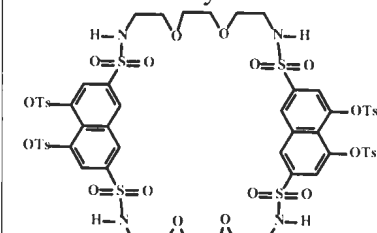
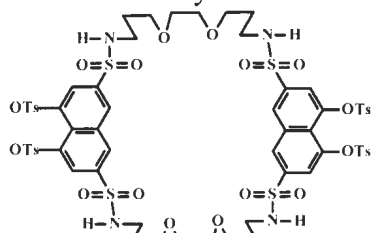


**Figure 3.17.**  $^1\text{H}$  NMR (300 MHz) titration curves for both singlet and NH signals of **25** ( $4.38 \times 10^{-4}$  M) with TBAI.

### 3.4.2.4 Comparison between the $K_{assoc}$ values of macrocycles **22** and **25** with TBAX salts

A comparison between the association constant values measured for the complexation of macrocycles **22** and **25** with TBAX salts is summarized in Table 3.7. The  $K_{assoc}$  values for **22** compared with those of macrocycle **25** are nearly 3-, 2.5- and 4-fold higher for the  $\text{Cl}^-$ ,  $\text{Br}^-$  and  $\text{I}^-$  salts respectively. There are several possible factors which could account for these differences between **22** and **25**. Firstly, the mode of complexation of the halide ion is presumed to be via hydrogen-bonding between the halide ions and the protons of the NH groups. As found by others in similar studies, the trend is:  $\text{Cl}^- > \text{Br}^- > \text{I}^-$ . Secondly, the tetrabutylammonium ion is non-coordinating so it is presumed that the ether oxygen atoms are not significant in the case of the TBAX salts as compared with the metal halides. Since presumably the distances between the NH groups in the two macrocycles are not different, a factor that could be more significant is the difference in the ring sizes leading to more conformational possibilities and a larger entropic effect therefore which needs to be overcome in the case of **25**.

**Table 3.7.**  $K_{assoc}$  values of macrocycles **22** and **25** with TBAX (X= halide) salts.

TBAX	$K_{assoc}(\text{M}^{-1})$	Macrocycle <b>22</b> 	Macrocycle <b>25</b> 
TBACl		808	252
TBABr		229	87
TBAI		222	52

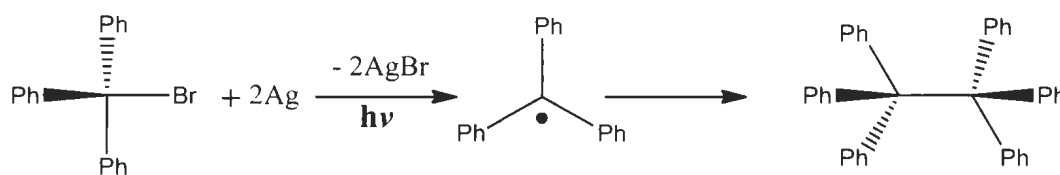
### 3.4.2.5 ESI-mass spectral data of **25** with tetrabutylammonium salts

A study of the complexation of **25** with the tetrabutylammonium salts was also conducted qualitatively using ESI-mass spectra in both positive and negative modes, conducted using an Agilent 1100 series SL LC/MSD (Trap) in the ESI mode with the following method parameters: Nebulizer (50 psi), dry gas (11 L/min), dry temperature (350 °C), for compound stability (50%), trap drive level (100%) and chloroform as a solvent. The ESI-MS of the TBACl:**25** solution in chloroform in the negative-ion mode showed a mass signal at  $m/z$  1573 corresponding to [**25** + Cl<sup>-</sup>], and in the positive-ion mode mass signals at  $m/z$  1779 and 1838 corresponding to [**25** + TBA<sup>+</sup>] and [**25** + TBACl + Na<sup>+</sup>], respectively.

For the TBABr:**25** solution the ESI-MS spectra in the negative-ion mode showed a mass signal at  $m/z$  1617 corresponding to [**25** + Br<sup>-</sup>], and in the positive-ion mode, mass signals at  $m/z$  1779 and 1882 corresponding to [**25** + TBA<sup>+</sup>] and [**25** + TBABr + Na<sup>+</sup>], respectively. But, as before, in the case of TBAI, using the same conditions and parameters of the ESI-MS spectra used for the chloride and bromide salts, no mass signals corresponding to any complexation in the positive-ion mode could be detected. However, when the solvent was changed from chloroform to methanol instead, and the dry temperature decreased to 200 °C on the Agilent instrument, as was done with sulfonamide **22**, the ESI-MS spectra in the negative-ion mode revealed a mass signal at  $m/z$  1663.6 corresponding to [**25** + I<sup>-</sup>] and in the positive-ion mode, mass signals at  $m/z$  1779, 1798 and 1929 corresponding to [**25** + TBA<sup>+</sup>], [**25** + TBA<sup>+</sup> + H<sub>2</sub>O] and [**25** + TBAI + Na<sup>+</sup>], respectively.

### 3.5 Photochemistry of sulfonamides

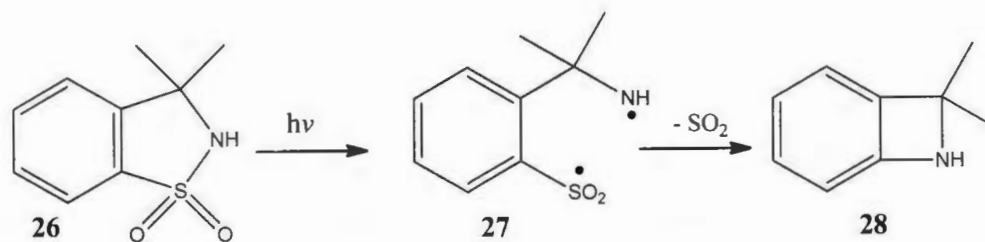
With regard to a photochemically-induced reaction observed with the [2+2] macrocyclic sulfonamides **22** and **25**, the following brief introduction to photochemistry is presented first. Photochemical reactions are an important branch of chemistry and deals with chemical reactions proceeding as a result of the absorption of light of various wavelengths by atoms or molecules. The activated atoms or molecules can result in a variety of different types of well-known transformations and it is noteworthy that Gomberg and co-workers<sup>30</sup> reported the first significant study in 1900 of a photochemical reaction involving the reaction of triphenylmethyl bromide with silver, as illustrated in Scheme 3.9.



**Scheme 3.9.** Gomberg's free radical reaction.

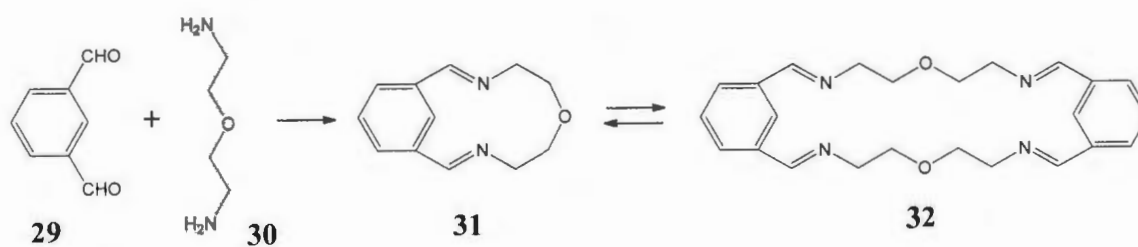
Photochemical reactions of sulfonamides in general have precedent in the literature and many are particularly of interest due to the fact that pharmaceutical aryl sulfonamide and sultam compounds may be photolabile<sup>31,32</sup> Döpp, for example, conducted photochemical studies on sultams related to saccharin and proposed several mechanisms to account for the resulting photoproducts obtained.<sup>33</sup> Weiss *et al.* also conducted a series of photochemical reactions on sulfonamides and included photo-Fries rearrangement among several different pathways proposed to account for their observed products.<sup>34</sup> In 1980 Lancaster and Smith<sup>35</sup> reported the photochemical extrusion of  $\text{SO}_2$  from

sulfonamide **26** via the presumed free-radical intermediate **27**, to form the bicyclic secondary amine **28** as shown in Scheme 3.10



**Scheme 3.10.** Lancaster and Smith sulfonamide photochemical reaction.

In a study which is of direct relevance to the phenomena seen in the work being described in this thesis, Jurczak and co-workers<sup>36</sup> synthesized the macrocyclic bis- and tetra-imines **31** and **32**, respectively, by the condensation of dialdehyde **29** with the diamine **30**. They also reported an equilibrium process between the [1+1] bis-imine **31** and the [2+2] tetra-imine **32**, which implied that the [1+1] compound formed first and then converted to the [2+2] compound or *vice versa* (Scheme 3.11).



**Scheme 3.11.** Synthesis and equilibrium process between the *bis*-**31** and *tetra*-imines **32**.

### 3.5.1 Photochemical reaction of macrocyclic sulfonamide **25**

When a chloroform solution of the [2+2] macrocyclic sulfonamide **25** was set aside to crystallize for three or four weeks in a closed vial on the bench-top it was noticed that

the color of the solution gradually changed from colorless to light yellow. It was suspected that a photochemical reaction might have occurred, as other solutions of the same compound which were protected from light with aluminum foil did not change in the same way. By way of contrast, solutions of the [1+1] macrocyclic sulfonamide **24** did not change in the same way, and afforded crystals whose X-ray structure was described previously. When crystals did form from the methanol:chloroform solution of the [2+2] macrocyclic sulfonamide **25**, it was anticipated that these would complement the X-ray structure for **24**. Surprisingly, the X-ray structure of the putative **25** however turned out to be identical to that obtained with **24**. This observation indicated that a photochemical disproportionation of the [2+2] macrocycle formed the corresponding [1+1] macrocycle.

To confirm this hypothesis, a sample of **25** was prepared by dissolving (5 mg) in 1 mL of deuterated chloroform in an NMR tube and then exposing the sample to a single low-energy 350-nm lamp in a Rayonet<sup>R</sup> photochemical reactor, for short periods and monitoring the solution directly by <sup>1</sup>H NMR. Preliminary experiments led to the optimal conditions which are described below.

Figure 3.18 shows the 300 MHz <sup>1</sup>H NMR spectra of the stepwise 350-nm photochemical reaction of the [2+2] macrocycle **25**. Increasing the light exposure time resulted in a gradual increase in the formation of the [1+1] macrocycle **24**. This can be followed by comparing the triplet NH signals of the different spectra with the triplet NH signals of the free macrocycles **24** and **25**. Thus, there is a gradual conversion of the [2+2] macrocycle into the [1+1] macrocycle. An analogous non-photochemical

disproportionation process was observed between the macrocycles reported by Jurczak and co-workers and summarized previously in Scheme 3.11.<sup>28</sup>

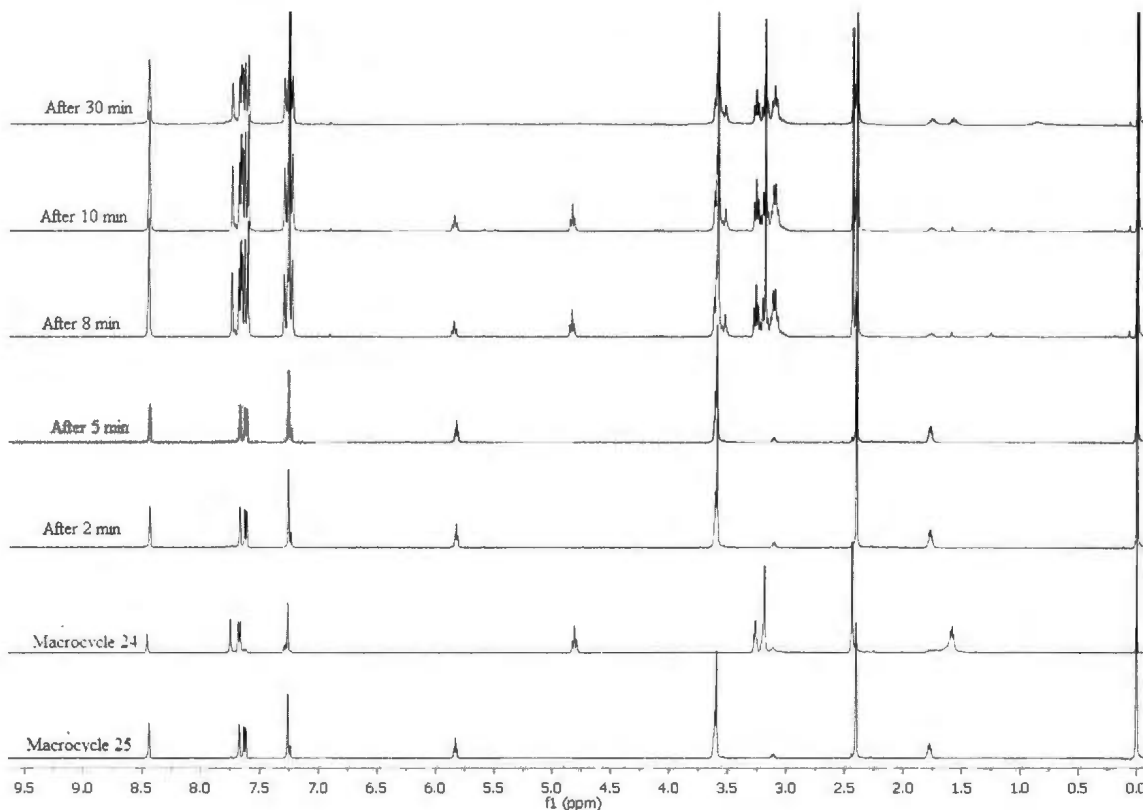


**Figure 3.18.** <sup>1</sup>H NMR (300 MHz) stepwise photochemical reaction spectra of **25**.

Figure 3.19 shows expanded sections of the <sup>1</sup>H NMR spectra of the triplet NH signals of compounds **24** and **25** (bottom two spectra, for reference). After 2 and 5 minutes of irradiation, the solution of **25** showed no changes. After 8 minutes irradiation however, the appearance of the NH triplet corresponding to the formation of the [1+1] macrocyclic sulfonamide **24** is obvious. After 10 minutes, there is an apparent increase in the relative proportion of **25** vs that of **24**. After 30 minutes of irradiation both species appear to have decomposed as the NH signals completely disappeared.

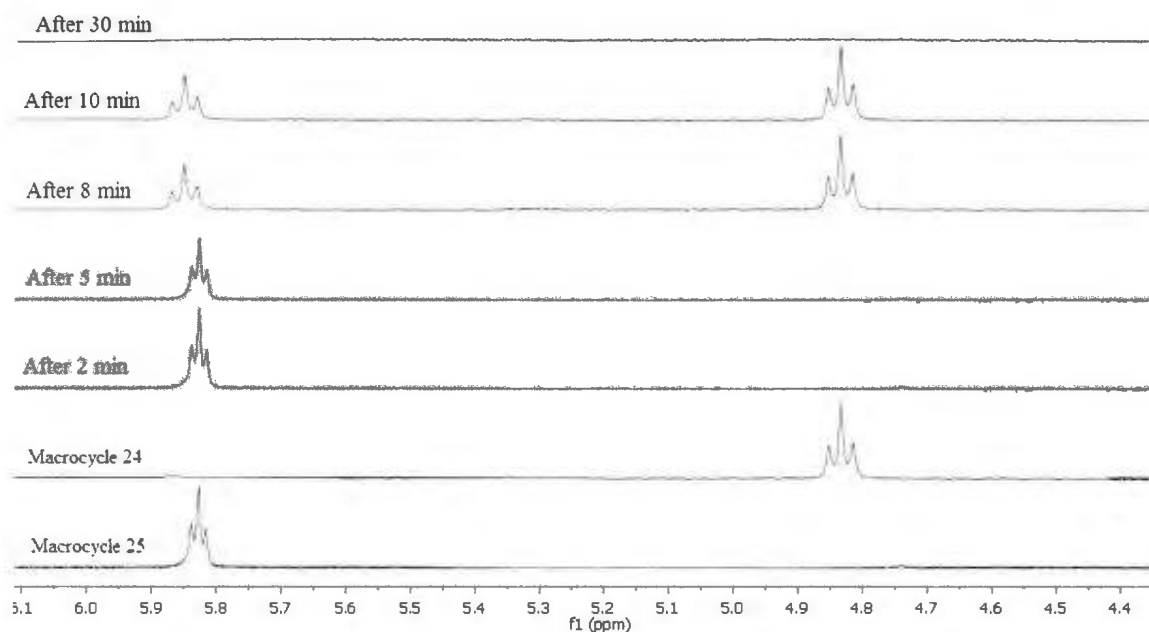
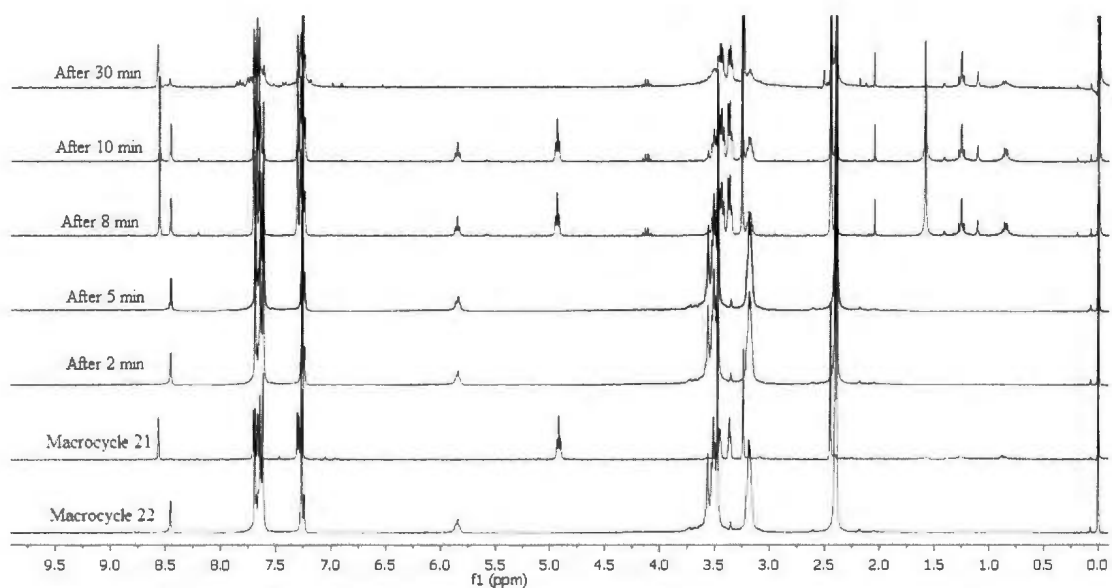


**Figure 3.19.** Expanded sections of  $^1\text{H}$  NMR (300 MHz) stepwise photochemical reaction spectra for the NH signals of **25**.

Confirmation of this process was obtained from the positive-mode APCI-mass spectra of the solution which had been irradiated for only 8 minutes which, in the positive mode, showed mass signals at  $m/z$  769 and 1538 corresponding to the masses of  $[\mathbf{24} + \text{H}^+]$  and  $[\mathbf{25} + \text{H}^+]$ , respectively.

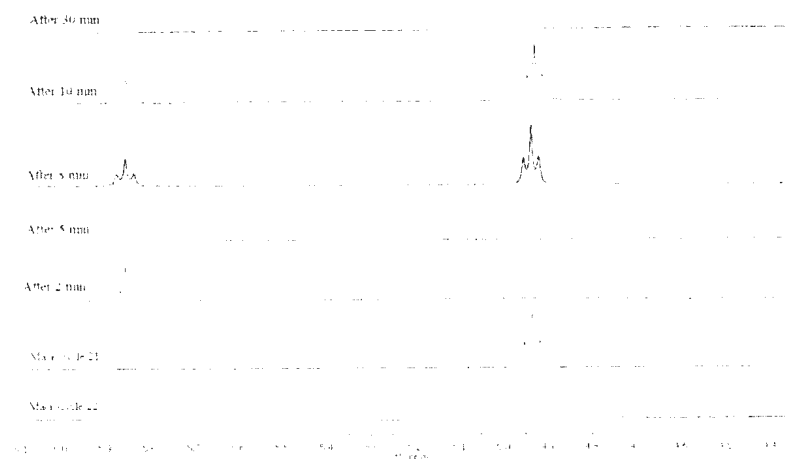
### 3.5.2 Photochemical reaction of macrocyclic sulfonamide **22**

Macrocyclic sulfonamide **22** showed a similar photochemical behaviour to that of **25**, as shown by the  $^1\text{H}$  NMR spectra of a similar timed 350 nm irradiation experiment of a solution of **22** under the same conditions that were used for **25** (Figure 3.20).



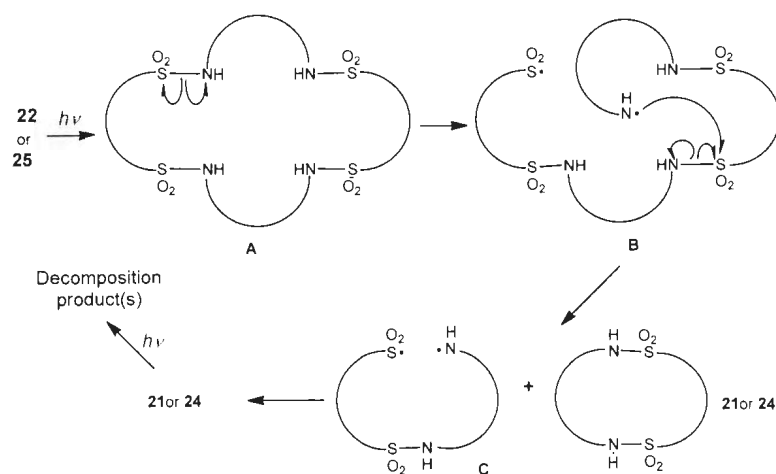
**Figure 3.20.**  $^1\text{H}$  NMR (300 MHz) stepwise photochemical reaction spectra of **22**.

Figure 3.20, and the expanded region spectra shown as Figure 3.21, show that, as was observed with macrocyclic sulfonamide **25**, the disappearance of the triplet signal of the NH protons of the [2+2] macrocycle **22** at 5.85 ppm and the emergence of the corresponding triplet of the NH groups of **21** at 4.94 ppm increased after 8 to 10 minutes of irradiation. After 30 minutes both triplet NH peaks at 4.9 and 5.8 ppm completely disappeared upon the prolonged irradiation. These findings were also confirmed by positive mode APCI-mass spectra which revealed mass signals at  $m/z$  741 and 1481 corresponding to  $[\mathbf{21} + \text{H}^+]$  and  $[\mathbf{22} + \text{H}^+]$  respectively, for the solution measured after 8 minutes of irradiation.



**Figure 3.21.** Expanded sections of  $^1\text{H}$  NMR (300 MHz) stepwise photochemical reaction spectra for the NH signals of **22**.

The mechanism can be proposed as shown in Scheme 3.12. It is presumed that a first step involves the homolytic cleavage of a sulfur-nitrogen bond in **22** (or **25**) as shown in **A** to form the di-radical species **B** which can then undergo an intramolecular homolytic bond cleavage and concomitant formation of **21** from **22** (or **24** from **25**) and the di-radical species **C** which can either form **21** or **24**, then directly undergo formation of decomposition products.



**Scheme 3.12.** Mechanism of the photochemical decomposition of compounds **22** and **25**.

### 3.6 Conclusions

Two new bis-sulfonamide macrocycles **21** and **24** and two tetrasulfonamide macrocycles **22** and **25** have been synthesized by reacting the ditosyl-protected chromotropic acid disulfonyl dichloride derivative **19** with 1,8-diamino-3,6-dioxaoctane ("Jeffamine<sup>®</sup> EDR 148") and 1,10-diamino-4,7-dioxadecane ("Jeffamine<sup>®</sup> EDR 176"), and their structures were fully characterized. The bisulfonamide macrocycle **24** afforded crystals which were suitable for a single-crystal X-ray crystallographic determination. Complexation studies of **22** and **25** were conducted with both alkali metal halides and tetrabutylammonium salts using both <sup>1</sup>H NMR and ESI MS indicating that these new macrocycles were moderately good hosts for 1:1 complexation with TBAX halides.

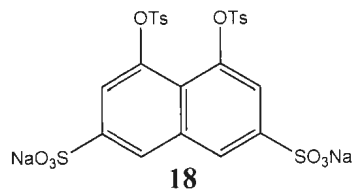
In addition, the [2+2] macrocycles **22** and **25** were shown to be photolabile and disproportionated into the corresponding [1+1] macrocyclic compounds **21** and **24** respectively, as determined by <sup>1</sup>H NMR and MS experiments.

### 3.7 Experimental section

General methods, materials, and instrumentation used were identical to those described in Chapter 2. The Huntsman Petrochemical Corporation is gratefully acknowledged for the generous gift of 1,8-diamino-3,6-dioxaoctane ("Jeffamine<sup>®</sup> EDR 148") and 1,10-diamino-4,7-dioxadecane ("Jeffamine<sup>®</sup> EDR 176").

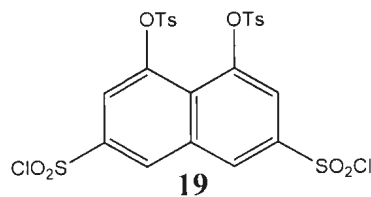
#### 3.7.1 Experimental

##### Disodium 4,5-ditosyloxynaphthalene-2,7-disulfonate (**18**)



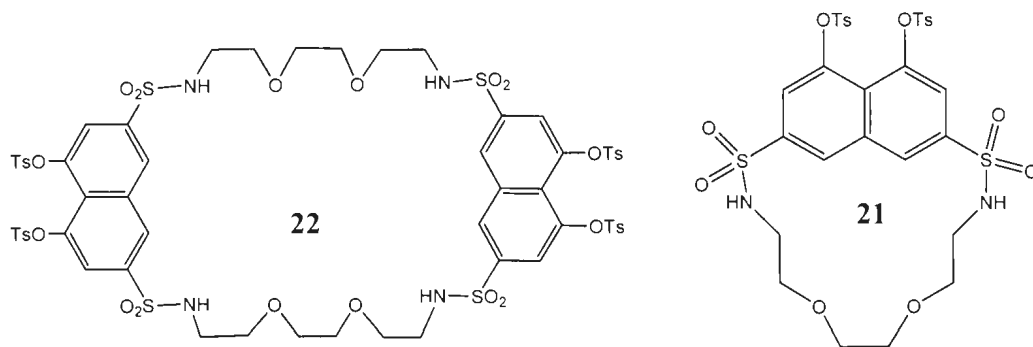
Disodium 4,5-ditosyloxynaphthalene-2,7-disulfonate (**18**) was prepared as described by K. Paruch *et al.*<sup>23</sup>

##### Ditosyloxynaphthalene-2,7-disulfonylchloride (**19**)



4,5-Ditosyloxynaphthalene-2,7-disulfonylchloride (**19**) was prepared as described by K. Paruch *et al.*<sup>23</sup>

### General conditions for the synthesis of macrocyclic sulfonamides **21** and **22**



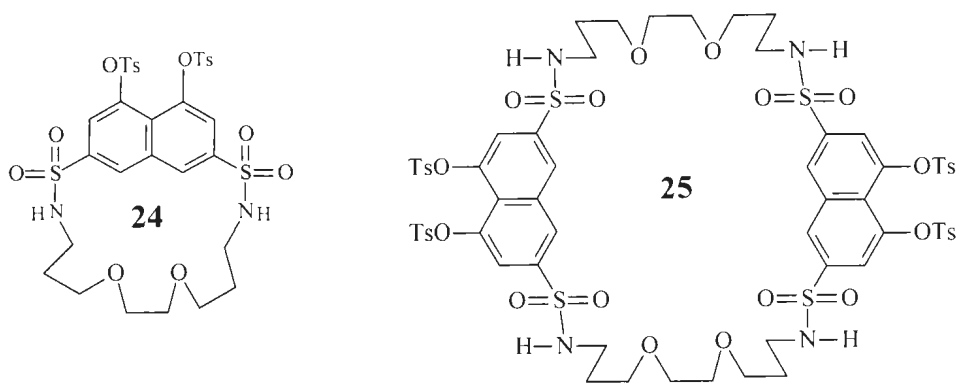
A solution of **19** (1.00 g, 1.50 mmol) in CH<sub>3</sub>CN (300 mL) was added dropwise over 1 h to a stirred solution of 1,8-diamino-3,6-dioxaoctane (**20**), (0.3 mL, 2 mmol) and triethylamine (0.4 mL, 5 mmol) in CH<sub>3</sub>CN (20 mL) at either 0 °C or -78 °C (Conditions “a”, Scheme 3.6); or by using dry methylene chloride (300 mL) at -100 °C (Conditions “b”, Scheme 3.6). In each case, the reaction solutions were maintained at the respective temperatures for 2 h and then allowed to warm to room temperature, with stirring over a period of 5 d. The reaction solutions were filtered and washed with brine (3 x 100 mL) and then with water (2 x 100 mL). The extracts were dried with anhydrous sodium sulfate and evaporated under reduced pressure to yield yellow solids, solids, which were purified by SiO<sub>2</sub> flash column chromatography using ethyl acetate–*n*-hexane (90:10) as eluent. Further purification of the fractions obtained was conducted by re-chromatographing twice by flash chromatography with the same eluent, and finally by preparative-layer thin-layer chromatography using ethyl acetate–methanol (85:15) as eluent.

Conditions “a” afforded the [1+1] macrocycle **21** (720 mg; 65%) as a colorless solid: mp 223–224 °C; <sup>1</sup>H NMR (CDCl<sub>3</sub>, 500 MHz): δ 2.45 (s, 6H), 3.24 (s, 4H), 3.36 (m, 4H), 3.45 (m, 4H), 4.90 (brt, 2H), 7.30 (d, *J* = 8.0 Hz, 4H), 7.66 (d, *J* = 1.5 Hz, 2H), 7.70 (d, *J*

= 8.0 Hz, 4H), 8.56 (d,  $J = 1.5$  Hz, 2H);  $^{13}\text{C}$  NMR ( $\text{CD}_3\text{OD}$ , 75 MHz):  $\delta$  20.1, 42.9, 68.8, 69.5, 119.8, 123.5, 127.8, 128.7, 129.4, 131.2, 134.7, 141.1, 143.6, 146.3; APCI-MS ( $m/z$ ): 741.0 (M+1, 100).

Conditions "b" afforded [1+1] macrocycle **21** (178 mg; 16%) whose spectral data was identical to that obtained from Conditions "a" and the [2+2] macrocycle **22** (520 mg; 47%) as a colourless solid: mp 175-176 °C;  $^1\text{H}$  NMR ( $\text{CDCl}_3$ , 300 MHz):  $\delta$  2.39 (s, 12H), 3.18 (m, 8H), 3.51 (m, 16H), 5.84 (t,  $J = 5.4$  Hz, 4H), 7.25 (d,  $J = 8.1$  Hz, 8H), 7.63 (d,  $J = 8.1$  Hz, 8H), 7.69 (d,  $J = 1.5$  Hz, 4H), 8.45 (d,  $J = 1.5$  Hz, 4H);  $^{13}\text{C}$  NMR ( $\text{CD}_2\text{Cl}_2$ , 75 MHz):  $\delta$  21.9, 43.5, 69.6, 70.5, 121.3, 128.5, 128.6, 129.3, 130.2, 131.7, 135.5, 139.8, 144.5, 146.8; APCI-MS ( $m/z$ ): 1481.3 (M+1, 100).

#### General conditions for the synthesis of macrocyclic sulfonamides **24** and **25**



A solution of **19** (2.00 g, 3.00 mmol) in  $\text{CH}_3\text{CN}$  (700 mL) was added dropwise over 2 hours to a stirred solution of 1,10-diamino-4,7-dioxadecane (**23**), (0.53 mL, 3 mmol) and triethylamine (0.8 mL, 11 mmol) in  $\text{CH}_3\text{CN}$  (20 mL) at either 0 °C or -78 °C (Conditions "a", Scheme 3.7); or by using dry methylene chloride (700 mL) at -100 °C (Conditions "b", Scheme 3.7). In each case, the reaction solutions were maintained at the

respective temperatures for 2 h and then allowed to warm to room temperature, with stirring over a period of 5 d. The reaction solutions were filtered and washed with brine (3 x 100 mL) and then with water (2 x 100 mL). The extracts were dried with anhydrous sodium sulfate and evaporated under reduced pressure to yield yellow solids, which were purified by using two column chromatography on silica using ethyl acetate/*n*-hexane (85:15) as eluent.

Conditions "a" afforded the [1+1] macrocycle **24** (1.7 g; 76%) as a colorless solid: mp 131-132 °C; <sup>1</sup>H NMR (CD<sub>3</sub>OD, 500 MHz): δ 1.32 (m, 4H), 2.34 (s, 6H), 2.83 (m, 4H), 2.93 (s, 4H), 3.02 (t, *J* = 6.0 Hz, 4H), 7.35 (d, *J* = 8.5 Hz, 4H), 7.50 (d, *J* = 1.5 Hz, 2H), 7.54 (d, *J* = 8.5 Hz, 4H), 8.71 (d, *J* = 1.5 Hz, 2H); <sup>13</sup>C NMR (CD<sub>3</sub>OD, 75 MHz): δ 21.6, 30.0, 41.1, 68.6, 70.7, 120.9, 122.2, 129.4, 130.2, 130.9, 132.7, 141.4, 145.5, 147.8, 162.8; APCI-MS (*m/z*): 769.0 (M+1, 100).

Conditions "b" afforded [1+1] macrocycle **24** (290 mg; 13%) whose spectral data was identical to that obtained from Conditions "a" and the [2+2] macrocycle **25** (1050 mg; 45%) as a colourless solid: mp 130-131 °C; <sup>1</sup>H NMR (CDCl<sub>3</sub>, 500 MHz): δ 1.77 (m, 8H), 2.40 (s, 12H), 3.11 (m, 8H), 3.59 (s, 8H), 3.62 (m, 8H), 5.83 (t, *J* = 6.1 Hz, 4H), 7.25 (d, *J* = 8.0 Hz, 8H), 7.62 (d, *J* = 8 Hz, 8H), 7.67 (d, *J* = 1.5, 4H), 8.44 (d, *J* = 1.5, 4H); <sup>13</sup>C NMR (DMSO-*d*<sub>6</sub>, 75 MHz): δ 22.2, 29.2, 57.9, 67.7, 69.6, 121.1, 124.2, 128.8, 129.4, 131.0, 131.3, 135.1, 140.3, 144.1, 147.1; APCI-MS (*m/z*): 1537.3 (M+1, 100).

### 3.8 References

1. (a) K. A. Connors, *Binding Constants*, Wiley, New York, 1987. (b) Association constants were calculated using non-linear curve fitting using the program ORIGINPrO 7.5 from OriginLab Corporation.
2. Eegriwe, E. *Anal. Chem.* **1937**, *110*, 22-25.
3. (a) Georghiou, P. E.; Ho, C. K. *Can. J. Chem.* **1989**, *67*, 871-876. (b) Georghiou, P. E.; Ho, C. K.; Jablonski, C. *Can. J. Chem.* **1991**, *69*, 1207-1211.
4. (a) Prand, C.; Rand, B.; Venturini, T. *J. Chromatogr. Sci.* **1981**, *19*, 308-314. b) Jandera, P.; Churacek, J. *J. Chromatogr.* **1980**, *197*, 181. c) Budesinsky, B. *Chelates in Analytical Chemistry*. Vol. 2, New York. 1969.
5. National Institute for Occupational Safety and Health, *Manual of analytical methods*, 2<sup>nd</sup> Ed. Vol. 1, Washington, DC. 1977.
6. Georghiou, P. E.; Ho, C. K.; Jablonski, C. *Can. J. Chem.* **1991**, *69*, 1207-1211.
7. Poh, B.; Lim, C.; Khoo, K. *Tetrahedron Lett.* **1989**, *30*, 1005-1008.
8. Gutsche, C. D. *Calixarenes Revisted*, The Royal Society of Chemistry, Cambridge, 1998.
9. Franca, Z.; Paola, V. *Archiv. Pharm.* **1998**, *331*, 219-223.
10. Hawing, F; Lawrence, J. *The Sulfonamides*; H. K. Lewis & Co. Ltd., 1950.
11. Lawrence, J.; Francis, J. *The Sulphonamides and Antibiotics in Man and Animals*; H.K. Lewis & Co. Ltd., 1953.
12. Claudiu, T. S.; Angela, C.; Andrea, S. *Med. Res. Rev.* **2003**, *23*, 535-558.

13. Lehn, J. M. *Supramolecular Chemistry*; Wiley-VCH: Weinheim, 1995.
14. Sneader, W. *Drug Discovery: A History, 1<sup>st</sup> Ed.*, John Willey and Sons 2005.
15. El-Atrouni, W. I.; Temesgen, Z. *Drugs Today* **2007**, *43*, 671-679.
16. Valiyaveetil, S.; Engbersen, J. F. J.; Verboom, W.; Reinhoudt, D. *Angew Chem. Int. Ed.* **1993**, *32*, 900-901.
17. a) Biernat, J. F.; Bradshaw, J. S.; Wilson, B. E.; Dalley, N. K.; Izatt, R. M. *J. Heterocyclic Chem.* **1986**, *23*, 1667-1671. b) Biernat, J. F.; Bochenska, M.; Bradshaw, J. S.; Koyama, H.; Lindh, G.; Lamb, J. D.; Christensen, J.; Izatt, R. M. *J. Inclu. Phenom.* **1987**, *5*, 729-738.
18. Eshghi, H.; Rahimizadeh, M.; Zokaei, M.; Eshghi, S.; Kihanyan, M. *Eur. J. Org. Chem.* **2011**, *2*, 47-50.
19. He, L.; An, Y.; Yuan, L.; Gong, B. *Chem. Commun.* **2005**, *30*, 3788-3790.
20. He, L.; An, Y.; Yuan, L.; Gong, B. *PNAS* **2006**, *103*, 10850-10855.
21. Bocheiqska, M.; Biernat, J. *J. Inclu. Phenom.* **1988**, *6*, 593-597.
22. Eshghi, H. *Synth. Commun.* **2008**, *38*, 2540-2547.
23. Paruch, K.; Vyklicky, L.; Katz, T.; Incarvito, C.; Rheingold, A. *J. Org. Chem.* **2000**, *65*, 8774-8782.
24. Jeffamines are the trade names for these amines supplied by Huntsman International.
25. Fielding, L. *Tetrahedron* **2000**, *56*, 6151-6170.

26. Georghiou, P. E.; Tran, A.H.; Stroud, S. S.; Thompson, D. W. *Tetrahedron* **2006**, *62*, 2036-2044.
27. Sleem, H. F.; Dawe, L. N.; Georghiou, P. E. *New J. Chem.* **2012**, *36*, 2451-2455.
28. Molecular modeling was conducted using the MMFF force field with Spartan'10 software by Wavefunction Inc., Irvine, CA
29. (a) Chmielewski, M. J.; Zielinski, T.; Jurczak, J. *Pure Appl. Chem.* **2007**, *79*, 1087-1089. (b) Chmielewski, M. J.; Jurczak, J. *Chem. Eur. J.* **2006**, *12*, 7605-7609. (c) Chmielewski, M. J.; Jurczak, J. *Chem. Eur. J.* **2005**, *11*, 6080. (d) Chmielewski, M.; Szumna, A.; Jurczak, J. *Tetrahedron Lett.* **2004**, *45*, 8699. (e) Szumna, A.; Jurczak, J. *Eur. J. Org. Chem.* **2001**, 4031.
30. Parsons, A. F. *An Introduction to Free Radical Chemistry*; Blackwell Science Ltd., 2000.
31. Taylor, T.; Francis, A. *Photostability of Drugs and Drug Formulations*, Ed. H. H., London, 1996.
32. Papageorgiou, G.; Corrie, T. *Tetrahedron* **1999**, *55*, 237-254.
33. Döpp, D. *International J. Photoenergy* **2001**, *3*, 41-48.
34. Weiss, B.; Dürr, H.; Haas, H. J. *Angew. Chem., Int. Ed. Engl.* **1980**, *19*, 648-650.
35. Lancaster, M.; Smith, D. J. H. *J. Chem. Soc., Chem. Commun.* **1980**, 471-472.
36. Ceborska, M.; Tarnowska, A.; Jurczak, J. *Tetrahedron* **2010**, *66*, 9532-9537.

## **Chapter 4**

### **$^1\text{H}$ -NMR Spectroscopic Studies of Tetrabutylammonium Halides**

## Chapter 4

### <sup>1</sup>H-NMR Spectroscopic Studies of Tetrabutylammonium Halides

#### 4.1 Introduction

This chapter describes a preliminary <sup>1</sup>H-NMR spectroscopic study of tetrabutylammonium halides (TBAX: X = Cl<sup>-</sup>, Br<sup>-</sup> or I<sup>-</sup>) alone in CDCl<sub>3</sub> solutions. It had previously been noticed in the titration experiments described in Chapters 2 and 3 that the reference residual proton signal (i.e. from CHCl<sub>3</sub>) in the solvent CDCl<sub>3</sub> was shifted downfield upon the successive addition amounts of TBAX salts to the solutions of the various host molecules studied. It was decided that a study of this phenomenon was warranted to quantify the extent of these chemical shift changes. From the resulting titration plots obtained from the addition of only the TBAX salts to the CDCl<sub>3</sub> solvent, linear concentration-chemical shift relationships in each case could be determined.

##### 4.1.1 NMR studies of the complexation of tetrabutylammonium halides (TBAX)

In 1968 Green and Martin<sup>1</sup> published an extensive and insightful study in which they reported the interactions of tetrabutylammonium halides (TBAX; where X = Cl<sup>-</sup>, Br<sup>-</sup> or I<sup>-</sup>) with various trihalomethanes, including chloroform, in two different solvents, acetonitrile and tetrachloromethane using both <sup>1</sup>H NMR and IR spectroscopy. They found that the <sup>1</sup>H NMR chemical shifts of the trihalomethane protons changed upon the addition of tetrabutylammonium halides in these solvents.

**Table 4.1.** Comparison between  $^1\text{H}$  NMR chemical induced shift changes and association constants of different trihalomethane-base complexes.<sup>1</sup>

Acceptor (trichloromethane)	Donor (base)	Solvent	K ( $\text{M}^{-1}$ )	Limiting shift (ppm)
$\text{CHF}_3$	$\text{Cl}^-$	$\text{CCl}_4$	$2.43 \pm 0.13$	$- 2.15 \pm 0.06$
	$\text{Br}^-$		$1.38 \pm 0.16$	$- 2.17 \pm 0.21$
	$\text{I}^-$		$0.55 \pm 0.30$	$- 3.10 \pm 1.7$
$\text{CHCl}_3$	$\text{Cl}^-$	$\text{CCl}_4$	$2.51 \pm 0.17$	$- 2.92 \pm 0.12$
	$\text{Br}^-$		$1.78 \pm 0.08$	$- 2.51 \pm 0.08$
	$\text{I}^-$		$1.07 \pm 0.43$	$- 2.30 \pm 0.90$
$\text{CHCl}_3$	$\text{Cl}^-$	$\text{CH}_3\text{CN}$	$1.18 \pm 0.05$	$- 3.08 \pm 0.11$
	$\text{Br}^-$		$0.73 \pm 0.09$	$- 2.76 \pm 0.33$
	$\text{I}^-$		$0.48 \pm 0.05$	$- 2.18 \pm 0.22$
$\text{CHBr}_3$	$\text{Cl}^-$	$\text{CCl}_4$	$2.45 \pm 0.16$	$- 2.29 \pm 0.10$
	$\text{Br}^-$		$1.86 \pm 0.09$	$- 2.82 \pm 0.04$
	$\text{I}^-$		$1.95 \pm 0.45$	$- 1.06 \pm 0.22$
$\text{CHBr}_3$	$\text{Cl}^-$	$\text{CH}_3\text{CN}$	$1.10 \pm 0.06$	$- 2.34 \pm 0.11$
	$\text{Br}^-$		$1.11 \pm 0.20$	$- 1.57 \pm 0.24$
	$\text{I}^-$		$1.17 \pm 0.09$	$- 0.83 \pm 0.05$
$\text{CHI}_3$	$\text{Cl}^-$	$\text{CH}_3\text{CN}$	$3.30 \pm 0.25$	$0.31 \pm 0.01$
	$\text{Br}^-$		$3.76 \pm 0.22$	$0.32 \pm 0.01$
	$\text{I}^-$		$3.56 \pm 0.18$	$0.36 \pm 0.01$
$\text{CHCl}_3$	Pyridine	$\text{CCl}_4$	$0.38 \pm 0.07$	$- 1.07 \pm 0.19$
$\text{CHBr}_3$	Pyridine		$0.34 \pm 0.05$	$- 1.16 \pm 0.17$
$\text{CHI}_3$	Pyridine		$0.93 \pm 0.07$	$- 0.38 \pm 0.06$

Table 4.1 shows the 60 MHz  $^1\text{H}$  NMR chemical shift changes and the resultant association constants of the trihalomethane protons with the addition of the tetrabutylammonium halides in  $\text{CH}_3\text{CN}$  or  $\text{CCl}_4$ . In particular, it can be seen that the highest  $K$  values for  $\text{CHCl}_3$  as the acceptor molecule in both solvents, were in the order of  $\text{Cl}^- > \text{Br}^- > \text{I}^-$  for the respective TBAX salts. This trend is typical of what was seen

when the same TBAX salts were used with the anion receptors reported in Chapters 2 and 3 of this thesis.

Figure 4.1, taken from Green and Martin's paper, shows a typical titration curve for the complex formation of  $\text{CHCl}_3$  with TBABr in  $\text{CH}_3\text{CN}$  solution. The  $K$  value determined by these authors using a modified Benesi-Hildebrand plot was  $0.73 \pm 0.09 \text{ M}^{-1}$ . Based upon the data in Figure 4.1, and using the non-linear 1:1 binding isotherm which has been used in all of the binding studies reported in the earlier chapters of this thesis, we determined a comparable value of  $0.94 \pm 0.04 \text{ M}^{-1}$ .

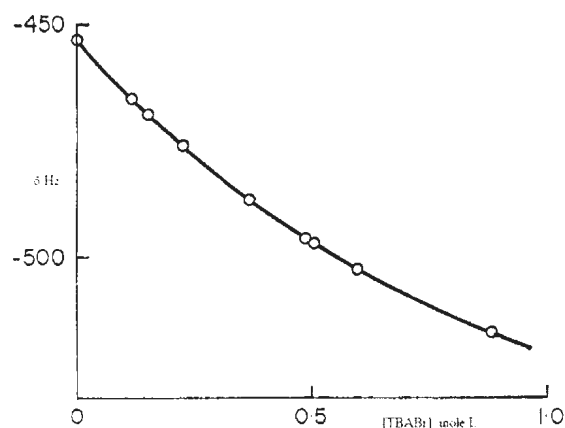


**Figure 4.1.** Proton shielding of 0.1 M  $\text{CHCl}_3$  in  $\text{CH}_3\text{CN}$  as a function of TBABr concentration. [Adapted with permission from ref. 1]

Green and Martin also reported an IR spectroscopic titration study of deuterated chloroform with TBACl and TBABr in  $\text{CCl}_4$  solvent in which the characteristic "C-D H-bonded stretch band"<sup>2,3</sup> in the  $2170\text{-}2200 \text{ cm}^{-1}$  range could be observed for each of the  $\text{CDCl}_3\text{:TBACl}$  and  $\text{CDCl}_3\text{:TBABr}$  complexes. The intensity of this band was found to be proportional to the concentration of the respective complex as measured by using the equilibrium constant that they obtained from the  $^1\text{H}$  NMR measurements. Linear

relationships between the complex concentration and the intensity of H-bond band could be clearly seen. The authors concluded that the observed association constants which increased with decreasing ionic radius of the anion (i.e.  $\text{Cl}^- > \text{Br}^- > \text{I}^-$ ) was as a result of strongly bound 1:1 complexes formed between the anions and the chloroform in the dilute solutions in the weakly interacting solvent. They concluded also that the association energies of the complexes are "...dominated by the polarization of the carbon-halogen structure of the molecule(s), rather than by the electrophilicity of the C—H fragment", and that "a simple monopole-dipole electrostatic model" could account for their observed data. For chloroform the evidence suggested that the interaction is between the halide ion and the hydrogen of chloroform whereas for tribromo- and triiodomethane the interactions are between the halide ion and the halogens.<sup>4</sup>

In 1963, another study reported by Kaiser revealed the effect of the chemical shift changes upon complexation of chloroform in dioxane.<sup>5</sup>

#### **4.2 Complexation studies of different TBAX halides in $\text{CDCl}_3$ solutions**

In preliminary studies conducted for this thesis, the maximum chemical shift changes were determined using saturated solutions of the TBAX halides in  $\text{CDCl}_3$  with TMS internal standard. For the titration studies however, aliquots of each of the TBAX salts were added into separate sample vials. To each of these samples, 1.00 mL volumes of  $\text{CDCl}_3$  were added and the resulting solutions were sonicated at room temperature for 30 min and then allowed to stand for 24 h before measuring their  $^1\text{H}$  NMR spectra (Figures 4.2, 4.4, 4.6 and 4.8). It can be noted that before each measurement the instrument was re-shimmed. Plots of the observed chemical shifts ( $\Delta\delta$  Hz) for the

residual proton signal of the  $\text{CDCl}_3$  solvent against the molar concentrations of the TBAX salts in the  $\text{CDCl}_3$  solutions were produced. These plots resemble the linear portion of Beer-Lambert plots rather than providing any evidence for 1:1 binding between the solvent and the TBAX salts. From the least-squares linear regression plots (Figures 4.3, 4.5, 4.7 and 4.9), slopes of 174, 162, 135 and 47  $\text{Hz}\cdot\text{M}^{-1}$  respectively, were obtained for the data (Tables 4.2 - 4.5) from the chloride, bromide, iodide and tetrafluoroborate salts.

#### 4.2.1 Titration of TBACl with $\text{CDCl}_3$

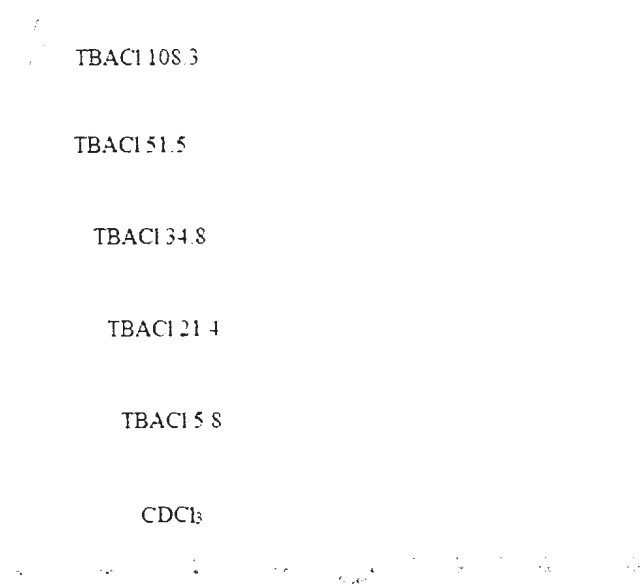


**Figure 4.2.**  $^1\text{H}$  NMR (300 MHz) expanded titration spectra for the residual proton signal of the  $\text{CDCl}_3$  solvent with increasing amounts of TBACl.

Figure 4.2 shows the titration spectra for TBACl with  $\text{CDCl}_3$  in which the downfield chemical shift changes from 7.26 ppm to 7.49 ppm can be seen for the residual proton signal of  $\text{CDCl}_3$ . Table 4.2 summarizes the data which were plotted in Figure 4.3.

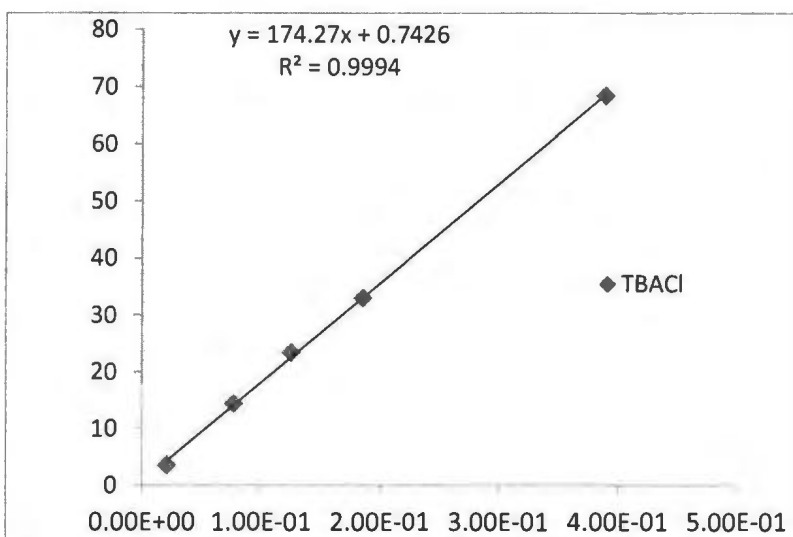


**Figure 4.3.** Least-squares linear regression plot for the  $\text{CDCl}_3$ : TBACl data of Table 4.2.

**Table 4.2.**  $^1\text{H}$  NMR (300 MHz) titration data from Figure 4.2.

Sample	TBACl (g)	moles of TBACl	[TBACl]	$\text{CDCl}_3$ $\delta$	$\Delta\delta$	Hz
				7.260	0	0
1	5.80E-03	2.09E-05	2.09E-02	7.272	0.01	3.6
2	2.14E-02	7.70E-05	7.70E-02	7.308	0.05	14.4
3	3.48E-02	1.25E-04	1.25E-01	7.338	0.08	23.4
4	5.15E-02	1.85E-04	1.85E-01	7.370	0.11	33
5	1.08E-01	3.90E-04	3.90E-01	7.488	0.23	68.4

### 4.2.2 Titration of TBABr with $\text{CDCl}_3$

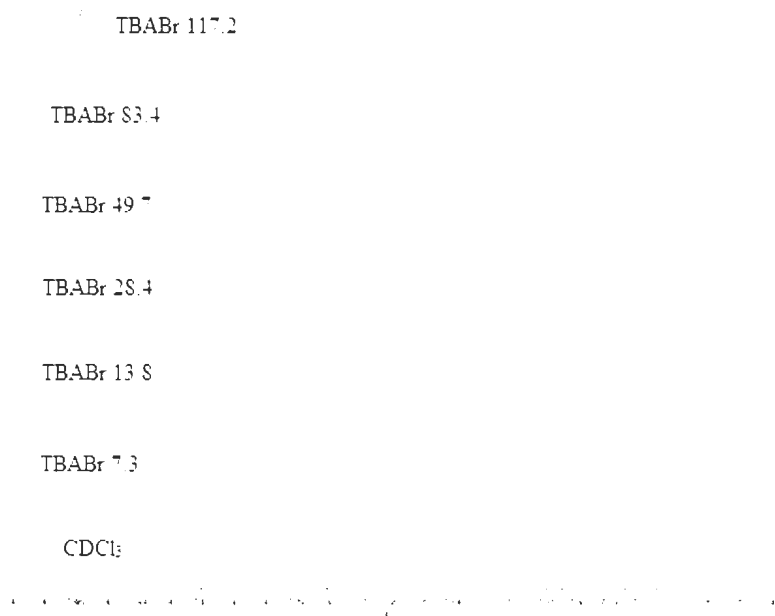


**Figure 4.4.**  $^1\text{H}$  NMR (300 MHz) expanded titration spectra for the residual proton signal of the  $\text{CDCl}_3$  solvent with increasing amounts of TBABr.

Figure 4.4 shows the titration spectra for TBABr with  $\text{CDCl}_3$  in which the downfield chemical shift changes from 7.26 ppm to 7.46 ppm can be seen for the residual proton signal of  $\text{CDCl}_3$ . Table 4.3 summarizes the data plotted in Figure 4.5.

**Table 4.3.**  $^1\text{H}$  NMR (300 MHz) titration data from Figure 4.4.

Sample	TBABr (g)	moles of TBABr	[TBABr]	$\text{CDCl}_3$ $\delta$	$\Delta\delta$	Hz	$1/\Delta\delta$
				7.260	0	0	
1	7.30E-03	2.26E-05	2.26E-02	7.274	0.01	4.2	0.238
2	1.38E-02	4.28E-05	4.28E-02	7.284	0.02	7.2	0.139
3	2.84E-02	8.81E-05	8.81E-02	7.310	0.05	15	0.067
4	4.97E-02	1.54E-04	1.54E-01	7.354	0.09	28.2	0.035
5	8.34E-02	2.59E-04	2.59E-01	7.402	0.14	42.6	0.023
6	1.17E-01	3.64E-04	3.64E-01	7.457	0.20	59.1	0.02

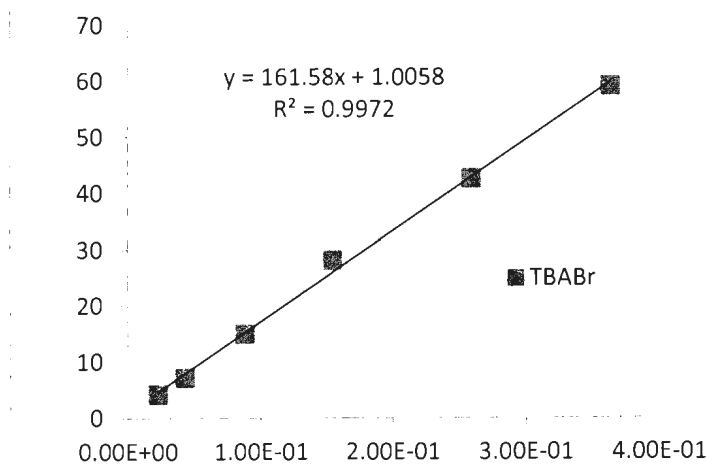


**Figure 4.5.** Least-squares linear regression plot for the  $\text{CDCl}_3$ : TBABr data of Table 4.3.

#### 4.2.3 Titration of TBAI with $\text{CDCl}_3$

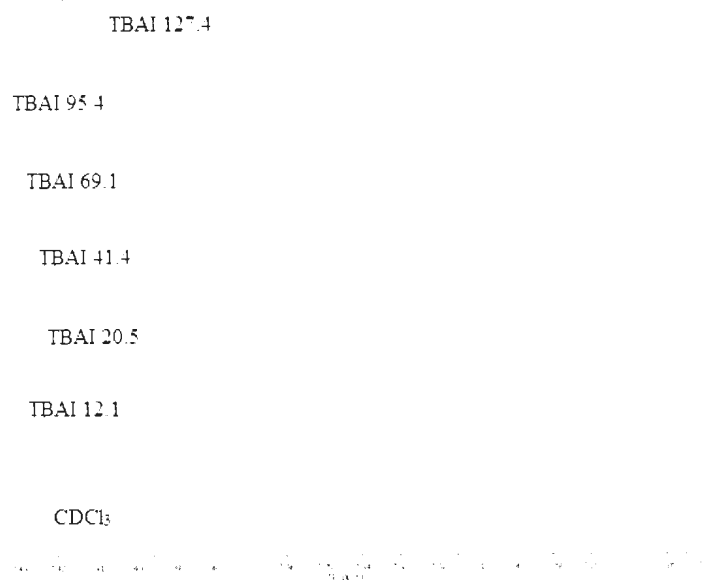


**Figure 4.6.**  $^1\text{H}$  NMR (300 MHz) expanded titration spectra for the  $\text{CDCl}_3$  solvent signal with TBAI.

Figure 4.6 shows the titration spectra for TBAI with  $\text{CDCl}_3$  in which the downfield chemical shift changes from 7.26 ppm to 7.42 ppm for the residual proton signal of  $\text{CDCl}_3$ . Table 4.4 summarizes the data plotted in Figure 4.7.

**Table 4.4.**  $^1\text{H}$  NMR (300 MHz) expanded titration data from Figure 4.6.

Sample	TBAI (g)	moles of TBAI	[TBAI]	$\text{CDCl}_3\delta$	$\Delta\delta$	Hz
				7.260	0	0
1	1.21E-02	3.28E-05	3.28E-02	7.277	0.02	5.1
2	2.05E-02	5.55E-05	5.55E-02	7.287	0.03	8.1
3	4.14E-02	1.12E-04	1.12E-01	7.314	0.05	16.2
4	6.91E-02	1.87E-04	1.87E-01	7.349	0.09	26.7
5	9.54E-02	2.58E-04	2.58E-01	7.379	0.12	35.7
6	1.27E-01	3.45E-04	3.45E-01	7.417	0.16	47.1

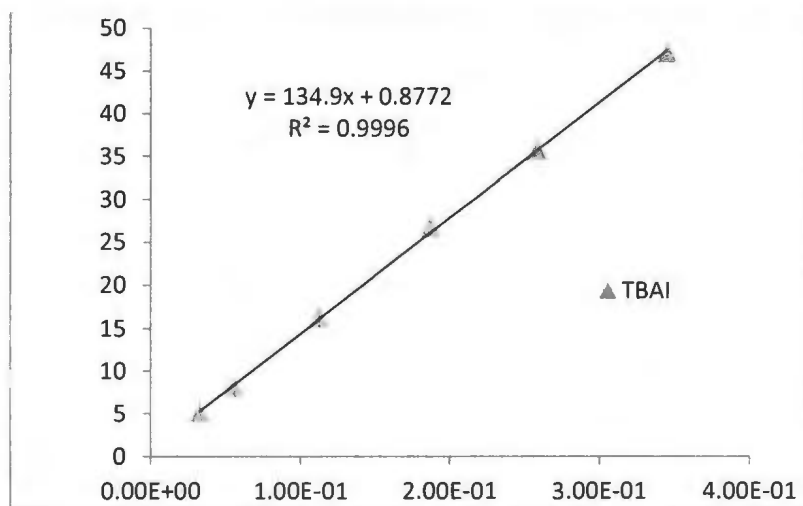


**Figure 4.7.** Least-squares linear regression plot for the  $\text{CDCl}_3$ : TBAI data of Table 4.4.

#### 4.2.4 Titration of TBABF<sub>4</sub> with CDCl<sub>3</sub>

Figure 4.8 shows the titration spectra for TBABF<sub>4</sub> with CDCl<sub>3</sub> in which the downfield chemical shift changes from 7.26 ppm to 7.33 ppm for the residual proton signal of CDCl<sub>3</sub>. Table 4.5 summarizes the data which were plotted in Figure 4.9.

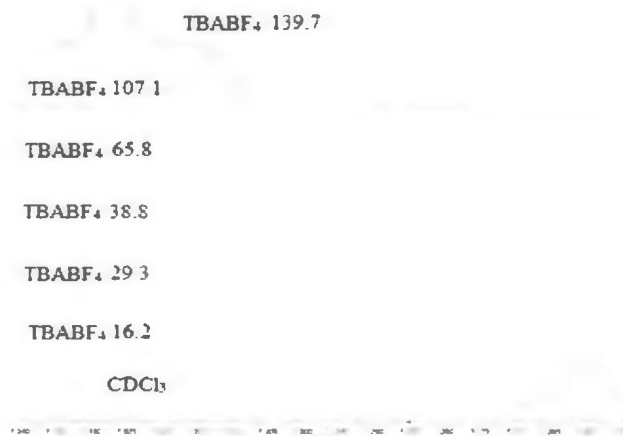


**Figure 4.8.** <sup>1</sup>H NMR (300 MHz) titration spectra for the residual proton signal of the CDCl<sub>3</sub> solvent with increasing amounts of TBABF<sub>4</sub>.

**Table 4.5.** <sup>1</sup>H NMR (300 MHz) titration data from Figure 4.10.

Sample	TBABF <sub>4</sub> (g)	moles of TBABF <sub>4</sub>	[TBABF <sub>4</sub> ]	CDCl <sub>3</sub> δ	Δδ	Hz
				7.260	0	0
1	1.62E-02	4.92E-05	4.92E-02	7.269	0.01	3
2	2.93E-02	8.90E-05	8.90E-02	7.276	0.02	5
3	3.88E-02	1.18E-04	1.18E-01	7.280	0.02	6
4	6.58E-02	2.00E-04	2.00E-01	7.294	0.03	10
5	1.07E-01	3.25E-04	3.25E-01	7.313	0.05	16
6	1.39E-01	4.21E-04	4.21E-01	7.328	0.07	20

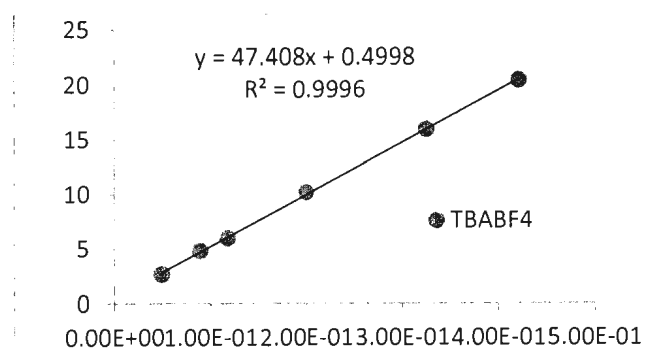


**Figure 4.9.** Least-squares linear regression plot for the  $\text{CDCl}_3$ : TBABr data of Table 4.5.

#### 4.2.5 Comparison between the slopes observed with the TBAX salts in $\text{CDCl}_3$

Table 4.6 summarizes the values of the slopes measured for the four TBAX salts in  $\text{CDCl}_3$  solutions. There are a couple of possible factors which could account for these differences. First, there is the obvious difference in the dielectric constants of the solutions, which however were not determined. Secondly, since the mode of complexation is presumed to be *via* hydrogen-bonding between the halide ions and the residual protons in the  $\text{CDCl}_3$  solvent, as more of the halide is added to the fixed amount of the solvent, complexation should increase. Therefore the chemical shift of the residual chloroform signal should change accordingly. However, since a true saturation between the “guest” (i.e. the TBAX salt) and the solvent was not reached, a “binding constant” could not be determined. Nevertheless, as found by others (and ourselves as noted in Chapter 2 of this thesis) in host-guest studies in which TBAX salts were employed, the trend in the slopes observed here is in a similar order to that observed for the binding constants observed in those studies, namely:  $\text{Cl}^- > \text{Br}^- > \text{I}^- > \text{BF}_4^-$ .

**Table 4.6.** Slope values of  $\text{CDCl}_3$  with TBAX ( $\text{X} = \text{Cl}^-$ ,  $\text{Br}^-$ ,  $\text{I}^-$  and  $\text{BF}_4^-$ ) salts.

TBAX	TBACl	TBABr	TBAI	TBABF <sub>4</sub>
Slope ( $\text{Hz}\cdot\text{M}^{-1}$ )	174	162	135	47

### 4.3 X-Ray structure of TBABr with $\text{CDCl}_3$

When one of the titration samples containing TBABr in  $\text{CDCl}_3$  was allowed to slowly crystallize at room temperature, colorless crystals formed. In spite of the crystals being irregular, Dr. L. N. Dawe succeeded to solve this problem by reprocessing the raw data using a FS process. PLATON was used to identify a twin law, which was applied by refining using the newly released SHELXL-2013 through OLEX2, to obtain the X-ray structure of TBABr: $\text{CDCl}_3$  shown in Figure 4.10.

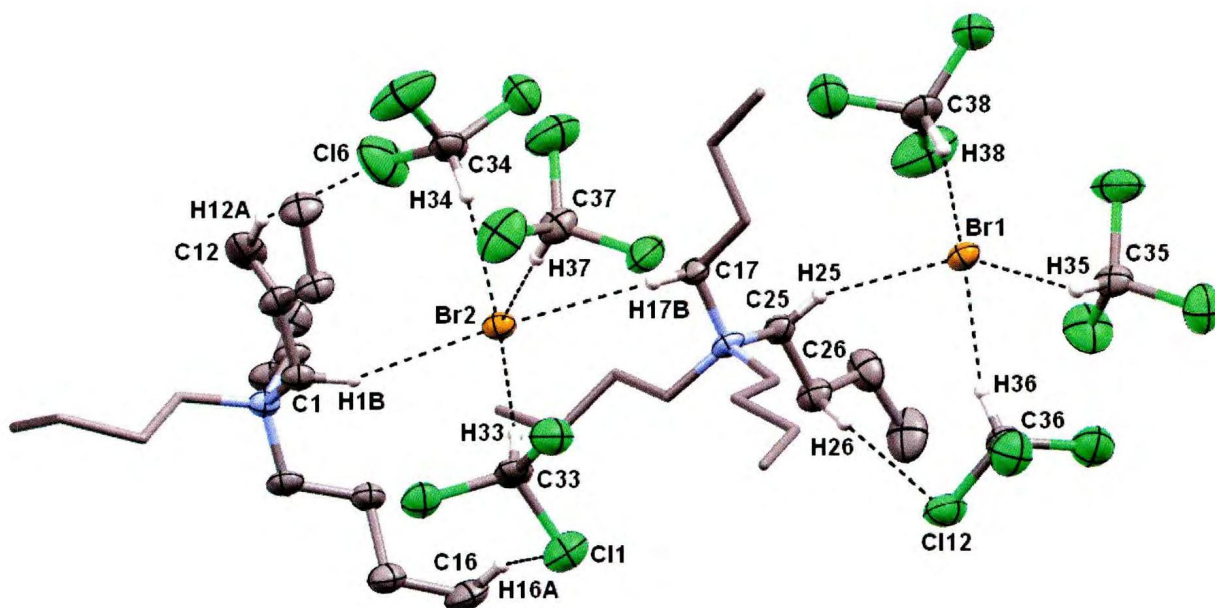


**Figure 4.10.** Asymmetric unit of TBABr: $\text{CHCl}_3$ . H-atoms not involved in halogen interactions omitted.  $\text{TBA}^+$  chains not involved in halogen interactions represented as capped sticks. All other non-hydrogen atoms represented as 30% probability ellipsoids.

**Table 4.7.** lists the short-contact distances for the bromide anion to chloroform protons derived from the X-ray structure shown in Figure 4.10.

<i>D—H...A</i>	<i>H...A</i>	<i>D...A</i>	<i>-vdW distance</i>
C33—H33...Br2	2.50	3.488 (11)	-0.547
C34—H34...Br2	2.56	3.551 (11)	-0.494
C37—H37...Br2	2.58	3.570 (13)	-0.464
C35—H35...Br1	2.59	3.514 (12)	-0.463
C36—H36...Br1	2.50	3.471 (12)	-0.551
C38—H38...Br1	2.59	3.572 (10)	-0.456

Gratifyingly, the X-ray structure obtained is very similar to the structure generated using semi-empirical (PM-3) molecular modeling<sup>6</sup> study with SpartanPro'10 for what was presumed to be a complex of TBABr with chloroform molecules. This structure is shown in Figure 4.11 and clearly shows that three CHCl<sub>3</sub> molecules surround each bromide ion.

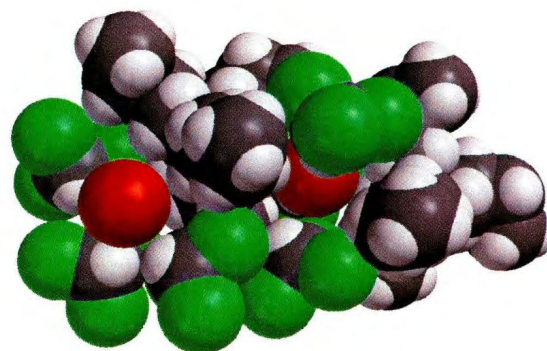


**Figure 4.11.** SpartanPro'10 molecular modeling of a putative (TBABr)<sub>2</sub>(CHCl<sub>3</sub>)<sub>6</sub> complex, green = chloride and red = bromide.

A recent paper by Unno and co-workers<sup>7</sup> reported the synthesis of a silanediol-based anion receptor **1**. A <sup>1</sup>H NMR titration of receptor **1** with TBACl in chloroform,

revealed a typical 1:1 binding with  $K_{assoc} = 1.44 \pm 0.11 \times 10^2 \text{ M}^{-1}$ ; and for 1:TBABr a  $K_{assoc} = 50 \pm 1.3 \text{ M}^{-1}$ .

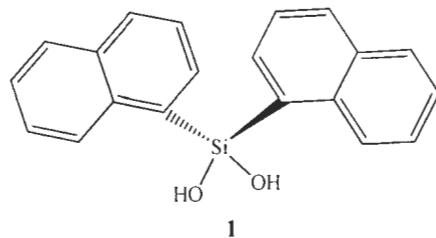
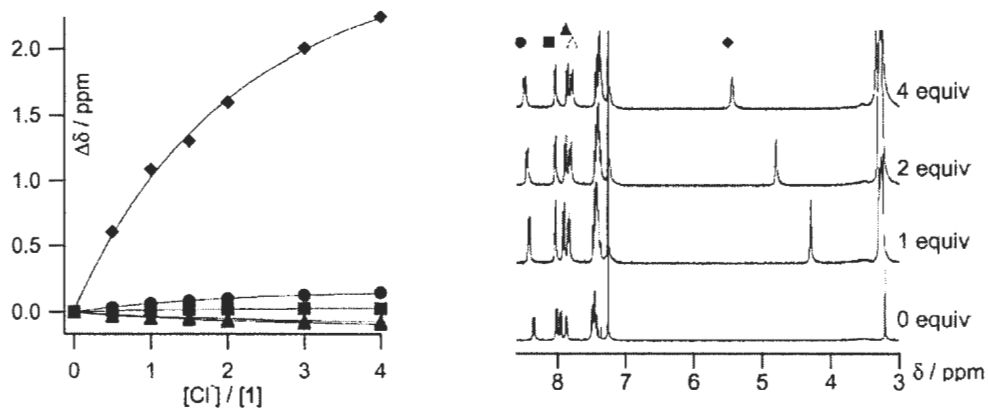
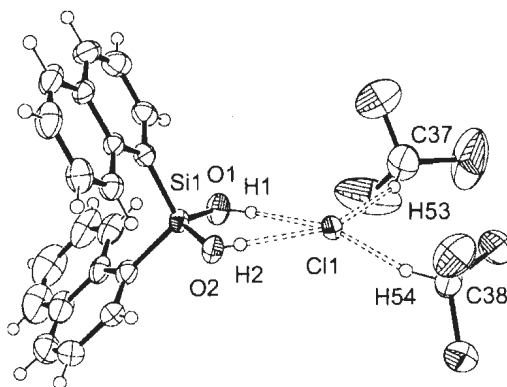


Figure 4.12 shows a  $^1\text{H}$  NMR titration curve of 1:TBACl in  $\text{CDCl}_3$ , arising from a downfield chemical shift changes in both the hydroxyl and aromatic signals of receptor 1.



**Figure 4.12.**  $^1\text{H}$  NMR titration curve and spectra of 1:TBACl in  $\text{CDCl}_3$ .<sup>7</sup>

In addition, they successfully determined an X-ray crystal structure of 1:TBACl (Figure 4.13) whose crystal they obtained from chloroform/hexane mixture. The structure clearly reveals hydrogen bonding between the hydroxyl hydrogen atoms (H1 and H2) of 1 and a  $\text{Cl}^-$  atom. Importantly as further support for our hypothesis that such hydrogen bonding accounts for the chemical shift changes seen for the residual proton in  $\text{CDCl}_3$ , which described in this chapter, a hydrogen bonding between the hydrogen atoms (H53 and H54) of the chloroform solvent and a  $\text{Cl}^-$  atom can also be seen.



**Figure 4.13.** X-ray crystal structure of **1**:TBACl.

#### 4.4 Conclusion

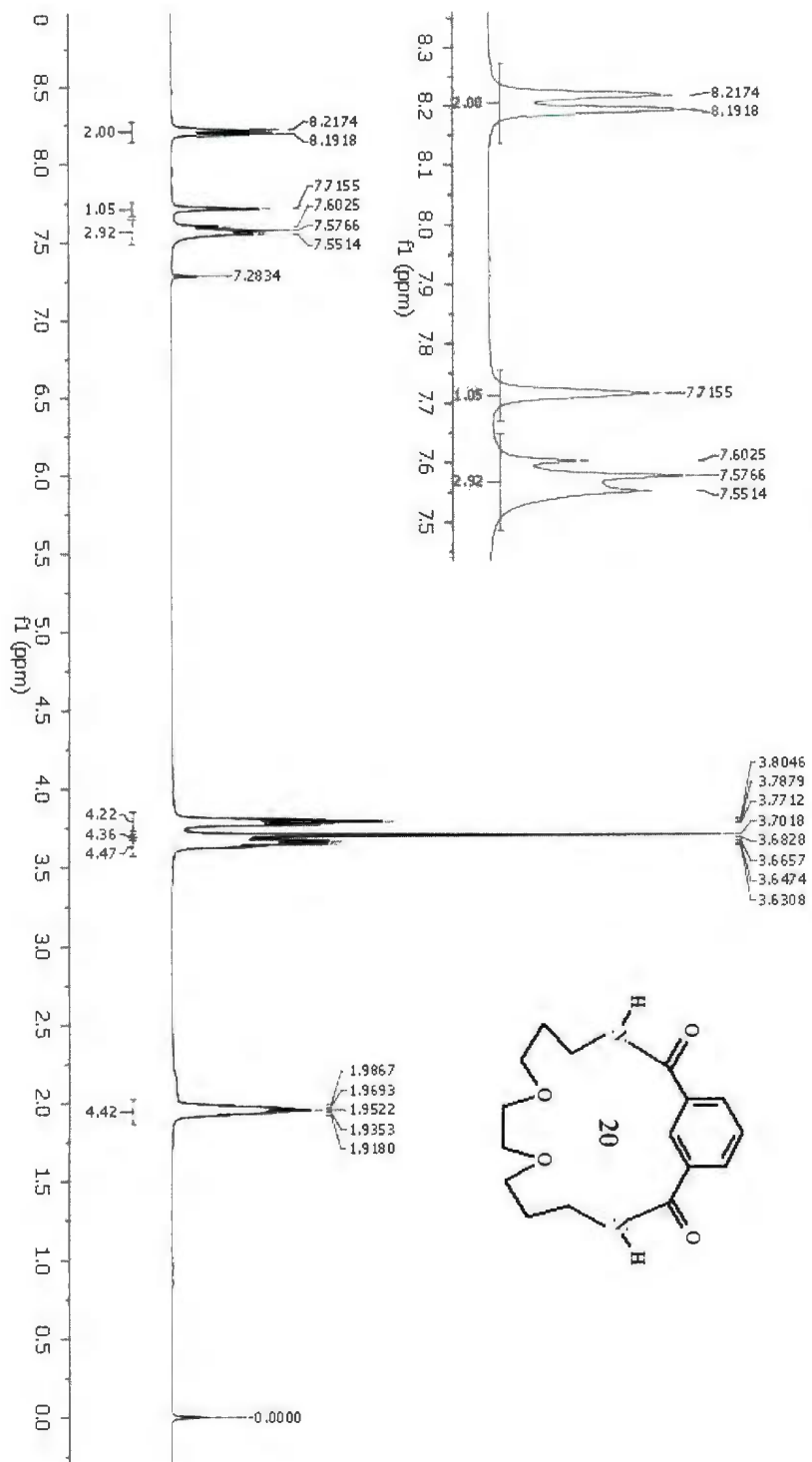
It has been shown that complexation occurs between chloroform and the halide ions of TBA salts, and that the chemical shift for the residual chloroform signal is significantly downfield shifted from the “reference” position of  $\delta = 7.26$  ppm. Thus, if  $^1\text{H}$  NMR spectra of host-guest titration studies are referenced only to this signal, significant errors could occur when determining the chemically-induced chemical shifts (CIS) of host signals affected by the complexation processes. These results were confirmed by the X-ray structure obtained for TBABr: $\text{CDCl}_3$  (Figure 4.10). In all of the determinations which were conducted and reported in this thesis, tetramethylsilane (TMS) was used as an internal standard and CIS were referenced to TMS at  $\delta = 0.00$  ppm.

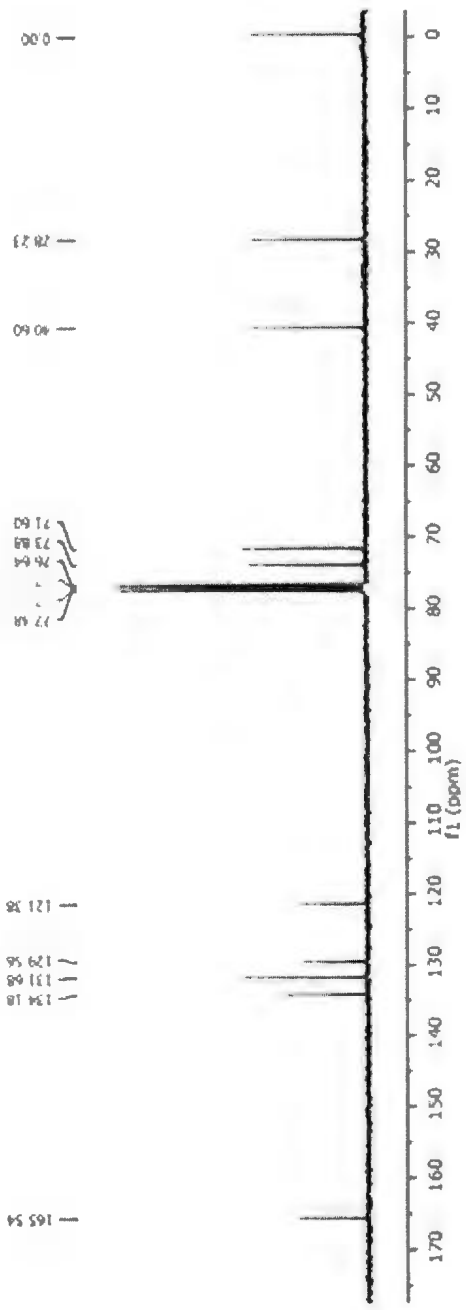
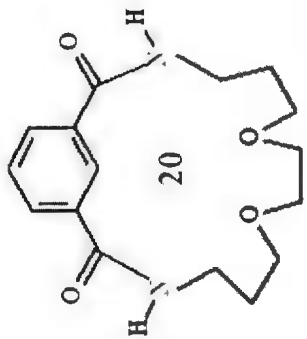
#### 4.5 References

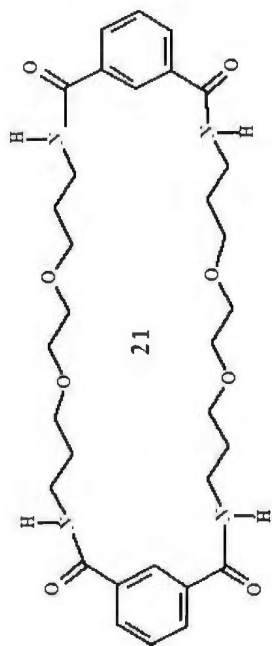
1. Green, R. D.; Martin, J. S. *J. Am. Chem. Soc.* **1968**, *90*, 3659-3668.
2. Pimentel, G. C.; McClellan, A. L. *The Hydrogen Bond* W. H. Freeman, San Francisco, California, 1960.
3. Allerhand, A.; Schleyer, P. R. *J. Am. Chem. Soc.* **1963**, *85*, 1715-1725.
4. Buckingham, A. D. *Can. J. Chem.* **1960**, *38*, 430-439.
5. Kaiser, R. *Can. J. Chem.* **1963**, *41*, 300-307.
6. Molecular modeling was conducted using SpartanPro'10 software by Wavefunction Inc., Irvine, CA.
7. Kondo, S.; Harada, T.; Tanaka, R.; Unno, M. *Org. Lett.* **2006**, *8*, 4621-4624.

## Appendix A

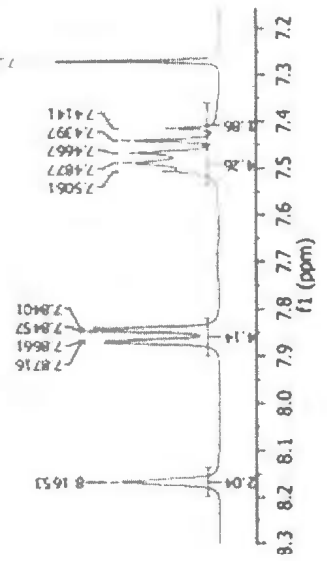
**$^1\text{H}$ ,  $^{13}\text{C}$  NMR and ESI-mass spectra for compounds described in Chapter 2**



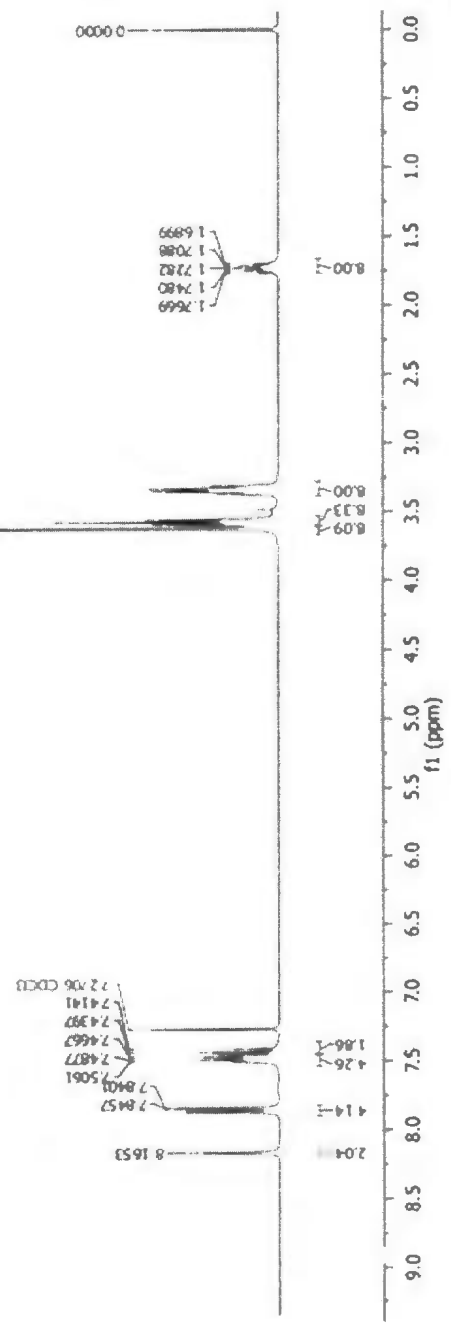




21



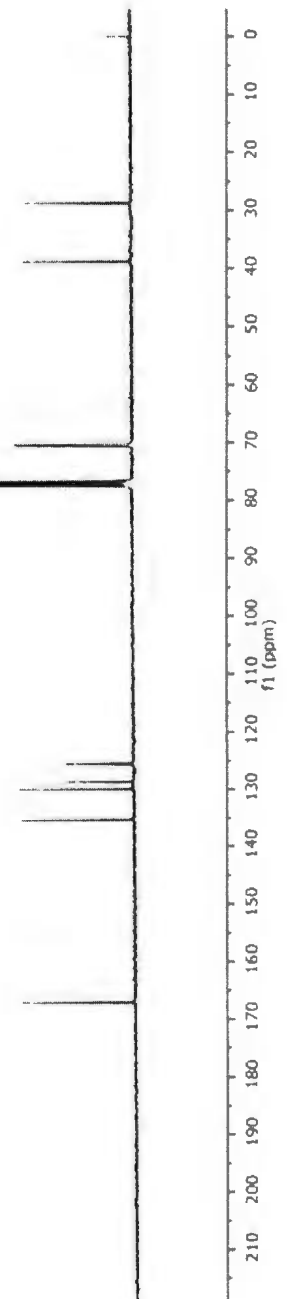
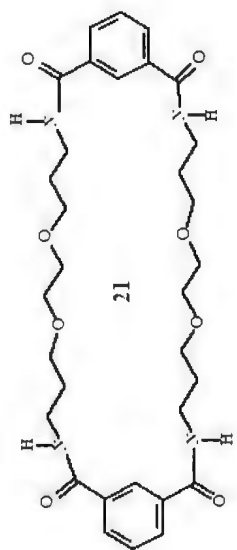
3.3117  
3.3307  
3.3508  
3.3699  
3.4800  
3.5568  
3.5756  
3.5945  
3.6238

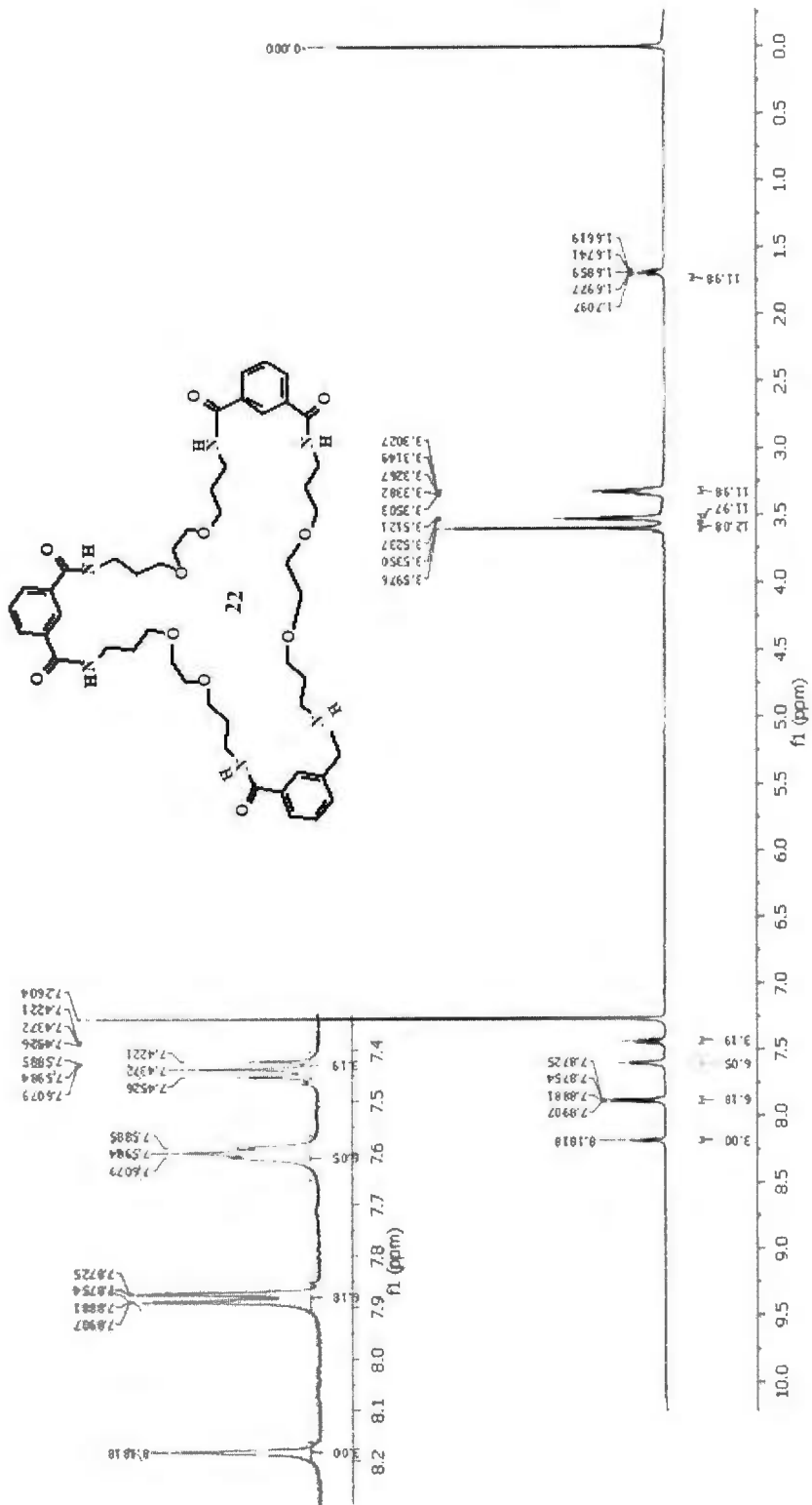


0.00  
 28.81  
 28.85  
 70.31  
 70.50  
 76.1  
 76.12  
 76.13  
 76.14  
 76.15

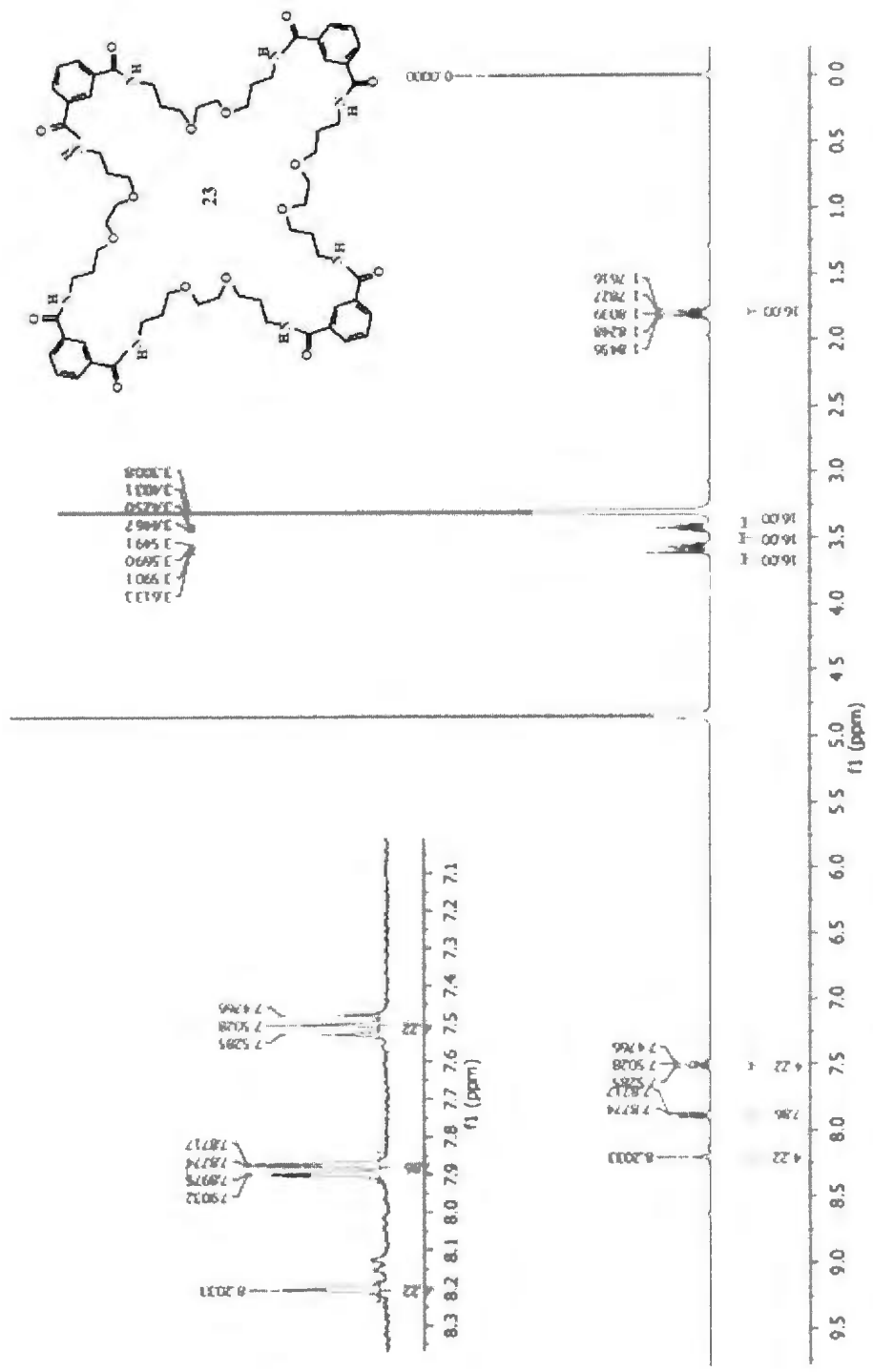
135.18  
 129.95  
 128.62  
 125.50

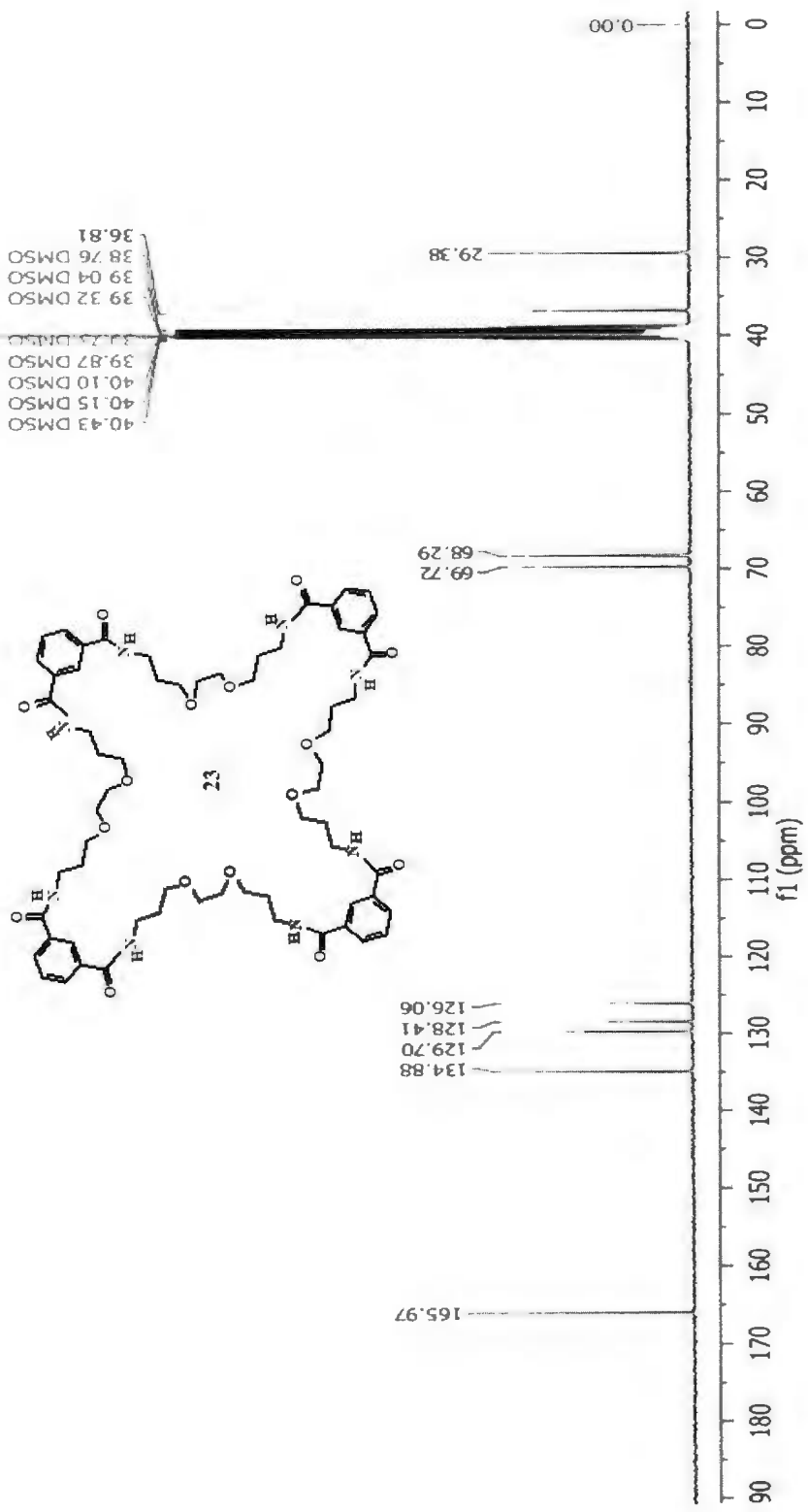
167.11

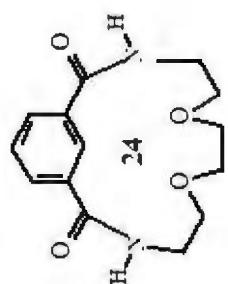












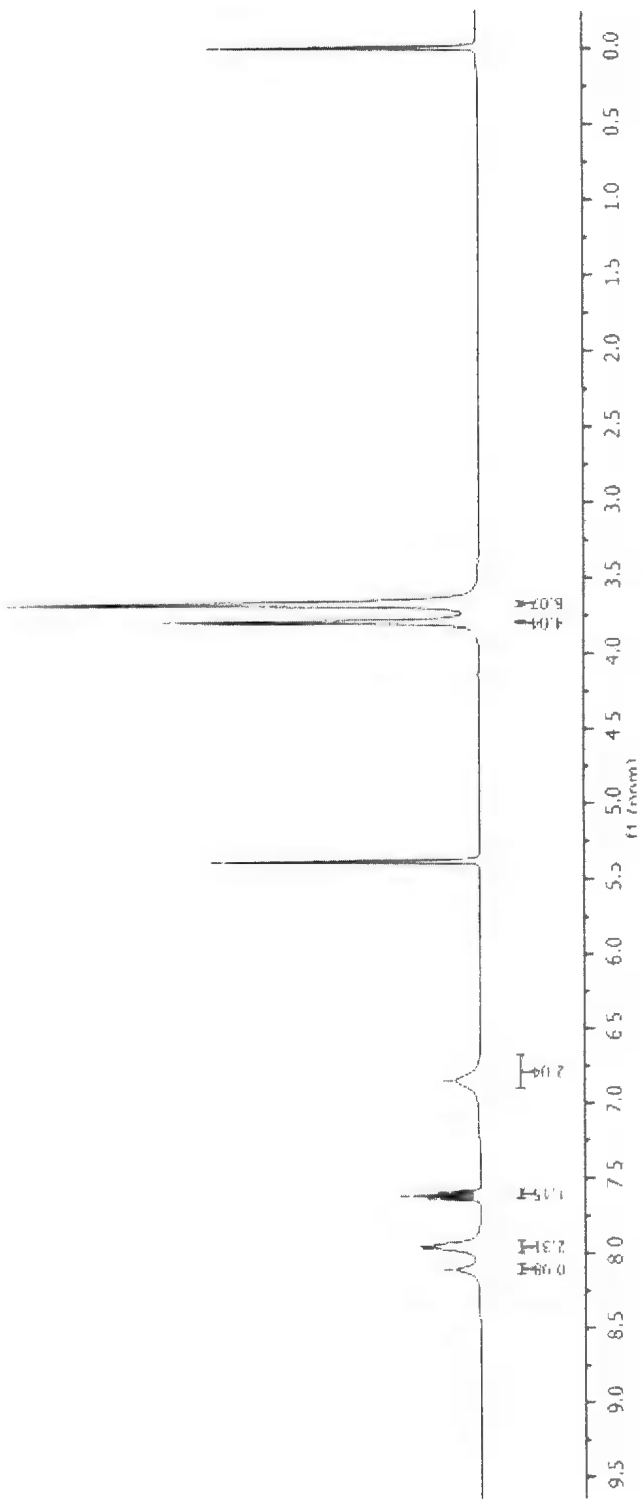
0.000

3.790  
3.673

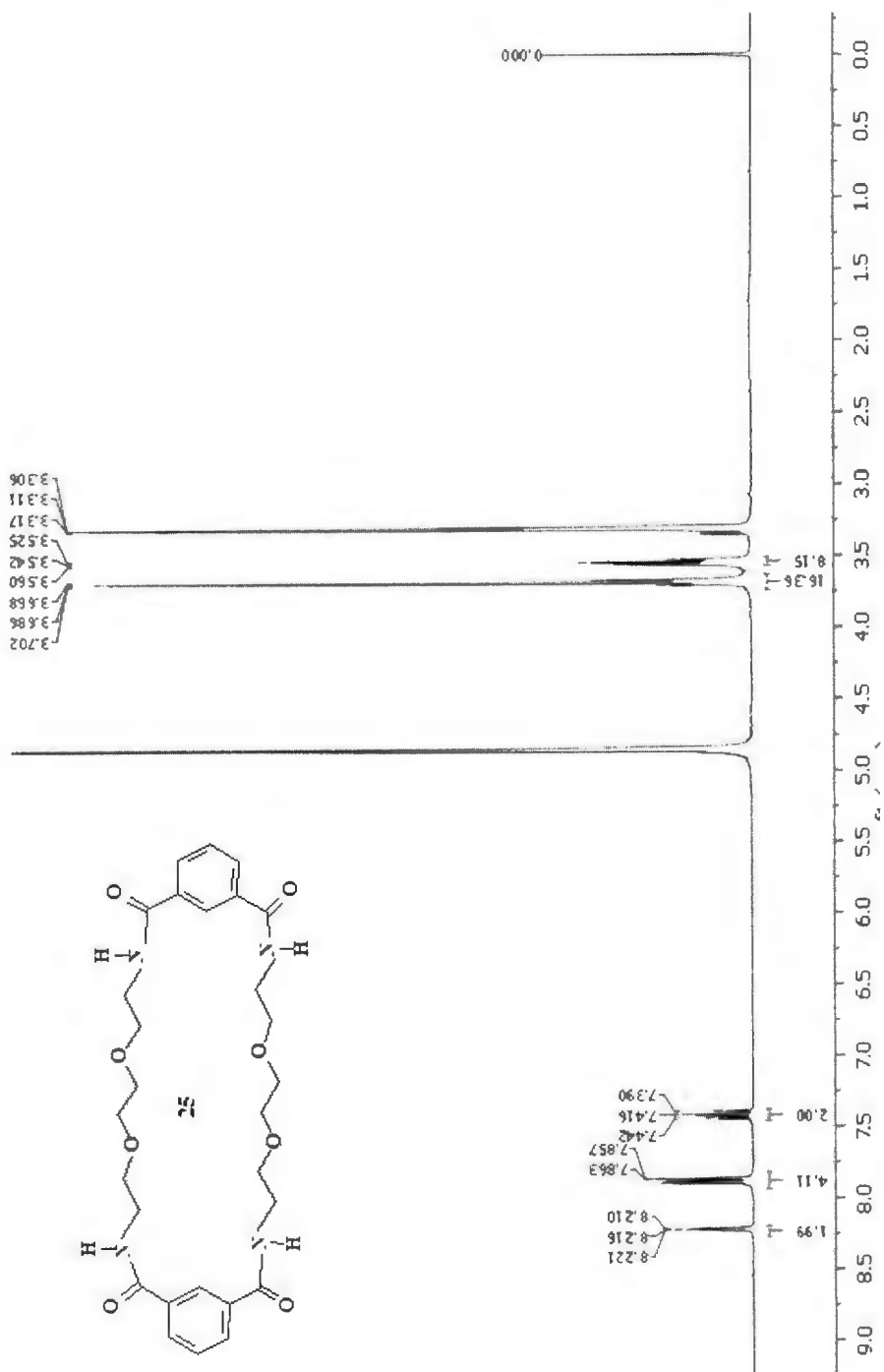
5.181

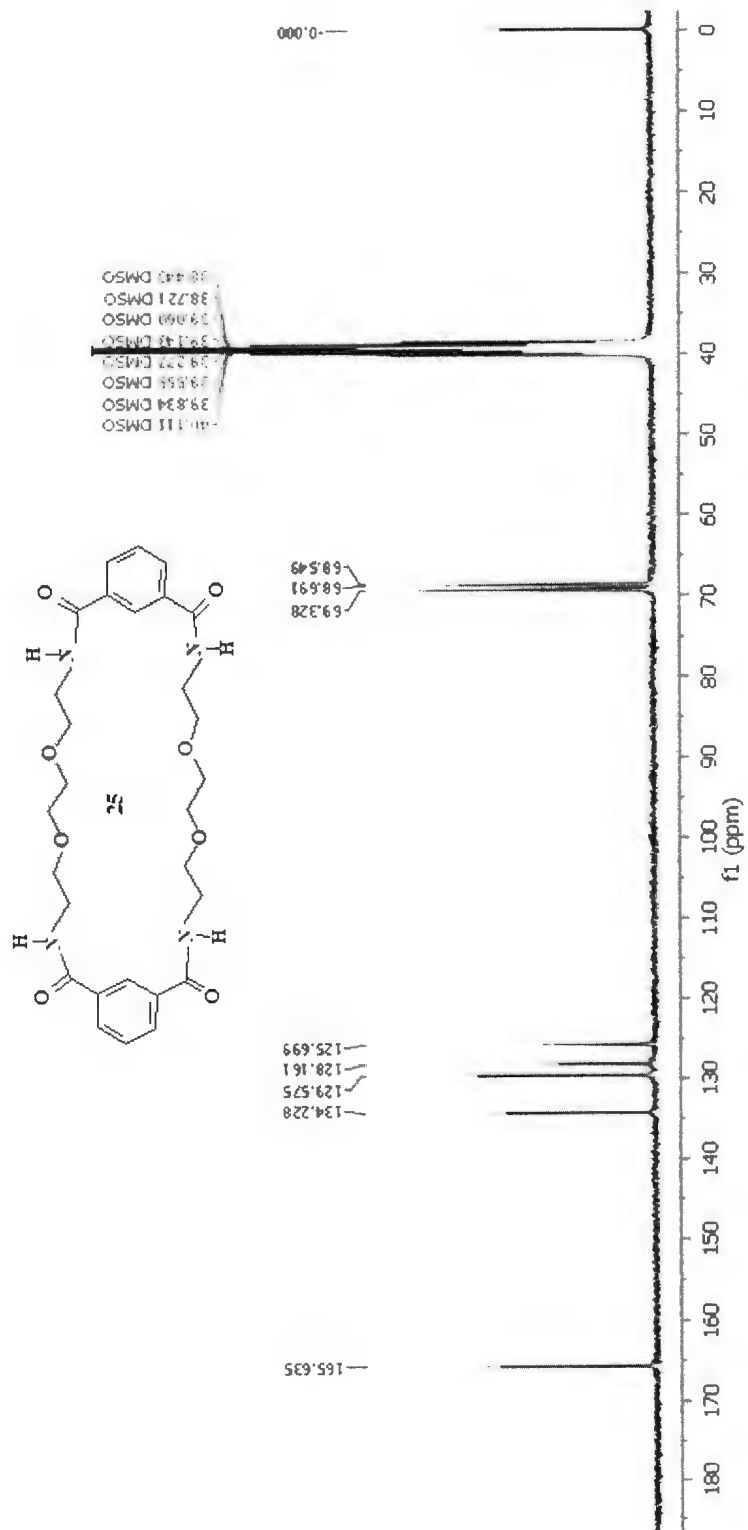
6.850

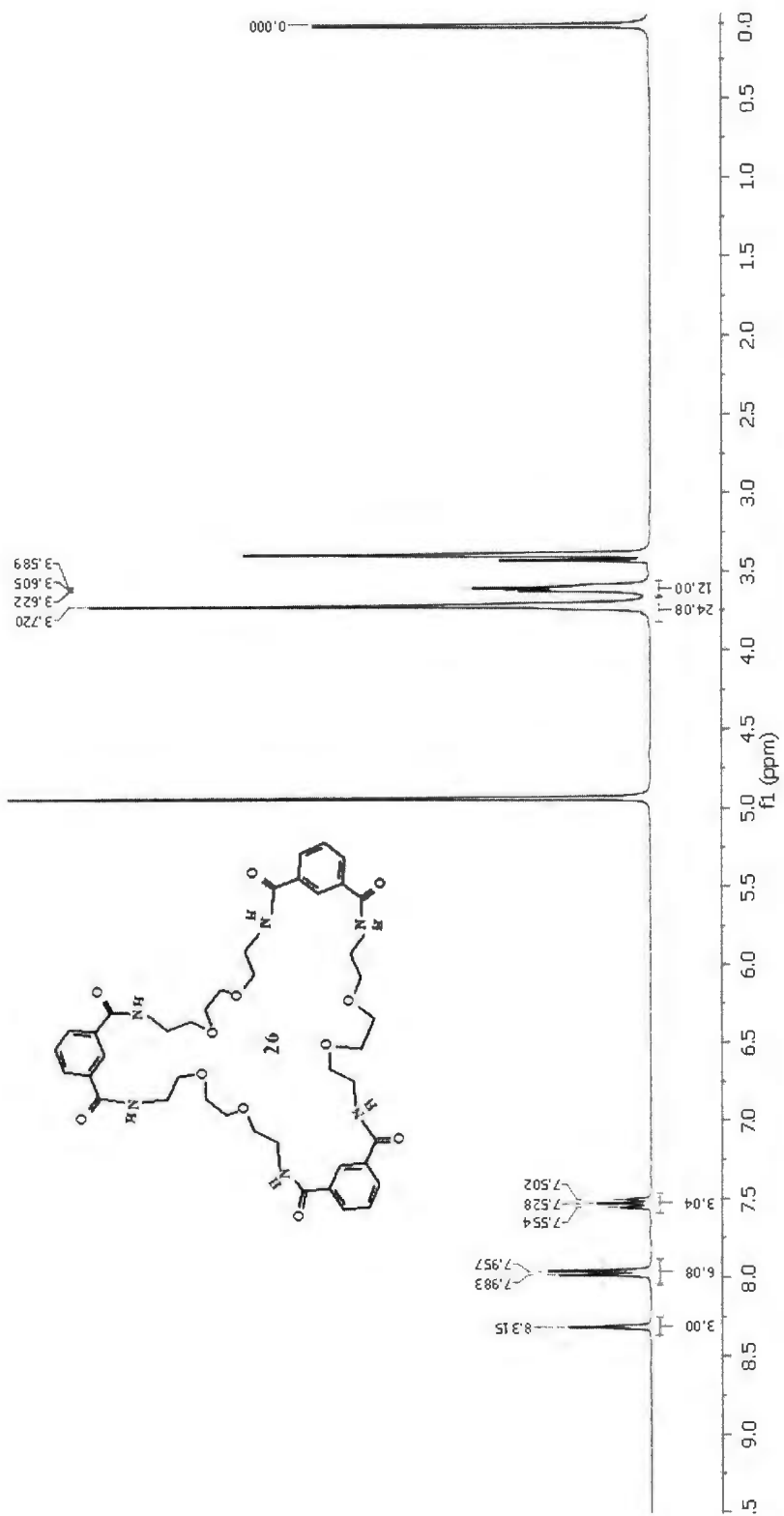
7.587  
7.612  
7.637  
7.949  
7.964  
8.184

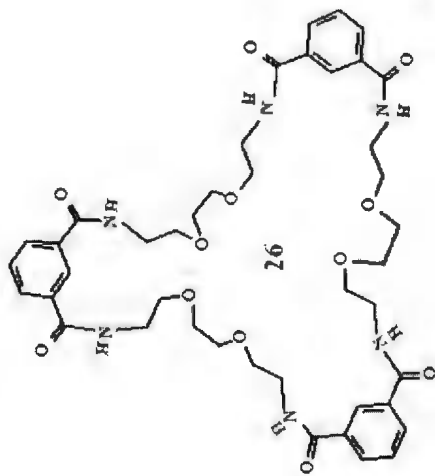










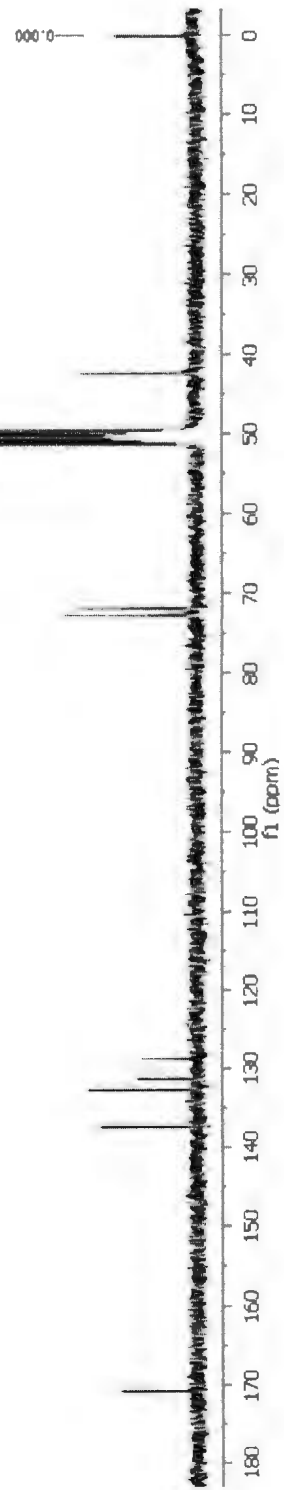


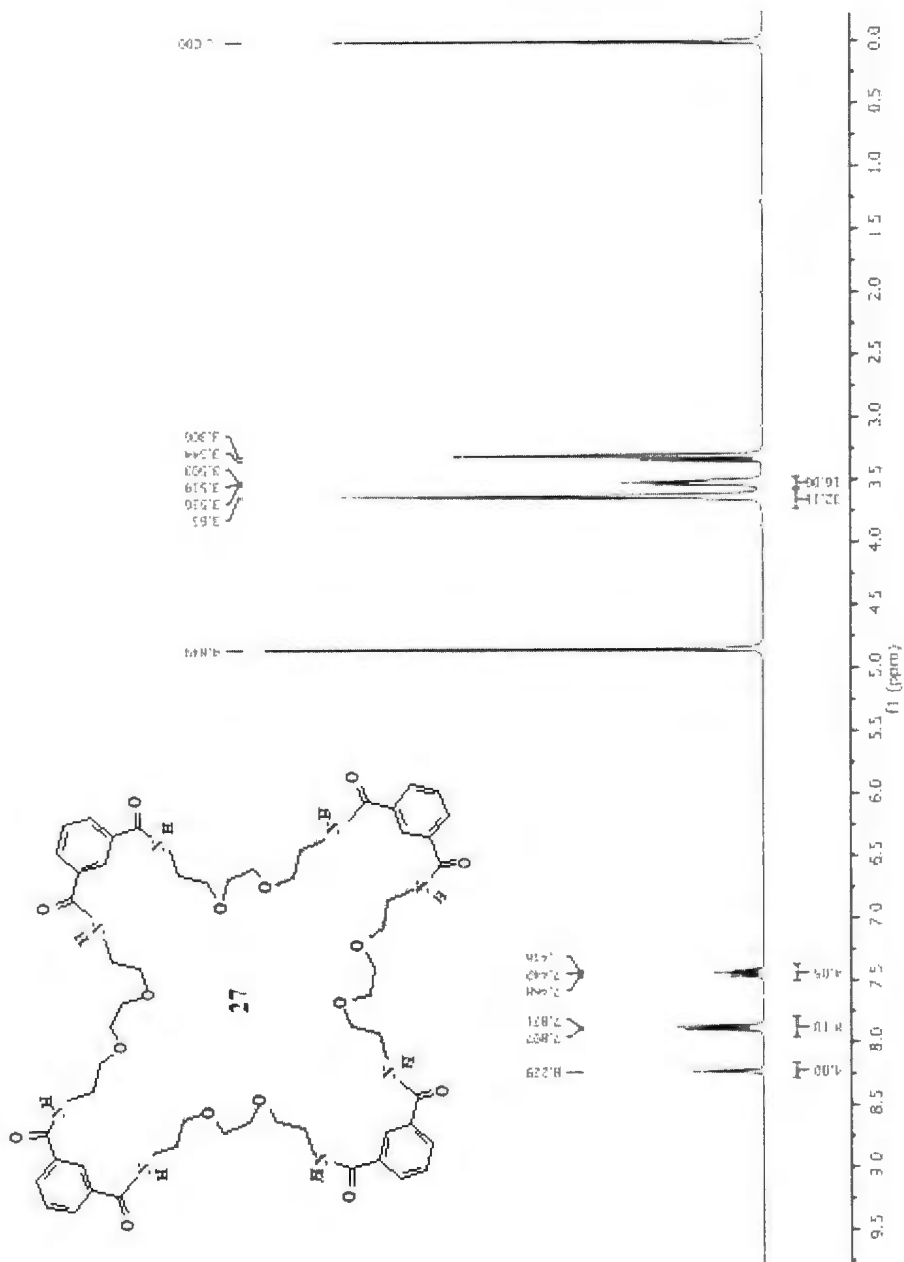
137.424  
132.753  
131.384  
128.599

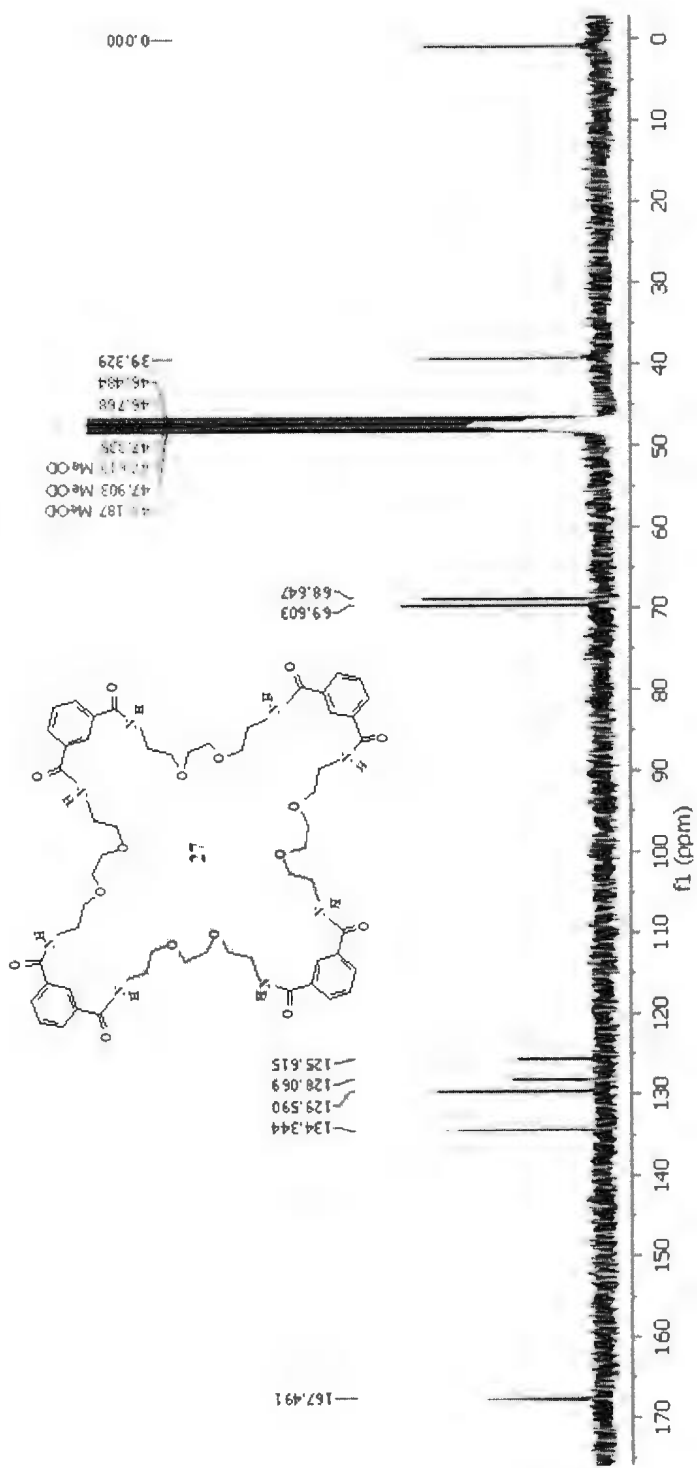
170.778

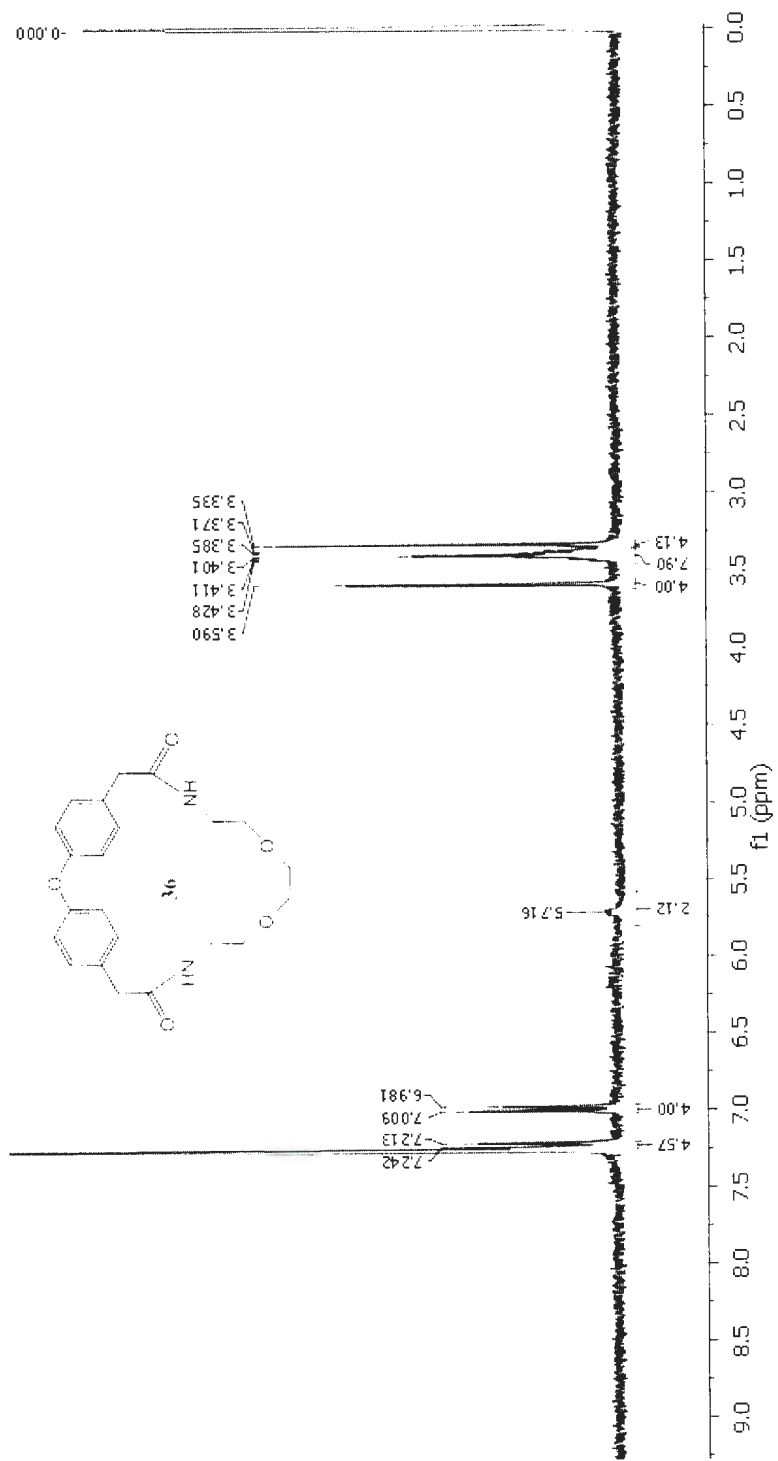
72.410  
71.591

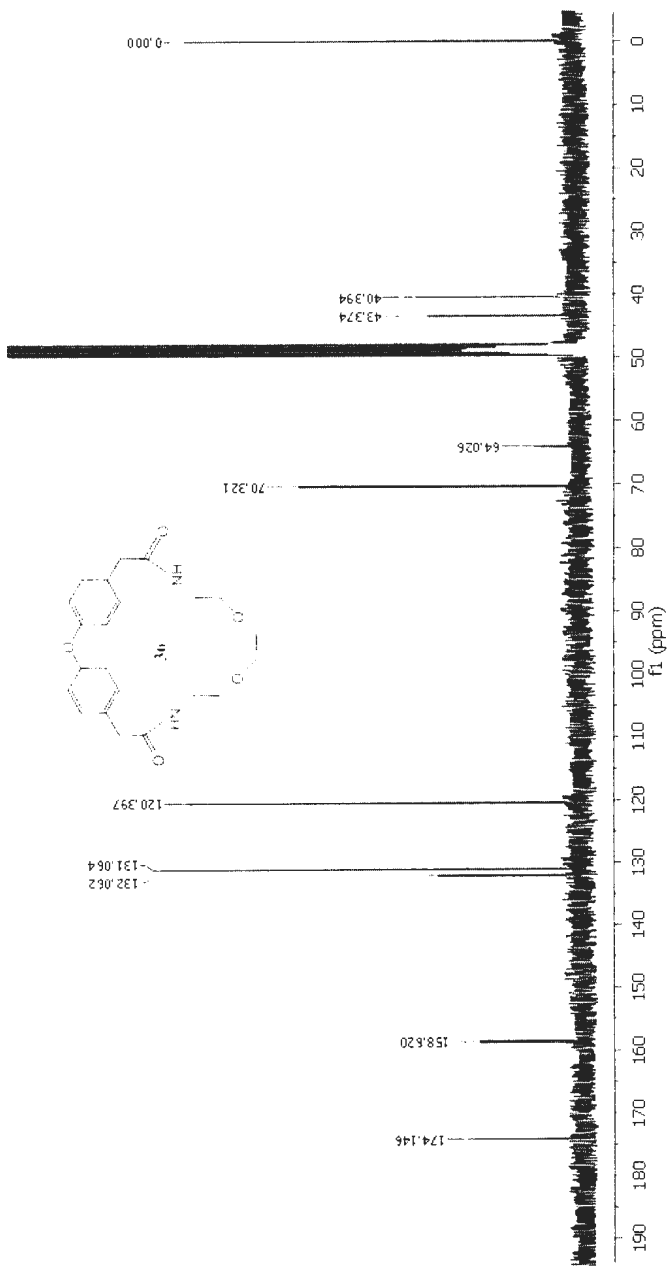
42.130

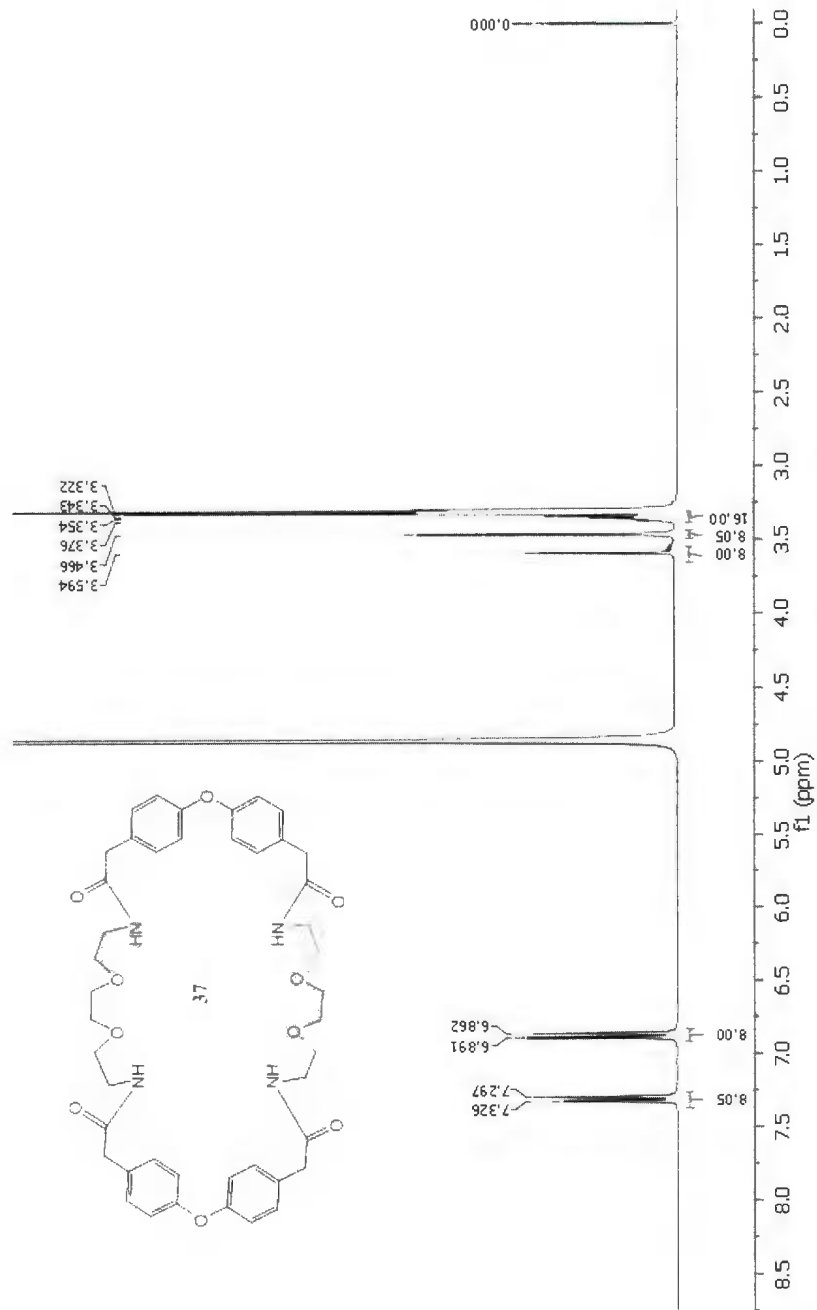


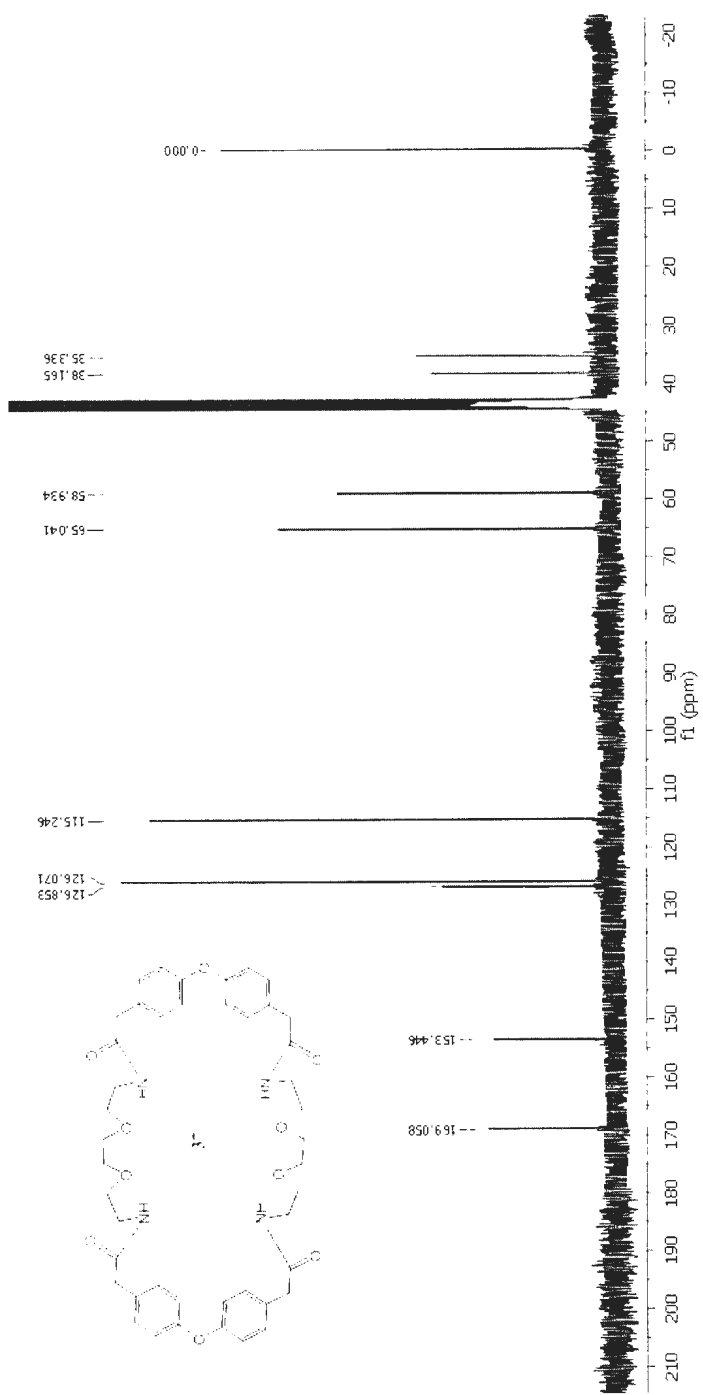


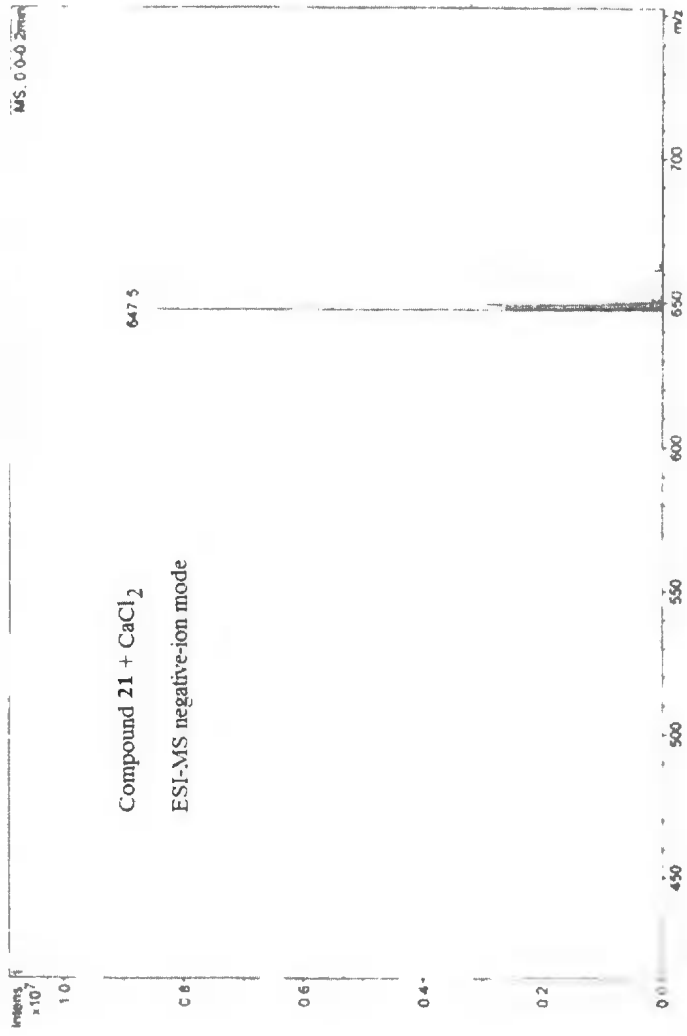


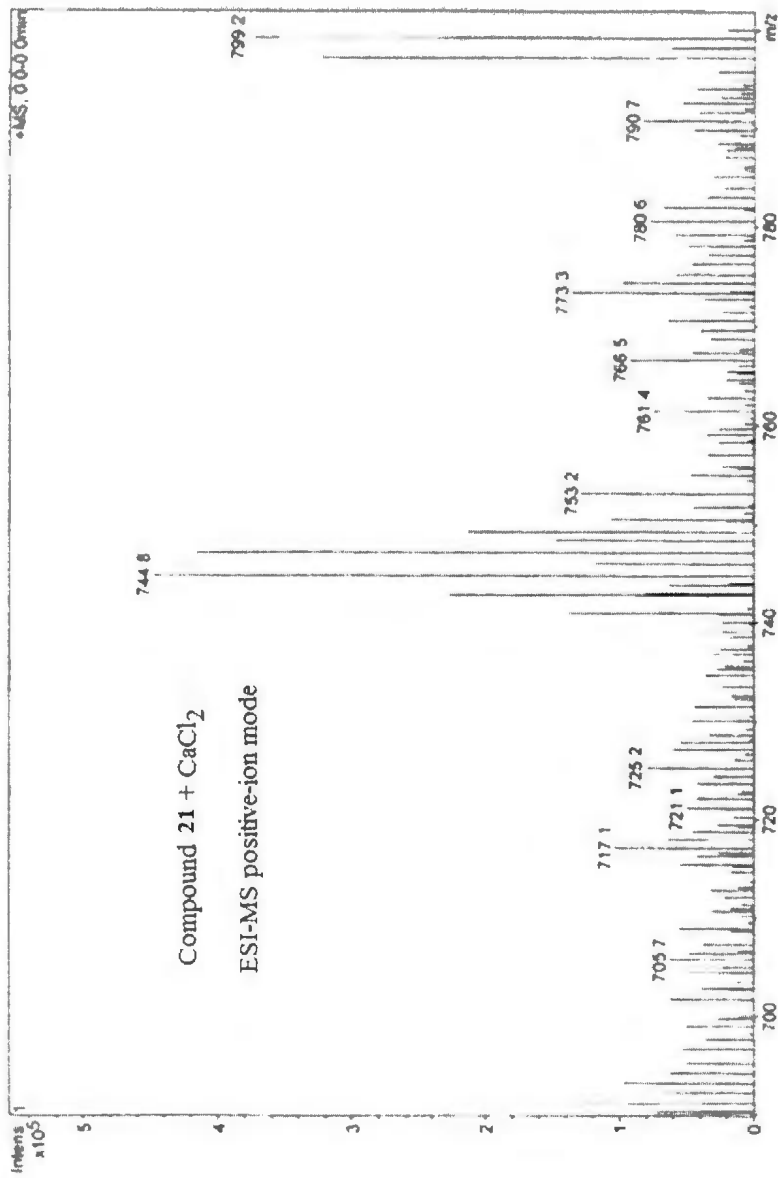


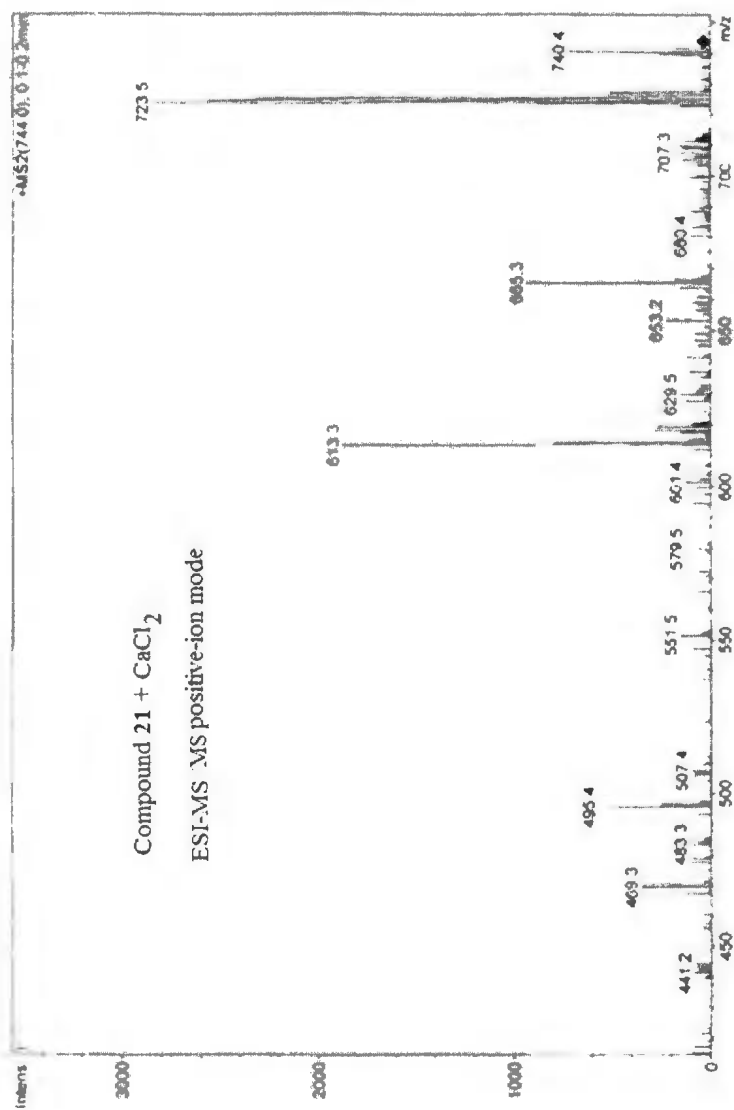


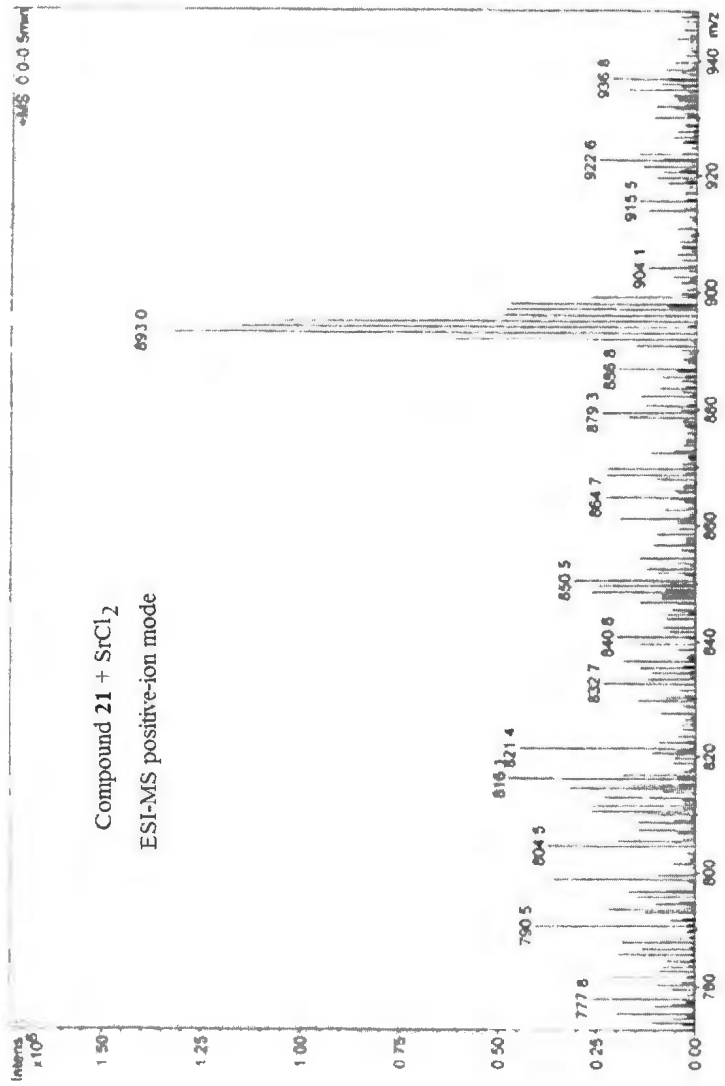


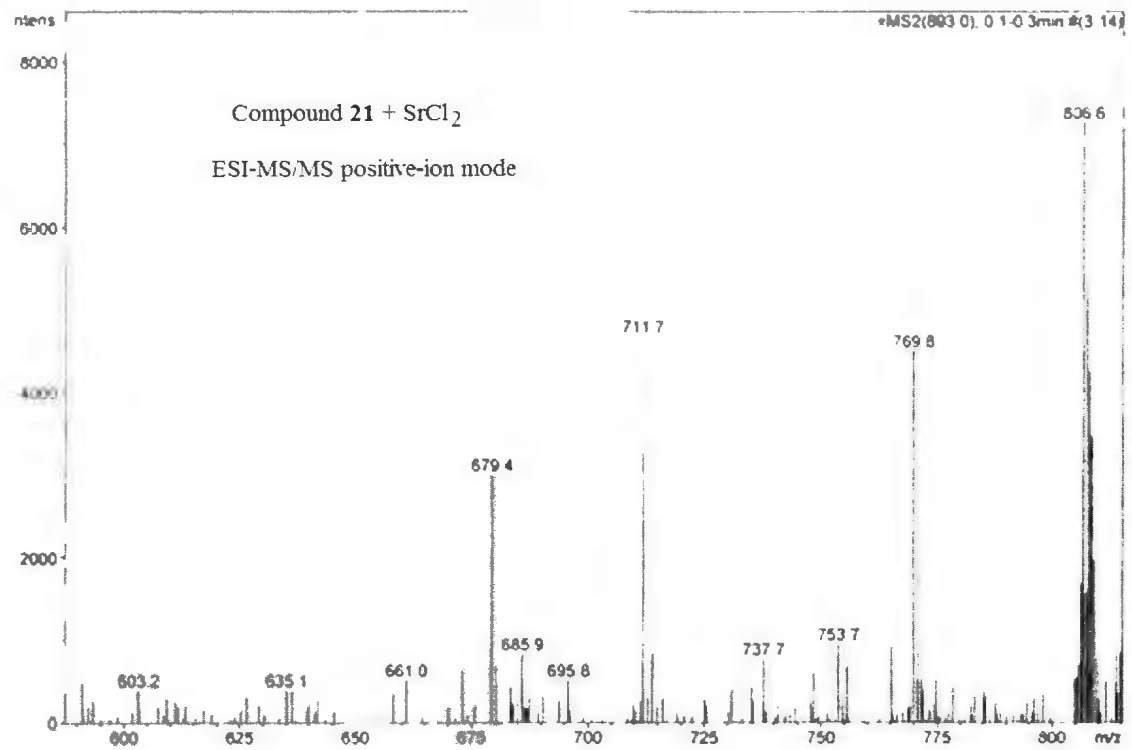


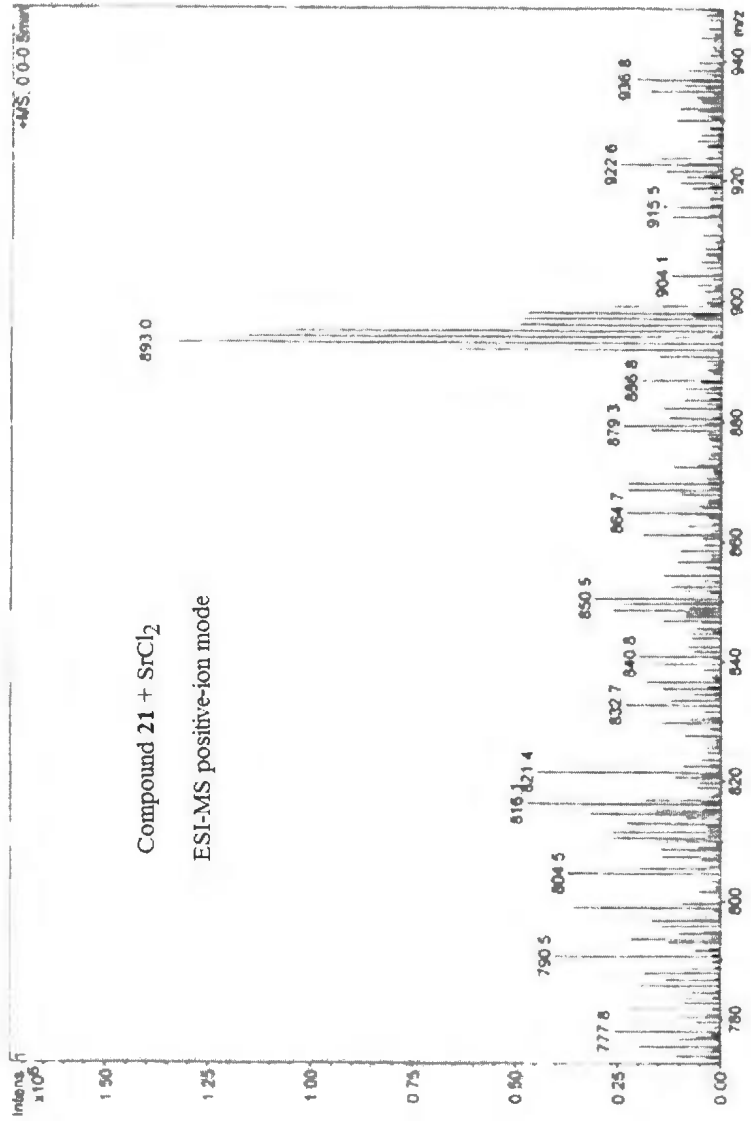


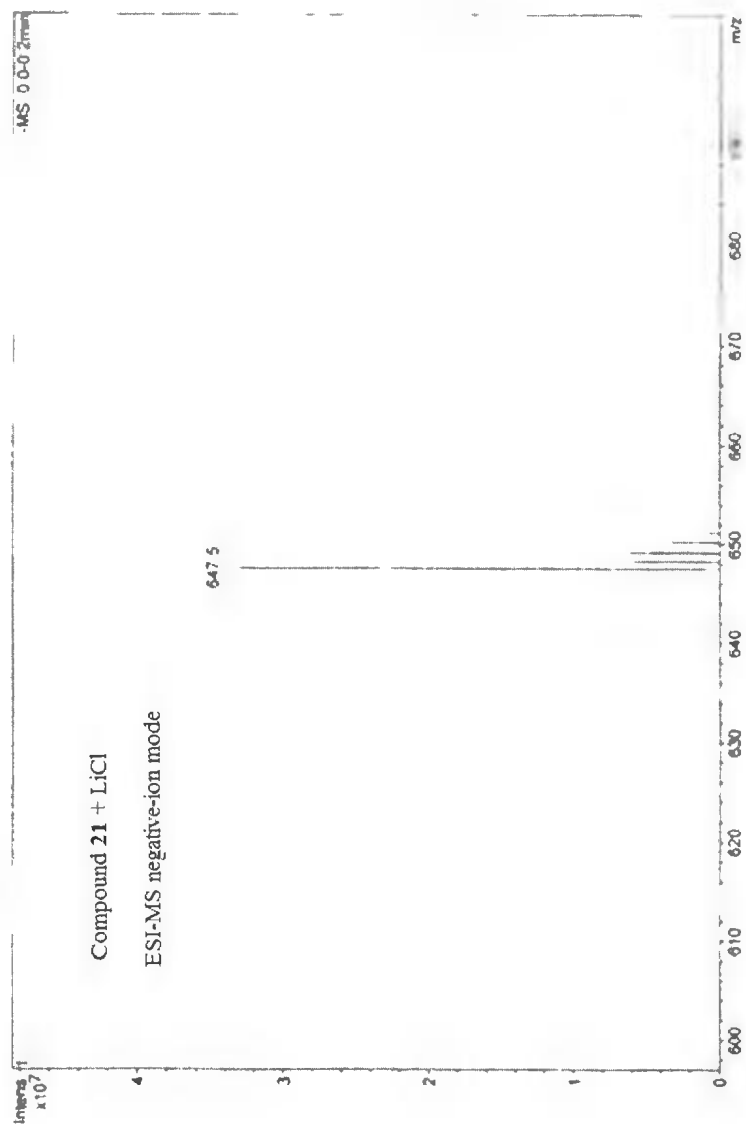


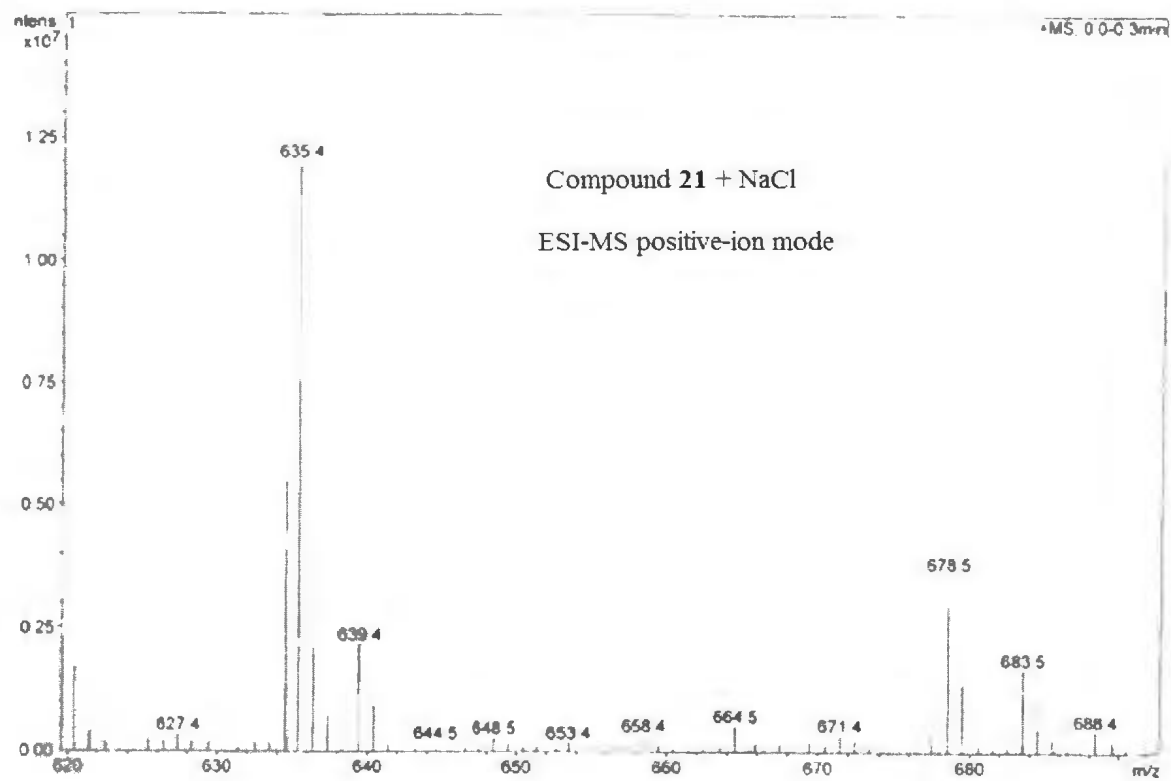


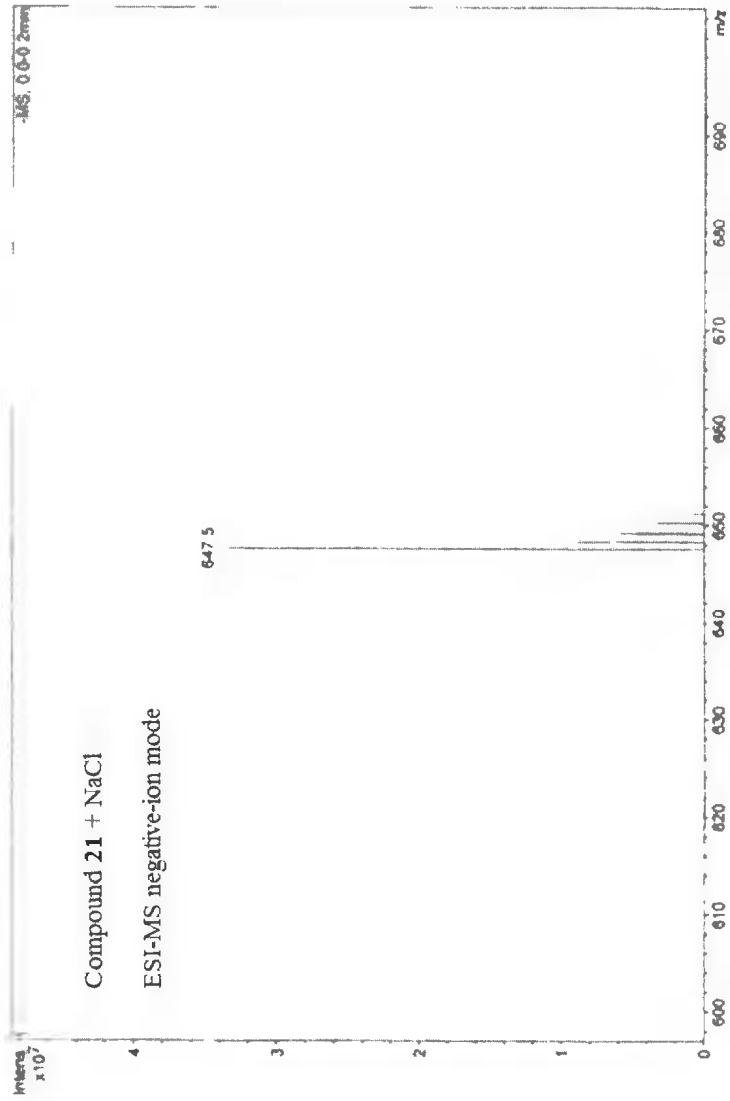


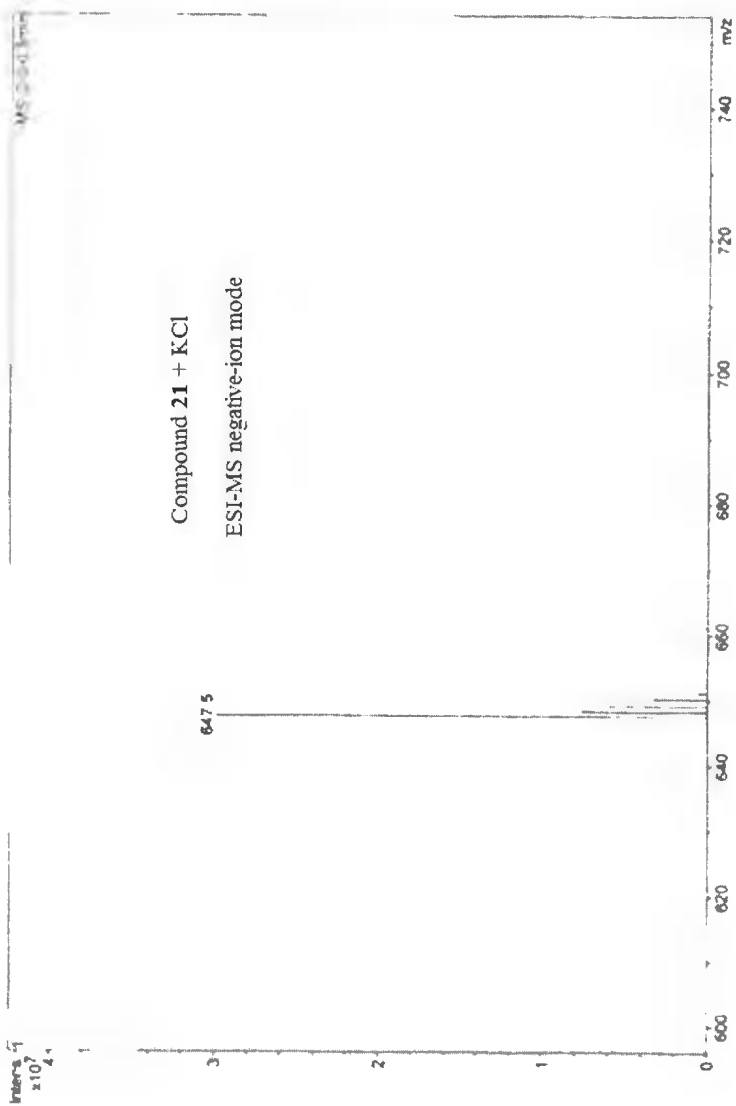


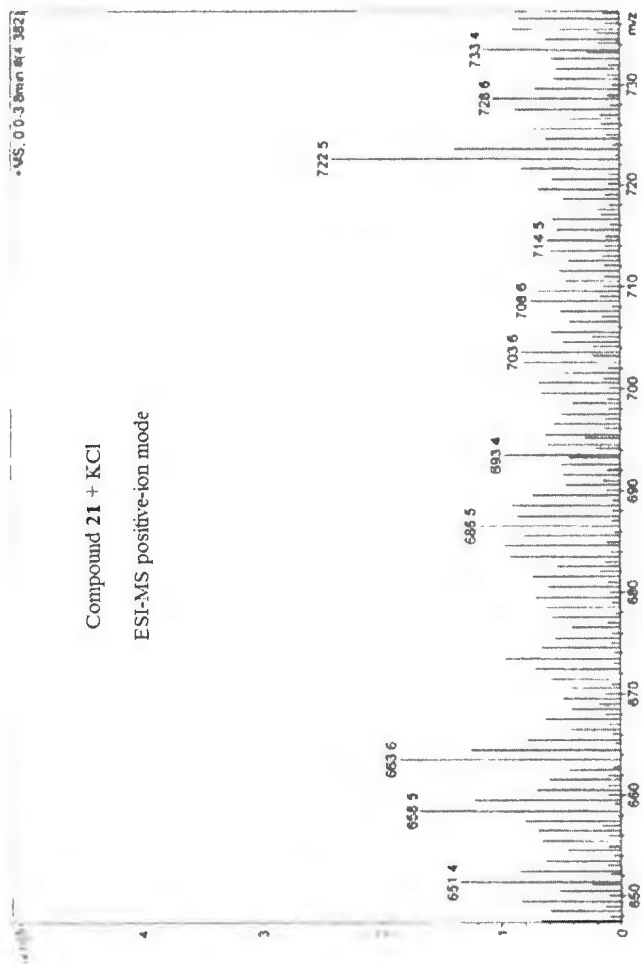


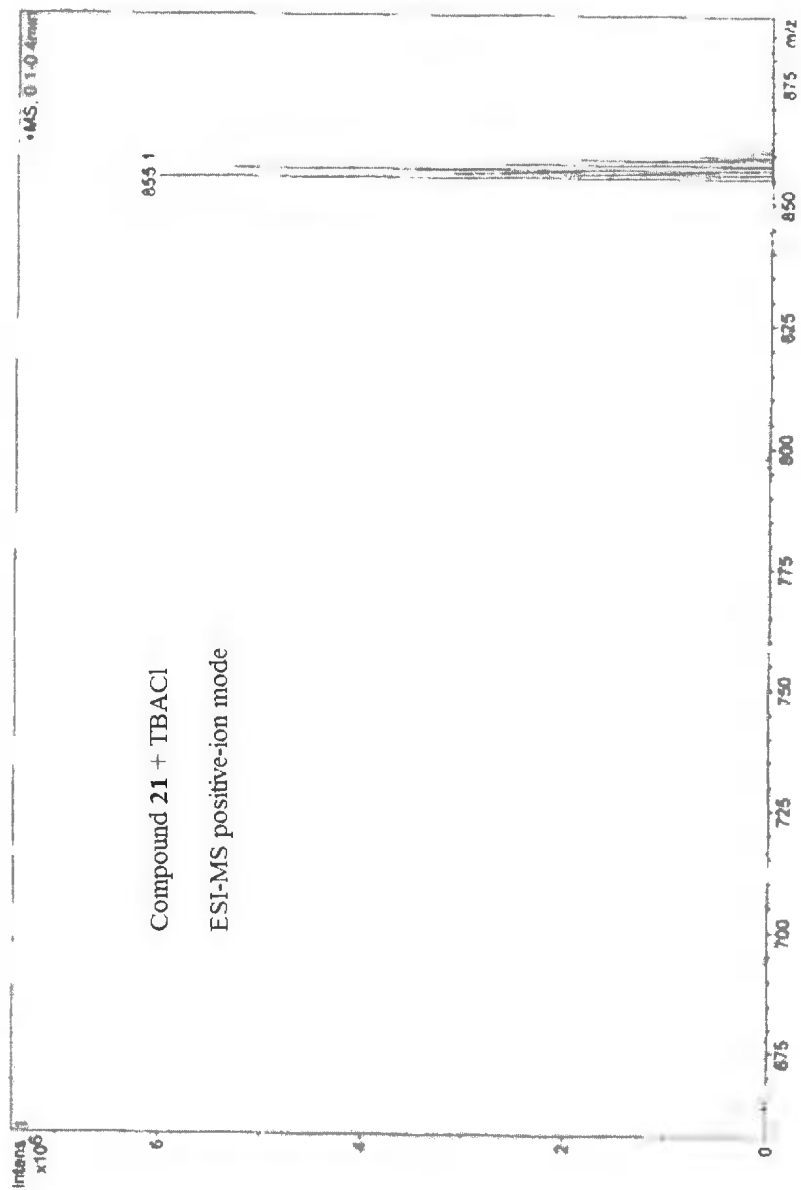




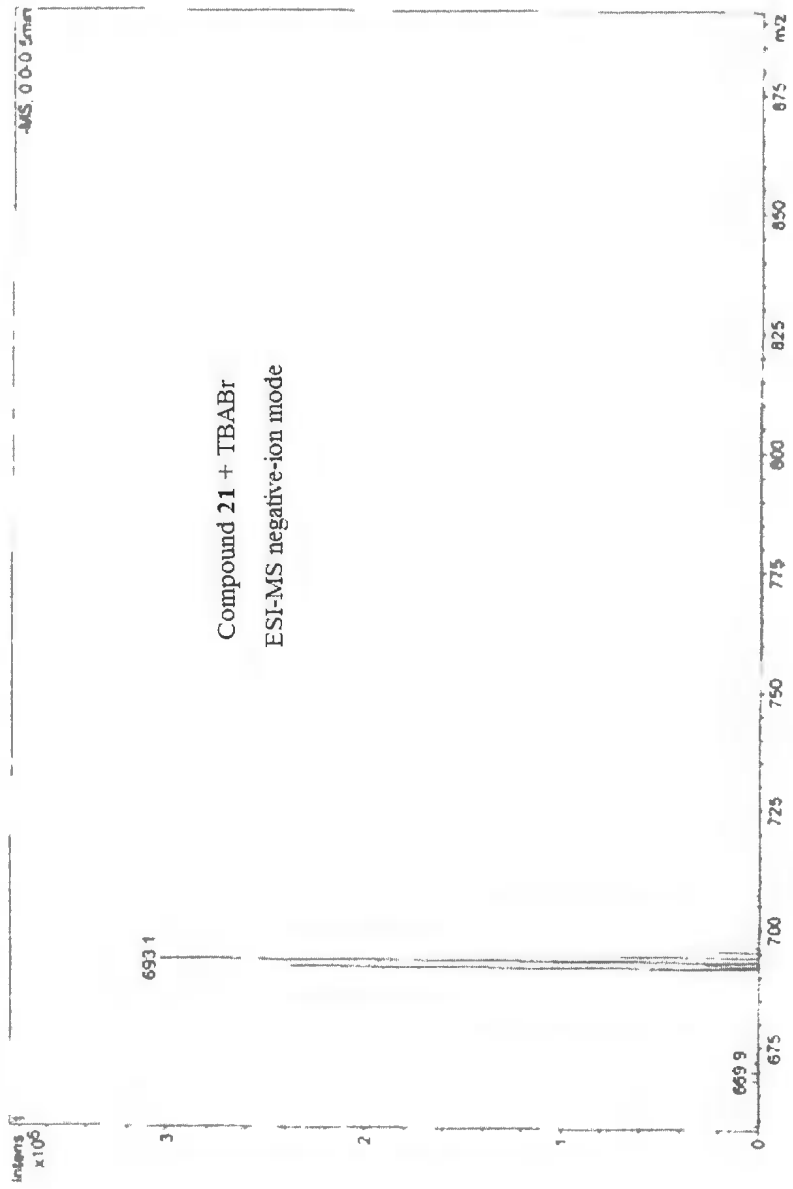


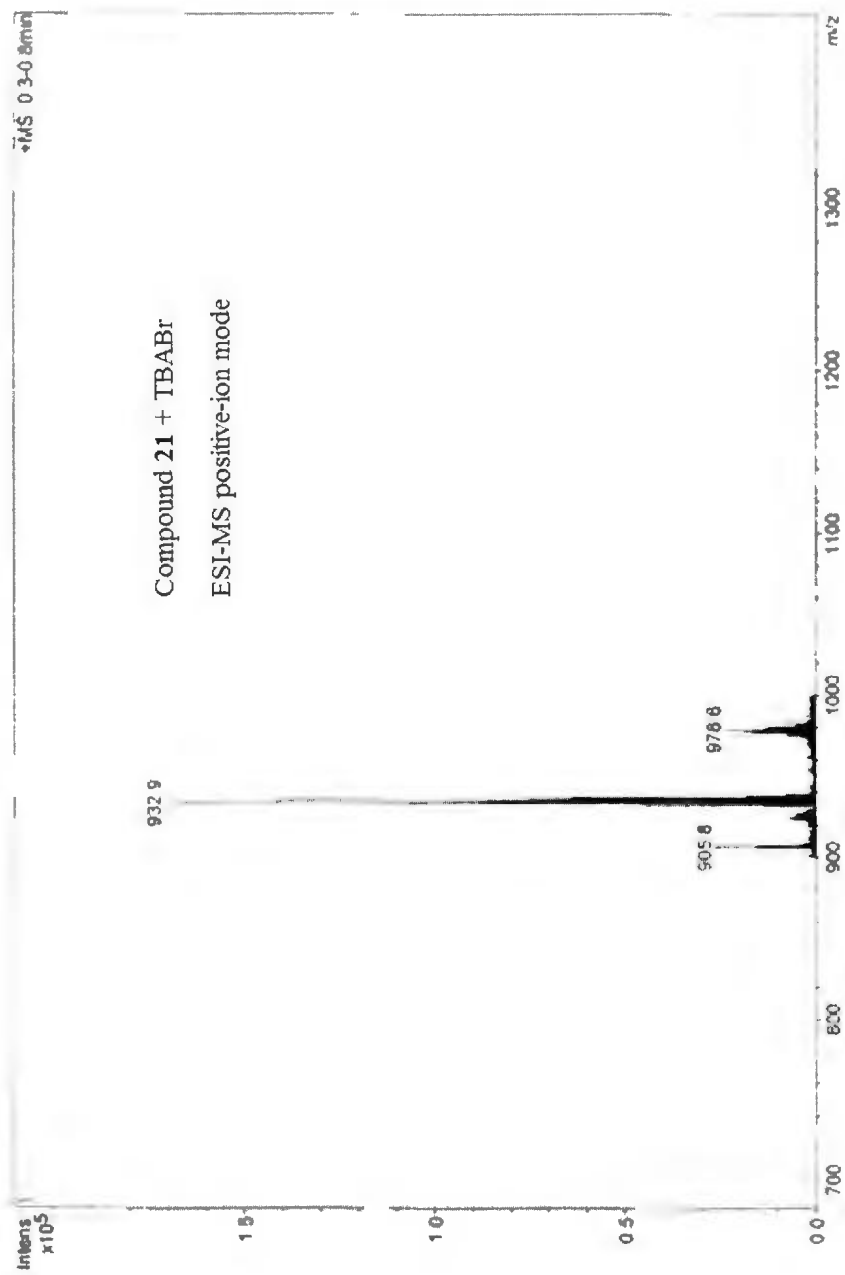


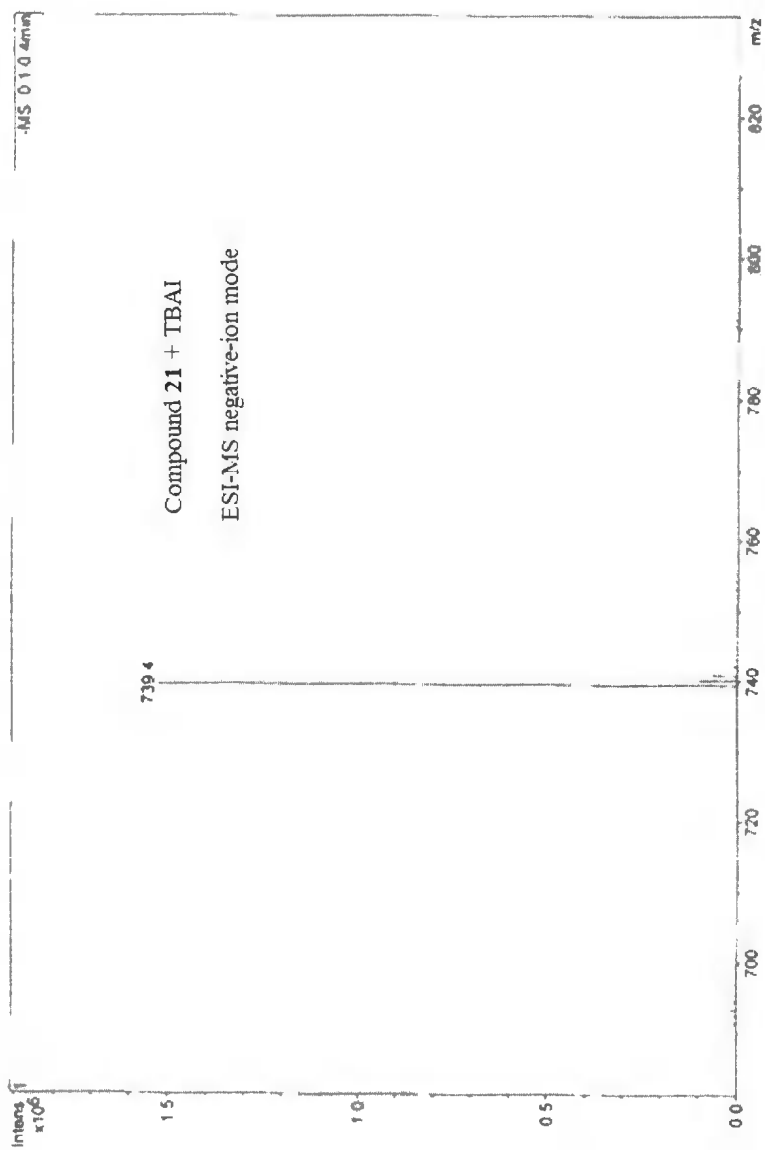


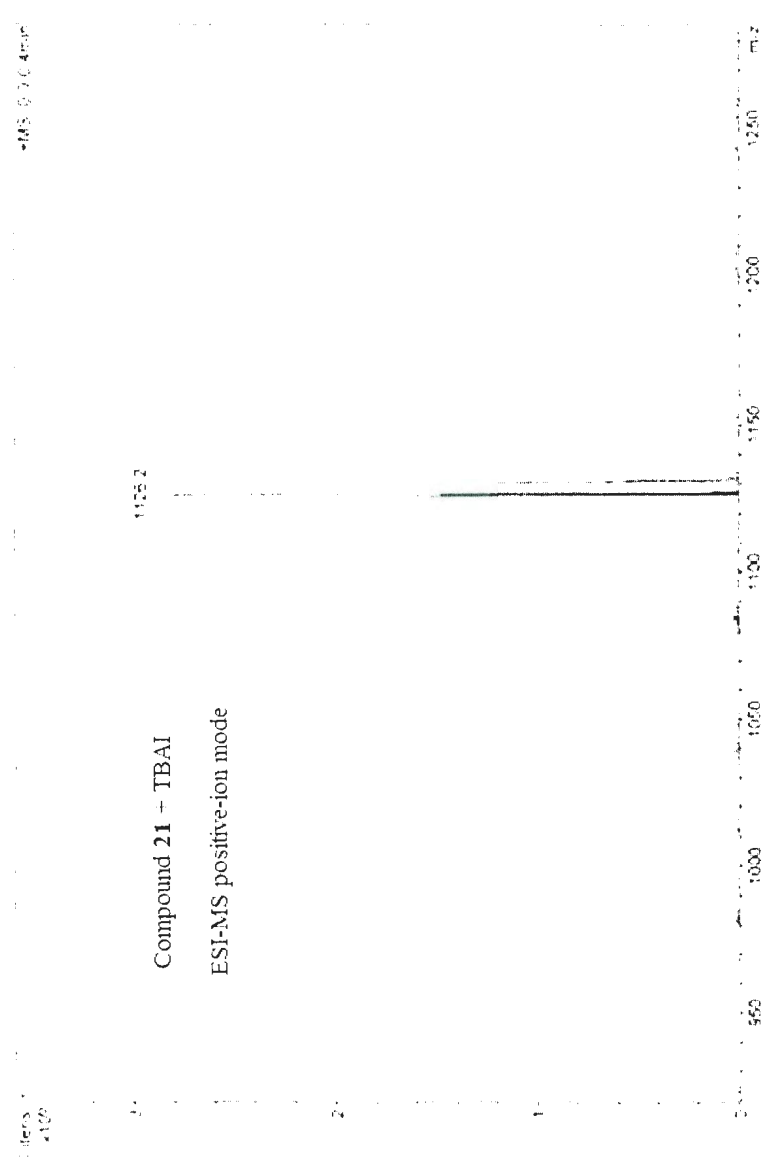




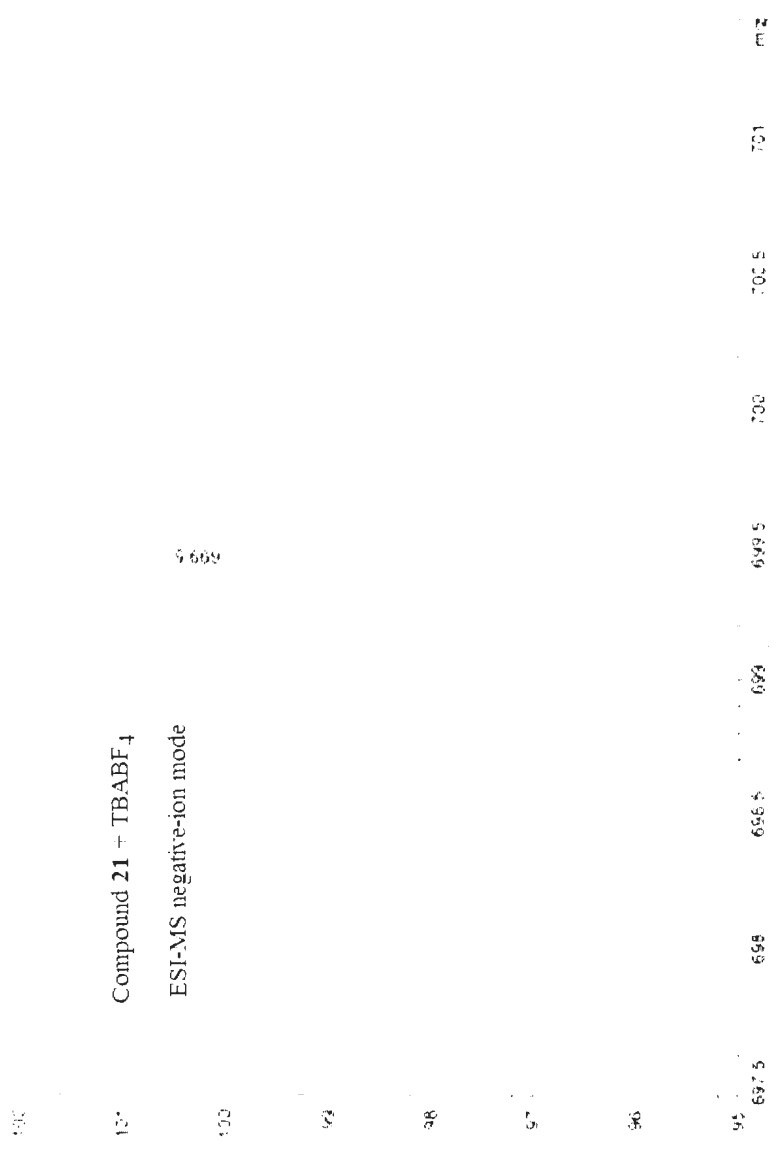


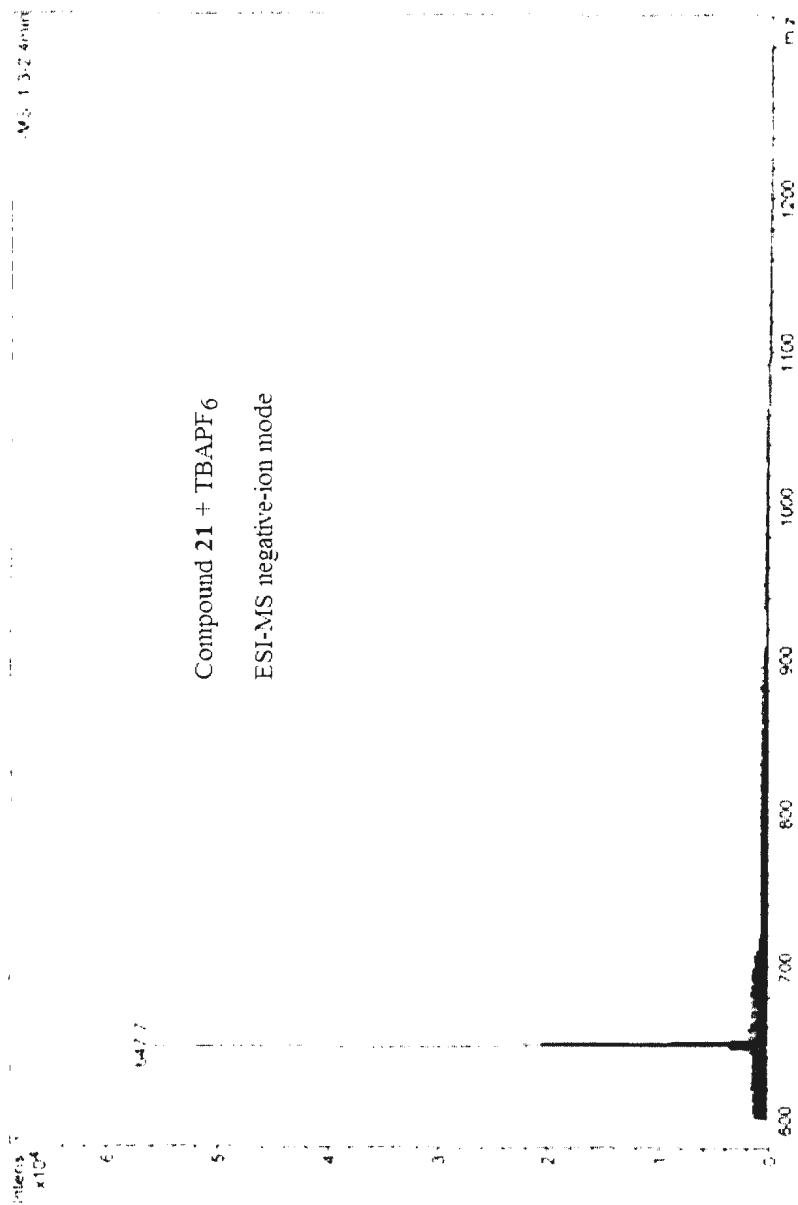


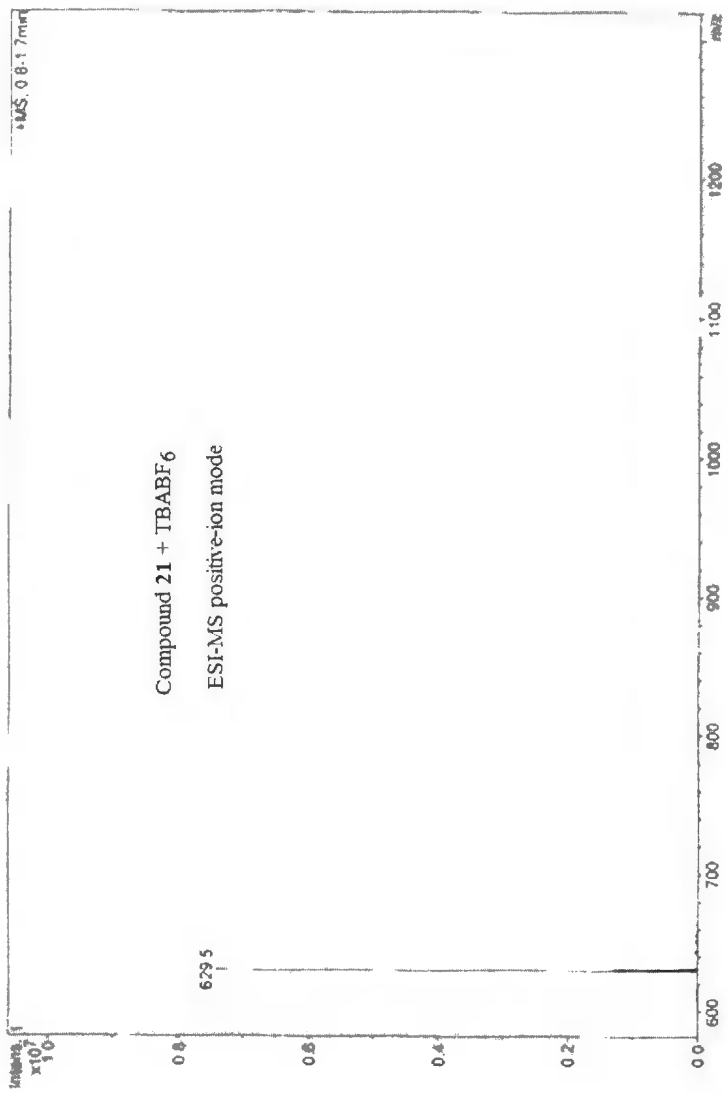






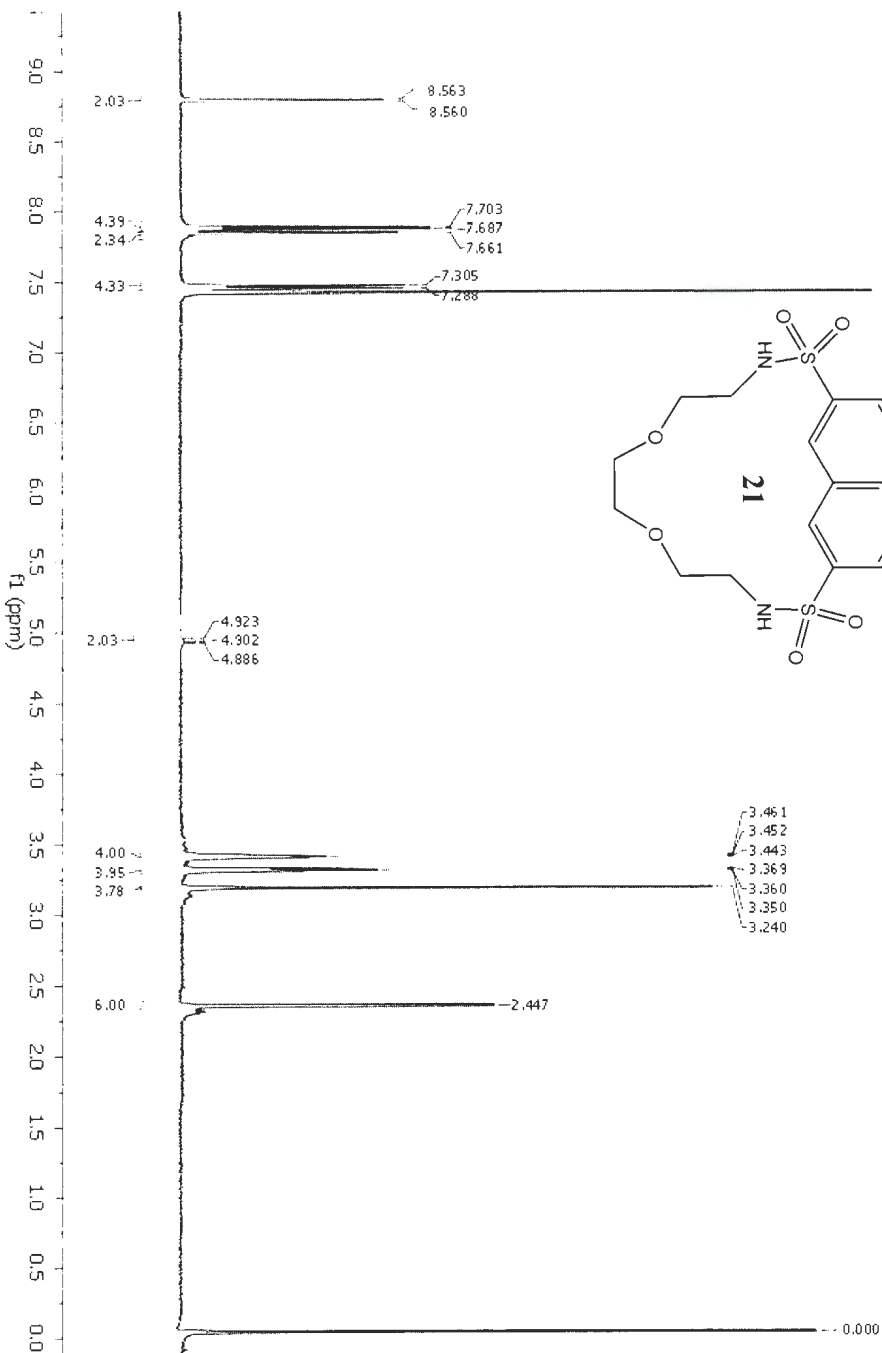


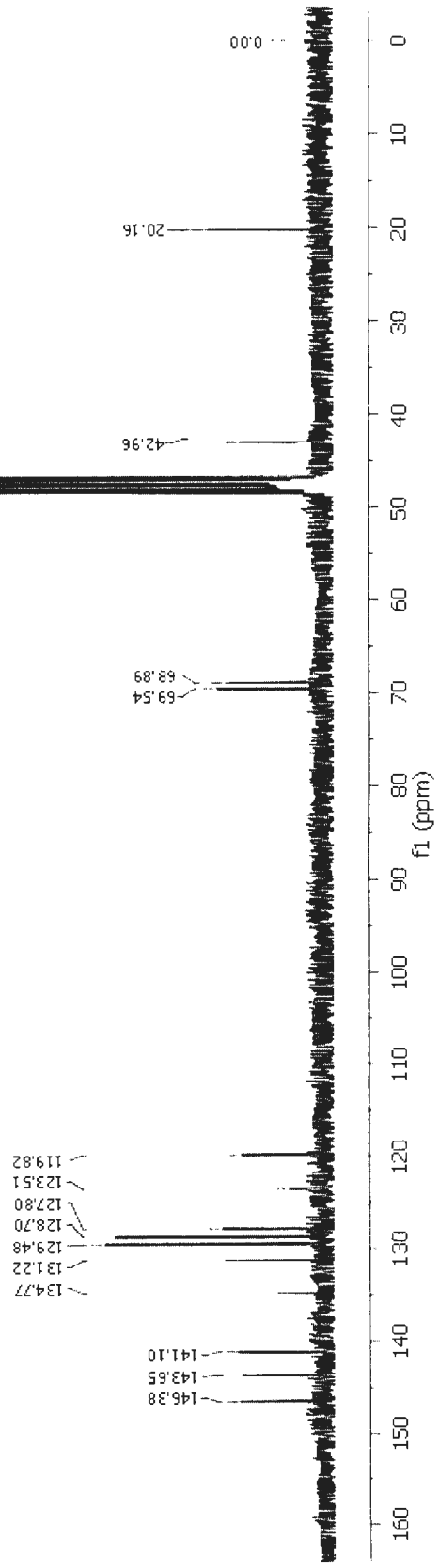
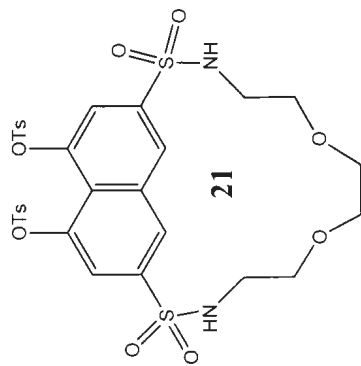


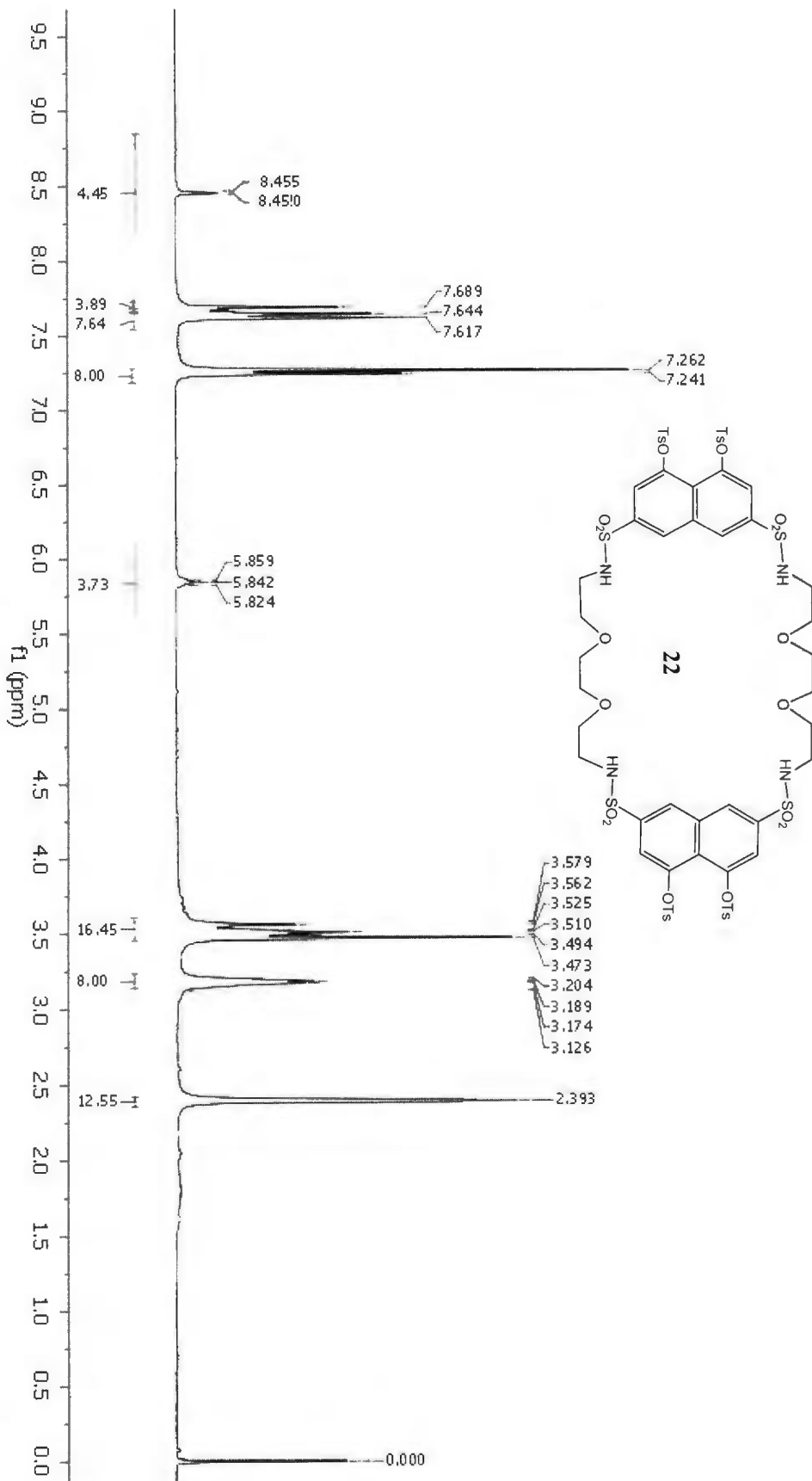


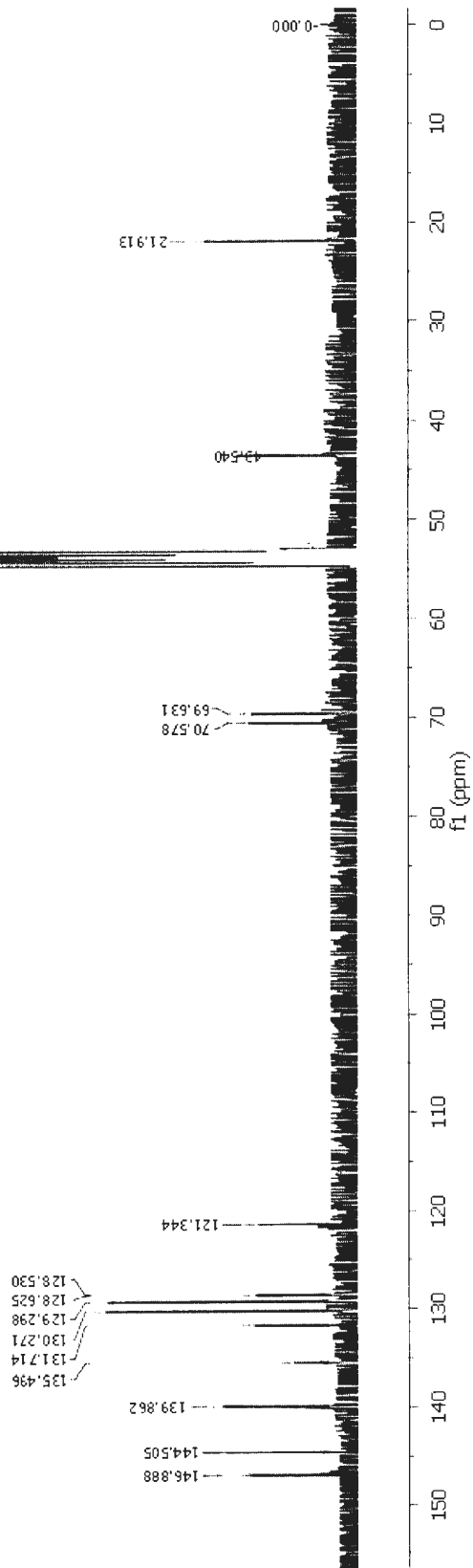
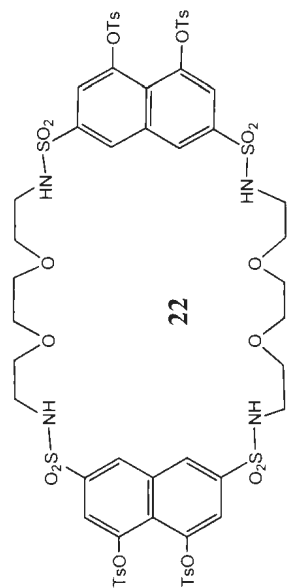
## **Appendix B**

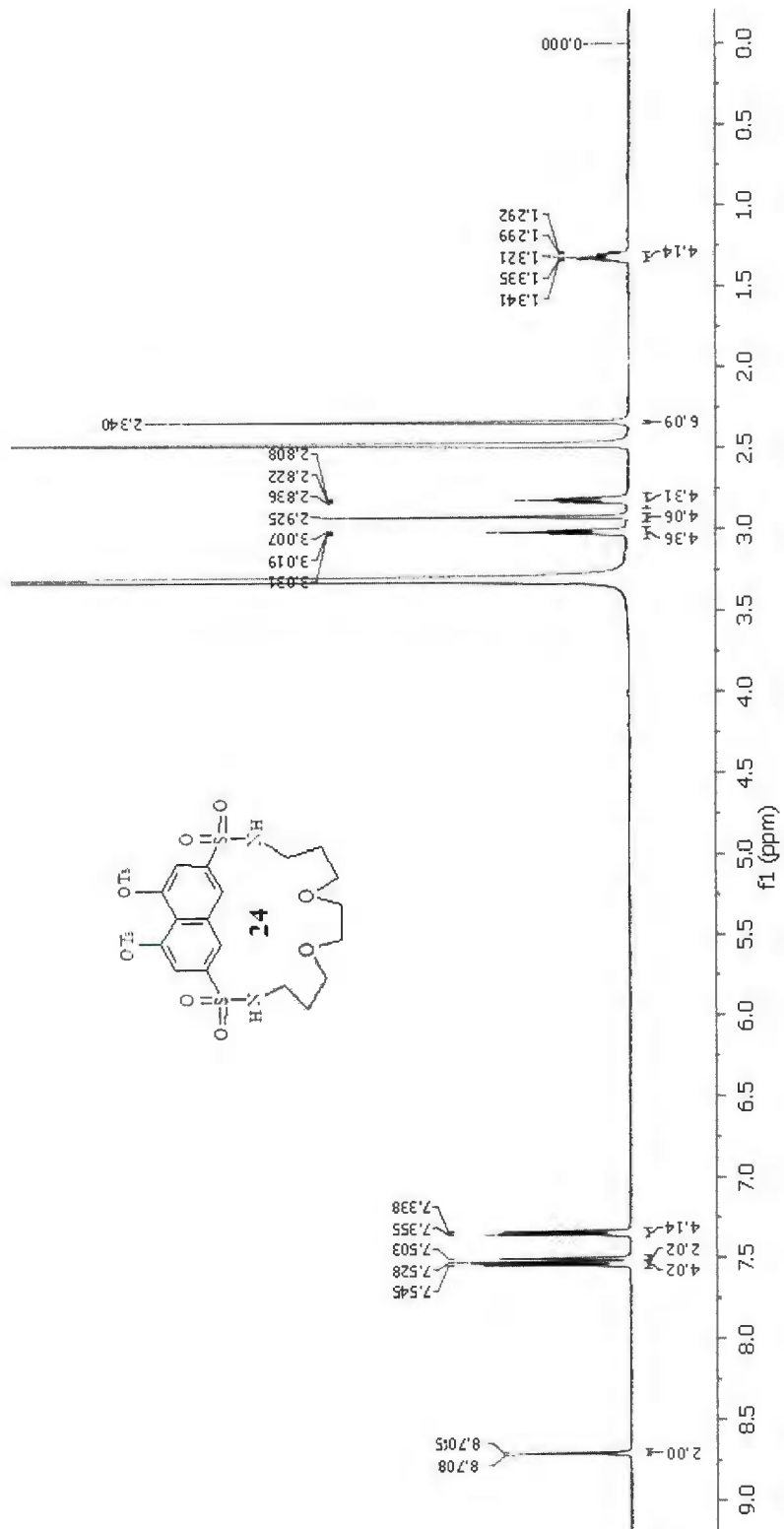
**$^1\text{H}$ ,  $^{13}\text{C}$  NMR and ESI-mass spectra for compounds described in Chapter 3**

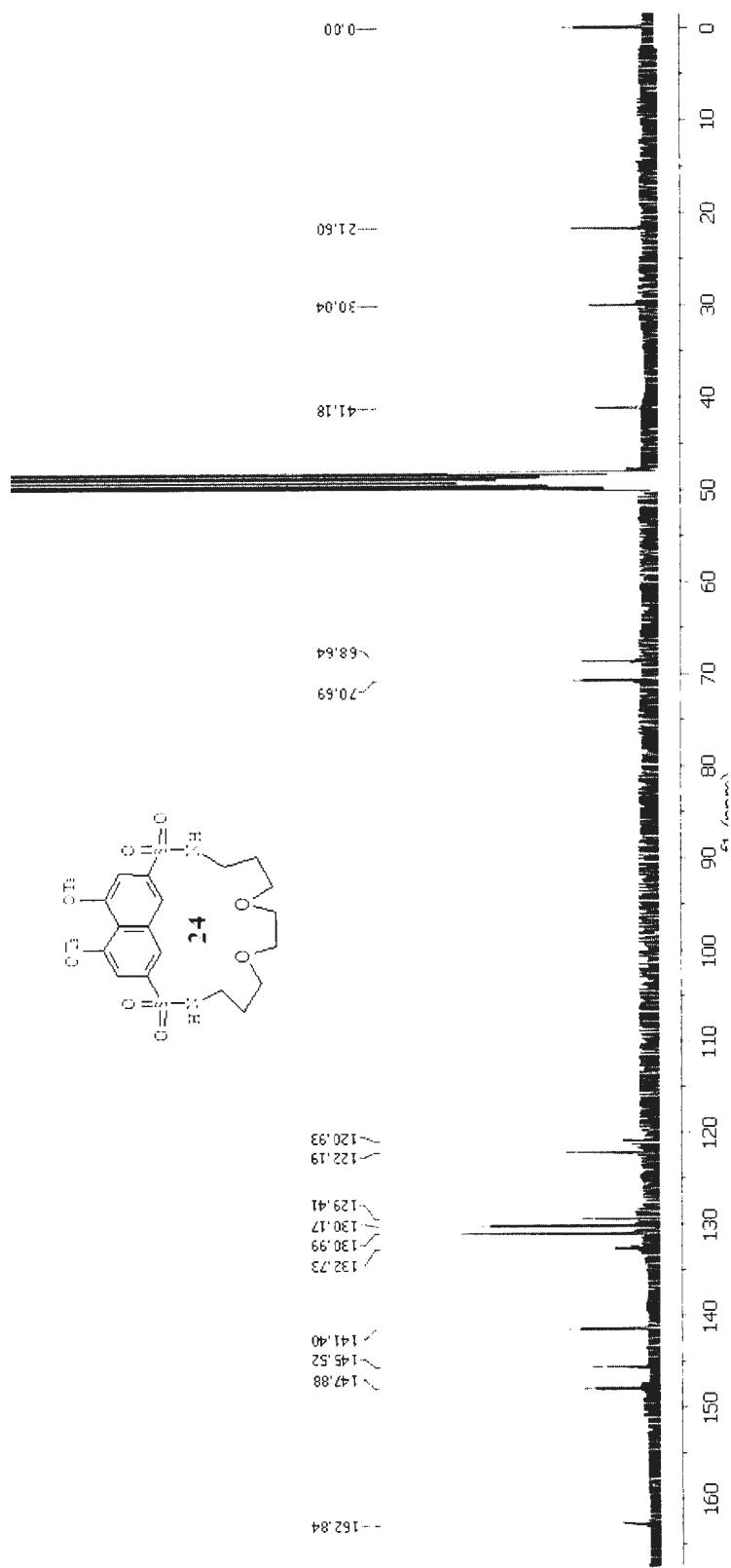


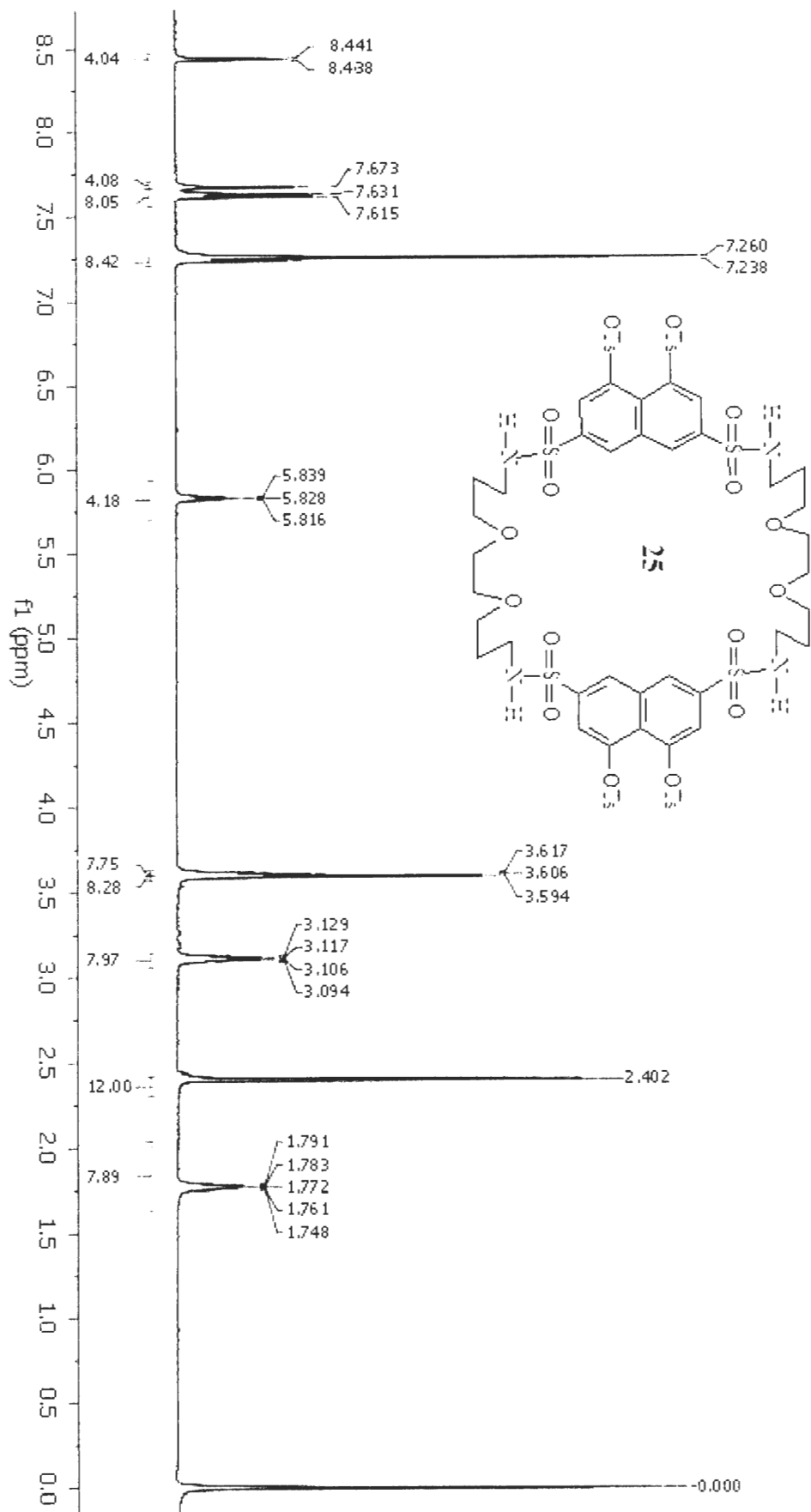


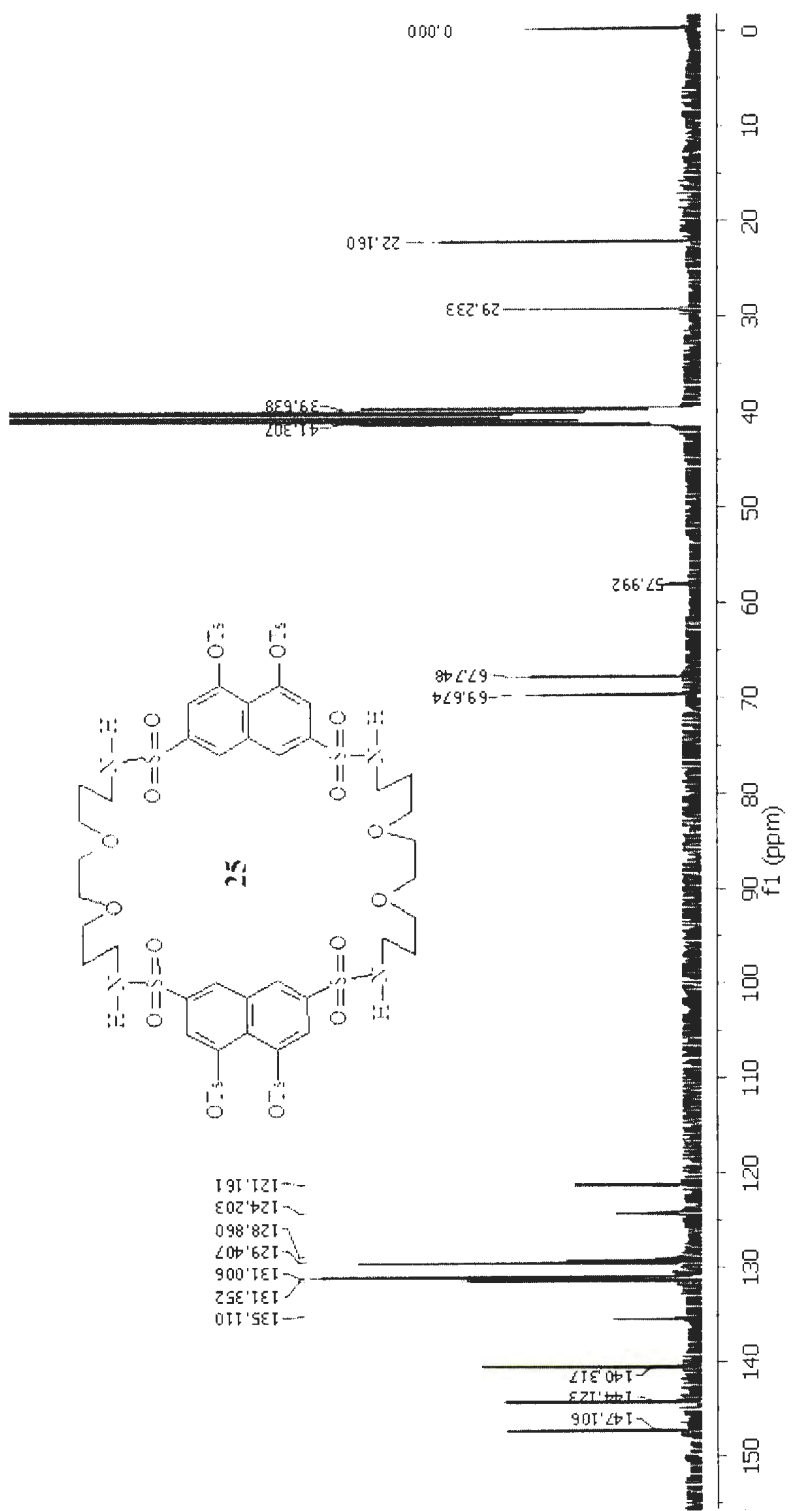






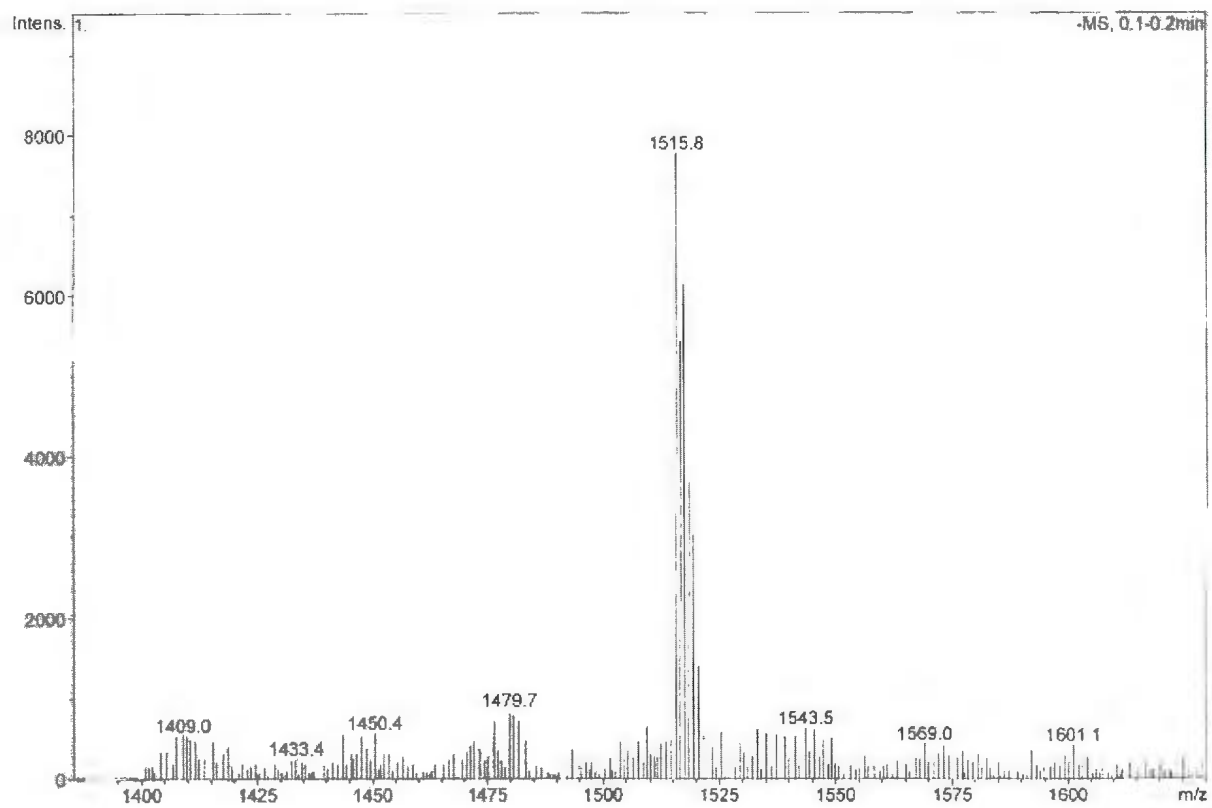




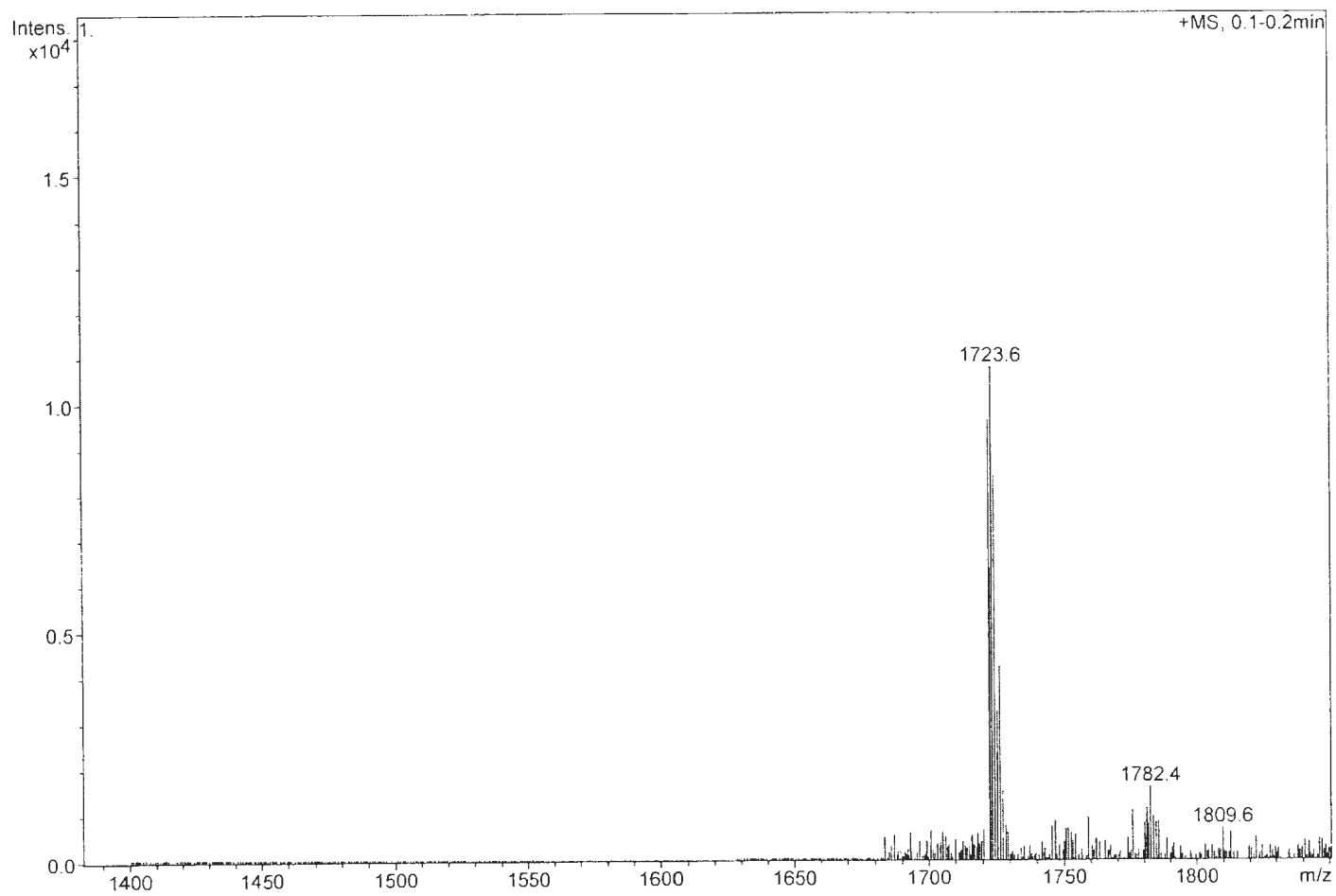


**ESI / MS of Compound "22"& TBACl complex in both -ve and +ve mode:**

**ESI-Mass (negative mode) of compound 22**

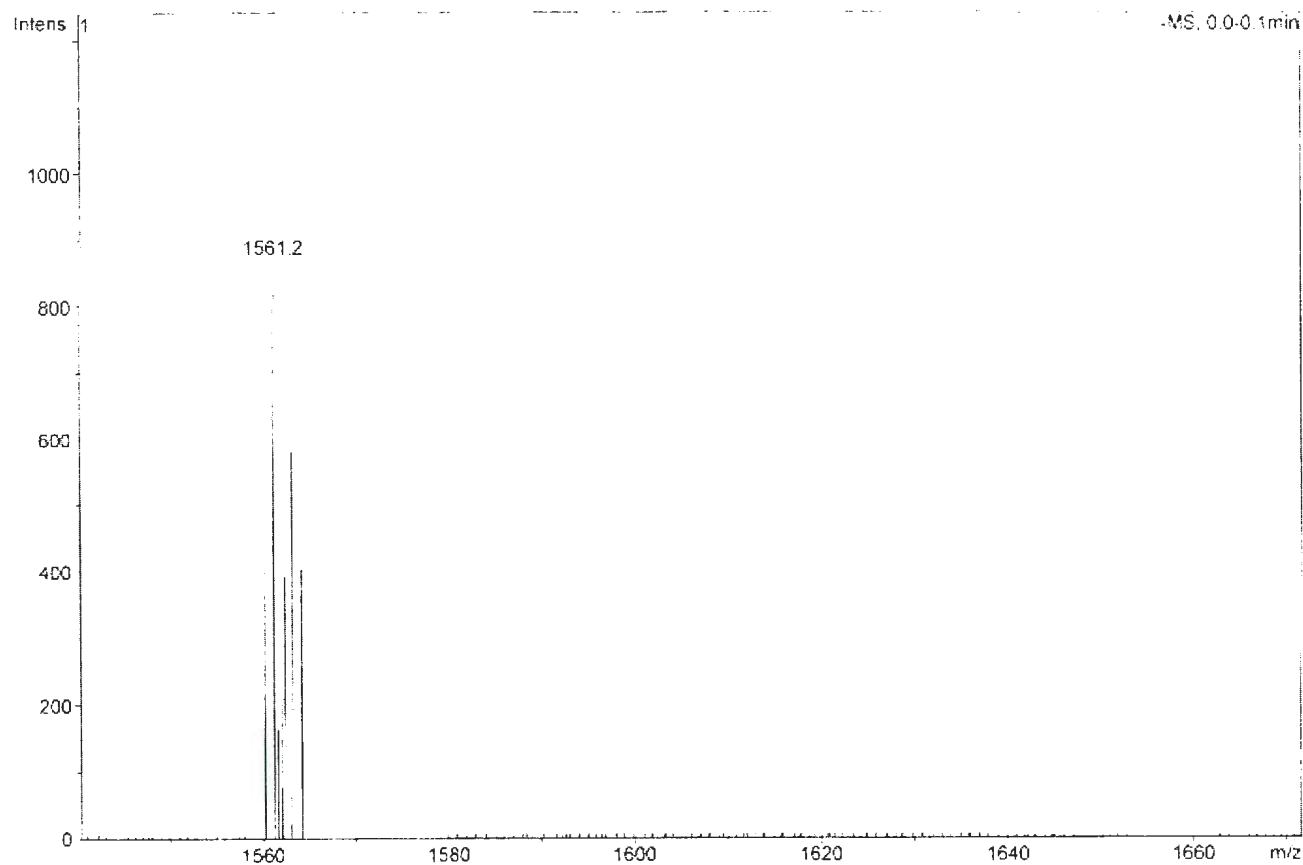


# ESI-Mass (positive mode) of compound **22**

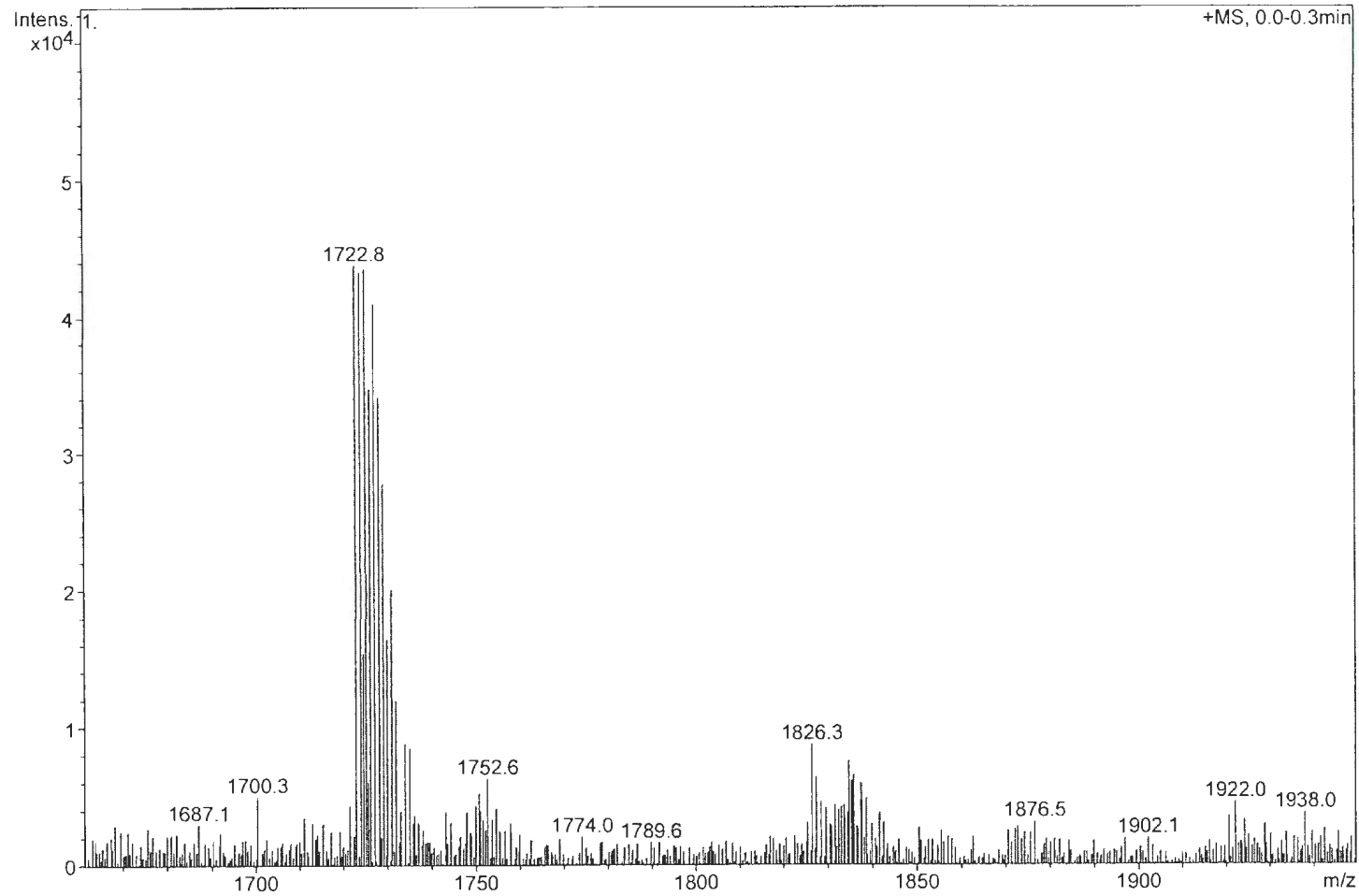


ESI / MS of Compound "22" & TBABr complex in both -ve and +ve mode:

ESI-Mass (negative mode) of compound 22

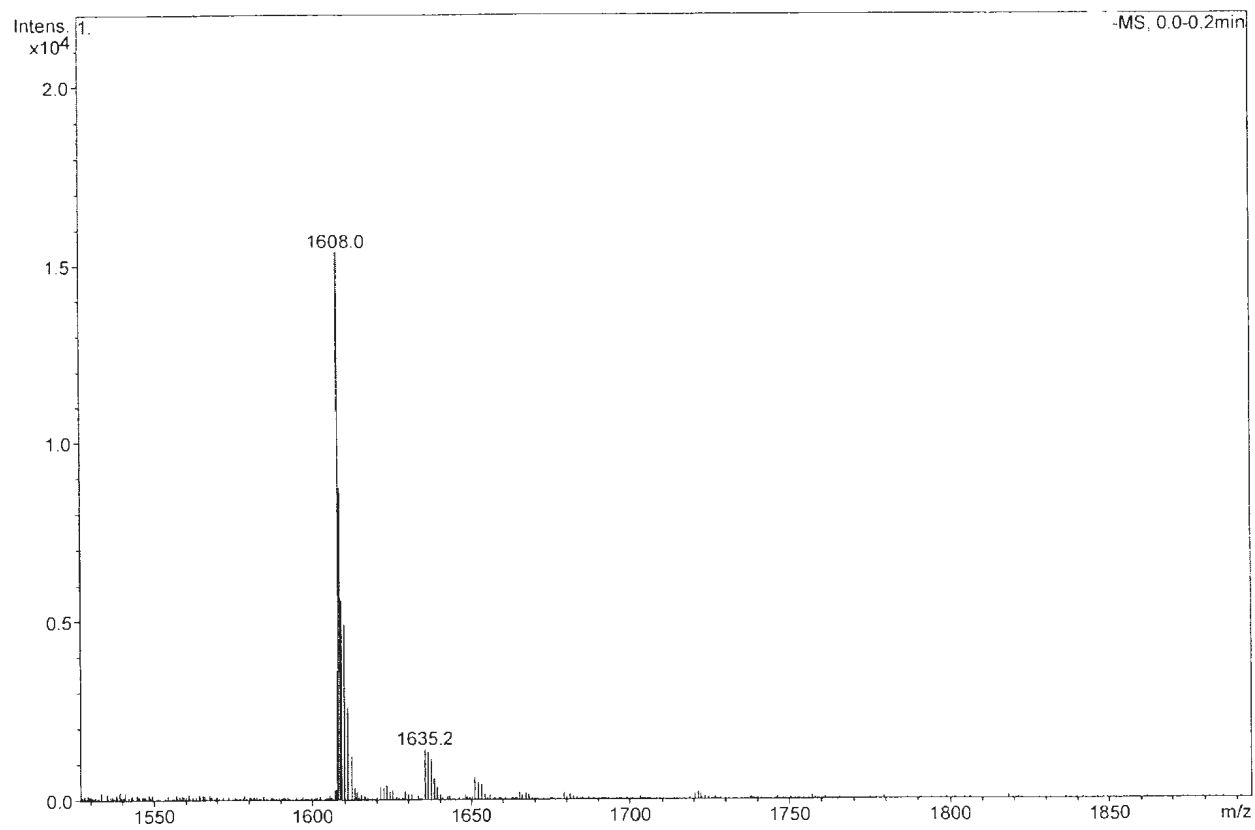


ESI-Mass (positive mode) of compound **22**

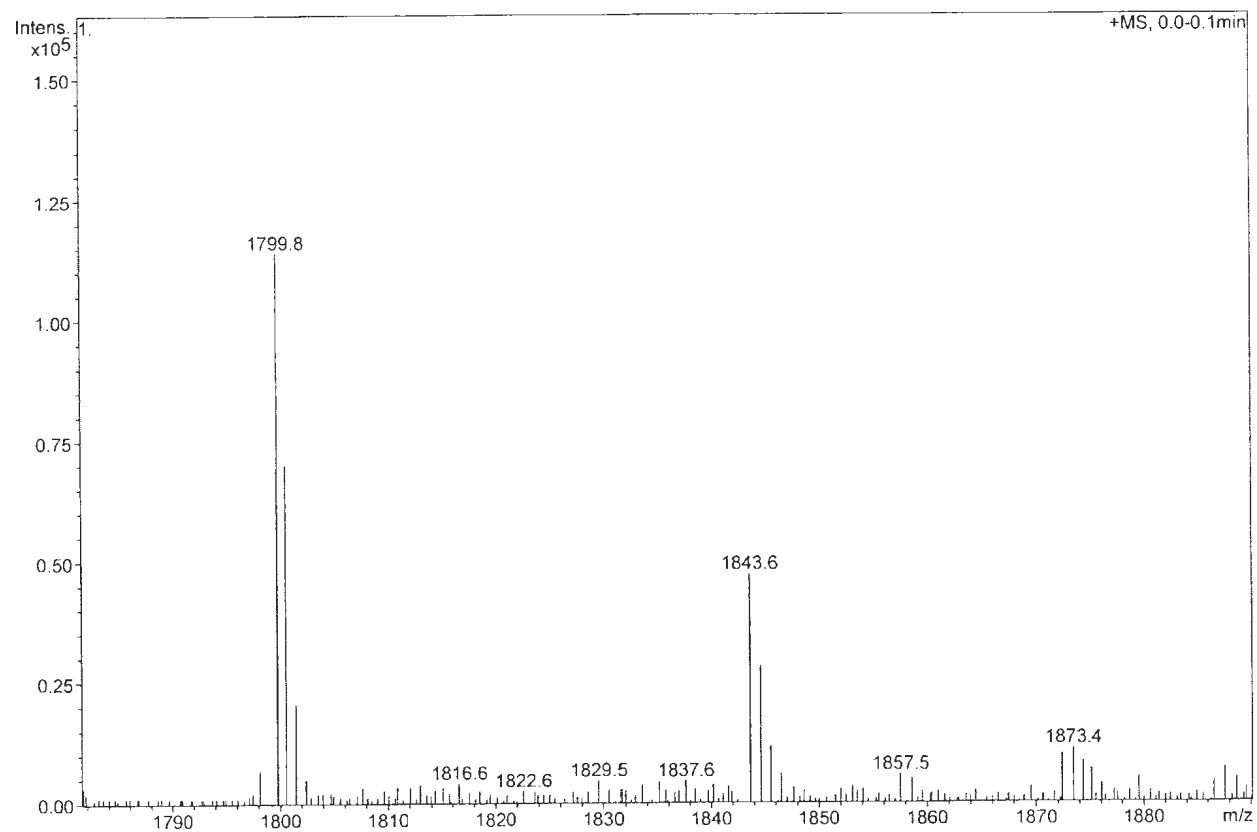


ESI / MS of Compound "22"& TBAI complex in both -ve and +ve mode:

ESI-Mass (negative mode) of compound **22**

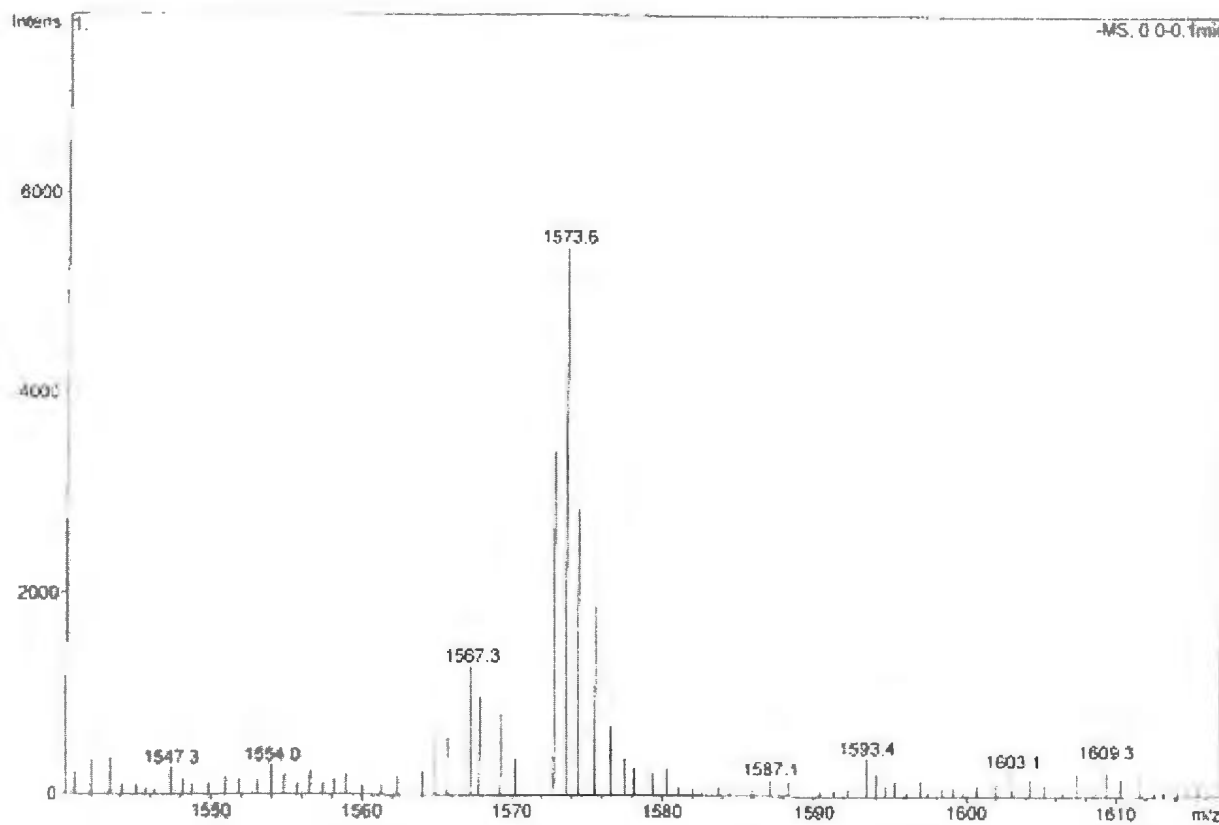


# ESI-Mass (positive mode) of compound 22

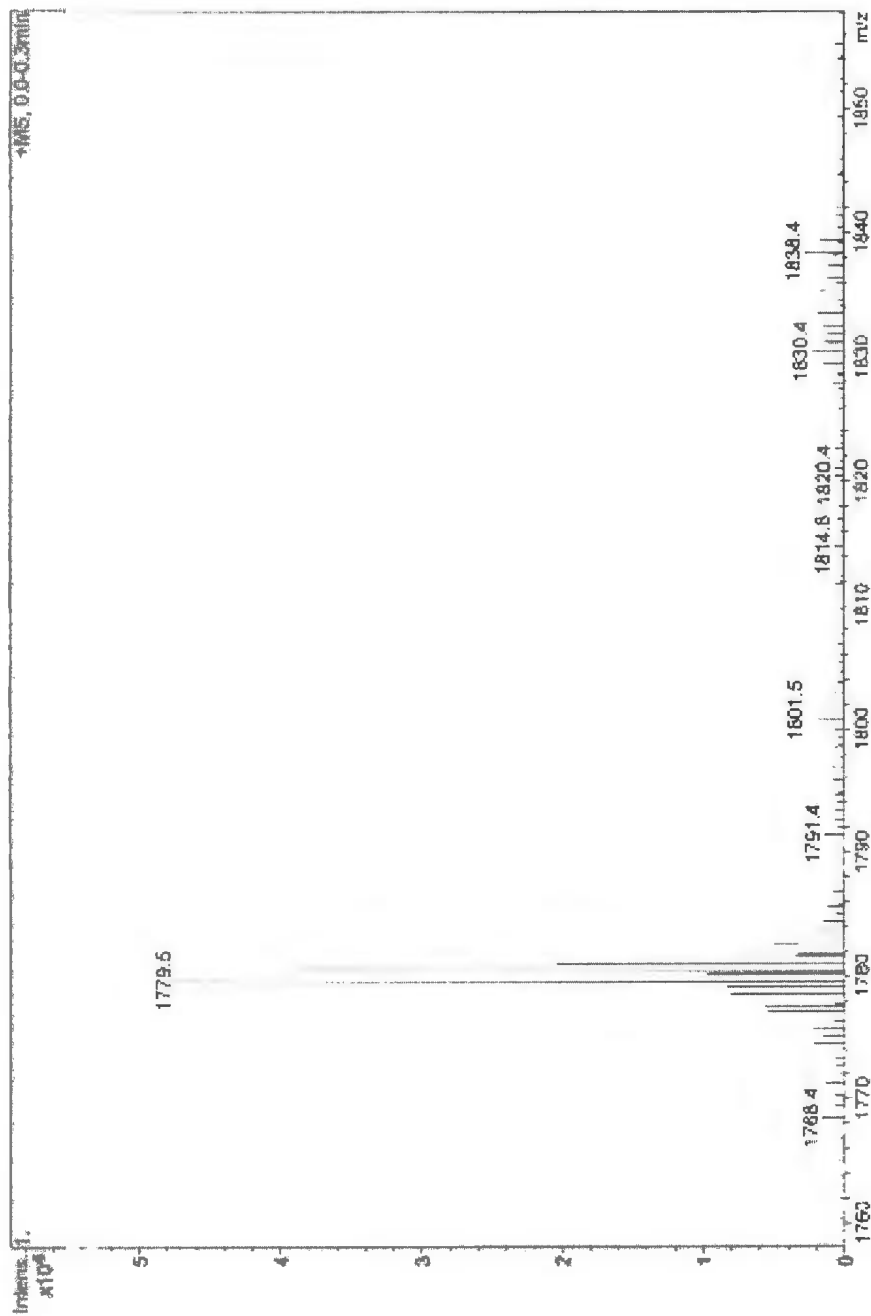


**ESI / MS of Compound "25"& TBACl complex in both -ve and +ve mode:**

ESI-Mass (negative mode) of compound **25**

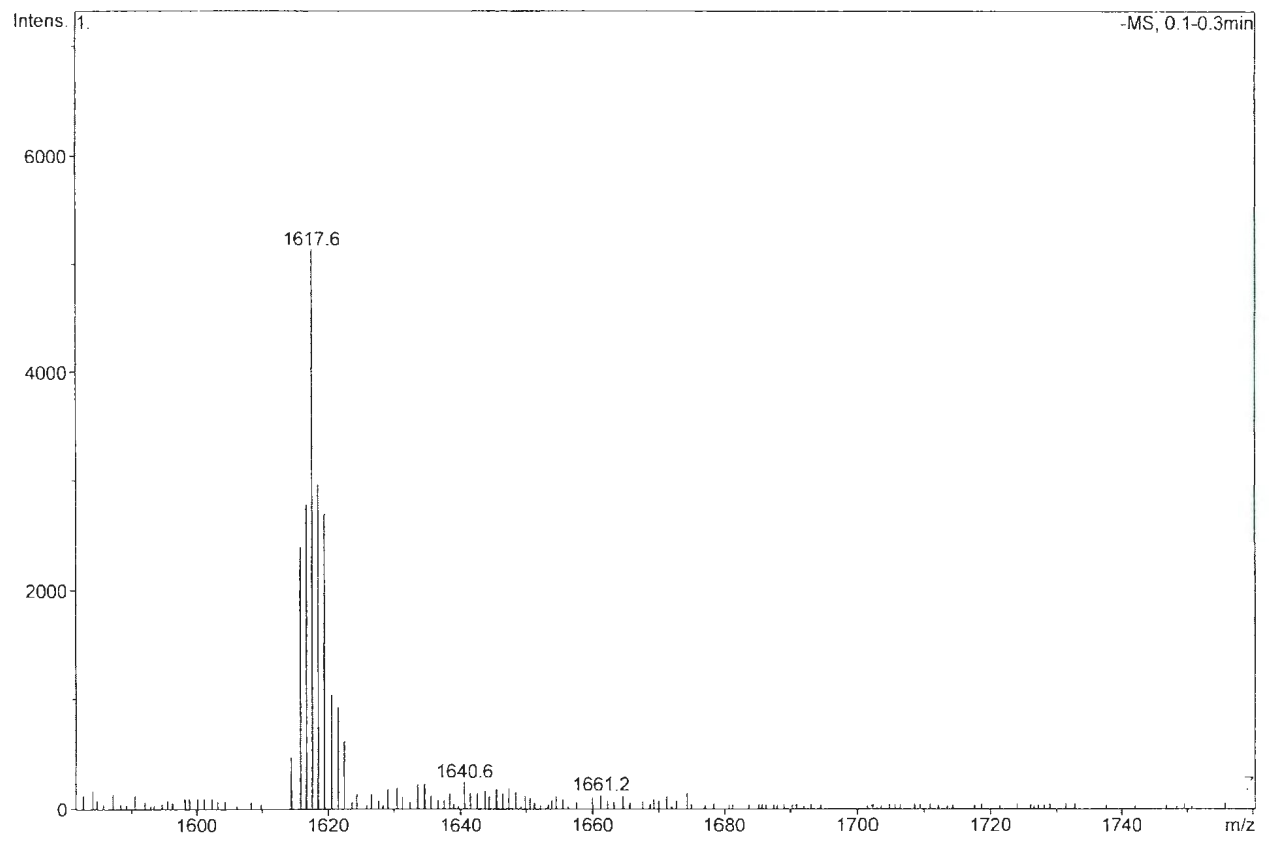


# ESI-Mass (positive mode) of compound 25

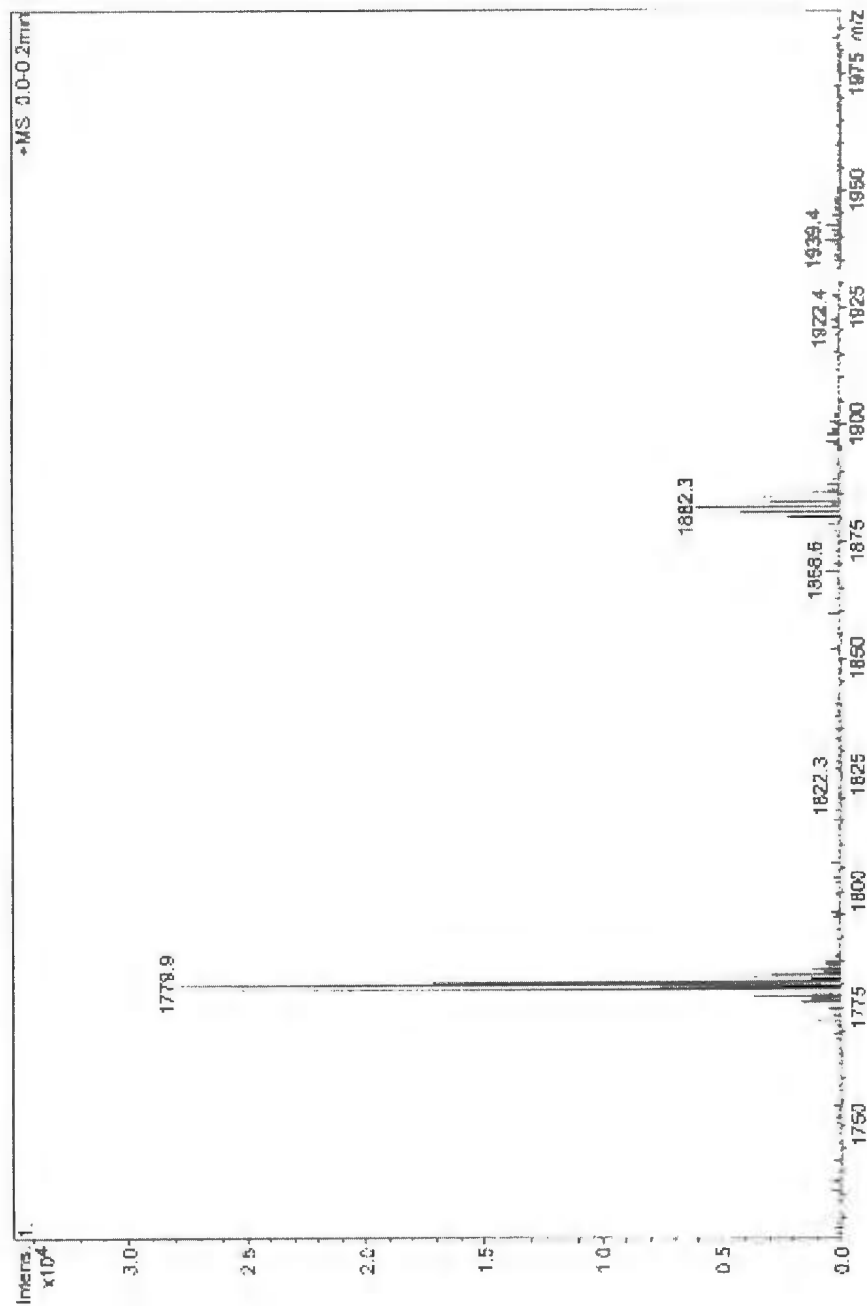


**ESI / MS of Compound "25"& TBABr complex in both -ve and +ve mode:**

ESI-Mass (negative mode) of compound **25**

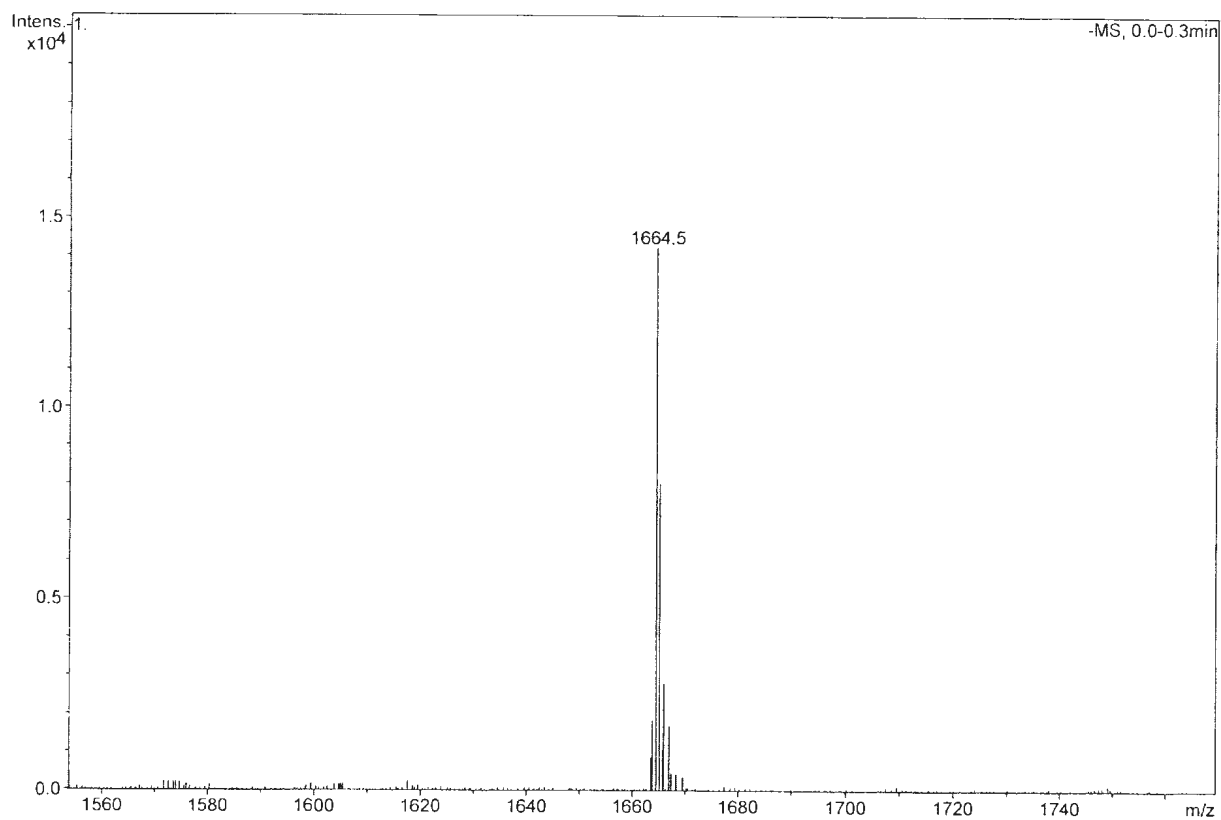


# ESI-Mass (positive mode) of compound 25

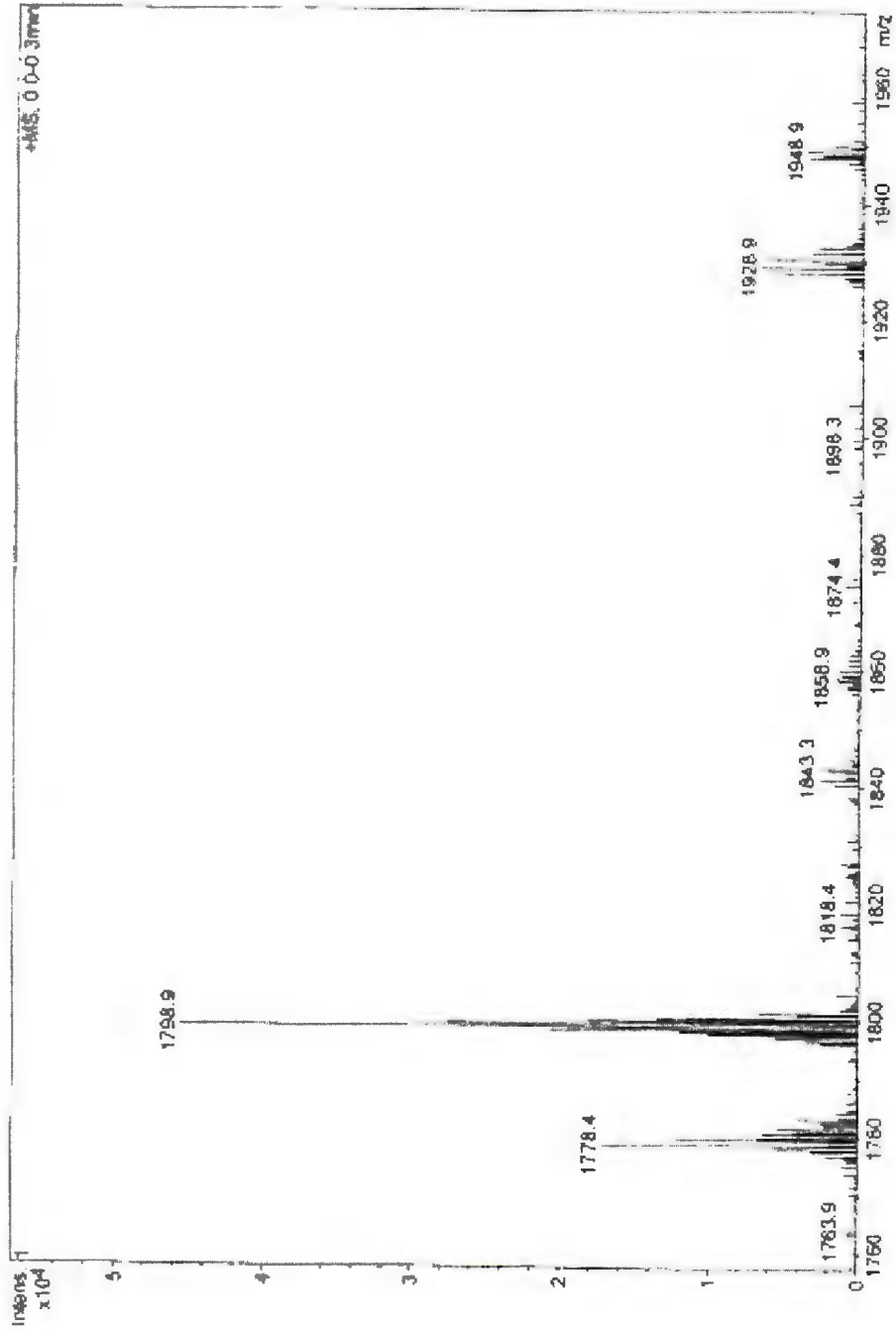


ESI / MS of Compound "25"& TBAI complex in both -ve and +ve mode:

ESI-Mass (negative mode) of compound 25



ESI-Mass (positive mode) of compound 25



## **Appendix C**

**X-ray crystallographic data reports for compounds  
in the order presented in Chapters 2-4**

**Appendix 2.1** X-ray crystallographic data report for compound **20** (Chapter 2)

X-ray Structure Report

for  
Dr. P. E. Georghiou

Prepared by

Louise N. Dawe, PhD

Centre for Chemical Analysis, Research and Training (C-CART)  
Department of Chemistry  
Memorial University of Newfoundland  
St. Johns, NL, A1B 3X7  
(709) 737-4556 (X-Ray Laboratory)

October 8, 2010

[Crystallographic data has been reported with the Cambridge crystallographic data centre as  
CCDC#896906]

Introduction

Collection, solution and refinement proceeded normally. H1N, H2N, H1W and H2W were introduced in difference map positions, and refined positionally with distance and angle restraints and with thermal parameters fixed 1.2 times that of their bonding partner. All other hydrogen atoms were introduced in calculated positions and refined on a riding model. All non-hydrogen atoms were refined anisotropically.

## Experimental

### Data Collection

A colorless prism crystal of  $C_{16}H_{24}N_2O_5$  having approximate dimensions of 0.53 x 0.41 x 0.33 mm was mounted on a low temperature diffraction loop. All measurements were made on a Rigaku Saturn CCD area detector equipped with a SHINE optic and Mo-K $\alpha$  radiation.

Indexing was performed from 360 images that were exposed for 7 seconds. The crystal-to-detector distance was 40.14 mm.

Cell constants and an orientation matrix for data collection corresponded to a primitive monoclinic cell with dimensions:

$$\begin{aligned} a &= 11.336(3) \text{ \AA} \\ b &= 10.813(3) \text{ \AA} \quad \beta = 129.643(6)^\circ \\ c &= 16.926(5) \text{ \AA} \\ V &= 1597.6(8) \text{ \AA}^3 \end{aligned}$$

For  $Z = 4$  and F.W. = 324.38, the calculated density is 1.348 g/cm $^3$ . The systematic absences of:

$$\begin{aligned} h0l: l \pm 2n \\ 0k0: k \pm 2n \end{aligned}$$

uniquely determine the space group to be:

$$P2_1/c \text{ (#14)}$$

The data were collected at a temperature of  $-120 \pm 1^\circ\text{C}$  to a maximum  $2\theta$  value of  $61.4^\circ$ . A total of 1080 oscillation images were collected. A sweep of data was done using  $\omega$  scans from  $-75.0$  to  $105.0^\circ$  in  $0.5^\circ$  step, at  $\chi=45.0^\circ$  and  $\phi = 90.0^\circ$ . The exposure rate was 14.0 [sec./ $^\circ$ ]. The detector swing angle was  $15.12^\circ$ . A second sweep was performed using  $\omega$  scans from  $-75.0$  to  $105.0^\circ$  in  $0.5^\circ$  step, at  $\chi=45.0^\circ$  and  $\phi = 180.0^\circ$ . The exposure rate was 14.0 [sec./ $^\circ$ ]. The detector swing angle was  $15.12^\circ$ . Another sweep was performed using  $\omega$  scans from  $-75.0$  to  $105.0^\circ$  in  $0.5^\circ$  step, at  $\chi=0.0^\circ$  and  $\phi = 0.0^\circ$ . The exposure rate was 14.0 [sec./ $^\circ$ ]. The detector swing angle was  $15.12^\circ$ . The crystal-to-detector distance was 40.14 mm. Readout was performed in the 0.137 mm pixel mode.

### Data Reduction

Of the 21578 reflections that were collected, 3649 were unique ( $R_{int} = 0.0230$ ). Data were collected and processed using CrystalClear (Rigaku). Net intensities and sigmas were derived as follows:

$$F^2 = [\sum(P_i - mB_{ave})] \cdot Lp^{-1}$$

where  $P_i$  is the value in counts of the  $i^{th}$  pixel  
 $m$  is the number of pixels in the integration area  
 $B_{ave}$  is the background average  
 $Lp$  is the Lorentz and polarization factor

$$B_{ave} = \sum(B_j)/n$$

where  $n$  is the number of pixels in the background area  
 $B_j$  is the value of the  $j^{th}$  pixel in counts

$$\sigma^2(F^2_{hkl}) = [(\sum P_i) + m((\sum(B_{ave} - B_j)^2)/(n-1))] \cdot Lp \cdot errmul + (erradd \cdot F^2)^2$$

where  $erradd = 0.00$   
 $errmul = 1.00$

The linear absorption coefficient,  $\mu$ , for Mo-K $\alpha$  radiation is 1.002 cm<sup>-1</sup>. A numerical absorption correction was applied which resulted in transmission factors ranging from 0.9642 to 0.9796. The data were corrected for Lorentz and polarization effects.

### Structure Solution and Refinement

The structure was solved by direct methods<sup>2</sup> and expanded using Fourier techniques<sup>3</sup>. The non-hydrogen atoms were refined anisotropically. Some hydrogen atoms were refined isotropically, some were refined using the riding model, and the rest were included in fixed positions. The final cycle of full-matrix least-squares refinement<sup>4</sup> on  $F^2$  was based on 3649 observed reflections and 221 variable parameters and converged (largest parameter shift was 0.00 times its esd) with unweighted and weighted agreement factors of:

$$R1 = \sum ||F_o| - |F_c|| / \sum |F_o| = 0.0389$$

$$wR2 = [ \sum ( w (F_o^2 - F_c^2)^2 ) / \sum w(F_o^2)^2 ]^{1/2} = 0.0992$$

The standard deviation of an observation of unit weight<sup>5</sup> was 1.06. Unit weights were used. The maximum and minimum peaks on the final difference Fourier map corresponded to 0.44 and -0.27 e<sup>-</sup>/Å<sup>3</sup>, respectively.

Neutral atom scattering factors were taken from Cromer and Waber<sup>6</sup>. Anomalous dispersion effects were included in F<sub>calc</sub><sup>7</sup>; the values for Δf' and Δf'' were those of Creagh and McAuley<sup>8</sup>. The values for the mass attenuation coefficients are those of Creagh and Hubbell<sup>9</sup>. All calculations were performed using the CrystalStructure<sup>10,11</sup> crystallographic software package except for refinement, which was performed using SHELXL-97<sup>2</sup>.

### References

(1) CrystalClear: Rigaku Corporation, 1999. CrystalClear Software User's Guide, Molecular Structure Corporation, (c) 2000. J.W. Pflugrath (1999) Acta Cryst. D55, 1718-1725.

(2) SHELX97: Sheldrick, G.M. Acta Cryst. 2008. A64, 112-122.

(3) DIRDIF99: Beurskens, P.T., Admiraal, G., Beurskens, G., Bosman, W.P., de Gelder, R., Israel, R. and Smits, J.M.M. (1999). The DIRDIF-99 program system, Technical Report of the Crystallography Laboratory, University of Nijmegen, The Netherlands.

(4) Least Squares function minimized: (SHELXL97)

$$\sum w(F_o^2 - F_c^2)^2 \quad \text{where } w = \text{Least Squares weights.}$$

(5) Standard deviation of an observation of unit weight:

$$[\sum w(F_o^2 - F_c^2)^2 / (N_o - N_v)]^{1/2}$$

where:            N<sub>o</sub> = number of observations  
                      N<sub>v</sub> = number of variables

(6) Cromer, D. T. & Waber, J. T.; "International Tables for X-ray Crystallography", Vol. IV, The Kynoch Press, Birmingham, England, Table 2.2 A (1974).

(7) Ibers, J. A. & Hamilton, W. C.; Acta Crystallogr., 17, 781 (1964).

(8) Creagh, D. C. & McAuley, W.J. ; "International Tables for Crystallography", Vol C, (A.J.C. Wilson, ed.), Kluwer Academic Publishers, Boston, Table 4.2.6.8, pages 219-222 (1992).

(9) Creagh, D. C. & Hubbell, J.H.; "International Tables for Crystallography", Vol C, (A.J.C. Wilson, ed.), Kluwer Academic Publishers, Boston, Table 4.2.4.3, pages 200-206 (1992).

(10) CrystalStructure 3.7.0: Crystal Structure Analysis Package, Rigaku and Rigaku/MSC (2000-2005). 9009 New Trails Dr. The Woodlands TX 77381 USA.

(11) CRYSTALS Issue 10: Watkin, D.J., Prout, C.K. Carruthers, J.R. & Betteridge, P.W. Chemical Crystallography Laboratory, Oxford, UK. (1996)

### EXPERIMENTAL DETAILS

#### A. Crystal Data

Empirical Formula	C <sub>16</sub> H <sub>24</sub> N <sub>2</sub> O <sub>5</sub>
Formula Weight	324.38
Crystal Color, Habit	colorless, prism
Crystal Dimensions	0.53 X 0.41 X 0.33 mm
Crystal System	monoclinic
Lattice Type	Primitive
Detector Position	40.14 mm
Pixel Size	0.137 mm
Lattice Parameters	a = 11.336(3) Å b = 10.813(3) Å c = 16.926(5) Å β = 129.643(6) ° V = 1597.6(8) Å <sup>3</sup>

Space Group	P2 <sub>1</sub> /c (#14)
Z value	4
D <sub>calc</sub>	1.348 g/cm <sup>3</sup>
F <sub>000</sub>	696
μ(MoKα)	1.00 cm <sup>-1</sup>

#### B. Intensity Measurements

Detector Goniometer	Rigaku Saturn Rigaku AFC8
Radiation	MoKα (λ = 0.71075 Å) graphite monochromated-Rigaku SHINE
Detector Aperture	70 mm x 70 mm
Data Images	1080 exposures
ω oscillation Range (χ=45.0, φ=90.0)	-75.0 - 105.0°
Exposure Rate	14.0 sec./°
Detector Swing Angle	15.12°
ω oscillation Range (χ=45.0, φ=180.0)	-75.0 - 105.0°
Exposure Rate	14.0 sec./°
Detector Swing Angle	15.12°
ω oscillation Range (χ=0.0, φ=0.0)	-75.0 - 105.0°
Exposure Rate	14.0 sec./°

Detector Swing Angle	15.12°
Detector Position	40.14 mm
Pixel Size	0.068 mm
2θ <sub>max</sub>	61.4°
No. of Reflections Measured	Total: 21578 Unique: 3649 (R <sub>int</sub> = 0.0230) I > 2σ(I): 3601
Corrections	Lorentz-polarization (trans. factors: 0.9642 - 0.9796)

### C. Structure Solution and Refinement

Structure Solution	Direct Methods (SHELX97)
Refinement	Full-matrix least-squares on F <sup>2</sup>
Function Minimized	$\sum w (F_o^2 - F_c^2)^2$
Least Squares Weights	$w = 1 / [ \sigma^2(F_o^2) + (0.0499 \cdot P)^2 + 0.5175 \cdot P ]$ where $P = (\text{Max}(F_o^2, 0) + 2F_c^2) / 3$
2θ <sub>max</sub> cutoff	55.0°
Anomalous Dispersion	All non-hydrogen atoms
No. Observations (All reflections)	3649
No. Variables	221
Reflection/Parameter Ratio	16.51
Residuals: R1 (I > 2.00σ(I))	0.0389

Residuals: R (All reflections)	0.0393
Residuals: wR2 (All reflections)	0.0992
Goodness of Fit Indicator	1.064
Max Shift/Error in Final Cycle	0.000
Maximum peak in Final Diff. Map	0.44 e <sup>-</sup> /Å <sup>3</sup>
Minimum peak in Final Diff. Map	-0.27 e <sup>-</sup> /Å <sup>3</sup>

**Appendix 2.2** X-ray crystallographic data report for compound **21** (Chapter 2)

X-ray Structure Report

for

Prof. Paris Georghiou

Prepared by

Louise N. Dawe, PhD

Centre for Chemical Analysis, Research and Training (C-CART)

Department of Chemistry

Memorial University of Newfoundland

St. Johns, NL, A1B 3X7

(709) 864-4556 (X-Ray Laboratory)

February 16, 2011

[Crystallographic data has been reported with the Cambridge crystallographic data centre as CCDC#896907]

Introduction

Multiple attempts were made to grow X-ray diffraction single crystals, however, the only successful collection, reported here, was performed on a very tiny needle that diffracted poorly. The high data statistics are the result of this weak data-set. Please note that this has also resulted in large esd's on some bond lengths and angles.

H1A and H2A were introduced in difference map positions, and were allowed to refine positionally, with isotropic displacement parameters fixed 1.2 times that of their bonding partners. All other hydrogen atoms were introduced in calculated positions and refined on a riding model. All non-hydrogen atoms were refined anisotropically.

## Experimental

### Data Collection

A colorless prism crystal of  $C_{32}H_{44}N_4O_8$  having approximate dimensions of 0.20 x 0.20 x 0.20 mm was mounted on a low temperature diffraction loop. All measurements were made on a Rigaku Saturn70 CCD diffractometer using graphite monochromated Mo-K $\alpha$  radiation, equipped with a SHINE optic.

The crystal-to-detector distance was 50.00 mm.

Cell constants and an orientation matrix for data collection corresponded to a primitive triclinic cell with dimensions:

$$\begin{aligned} a &= 5.0083(18) \text{ \AA} & \alpha &= 85.179(8)^\circ \\ b &= 9.048(3) \text{ \AA} & \beta &= 82.023(9)^\circ \\ c &= 17.725(6) \text{ \AA} & \gamma &= 75.645(9)^\circ \\ V &= 769.6(5) \text{ \AA}^3 \end{aligned}$$

For  $Z = 1$  and F.W. = 612.72, the calculated density is 1.322 g/cm<sup>3</sup>. Based on a statistical analysis of intensity distribution, and the successful solution and refinement of the structure, the space group was determined to be:

P-1 (#2)

The data were collected at a temperature of  $-110 \pm 1^\circ\text{C}$  to a maximum  $2\theta$  value of  $55.0^\circ$ . A total of 1314 oscillation images were collected. A sweep of data was done using  $\omega$  scans from  $-70.0$  to  $110.0^\circ$  in  $0.5^\circ$  step, at  $\chi=45.0^\circ$  and  $\phi = 180.0^\circ$ . The exposure rate was 80.0 [sec./ $^\circ$ ]. The detector swing angle was  $20.00^\circ$ . A second sweep was performed using  $\omega$  scans from  $-36.0$  to  $99.0^\circ$  in  $0.5^\circ$  step, at  $\chi=0.0^\circ$  and  $\phi = 0.0^\circ$ . The exposure rate was 80.0 [sec./ $^\circ$ ]. The detector swing angle was  $20.00^\circ$ . Another sweep was performed using  $\omega$  scans from  $-70.0$  to  $110.0^\circ$  in  $0.5^\circ$  step, at  $\chi=45.0^\circ$  and  $\phi = 90.0^\circ$ . The exposure rate was 80.0 [sec./ $^\circ$ ]. The detector swing angle was  $20.00^\circ$ . Another sweep was performed using  $\omega$  scans from  $-70.0$  to  $92.0^\circ$  in  $0.5^\circ$  step, at  $\chi=45.0^\circ$  and  $\phi = 0.0^\circ$ . The exposure rate was 80.0 [sec./ $^\circ$ ]. The detector swing angle was  $20.00^\circ$ . The crystal-to-detector distance was 50.00 mm. Readout was performed in the 0.068 mm pixel mode.

## Data Reduction

Of the 8677 reflections that were collected, 2656 were unique ( $R_{\text{int}} = 0.1457$ ); equivalent reflections were merged. Data were collected and processed using CrystalClear (Rigaku).

The linear absorption coefficient,  $\mu$ , for Mo-K $\alpha$  radiation is  $0.95 \text{ cm}^{-1}$ . An empirical absorption correction was applied which resulted in transmission factors ranging from 0.323 to 1.000. The data were corrected for Lorentz and polarization effects.

## Structure Solution and Refinement

The structure was solved by direct methods<sup>2</sup> and expanded using Fourier techniques. The non-hydrogen atoms were refined anisotropically. Hydrogen atoms were refined using the riding model. The final cycle of full-matrix least-squares refinement<sup>3</sup> on  $F^2$  was based on 2656 observed reflections and 205 variable parameters and converged (largest parameter shift was 0.00 times its esd) with unweighted and weighted agreement factors of:

$$R1 = \sum ||F_o| - |F_c|| / \sum |F_o| = 0.1365$$

$$wR2 = [ \sum ( w (F_o^2 - F_c^2)^2 ) / \sum w(F_o^2)^2 ]^{1/2} = 0.3084$$

The standard deviation of an observation of unit weight<sup>4</sup> was 1.11. Unit weights were used. The maximum and minimum peaks on the final difference Fourier map corresponded to 0.30 and  $-0.29 \text{ e}^{-}/\text{\AA}^3$ , respectively.

Neutral atom scattering factors were taken from Cromer and Waber<sup>5</sup>. Anomalous dispersion effects were included in  $F_{\text{calc}}$ <sup>6</sup>; the values for  $\Delta f'$  and  $\Delta f''$  were those of Creagh and McAuley<sup>7</sup>. The values for the mass attenuation coefficients are those of Creagh and Hubbell<sup>8</sup>. All calculations were performed using the CrystalStructure<sup>9</sup> crystallographic software package except for refinement, which was performed using SHELXL-97<sup>2</sup>.

## References

(1) CrystalClear: Rigaku Corporation, 1999. CrystalClear Software User's Guide, Molecular Structure Corporation, (c) 2000. J.W. Pflugrath (1999) Acta Cryst. D55, 1718-1725.

(2) SHELX97: Sheldrick, G.M. Acta Cryst. 2008, A64, 112-122

(3) Least Squares function minimized: (SHELXL97)

$$\sum w(F_o^2 - F_c^2)^2 \quad \text{where } w = \text{Least Squares weights.}$$

(4) Standard deviation of an observation of unit weight:

$$[\sum w(F_o^2 - F_c^2)^2 / (N_o - N_v)]^{1/2}$$

where:  $N_o$  = number of observations  
 $N_v$  = number of variables

(5) Cromer, D. T. & Waber, J. T.; "International Tables for X-ray Crystallography", Vol. IV, The Kynoch Press, Birmingham, England, Table 2.2 A (1974).

(6) Ibers, J. A. & Hamilton, W. C.; Acta Crystallogr., 17, 781 (1964).

(7) Creagh, D. C. & McAuley, W.J. ; "International Tables for Crystallography", Vol C, (A.J.C. Wilson, ed.), Kluwer Academic Publishers, Boston, Table 4.2.6.8, pages 219-222 (1992).

(8) Creagh, D. C. & Hubbell, J.H.; "International Tables for Crystallography", Vol C, (A.J.C. Wilson, ed.), Kluwer Academic Publishers, Boston, Table 4.2.4.3, pages 200-206 (1992).

(9) CrystalStructure 4.0: Crystal Structure Analysis Package, Rigaku and Rigaku Americas (2000-2010). 9009 New Trails Dr. The Woodlands TX 77381 USA.

## EXPERIMENTAL DETAILS

### A. Crystal Data

Empirical Formula	$C_{32}H_{44}N_4O_8$
Formula Weight	612.72
Crystal Color, Habit	colorless, prism
Crystal Dimensions	0.20 X 0.20 X 0.20 mm
Crystal System	triclinic
Lattice Type	Primitive
Lattice Parameters	$a = 5.0083(18) \text{ \AA}$ $b = 9.048(3) \text{ \AA}$ $c = 17.725(6) \text{ \AA}$ $\alpha = 85.179(8)^\circ$ $\beta = 82.023(9)^\circ$ $\gamma = 75.645(9)^\circ$ $V = 769.6(5) \text{ \AA}^3$
Space Group	P-1 (#2)
Z value	1
$D_{\text{calc}}$	$1.322 \text{ g/cm}^3$
F000	328
$\mu(\text{MoK}\alpha)$	$0.95 \text{ cm}^{-1}$

## B. Intensity Measurements

Diffractometer	Rigaku Saturn70 CCD
Radiation	MoK $\alpha$ ( $\lambda = 0.71075 \text{ \AA}$ ) graphite monochromated-Rigaku SHINE
Voltage, Current	50kV, 40mA
Temperature	-110.0 $^{\circ}$ C
Detector Aperture	70 x 70 mm
Data Images	1314 exposures
$\omega$ oscillation Range ( $\chi=45.0, \phi=180.0$ )	-70.0 - 110.0 $^{\circ}$
Exposure Rate	80.0 sec./ $^{\circ}$
Detector Swing Angle	20.00 $^{\circ}$
$\omega$ oscillation Range ( $\chi=0.0, \phi=0.0$ )	-36.0 - 99.0 $^{\circ}$
Exposure Rate	80.0 sec./ $^{\circ}$
Detector Swing Angle	20.00 $^{\circ}$
$\omega$ oscillation Range ( $\chi=45.0, \phi=90.0$ )	-70.0 - 110.0 $^{\circ}$
Exposure Rate	80.0 sec./ $^{\circ}$
Detector Swing Angle	20.00 $^{\circ}$
$\omega$ oscillation Range ( $\chi=45.0, \phi=0.0$ )	-70.0 - 92.0 $^{\circ}$
Exposure Rate	80.0 sec./ $^{\circ}$
Detector Swing Angle	20.00 $^{\circ}$
Detector Position	50.00 mm

Pixel Size	0.137 mm
$2\theta_{\max}$	55.0°
No. of Reflections Measured	Total: 8677 Unique: 2656 ( $R_{\text{int}} = 0.1457$ ) $I > 2\sigma(I)$ : 1356
Corrections	Lorentz-polarization (trans. factors: 0.323 - 1.000)

### C. Structure Solution and Refinement

Structure Solution	Direct Methods
Refinement	Full-matrix least-squares on $F^2$
Function Minimized	$\sum w (F_o^2 - F_c^2)^2$
Least Squares Weights	$w = 1 / [ \sigma^2(F_o^2) + (0.0977 \cdot P)^2 + 1.0970 \cdot P ]$ where $P = (\text{Max}(F_o^2, 0) + 2F_c^2) / 3$
$2\theta_{\max}$ cutoff	50.0°
Anomalous Dispersion	All non-hydrogen atoms
No. Observations (All reflections)	2656
No. Variables	205
Reflection/Parameter Ratio	12.96
Residuals: $R_1 (I > 2.00\sigma(I))$	0.1365
Residuals: $R$ (All reflections)	0.2347
Residuals: $wR_2$ (All reflections)	0.3084

Goodness of Fit Indicator	1.107
Max Shift/Error in Final Cycle	0.000
Maximum peak in Final Diff. Map	0.30 e <sup>-</sup> /Å <sup>3</sup>
Minimum peak in Final Diff. Map	-0.29 e <sup>-</sup> /Å <sup>3</sup>

**Appendix 2.3** X-ray crystallographic data report for compound **24** (Chapter 2)

X-ray Structure Report

for

Prof. Paris Georghiou

Prepared by

Louise N. Dawe, PhD

Centre for Chemical Analysis, Research and Training (C-CART)  
and Department of Chemistry  
Memorial University of Newfoundland  
St. Johns, NL, A1B 3X7  
(709) 864-4556 (X-Ray Laboratory)  
(709) 864-8904 (Office)

November 21, 2012

Introduction

Collection, solution and refinement proceeded normally. N-H hydrogen atoms were located in difference map positions and refined with fixed Uiso (1.5Ueq of their bonding partners), and with distance restraints. All other hydrogen atoms were introduced in calculated positions and refined on a riding model. All non-hydrogen atoms were refined anisotropically.

*Experimental*

## Data Collection

A colorless prism crystal of  $C_{15}H_{19}N_2O_4Cl_3$  having approximate dimensions of 0.42 x 0.09 x 0.05 mm was mounted on a low temperature diffraction loop. All measurements were made on a Rigaku Saturn70 CCD diffractometer using graphite monochromated Mo-K $\alpha$  radiation, equipped with a SHINE optic.

The crystal-to-detector distance was 50.20 mm.

Cell constants and an orientation matrix for data collection corresponded to a primitive monoclinic cell with dimensions:

$$\begin{aligned}a &= 8.662(7) \text{ \AA} \\b &= 8.329(7) \text{ \AA} \quad \beta = 99.006(11)^\circ \\c &= 12.672(10) \text{ \AA} \\V &= 903.0(13) \text{ \AA}^3\end{aligned}$$

For  $Z = 2$  and F.W. = 397.69, the calculated density is 1.463 g/cm<sup>3</sup>. Based on the reflection conditions of:

$$0k0: k = 2n$$

packing considerations, a statistical analysis of intensity distribution, and the successful solution and refinement of the structure, the space group was determined to be:

$$P2_1 (\#4)$$

The data were collected at a temperature of  $-150 \pm 1^\circ\text{C}$  to a maximum  $2\theta$  value of  $59.8^\circ$ . A total of 1004 oscillation images were collected. A sweep of data was done using  $\omega$  scans from  $-70.0$  to  $110.0^\circ$  in  $0.5^\circ$  step, at  $\chi=0.0^\circ$  and  $\phi = 90.0^\circ$ . The exposure rate was 24.0 [sec./ $^\circ$ ]. The detector swing angle was  $20.11^\circ$ . A second sweep was performed using  $\omega$  scans from  $-70.0$  to  $102.0^\circ$  in  $0.5^\circ$  step, at  $\chi=45.0^\circ$  and  $\phi = 90.0^\circ$ . The exposure rate was 24.0 [sec./ $^\circ$ ]. The detector swing angle was  $20.11^\circ$ . Another sweep was performed using  $\omega$  scans from  $-70.0$  to  $80.0^\circ$  in  $0.5^\circ$  step, at  $\chi=45.0^\circ$  and  $\phi = 0.0^\circ$ . The exposure rate was 24.0 [sec./ $^\circ$ ]. The detector swing angle was  $20.11^\circ$ . The crystal-to-detector distance was 50.20 mm. Readout was performed in the 0.137 mm pixel mode.

## Data Reduction

Of the 8478 reflections that were collected, 3076 were unique ( $R_{int} = 0.0357$ ). Data were collected and processed using CrystalClear (Rigaku).

The linear absorption coefficient,  $\mu$ , for Mo-K $\alpha$  radiation is 5.29 cm<sup>-1</sup>. An empirical absorption correction was applied which resulted in transmission factors ranging from 0.982 to 0.998. The data were corrected for Lorentz and polarization effects.

## Structure Solution and Refinement

The structure was solved by direct methods<sup>2</sup> and expanded using Fourier techniques. The non-hydrogen atoms were refined anisotropically. Some hydrogen atoms were refined isotropically, some were refined using the riding model, and the rest were included in fixed positions. The final cycle of full-matrix least-squares refinement<sup>3</sup> on  $F^2$  was based on 3076 observed reflections and 223 variable parameters and converged (largest parameter shift was 0.00 times its esd) with unweighted and weighted agreement factors of:

$$R1 = \sum ||F_o| - |F_c|| / \sum |F_o| = 0.0368$$

$$wR2 = [ \sum ( w (F_o^2 - F_c^2)^2 ) / \sum w(F_o^2)^2 ]^{1/2} = 0.0953$$

The standard deviation of an observation of unit weight<sup>4</sup> was 1.06. Unit weights were used. The maximum and minimum peaks on the final difference Fourier map corresponded to 0.29 and -0.29 e<sup>-</sup>/Å<sup>3</sup>, respectively. The absolute structure was deduced based on Flack parameter, 0.07(7), using 1153 Friedel pairs.<sup>5</sup>

Neutral atom scattering factors were taken from Cromer and Waber<sup>6</sup>. Anomalous dispersion effects were included in  $F_{calc}$ <sup>7</sup>; the values for  $\Delta f'$  and  $\Delta f''$  were those of Creagh and McAuley<sup>8</sup>. The values for the mass attenuation coefficients are those of Creagh and Hubbell<sup>9</sup>. All calculations were performed using the CrystalStructure<sup>10</sup> crystallographic software package except for refinement, which was performed using SHELXL-97<sup>2</sup>.

## References

(1) CrystalClear: Rigaku Corporation, 1999. CrystalClear Software User's Guide, Molecular Structure Corporation, (c) 2000. J.W. Pflugrath (1999) Acta Cryst. D55, 1718-1725.

(2) SHELX97: Sheldrick, G.M. Acta Cryst. 2008, A64, 112-122.

(3) Least Squares function minimized: (SHELXL97)

$$\sum w(F_o^2 - F_c^2)^2 \quad \text{where } w = \text{Least Squares weights.}$$

(4) Standard deviation of an observation of unit weight:

$$[\sum w(F_o^2 - F_c^2)^2 / (N_o - N_v)]^{1/2}$$

where:  $N_o$  = number of observations  
 $N_v$  = number of variables

(5) Flack, H. D. (1983), Acta Cryst. A39, 876-881.

(6) Cromer, D. T. & Waber, J. T.; "International Tables for X-ray Crystallography", Vol. IV, The Kynoch Press, Birmingham, England, Table 2.2 A (1974).

(7) Ibers, J. A. & Hamilton, W. C.; Acta Crystallogr., 17, 781 (1964).

(8) Creagh, D. C. & McAuley, W.J. ; "International Tables for Crystallography", Vol C, (A.J.C. Wilson, ed.), Kluwer Academic Publishers, Boston, Table 4.2.6.8, pages 219-222 (1992).

(9) Creagh, D. C. & Hubbell, J.H.; "International Tables for Crystallography", Vol C, (A.J.C. Wilson, ed.), Kluwer Academic Publishers, Boston, Table 4.2.4.3, pages 200-206 (1992).

(10) CrystalStructure 4.0: Crystal Structure Analysis Package, Rigaku and Rigaku Americas (2000-2010). 9009 New Trails Dr. The Woodlands TX 77381 USA.

## EXPERIMENTAL DETAILS

### A. Crystal Data

Empirical Formula	$C_{15}H_{19}N_2O_4Cl_3$
Formula Weight	397.69
Crystal Color, Habit	colorless, prism
Crystal Dimensions	0.42 X 0.09 X 0.05 mm
Crystal System	monoclinic
Lattice Type	Primitive
Lattice Parameters	$a = 8.662(7) \text{ \AA}$ $b = 8.329(7) \text{ \AA}$ $c = 12.672(10) \text{ \AA}$ $\beta = 99.006(11)^\circ$ $V = 903.0(13) \text{ \AA}^3$
Space Group	$P2_1$ (#4)
Z value	2
$D_{\text{calc}}$	$1.463 \text{ g/cm}^3$
F <sub>000</sub>	412
$\mu(\text{MoK}\alpha)$	$5.29 \text{ cm}^{-1}$

## B. Intensity Measurements

Diffractometer	Rigaku Saturn70 CCD
Radiation	MoK $\alpha$ ( $\lambda = 0.71075 \text{ \AA}$ ) graphite monochromated-Rigaku SHINE
Voltage, Current	50kV, 30mA
Temperature	-150.0°C
Detector Aperture	70 x 70 mm
Data Images	1004 exposures
$\omega$ oscillation Range ( $\chi=0.0, \phi=90.0$ )	-70.0 - 110.0°
Exposure Rate	24.0 sec./°
Detector Swing Angle	20.11°
$\omega$ oscillation Range ( $\chi=45.0, \phi=90.0$ )	-70.0 - 102.0°
Exposure Rate	24.0 sec./°
Detector Swing Angle	20.11°
$\omega$ oscillation Range ( $\chi=45.0, \phi=0.0$ )	-70.0 - 80.0°
Exposure Rate	24.0 sec./°
Detector Swing Angle	20.11°
Detector Position	50.20 mm
Pixel Size	0.068 mm
$2\theta_{\max}$	59.8°
No. of Reflections Measured	Total: 8478 Unique: 3076 ( $R_{\text{int}} = 0.0357$ ) $I > 2\sigma(I)$ : 2960 Friedel pairs: 1153

Corrections	Lorentz-polarization (trans. factors: 0.982 - 0.998)
-------------	---

### C. Structure Solution and Refinement

Structure Solution	Direct Methods
Refinement	Full-matrix least-squares on $F^2$
Function Minimized	$\sum w (F_o^2 - F_c^2)^2$
Least Squares Weights	$w = 1 / [ \sigma^2(F_o^2) + (0.0371 \cdot P)^2 + 0.6641 \cdot P ]$ where $P = (\text{Max}(F_o^2, 0) + 2F_c^2) / 3$
$2\theta_{\text{max}}$ cutoff	53.0°
Anomalous Dispersion	All non-hydrogen atoms
No. Observations (All reflections)	3076
No. Variables	223
Reflection/Parameter Ratio	13.79
Residuals: R1 ( $I > 2.00\sigma(I)$ )	0.0368
Residuals: R (All reflections)	0.0402
Residuals: wR2 (All reflections)	0.0953
Goodness of Fit Indicator	1.062
Flack Parameter (Friedel pairs = 1153)	0.07(7)
Max Shift/Error in Final Cycle	0.001
Maximum peak in Final Diff. Map	0.29 e <sup>-</sup> /Å <sup>3</sup>
Minimum peak in Final Diff. Map	-0.29 e <sup>-</sup> /Å <sup>3</sup>

## Appendix 2.4 X-ray crystallographic data report for compound 25 (Chapter 2)

### X-ray Structure Report

for  
Dr. P.E. Georghiou

Prepared by

Louise N. Dawe, PhD

Department of Chemistry and  
Centre for Chemical Analysis, Research and Training (C-CART)  
Memorial University of Newfoundland  
St. Johns, NL, A1B 3X7  
(709) 864-4556 (X-Ray Laboratory)

December 16, 2012

### Introduction

All non-hydrogen atoms were refined anisotropically. HN1 and HN2 were introduced in their difference map positions and refined with  $U_{\text{iso}} = 1.5 U_{\text{eq}}$  of N1 and N2 respectively. All other H-atoms were introduced in calculated positions and refined on a riding model.

### *Experimental*

#### Data Collection

A colorless prism crystal of  $\text{C}_{28}\text{H}_{36}\text{N}_4\text{O}_8$  having approximate dimensions of 0.13 x 0.07 x 0.07 mm was mounted on a low temperature collection loop. All measurements were made on a Rigaku Saturn70 CCD diffractometer, equipped with a SHINE optic, using graphite monochromated Mo-K $\alpha$  radiation.

The crystal-to-detector distance was 50.18 mm.

Cell constants and an orientation matrix for data collection corresponded to a primitive triclinic cell with dimensions:

$$\begin{aligned} a &= 9.293(10) \text{ \AA} & \alpha &= 91.525(8)^\circ \\ b &= 9.4262(10) \text{ \AA} & \beta &= 110.407(3)^\circ \\ c &= 9.600(9) \text{ \AA} & \gamma &= 115.256(16)^\circ \\ V &= 697.4(10) \text{ \AA}^3 \end{aligned}$$

For  $Z = 1$  and F.W. = 556.61, the calculated density is  $1.325 \text{ g/cm}^3$ . Based on a statistical analysis of intensity distribution, and the successful solution and refinement of the structure, the space group was determined to be:

P-1 (#2)

The data were collected at a temperature of  $-150 \pm 1^\circ\text{C}$  to a maximum  $2\theta$  value of  $59.7^\circ$ . A total of 966 oscillation images were collected. A sweep of data was done using  $\omega$  scans from  $-70.0$  to  $110.0^\circ$  in  $0.5^\circ$  step, at  $\chi=45.0^\circ$  and  $\phi = 0.0^\circ$ . The exposure rate was  $40.0 \text{ [sec./}^\circ]$ . The detector swing angle was  $20.08^\circ$ . A second sweep was performed using  $\omega$  scans from  $-70.0$  to  $110.0^\circ$  in  $0.5^\circ$  step, at  $\chi=45.0^\circ$  and  $\phi = 180.0^\circ$ . The exposure rate was  $40.0 \text{ [sec./}^\circ]$ . The detector swing angle was  $20.08^\circ$ . Another sweep was performed using  $\omega$  scans from  $-12.0$  to  $50.0^\circ$  in  $0.5^\circ$  step, at  $\chi=0.0^\circ$  and  $\phi = 90.0^\circ$ . The exposure rate was  $40.0 \text{ [sec./}^\circ]$ . The detector swing angle was  $20.08^\circ$ . Another sweep was performed using  $\omega$  scans from  $-70.0$  to  $-9.0^\circ$  in  $0.5^\circ$  step, at  $\chi=45.0^\circ$  and  $\phi = 90.0^\circ$ . The exposure rate was  $40.0 \text{ [sec./}^\circ]$ . The detector swing angle was  $20.08^\circ$ . The crystal-to-detector distance was  $50.18 \text{ mm}$ . Readout was performed in the  $0.137 \text{ mm}$  pixel mode.

#### Data Reduction

Of the 7058 reflections that were collected, 3149 were unique ( $R_{\text{int}} = 0.0485$ ). Data were collected and processed using CrystalClear (Rigaku).

The linear absorption coefficient,  $\mu$ , for Mo-K $\alpha$  radiation is  $0.98 \text{ cm}^{-1}$ . An empirical absorption correction was applied which resulted in transmission factors ranging from 0.992 to 0.999. The data were corrected for Lorentz and polarization effects.

## Structure Solution and Refinement

The structure was solved by direct methods<sup>2</sup> and expanded using Fourier techniques. The non-hydrogen atoms were refined anisotropically. Hydrogen atoms were refined using the riding model. The final cycle of full-matrix least-squares refinement<sup>3</sup> on  $F^2$  was based on 3149 observed reflections and 187 variable parameters and converged (largest parameter shift was 0.00 times its esd) with unweighted and weighted agreement factors of:

$$R1 = \sum ||F_o| - |F_c|| / \sum |F_o| = 0.0711$$

$$wR2 = [ \sum ( w (F_o^2 - F_c^2)^2 ) / \sum w(F_o^2)^2 ]^{1/2} = 0.2045$$

The standard deviation of an observation of unit weight<sup>4</sup> was 1.09. Unit weights were used. The maximum and minimum peaks on the final difference Fourier map corresponded to 0.42 and -0.31 e<sup>-</sup>/Å<sup>3</sup>, respectively.

Neutral atom scattering factors were taken from Cromer and Waber<sup>5</sup>. Anomalous dispersion effects were included in  $F_{calc}$ <sup>6</sup>; the values for  $\Delta f'$  and  $\Delta f''$  were those of Creagh and McAuley<sup>7</sup>. The values for the mass attenuation coefficients are those of Creagh and Hubbell<sup>8</sup>. All calculations were performed using the CrystalStructure<sup>9</sup> crystallographic software package except for refinement, which was performed using SHELXL-97<sup>10</sup>.

## *References*

- (1) CrystalClear: Rigaku Corporation, 1999. CrystalClear Software User's Guide, Molecular Structure Corporation, (c) 2000. J.W. Pflugrath (1999) Acta Cryst. D55, 1718-1725.
- (2) SIR2004: M.C. Burla, R. Caliendo, M. Camalli, B. Carrozzini, G.L. Cascarano, L. De Caro, C. Giacovazzo, G. Polidori, R. Spagna (2005)
- (3) Least Squares function minimized: (SHELXL97)

$$\sum w(F_o^2 - F_c^2)^2 \quad \text{where } w = \text{Least Squares weights.}$$

- (4) Standard deviation of an observation of unit weight:

$$[\sum w(F_o^2 - F_c^2)^2 / (N_o - N_v)]^{1/2}$$

where:  $N_O$  = number of observations  
 $N_V$  = number of variables

(5) Cromer, D. T. & Waber, J. T.; "International Tables for X-ray Crystallography", Vol. IV, The Kynoch Press, Birmingham, England, Table 2.2 A (1974).

(6) Ibers, J. A. & Hamilton, W. C.; Acta Crystallogr., 17, 781 (1964).

(7) Creagh, D. C. & McAuley, W.J. ; "International Tables for Crystallography", Vol C, (A.J.C. Wilson, ed.), Kluwer Academic Publishers, Boston, Table 4.2.6.8, pages 219-222 (1992).

(8) Creagh, D. C. & Hubbell, J.H.; "International Tables for Crystallography", Vol C, (A.J.C. Wilson, ed.), Kluwer Academic Publishers, Boston, Table 4.2.4.3, pages 200-206 (1992).

(9) CrystalStructure 4.0: Crystal Structure Analysis Package, Rigaku and Rigaku Americas (2000-2010). 9009 New Trails Dr. The Woodlands TX 77381 USA.

(10) SHELX97: Sheldrick, G.M. Acta Cryst. 2008, A64, 112-122

#### EXPERIMENTAL DETAILS

##### A. Crystal Data

Empirical Formula	$C_{28}H_{36}N_4O_8$
Formula Weight	556.61
Crystal Color, Habit	colorless, prism
Crystal Dimensions	0.13 X 0.07 X 0.07 mm
Crystal System	triclinic
Lattice Type	Primitive
Lattice Parameters	$a = 9.293(10) \text{ \AA}$ $b = 9.4262(10) \text{ \AA}$ $c = 9.600(9) \text{ \AA}$ $\alpha = 91.525(8)^\circ$ $\beta = 110.407(3)^\circ$ $\gamma = 115.256(16)^\circ$

	$V = 697.4(10) \text{ \AA}^3$
Space Group	P-1 (#2)
Z value	1
$D_{\text{calc}}$	$1.325 \text{ g/cm}^3$
F000	296
$\mu(\text{MoK}\alpha)$	$0.98 \text{ cm}^{-1}$

#### B. Intensity Measurements

Diffractometer	Rigaku Saturn70 CCD
Radiation	MoK $\alpha$ ( $\lambda = 0.71075 \text{ \AA}$ ) graphite monochromated-Rigaku SHINE
Voltage, Current	50kV, 30mA
Temperature	$-150.0^\circ\text{C}$
Detector Aperture	70 x 70 mm
Data Images	966 exposures
$\omega$ oscillation Range ( $\chi=45.0, \phi=0.0$ )	$-70.0 - 110.0^\circ$
Exposure Rate	$40.0 \text{ sec./}^\circ$
Detector Swing Angle	$20.08^\circ$
$\omega$ oscillation Range ( $\chi=45.0, \phi=180.0$ )	$-70.0 - 110.0^\circ$
Exposure Rate	$40.0 \text{ sec./}^\circ$
Detector Swing Angle	$20.08^\circ$
$\omega$ oscillation Range ( $\chi=0.0, \phi=90.0$ )	$-12.0 - 50.0^\circ$
Exposure Rate	$40.0 \text{ sec./}^\circ$

Detector Swing Angle	20.08°
$\omega$ oscillation Range ( $\chi=45.0$ , $\phi=90.0$ )	-70.0 - -9.0°
Exposure Rate	40.0 sec./°
Detector Swing Angle	20.08°
Detector Position	50.18 mm
Pixel Size	0.137 mm
$2\theta_{\max}$	59.7°
No. of Reflections Measured	Total: 7058 Unique: 3149 ( $R_{\text{int}} = 0.0485$ ) $I > 2\sigma(I)$ : 2268
Corrections	Lorentz-polarization (trans. factors: 0.992 – 0.999)

### C. Structure Solution and Refinement

Structure Solution	Direct Methods
Refinement	Full-matrix least-squares on $F^2$
Function Minimized	$\sum w (F_o^2 - F_c^2)^2$
Least Squares Weights	$w = 1 / [ \sigma^2(F_o^2) + (0.0948 \cdot P)^2 + 0.3294 \cdot P ]$ where $P = (\text{Max}(F_o^2, 0) + 2F_c^2) / 3$
$2\theta_{\max}$ cutoff	55.0°
Anomalous Dispersion	All non-hydrogen atoms

No. Observations (All reflections)	3149
No. Variables	187
Reflection/Parameter Ratio	16.84
Residuals: R1 ( $I > 2.00\sigma(I)$ )	0.0711
Residuals: R (All reflections)	0.0958
Residuals: wR2 (All reflections)	0.2045
Goodness of Fit Indicator	1.088
Max Shift/Error in Final Cycle	0.000
Maximum peak in Final Diff. Map	0.42 e <sup>-</sup> /Å <sup>3</sup>
Minimum peak in Final Diff. Map	-0.31 e <sup>-</sup> /Å <sup>3</sup>

**Appendix 2.5** X-ray crystallographic data report for compound **36** (Chapter 2)

X-ray Structure Report

for

Prof. Paris Georghiou

Prepared by

Louise N. Dawe, PhD

Centre for Chemical Analysis, Research and Training (C-CART)  
Department of Chemistry  
Memorial University of Newfoundland  
St. Johns, NL, A1B 3X7  
(709) 864-4556 (X-Ray Laboratory)  
(709) 864-8904 (Office)

July 6, 2011

Introduction

Collection, solution and refinement proceeded normally. All non-hydrogen atoms were refined anisotropically. All H-atoms were introduced in calculated positions and refined on a riding model, except the N-bound H1, which was introduced from its difference map position, and was refined positionally, with its isotropic displacement ellipsoid fixed 1.2 times of N1, at the time the atom was introduced.

## Experimental

### Data Collection

A colorless needle crystal of  $C_{22}H_{26}N_2O_5$  having approximate dimensions of 0.25 x 0.05 x 0.03 mm was mounted on a glass fiber. All measurements were made on a Rigaku Saturn70 CCD diffractometer using graphite monochromated Mo- $K\alpha$  radiation, equipped with a SHINE optic.

The crystal-to-detector distance was 50.00 mm.

Cell constants and an orientation matrix for data collection corresponded to a C-centered monoclinic cell with dimensions:

$$\begin{aligned} a &= 4.7848(10) \text{ \AA} \\ b &= 18.335(4) \text{ \AA} \quad \beta = 93.032(7)^\circ \\ c &= 23.767(6) \text{ \AA} \\ V &= 2082.1(8) \text{ \AA}^3 \end{aligned}$$

For  $Z = 4$  and F.W. = 398.46, the calculated density is 1.271 g/cm<sup>3</sup>. Based on the reflection conditions of:

$$\begin{aligned} hkl: & h+k = 2n \\ h0l: & l = 2n \end{aligned}$$

packing considerations, a statistical analysis of intensity distribution, and the successful solution and refinement of the structure, the space group was determined to be:

C2/c (#15)

The data were collected at a temperature of  $-110 \pm 1^\circ\text{C}$  to a maximum  $2\theta$  value of  $55.0^\circ$ . A total of 598 oscillation images were collected. A sweep of data was done using  $\omega$  scans from  $-70.0$  to  $110.0^\circ$  in  $1.0^\circ$  step, at  $\chi=0.0^\circ$  and  $\phi = 180.0^\circ$ . The exposure rate was 45.0 [sec./ $^\circ$ ]. The detector swing angle was  $20.00^\circ$ . A second sweep was performed using  $\omega$  scans from  $-70.0$  to  $78.0^\circ$  in  $1.0^\circ$  step, at  $\chi=0.0^\circ$  and  $\phi = 0.0^\circ$ . The exposure rate was 45.0 [sec./ $^\circ$ ]. The detector swing angle was  $20.00^\circ$ . Another sweep was performed using  $\omega$  scans from  $-70.0$  to  $80.0^\circ$  in  $1.0^\circ$  step, at  $\chi=45.0^\circ$  and  $\phi = 0.0^\circ$ . The exposure rate was 45.0 [sec./ $^\circ$ ]. The detector swing angle was  $20.00^\circ$ . Another sweep was performed using  $\omega$  scans from  $-70.0$  to  $50.0^\circ$  in  $1.0^\circ$  step, at  $\chi=45.0^\circ$  and  $\phi = 180.0^\circ$ . The exposure rate was 45.0 [sec./ $^\circ$ ]. The detector swing angle was  $20.00^\circ$ . The crystal-to-detector distance was 50.00 mm. Readout was performed in the 0.137 mm pixel mode.

## Data Reduction

Of the 8693 reflections that were collected, 1753 were unique ( $R_{\text{int}} = 0.1174$ ). Data were collected and processed using CrystalClear (Rigaku).

The linear absorption coefficient,  $\mu$ , for Mo-K $\alpha$  radiation is 0.90 cm<sup>-1</sup>. An empirical absorption correction was applied which resulted in transmission factors ranging from 0.382 to 1.000. The data were corrected for Lorentz and polarization effects.

## Structure Solution and Refinement

The structure was solved by direct methods<sup>2</sup> and expanded using Fourier techniques. The non-hydrogen atoms were refined anisotropically. Some hydrogen atoms were refined isotropically, some were refined using the riding model, and the rest were included in fixed positions. The final cycle of full-matrix least-squares refinement<sup>3</sup> on  $F^2$  was based on 1752 observed reflections and 135 variable parameters and converged (largest parameter shift was 0.00 times its esd) with unweighted and weighted agreement factors of:

$$R1 = \Sigma ||F_o| - |F_c|| / \Sigma |F_o| = 0.0907$$

$$wR2 = [ \Sigma ( w (F_o^2 - F_c^2)^2 ) / \Sigma w(F_o^2)^2 ]^{1/2} = 0.2483$$

The standard deviation of an observation of unit weight<sup>4</sup> was 1.05. Unit weights were used. The maximum and minimum peaks on the final difference Fourier map corresponded to 0.29 and -0.21 e<sup>-</sup>/Å<sup>3</sup>, respectively.

Neutral atom scattering factors were taken from Cromer and Waber<sup>5</sup>. Anomalous dispersion effects were included in  $F_{\text{calc}}$ <sup>6</sup>; the values for  $\Delta f'$  and  $\Delta f''$  were those of Creagh and McAuley<sup>7</sup>. The values for the mass attenuation coefficients are those of Creagh and Hubbell<sup>8</sup>. All calculations were performed using the CrystalStructure<sup>9</sup> crystallographic software package except for refinement, which was performed using SHELXL-97<sup>10</sup>.

## References

(1) CrystalClear: Rigaku Corporation, 1999. CrystalClear Software User's Guide, Molecular Structure Corporation, (c) 2000. J.W. Pflugrath (1999) Acta Cryst. D55, 1718-1725.

(2) SIR2004: M.C. Burla, R. Caliandro, M. Camalli, B. Carrozzini, G.L. Casciarano, L. De Caro, C. Giacovazzo, G. Polidori, R. Spagna (2005)

(3) Least Squares function minimized: (SHELXL97)

$$\sum w(F_o^2 - F_c^2)^2 \quad \text{where } w = \text{Least Squares weights.}$$

(4) Standard deviation of an observation of unit weight:

$$[\sum w(F_o^2 - F_c^2)^2 / (N_o - N_v)]^{1/2}$$

where:  $N_o$  = number of observations  
 $N_v$  = number of variables

(5) Cromer, D. T. & Waber, J. T.; "International Tables for X-ray Crystallography", Vol. IV, The Kynoch Press, Birmingham, England, Table 2.2 A (1974).

(6) Ibers, J. A. & Hamilton, W. C.; Acta Crystallogr., 17, 781 (1964).

(7) Creagh, D. C. & McAuley, W. J. ; "International Tables for Crystallography", Vol C, (A.J.C. Wilson, ed.), Kluwer Academic Publishers, Boston, Table 4.2.6.8, pages 219-222 (1992).

(8) Creagh, D. C. & Hubbell, J.H.; "International Tables for Crystallography", Vol C, (A.J.C. Wilson, ed.), Kluwer Academic Publishers, Boston, Table 4.2.4.3, pages 200-206 (1992).

(9) CrystalStructure 4.0: Crystal Structure Analysis Package, Rigaku and Rigaku Americas (2000-2010). 9009 New Trails Dr. The Woodlands TX 77381 USA.

(10) SHELX97: Sheldrick, G.M. Acta Cryst. 2008, A64, 112-122

## EXPERIMENTAL DETAILS

### A. Crystal Data

Empirical Formula	C <sub>22</sub> H <sub>26</sub> N <sub>2</sub> O <sub>5</sub>
Formula Weight	398.46
Crystal Color, Habit	colorless, needle
Crystal Dimensions	0.25 X 0.05 X 0.03 mm
Crystal System	monoclinic
Lattice Type	C-centered
Lattice Parameters	a = 4.7848(10) Å b = 18.335(4) Å c = 23.767(6) Å β = 93.032(7) ° V = 2082.1(8) Å <sup>3</sup>
Space Group	C2/c (#15)
Z value	4
D <sub>calc</sub>	1.271 g/cm <sup>3</sup>
F <sub>000</sub>	848
μ(MoKα)	0.90 cm <sup>-1</sup>

## B. Intensity Measurements

Diffractometer	Rigaku Saturn70 CCD
Radiation	MoK $\alpha$ ( $\lambda = 0.71075 \text{ \AA}$ ) graphite monochromated-Rigaku SHINE
Voltage, Current	50kV, 30mA
Temperature	-110.0°C
Detector Aperture	70 x 70 mm
Data Images	598 exposures
$\omega$ oscillation Range ( $\chi=0.0, \phi=180.0$ )	-70.0 - 110.0°
Exposure Rate	45.0 sec./°
Detector Swing Angle	20.00°
$\omega$ oscillation Range ( $\chi=0.0, \phi=0.0$ )	-70.0 - 78.0°
Exposure Rate	45.0 sec./°
Detector Swing Angle	20.00°
$\omega$ oscillation Range ( $\chi=45.0, \phi=0.0$ )	-70.0 - 80.0°
Exposure Rate	45.0 sec./°
Detector Swing Angle	20.00°
$\omega$ oscillation Range ( $\chi=45.0, \phi=180.0$ )	-70.0 - 50.0°
Exposure Rate	45.0 sec./°
Detector Swing Angle	20.00°
Detector Position	50.00 mm
Pixel Size	0.137mm

$2\theta_{\max}$	55.0°
No. of Reflections Measured	Total: 8693 Unique: 1752 ( $R_{\text{int}} = 0.1174$ ) $I > 2\sigma(I)$ : 889
Corrections	Lorentz-polarization (trans. factors: 0.382 - 1.000)

### C. Structure Solution and Refinement

Structure Solution	Direct Methods
Refinement	Full-matrix least-squares on $F^2$
Function Minimized	$\sum w (F_o^2 - F_c^2)^2$
Least Squares Weights	$w = 1 / [ \sigma^2(F_o^2) + (0.1066 \cdot P)^2 + 0.0706 \cdot P ]$ where $P = (\text{Max}(F_o^2, 0) + 2F_c^2) / 3$
$2\theta_{\max}$ cutoff	50.0°
Anomalous Dispersion	All non-hydrogen atoms
No. Observations (All reflections)	1752
No. Variables	135
Reflection/Parameter Ratio	12.98
Residuals: $R_1$ ( $I > 2.00\sigma(I)$ )	0.0907
Residuals: $R$ (All reflections)	0.1713
Residuals: $wR_2$ (All reflections)	0.2483
Goodness of Fit Indicator	1.049
Max Shift/Error in Final Cycle	0.000
Maximum peak in Final Diff. Map	0.29 e <sup>-</sup> /Å <sup>3</sup>
Minimum peak in Final Diff. Map	-0.21 e <sup>-</sup> /Å <sup>3</sup>

## Appendix 2.6 X-ray crystallographic data report for compound 38 (Chapter 2)

X-ray Structure Report

for

Prof. Paris Georghiou

Prepared by

Louise N. Dawe, PhD

Centre for Chemical Analysis, Research and Training (C-CART)

Department of Chemistry

Memorial University of Newfoundland

St. Johns, NL, A1B 3X7

(709) 864-4556 (X-Ray Laboratory)

(709) 864-8904 (Office)

June 28, 2011

[Crystallographic data has been reported with the Cambridge crystallographic data centre as CCDC#2182]

### Introduction

Collection, solution and refinement proceeded normally. O-H hydrogen atoms were located in difference map positions and refined with fixed Uiso (1.5Ueq of their bonding partners), and with distance (DFIX) and angle (DANG) restraints. H-bond D-A vectors were carefully considered after O-H hydrogen atoms were located, and while H12 is not oriented towards O9 or O10 (possible H-bond acceptors), forcing it into either of those orientations leads to very short (1.2 Å) H-H intermolecular distances that were not considered to be physically possible. All other hydrogen atoms were introduced in calculated positions and refined on a riding model. All non-hydrogen atoms were refined anisotropically.

BVS calculations were performed<sup>10</sup>, and indicate that all U atoms are in the +6 oxidation state. Charge balance has been achieved, since O(5,6,7,9 and 10) are each oxide (O<sup>2-</sup>), while the asymmetric unit also contains two acetates (CH<sub>3</sub>COO<sup>-</sup>).

Atom no.	Valence state assumed	Most consistent valence state	Bond Valence Sum	% Deviation from assumed valence state
U1	U1 (2)		6.726	236
U1	U1 (4)		7.335	83
U1	U1 (5)		6.637	33
U1	U1 (6)	*	6.1	2
U2	U2 (2)		6.696	235
U2	U2 (4)		7.299	82
U2	U2 (5)		6.605	32
U2	U2 (6)	*	6.033	1

### Experimental

#### Data Collection

A yellow prism crystal of  $C_{10}H_{28}O_{24}U_4$  having approximate dimensions of 0.10 x 0.07 x 0.05 mm was mounted on a low temperature diffraction loop. All measurements were made on a Rigaku Saturn70 CCD diffractometer using graphite monochromated Mo-K $\alpha$  radiation, equipped with a SHINE optic.

The crystal-to-detector distance was 50.14 mm.

Cell constants and an orientation matrix for data collection corresponded to a primitive monoclinic cell with dimensions:

$$\begin{aligned}
 a &= 8.334(3) \text{ \AA} \\
 b &= 10.649(3) \text{ \AA} \quad \beta = 107.632(4)^\circ \\
 c &= 16.763(5) \text{ \AA} \\
 V &= 1417.8(8) \text{ \AA}^3
 \end{aligned}$$

For  $Z = 2$  and F.W. = 1484.43, the calculated density is 3.477 g/cm<sup>3</sup>. The reflection conditions of:

$$\begin{aligned}
 h0l: l &= 2n \\
 0k0: k &= 2n
 \end{aligned}$$

uniquely determine the space group to be:

$$P2_1/c \text{ (#14)}$$

The data were collected at a temperature of  $-110 \pm 1^\circ\text{C}$  to a maximum  $2\theta$  value of  $59.6^\circ$ . A total of 1058 oscillation images were collected. A sweep of data was done using  $\omega$  scans from  $-70.0$  to  $107.0^\circ$  in  $0.5^\circ$  step, at  $\chi=45.0^\circ$  and  $\phi = 180.0^\circ$ . The exposure rate was  $30.0$  [sec./ $^\circ$ ]. The detector swing angle was  $20.10^\circ$ . A second sweep was performed using  $\omega$  scans from  $-70.0$  to  $110.0^\circ$  in  $0.5^\circ$  step, at  $\chi=0.0^\circ$  and  $\phi = 0.0^\circ$ . The exposure rate was  $30.0$  [sec./ $^\circ$ ]. The detector swing angle was  $20.10^\circ$ . Another sweep was performed using  $\omega$  scans from  $-70.0$  to  $102.0^\circ$  in  $0.5^\circ$  step, at  $\chi=45.0^\circ$  and  $\phi = 0.0^\circ$ . The exposure rate was  $30.0$  [sec./ $^\circ$ ]. The detector swing angle was  $20.10^\circ$ . The crystal-to-detector distance was  $50.14$  mm. Readout was performed in the  $0.137$  mm pixel mode.

### Data Reduction

Of the 15153 reflections that were collected, 3257 were unique ( $R_{\text{int}} = 0.0758$ ). Data were collected and processed using CrystalClear (Rigaku).

The linear absorption coefficient,  $\mu$ , for Mo-K $\alpha$  radiation is  $228.751 \text{ cm}^{-1}$ . An empirical absorption correction was applied which resulted in transmission factors ranging from  $0.638$  to  $0.880$ . The data were corrected for Lorentz and polarization effects.

### Structure Solution and Refinement

The structure was solved by direct methods<sup>2</sup> and expanded using Fourier techniques. The non-hydrogen atoms were refined anisotropically. Hydrogen atoms were refined using the riding model. The final cycle of full-matrix least-squares refinement<sup>3</sup> on  $F^2$  was based on 3257 observed reflections and 190 variable parameters and converged (largest parameter shift was  $0.00$  times its esd) with unweighted and weighted agreement factors of:

$$R1 = \sum ||F_o| - |F_c|| / \sum |F_o| = 0.0341$$

$$wR2 = [ \sum ( w (F_o^2 - F_c^2)^2 ) / \sum w(F_o^2)^2 ]^{1/2} = 0.1089$$

The standard deviation of an observation of unit weight<sup>4</sup> was  $1.18$ . Unit weights were used. The maximum and minimum peaks on the final difference Fourier map corresponded to  $1.93$  and  $-3.79 \text{ e}^-/\text{\AA}^3$ , respectively.

Neutral atom scattering factors were taken from Cromer and Waber<sup>5</sup>. Anomalous dispersion effects were included in  $F_{calc}$ <sup>6</sup>; the values for  $\Delta f'$  and  $\Delta f''$  were those of Creagh and McAuley<sup>7</sup>. The values for the mass attenuation coefficients are those of Creagh and Hubbell<sup>8</sup>. All calculations were performed using the CrystalStructure<sup>9</sup> crystallographic software package except for refinement, which was performed using SHELXL-97<sup>2</sup>.

### References

(1) CrystalClear: Rigaku Corporation, 1999. CrystalClear Software User's Guide, Molecular Structure Corporation, (c) 2000. J.W. Pflugrath (1999) Acta Cryst. D55, 1718-1725.

(2) SHELX97: Sheldrick, G.M. Acta Cryst. 2008, A64, 112-122

(3) Least Squares function minimized: (SHELXL97)

$$\sum w(F_o^2 - F_c^2)^2 \quad \text{where } w = \text{Least Squares weights.}$$

(4) Standard deviation of an observation of unit weight:

$$[\sum w(F_o^2 - F_c^2)^2 / (N_o - N_v)]^{1/2}$$

where:  $N_o$  = number of observations  
 $N_v$  = number of variables

(5) Cromer, D. T. & Waber, J. T.; "International Tables for X-ray Crystallography", Vol. IV, The Kynoch Press, Birmingham, England, Table 2.2 A (1974).

(6) Ibers, J. A. & Hamilton, W. C.; Acta Crystallogr., 17, 781 (1964).

(7) Creagh, D. C. & McAuley, W.J. ; "International Tables for Crystallography", Vol C, (A.J.C. Wilson, ed.), Kluwer Academic Publishers, Boston, Table 4.2.6.8, pages 219-222 (1992).

(8) Creagh, D. C. & Hubbell, J.H.; "International Tables for Crystallography", Vol C, (A.J.C. Wilson, ed.), Kluwer Academic Publishers, Boston, Table 4.2.4.3, pages 200-206 (1992).

(9) CrystalStructure 4.0: Crystal Structure Analysis Package, Rigaku and Rigaku Americas (2000-2010). 9009 New Trails Dr. The Woodlands TX 77381 USA.

(10) A.S. Wills, VaList, Program available from [www.ccp14.ac.uk](http://www.ccp14.ac.uk)

## EXPERIMENTAL DETAILS

### A. Crystal Data

Empirical Formula	$C_{10}H_{28}O_{24}U_4$
Formula Weight	1484.43
Crystal Color, Habit	yellow, prism
Crystal Dimensions	0.10 X 0.07 X 0.05 mm
Crystal System	monoclinic
Lattice Type	Primitive
Lattice Parameters	$a = 8.334(3) \text{ \AA}$ $b = 10.649(3) \text{ \AA}$ $c = 16.763(5) \text{ \AA}$ $\beta = 107.632(4)^\circ$ $V = 1417.8(8) \text{ \AA}^3$
Space Group	$P2_1/c$ (#14)
Z value	2
$D_{\text{calc}}$	$3.477 \text{ g/cm}^3$
$F_{000}$	1296
$\mu(\text{MoK}\alpha)$	$228.75 \text{ cm}^{-1}$

### B. Intensity Measurements

Diffractionmeter	Rigaku Saturn70 CCD
Radiation	$\text{MoK}\alpha$ ( $\lambda = 0.71075 \text{ \AA}$ ) graphite monochromated-Rigaku SHINE
Voltage, Current	50kV, 30mA

Temperature	-110.0°C
Detector Aperture	70 x 70 mm
Data Images	1058 exposures
$\omega$ oscillation Range ( $\chi=45.0, \phi=180.0$ )	-70.0 - 107.0°
Exposure Rate	30.0 sec./°
Detector Swing Angle	20.10°
$\omega$ oscillation Range ( $\chi=0.0, \phi=0.0$ )	-70.0 - 110.0°
Exposure Rate	30.0 sec./°
Detector Swing Angle	20.10°
$\omega$ oscillation Range ( $\chi=45.0, \phi=0.0$ )	-70.0 - 102.0°
Exposure Rate	30.0 sec./°
Detector Swing Angle	20.10°
Detector Position	50.14 mm
Pixel Size	0.137 mm
$2\theta_{\max}$	59.6°

No. of Reflections Measured	Total: 15153 Unique: 3257 ( $R_{int} = 0.0758$ ) $I > 2\sigma(I)$ : 3136
-----------------------------	--

Corrections	Lorentz-polarization (trans. factors: 0.638 - 0.880)
-------------	---

### C. Structure Solution and Refinement

Structure Solution	Direct Methods
Refinement	Full-matrix least-squares on $F^2$
Function Minimized	$\sum w (F_o^2 - F_c^2)^2$
Least Squares Weights	$w = 1 / [ \sigma^2(F_o^2) + (0.0617 \cdot P)^2 + 5.0464 \cdot P ]$ where $P = (\text{Max}(F_o^2, 0) + 2F_c^2) / 3$
$2\theta_{max}$ cutoff	55.0°
Anomalous Dispersion	All non-hydrogen atoms
No. Observations (All reflections)	3257
No. Variables	190
Reflection/Parameter Ratio	17.14
Residuals: $R_1$ ( $I > 2.00\sigma(I)$ )	0.0341
Residuals: $R$ (All reflections)	0.0373
Residuals: $wR_2$ (All reflections)	0.1089
Goodness of Fit Indicator	1.184
Max Shift/Error in Final Cycle	0.001
Maximum peak in Final Diff. Map	1.93 e <sup>-</sup> /Å <sup>3</sup>
Minimum peak in Final Diff. Map	-3.79 e <sup>-</sup> /Å <sup>3</sup>

**Appendix 2.7** X-ray crystallographic data report for compound **24** (Chapter 3)

X-ray Structure Report

for  
Dr. P. E. Georghiou

Prepared by

Louise N. Dawe, PhD

Centre for Chemical Analysis, Research and Training (C-CART)  
Department of Chemistry  
Memorial University of Newfoundland  
St. Johns, NL, A1B 3X7  
(709) 864-4556 (X-Ray Laboratory)

October 22, 2010

[Crystallographic data has been reported with the Cambridge crystallographic data centre as  
CCDC#924367]

Introduction

Collection, solution and refinement proceeded normally. H1N and H2N were located in their difference map positions. Their isotropic ellipses were set 1.2 times greater than their bonding partners, and they were refined positionally. All other hydrogen atoms were introduced in calculated positions and refined on a riding model. All non-hydrogen atoms were refined anisotropically. C16-18 and C19-21 make up two PARTs of a disordered chain. Their occupancies were refined (sum to one) and the distances between C-atoms in each PART was restrained.

## Experimental

### Data Collection

A colorless prism crystal of  $C_{32}H_{36}N_2O_{12}S_4$  having approximate dimensions of 0.11 x 0.08 x 0.07 mm was mounted on a low temperature diffraction loop. All measurements were made on a Rigaku Saturn CCD area detector equipped with a SHINE optic and Mo-K $\alpha$  radiation.

Indexing was performed from 300 images that were exposed for 25 seconds. The crystal-to-detector distance was 40.15 mm.

Cell constants and an orientation matrix for data collection corresponded to a primitive orthorhombic cell with dimensions:

$$\begin{aligned}a &= 10.7751(12) \text{ \AA} \\b &= 15.8213(18) \text{ \AA} \\c &= 20.683(2) \text{ \AA} \\V &= 3525.9(7) \text{ \AA}^3\end{aligned}$$

For  $Z = 4$  and F.W. = 768.88, the calculated density is 1.448 g/cm<sup>3</sup>. The systematic absences of:

$$\begin{aligned}h00: & h \pm 2n \\0k0: & k \pm 2n \\00l: & l \pm 2n\end{aligned}$$

uniquely determine the space group to be:

$$P2_12_12_1 \text{ (#19)}$$

The data were collected at a temperature of  $-115 \pm 1^\circ\text{C}$  to a maximum  $2\theta$  value of  $62.0^\circ$ . A total of 600 oscillation images were collected. A sweep of data was done using  $\omega$  scans from  $-75.0$  to  $75.0^\circ$  in  $0.5^\circ$  step, at  $\chi=45.0^\circ$  and  $\phi = 0.0^\circ$ . The exposure rate was 50.0 [sec./ $^\circ$ ]. The detector swing angle was  $15.09^\circ$ . A second sweep was performed using  $\omega$  scans from  $-75.0$  to  $75.0^\circ$  in  $0.5^\circ$  step, at  $\chi=0.0^\circ$  and  $\phi = 0.0^\circ$ . The exposure rate was 50.0 [sec./ $^\circ$ ]. The detector swing angle was  $15.09^\circ$ . The crystal-to-detector distance was 40.15 mm. Readout was performed in the 0.137 mm pixel mode.

## Data Reduction

Of the 28047 reflections that were collected, 8063 were unique ( $R_{int} = 0.0531$ ); equivalent reflections were merged. Data were collected and processed using CrystalClear (Rigaku). Net intensities and sigmas were derived as follows:

$$F^2 = [\sum(P_i - mB_{ave})] \cdot Lp^{-1}$$

where  $P_i$  is the value in counts of the  $i^{\text{th}}$  pixel  
 $m$  is the number of pixels in the integration area  
 $B_{ave}$  is the background average  
 $Lp$  is the Lorentz and polarization factor

$$B_{ave} = \sum(B_j)/n$$

where  $n$  is the number of pixels in the background area  
 $B_j$  is the value of the  $j^{\text{th}}$  pixel in counts

$$\sigma^2(F^2_{hkl}) = [(\sum P_i) + m((\sum(B_{ave} - B_j)^2)/(n-1))] \cdot Lp \cdot \text{errmul} + (\text{erradd} \cdot F^2)^2$$

where  $\text{erradd} = 0.00$   
 $\text{errmul} = 1.00$

The linear absorption coefficient,  $\mu$ , for Mo-K $\alpha$  radiation is  $3.342 \text{ cm}^{-1}$ . A numerical absorption correction was applied which resulted in transmission factors ranging from 0.9696 to 0.9872. The data were corrected for Lorentz and polarization effects.

## Structure Solution and Refinement

The structure was solved by direct methods<sup>2</sup> and expanded using Fourier techniques<sup>3</sup>. The non-hydrogen atoms were refined anisotropically. Hydrogen atoms were refined using the riding model. The final cycle of full-matrix least-squares refinement<sup>4</sup> on  $F^2$  was based on 8063 observed reflections and 485 variable parameters and converged (largest parameter shift was 0.00 times its esd) with unweighted and weighted agreement factors of:

$$R1 = \sum ||F_o| - |F_c|| / \sum |F_o| = 0.0528$$

$$wR2 = [ \sum ( w (F_o^2 - F_c^2)^2 ) / \sum w(F_o^2)^2 ]^{1/2} = 0.1248$$

The standard deviation of an observation of unit weight<sup>5</sup> was 1.12. Unit weights were used. The maximum and minimum peaks on the final difference Fourier map corresponded to 0.34 and -0.43 e<sup>-</sup>/Å<sup>3</sup>, respectively.

Neutral atom scattering factors were taken from Cromer and Waber<sup>6</sup>. Anomalous dispersion effects were included in F<sub>calc</sub><sup>7</sup>; the values for Δf' and Δf'' were those of Creagh and McAuley<sup>8</sup>. The values for the mass attenuation coefficients are those of Creagh and Hubbell<sup>9</sup>. All calculations were performed using the CrystalStructure<sup>10,11</sup> crystallographic software package except for refinement, which was performed using SHELXL-97<sup>2</sup>.

### References

(1) CrystalClear: Rigaku Corporation, 1999. CrystalClear Software User's Guide, Molecular Structure Corporation, (c) 2000. J.W. Pflugrath (1999) Acta Cryst. D55, 1718-1725.

(2) SHELXL97: Sheldrick, G.M. Acta Cryst. 2008. A64, 112-122

(3) DIRDIF99: Beurskens, P.T., Admiraal, G., Beurskens, G., Bosman, W.P., de Gelder, R., Israel, R. and Smits, J.M.M. (1999). The DIRDIF-99 program system, Technical Report of the Crystallography Laboratory, University of Nijmegen, The Netherlands.

(4) Least Squares function minimized: (SHELXL97)

$$\sum w(F_o^2 - F_c^2)^2 \quad \text{where } w = \text{Least Squares weights.}$$

(5) Standard deviation of an observation of unit weight:

$$[\sum w(F_o^2 - F_c^2)^2 / (N_o - N_v)]^{1/2}$$

where:        N<sub>o</sub> = number of observations  
               N<sub>v</sub> = number of variables

(6) Cromer, D. T. & Waber, J. T.; "International Tables for X-ray Crystallography", Vol. IV, The Kynoch Press, Birmingham, England, Table 2.2 A (1974).

(7) Ibers, J. A. & Hamilton, W. C.; Acta Crystallogr., 17, 781 (1964).

(8) Creagh, D. C. & McAuley, W.J. ; "International Tables for Crystallography", Vol C, (A.J.C. Wilson, ed.), Kluwer Academic Publishers, Boston, Table 4.2.6.8, pages 219-222 (1992).

(9) Creagh, D. C. & Hubbell, J.H.; "International Tables for Crystallography", Vol C, (A.J.C. Wilson, ed.), Kluwer Academic Publishers, Boston, Table 4.2.4.3, pages 200-206 (1992).

(10) CrystalStructure 3.7.0: Crystal Structure Analysis Package, Rigaku and Rigaku/MSC (2000-2005). 9009 New Trails Dr. The Woodlands TX 77381 USA.

(11) CRYSTALS Issue 10: Watkin, D.J., Prout, C.K. Carruthers, J.R. & Betteridge, P.W. Chemical Crystallography Laboratory, Oxford, UK. (1996)

### EXPERIMENTAL DETAILS

#### A. Crystal Data

Empirical Formula	$C_{32}H_{36}N_2O_{12}S_4$
Formula Weight	768.88
Crystal Color, Habit	colorless, prism
Crystal Dimensions	0.11 X 0.08 X 0.07 mm
Crystal System	orthorhombic
Lattice Type	Primitive
Detector Position	40.15 mm
Pixel Size	0.137 mm
Lattice Parameters	a = 10.7751(12) Å b = 15.8213(18) Å c = 20.683(2) Å V = 3525.9(7) Å <sup>3</sup>
Space Group	P2 <sub>1</sub> 2 <sub>1</sub> 2 <sub>1</sub> (#19)

Z value	4
D <sub>calc</sub>	1.448 g/cm <sup>3</sup>
F <sub>000</sub>	1608
μ(MoKα)	3.34 cm <sup>-1</sup>

#### B. Intensity Measurements

Detector	Rigaku Saturn
Goniometer	Rigaku AFC8
Radiation	MoKα (λ = 0.71075 Å) graphite monochromated-Rigaku SHINE
Detector Aperture	70 mm x 70 mm
Data Images	600 exposures
ω oscillation Range (χ=45.0, φ=0.0)	-75.0 - 75.0°
Exposure Rate	50.0 sec./°
Detector Swing Angle	15.09°
ω oscillation Range (χ=0.0, φ=0.0)	-75.0 - 75.0°
Exposure Rate	50.0 sec./°
Detector Swing Angle	15.09°
Detector Position	40.15 mm
Pixel Size	0.068 mm
2θ <sub>max</sub>	62.0°
No. of Reflections Measured	Total: 28047 Unique: 8063 (R <sub>int</sub> = 0.0531) I>2σ(I): 7506

Corrections	Lorentz-polarization (trans. factors: 0.9696 - 0.9872)
-------------	---

### C. Structure Solution and Refinement

Structure Solution	Direct Methods (SHELX97)
Refinement	Full-matrix least-squares on $F^2$
Function Minimized	$\sum w (F_o^2 - F_c^2)^2$
Least Squares Weights	$w = 1 / [ \sigma^2(F_o^2) + (0.0555 \cdot P)^2 + 0.7241 \cdot P ]$ where $P = (\text{Max}(F_o^2, 0) + 2F_c^2) / 3$
$2\theta_{\text{max}}$ cutoff	55.0°
Anomalous Dispersion	All non-hydrogen atoms
No. Observations (All reflections)	8063
No. Variables	485
Reflection/Parameter Ratio	16.62
Residuals: $R_1$ ( $ I  > 2.00\sigma(I)$ )	0.0528
Residuals: $R$ (All reflections)	0.0571
Residuals: $wR_2$ (All reflections)	0.1248
Goodness of Fit Indicator	1.115
Max Shift/Error in Final Cycle	0.000
Maximum peak in Final Diff. Map	0.34 e <sup>-</sup> /Å <sup>3</sup>
Minimum peak in Final Diff. Map	-0.43 e <sup>-</sup> /Å

## Appendix 2.8 X-ray crystallographic data report for compound TBABr + CHCl<sub>3</sub> (Chapter 4)

X-ray Structure Report  
for  
Dr. P.E. Georghiou  
Prepared by  
Louise N. Dawe, PhD  
Department of Chemistry and  
Centre for Chemical Analysis, Research and Training (C-CART)  
Memorial University of Newfoundland  
St. Johns, NL, A1B 3X7  
(709) 864-4556 (X-Ray Laboratory)

May 2, 2013

### Experimental

An irregular, colourless crystal of C<sub>38</sub>H<sub>78</sub>N<sub>2</sub>Br<sub>2</sub>Cl<sub>18</sub> was selected and mounted on a low temperature loop on a Rigaku Saturn70 (2x2 bin mode) diffractometer. The crystal was kept at 163 K during data collection. Using Olex2 [1], the structure was solved with the ShelXS [2] structure solution program using Direct Methods and refined with the ShelXL [3] refinement package using Least Squares minimisation. A twin law was detected using PLATON's TwinRotMap [4], and incorporation of this law, and refinement of BASF, yielded a suitable result.

1. O. V. Dolomanov, L. J. Bourhis, R. J. Gildea, J. A. K. Howard and H. Puschmann, OLEX2: a complete structure solution, refinement and analysis program. *J. Appl. Cryst.* (2009). 42, 339-341.
2. SHELXS, G.M. Sheldrick, *Acta Cryst.* (2008). A64, 112-122
3. SHELXL, G.M. Sheldrick, *Acta Cryst.* (2008). A64, 112-122
4. PLATON, A.L. Spek, *J. Appl. Cryst.* (2003), 36, 7-13.

### Crystal structure determination of TBABr + CHCl<sub>3</sub>

**Crystal Data** for C<sub>38</sub>H<sub>78</sub>N<sub>2</sub>Br<sub>2</sub>Cl<sub>18</sub> (*M* = 799.88): monoclinic, space group P2<sub>1</sub>/n (no. 14), *a* = 19.994(14) Å, *b* = 16.011(11) Å, *c* = 20.472(15) Å, β = 106.409(8)°, *V* = 6287(8) Å<sup>3</sup>, *Z* = 4, *T* = 163 K, μ(MoKα) = 2.082 mm<sup>-1</sup>, *D*<sub>calc</sub> = 1.438 g/mm<sup>3</sup>, 63646 reflections measured (5.982 ≤ 2θ ≤ 53), 13113 unique (*R*<sub>int</sub> = 0.1323) which were used in all calculations. The final *R*<sub>1</sub> was 0.1149 (*I* > 2σ(*I*)) and *wR*<sub>2</sub> was 0.3580 (all data).

Table 1 Crystal data and structure refinement for **TBABr + CHCl<sub>3</sub>**

Identification code	TBABr84-31D
Empirical formula	C <sub>38</sub> H <sub>78</sub> N <sub>2</sub> Br <sub>2</sub> Cl <sub>18</sub>
Formula weight	799.88
Temperature/K	163
Crystal system	monoclinic
Space group	P2 <sub>1</sub> /n
a/Å	19.994(14)
b/Å	16.011(11)
c/Å	20.472(15)
α/°	90
β/°	106.409(8)
γ/°	90
Volume/Å <sup>3</sup>	6287(8)
Z	4
ρ <sub>calc</sub> /mg/mm <sup>3</sup>	1.438
m/mm <sup>-1</sup>	2.082
F(000)	2784.0
Crystal size/mm <sup>3</sup>	0.37 × 0.32 × 0.28
2θ range for data collection	5.982 to 53°
Index ranges	-25 ≤ h ≤ 25, -20 ≤ k ≤ 20, -23 ≤ l ≤ 25
Reflections collected	63646
Independent reflections	13113[R(int) = 0.1323]
Data/restraints/parameters	13113/0/550
Goodness-of-fit on F <sup>2</sup>	1.190
Final R indexes [I ≥ 2σ(I)]	R <sub>1</sub> = 0.1149, wR <sub>2</sub> = 0.3168
Final R indexes [all data]	R <sub>1</sub> = 0.1529, wR <sub>2</sub> = 0.3580
Largest diff. peak/hole / e Å <sup>-3</sup>	1.87/-0.94

